Title
The Potential Role of Pericytes and Genetic Regulation of Fibroblasts in Cardiac Fibrosis

Author
Park, Shuin

Publication Date
2020

Peer reviewed|Thesis/dissertation

UNIVERSITY OF CALIFORNIA

Los Angeles

The Potential Role of Pericytes and Genetic Regulation of Fibroblasts in Cardiac Fibrosis

A dissertation submitted in partial satisfaction of

the requirements for the degree Doctor of Philosophy in

Molecular, Cellular, and Integrative Physiology

by

Shuin Park

2020

ABSTRACT OF THE DISSERTATION

The Potential Role of Pericytes and

Genetic Regulation of Fibroblasts in Cardiac Fibrosis

by

Shuin Park

Doctor of Philosophy in Molecular, Cellular, and Integrative Physiology

University of California, Los Angeles, 2020

Professor Reza Ardehali, Chair

Cardiovascular disease (CVD) is the leading cause of mortality in the developed world and is exacerbated by the presence of cardiac fibrosis. Cardiac fibrosis is defined as the accumulation of extracellular matrix (ECM) proteins that form scar tissue. The presence of fibrosis in the heart can lead to arrhythmia and reduced contractility, increasing the risk for heart failure. There is currently a deficit of effective treatments to prevent or reverse the process of developing cardiac fibrosis in CVD. Studies are currently focused on understanding the complex myriad of cells that contribute to this process. This dissertation focuses on two different cell types in the heart and their contributions to fibrosis: pericytes and fibroblasts. Understanding these cells and their roles in cardiac fibrosis may unveil potential therapeutic targets for treating CVD.

Cardiac pericytes are a heterogeneous mural cell population that interact closely with endothelial cells to maintain vascular stability. Pericytes in other organs have previously been reported to also play a functional role in ischemic injury response. Findings in spinal cord injury or kidney ischemia have identified pericytes to express ECM proteins and directly contribute to the formation of scar tissue. In order to determine whether pericytes in the heart play a similar role, we used *NG2*$^{CreER/+}$ mice to lineage-trace NG2+ cardiac pericytes and determined that a subset of these cells proliferate and express ECM proteins after myocardial infarction (MI).

However, due to the heterogeneity of the pericyte population, we noted that NG2 may only label a subpopulation of pericytes in the heart. Therefore, we developed a protocol in which pericytes could be enriched for analysis at the single cell resolution without using any markers. By using this protocol on uninjured murine hearts and hearts that had undergone MI, we identified a subpopulation of pericytes that are potentially responsive to injury. These findings provide a foundation for future studies on cardiac pericytes and their functional role in cardiac fibrosis.

Cardiac fibroblasts (CFbs) are known to be the major cellular source for ECM proteins in the heart. We sought to answer two questions regarding this cell type: 1) whether CFbs from various genetic backgrounds contribute to fibrosis uniquely and 2) whether CFbs express any circulating biomarkers that can be used for detecting fibrosis. CFbs from mice with varying susceptibility to isoproterenol-induced cardiac fibrosis were characterized based on their levels of proliferation and activation. While levels of activation correlated with extent of fibrosis, the levels of proliferation in these cells did not. We then looked at secreted proteins that were expressed by CFbs after injury and validated a significant decrease in circulating levels of the full-length CILP protein in heart failure patients compared to healthy volunteers. These findings support the growing body of research being done on CFbs and their role in developing cardiac fibrosis.

The dissertation of Shuin Park is approved.

Luisa Iruela-Arispe

Aldons J. Lusis

Yibin Wang

Reza Ardehali, Committee Chair

University of California, Los Angeles

2020

To my family for their endless support.

TABLE OF CONTENTS

LIST OF FIGURES

Chapter 2

Chapter 3

Chapter 4

Chapter 5

ACKNOWLEDGEMENTS

I'd first like to thank my parents and my brother because I would not have even started this journey if it wasn't for their support. Thank you for everything and I love you.

I'd like to thank Dr. Ardehali for giving me the opportunity to work in his lab for the last 6 years and allowing me to become the scientist I am today. It is difficult to describe in words how much I have learned and grown under his mentorship. I would also like to thank the past and present members of the Ardehali lab for being the best colleagues anyone could have asked for. Special thanks to Ngoc, Arash, Peng, Lingjun, Rong, James, and Sara for being a part of my daily life for all these years. Thank you all for helping me, teaching me, eating cake with me, and making my days that much more enjoyable.

I will always be thankful for the support I've received from the UCLA community. I'd like to thank my committee members Dr. Arispe, Dr. Wang, and Dr. Lusis for their continuous guidance and only wish that I had reached out to them more throughout my time at UCLA. I'd like to thank Dr. Tidball, Dr. Frye, and Yesenia for making MCIP my home and giving me the confidence to push through graduate school. I'd like to give special thanks to Felicia, Jessica, and Jeffery at the FACS core for all those hours making my experiments even possible. And finally, to all the friends that I've grabbed a coffee with, hiked with, studied with, celebrated achievements with, laughed with, and drank beer with, you are what made my time at UCLA truly special. My dissertation would not have been possible without any of you.

Last, but not least, I'd like to thank Jordan for literally feeding me through graduate school. You're the best thing LA could have given me. pew pew.

The work I have completed has been supported by the NIH (HL127728, HL28481, HL123295), the AHA (18IPA34170309, 14GRNT20480340, 16IRG27260285), and Eli & Edythe Broad Center of Regenerative Medicine and Stem Cell Research Center at UCLA. I have personally

been supported by the MCIP program via an NIH Institutional Training Grant (5T32GM65823-12) and the UCLA Vascular Biology Training Program (T32HL69766).

Chapter 4 is a modified version of a published manuscript printed with permission:

Park, S., Ranjbarvaziri, S., Lay, F.D., Zhao, P., Miller, M.J., Dhaliwal, J.S., Huertas-Vazquez, A., Wu, X., Qiao, R., Soffer, J.M., Mikkola, H.K.A., Lusis, A.J., and Ardehali, R. “Genetic Regulation of Fibroblast Activation and Proliferation in Cardiac Fibrosis”. *Circulation.* 138, 1224–1235 (2018). https://doi.org/10.1161/CIRCULATIONAHA.118.035420

S.R., S.P., and R.A. conceived the project and designed the experiments. X.W. and A. J. L. assisted with the initial design. S.P. and S.R. performed all experiments, analyzed data and prepared the figures. S.P. and S.R. had full access to all the data in the study and take responsibility for the integrity of the data and the accuracy of the data analysis. S.P., S.R., and R.A. wrote the manuscript. H.K.A.M. and F.D. L. helped with the analysis of RNA-sequencing data and acknowledge support the Quantitative and Computational Biosciences Community directed by Matteo Pellegrini. A.H-V. assisted with obtaining human serum samples. M.J.M., J.S.D., R.Q., and J.M.S. assisted with all stainings. P.Z. performed all surgeries. All authors reviewed the manuscript. Echocardiograms were performed in Dr. Yibin Wang’s lab. We would like to acknowledge Shuxun Ren with his assistance in the initial surgeries. The LTBP2 antibody was a generous gift from Dr. Marko Hyytiäinen from the University of Helsinki, Finland. We are grateful for the expert technical assistance from the UCLA Broad Stem Cell Research Center Flow Cytometry Core, Confocal Microscopy Core, and Clinical Microarray Core. We acknowledge Ngoc B. Nguyen and James L. Engel for their critical reading of this article. This work was supported by the NIH DP2 HL127728 (R.A); UCLA Broad Stem Cell Research Center-Rose Hills Foundation Research Award (R.A.); the Eli & Edythe Broad Center of Regenerative Medicine and Stem Cell Research Center at UCLA Research Award (R.A. and H.K.A.M.); NIH HL28481 (A.H-V., X.W., and A.J.L.); NIH HL123295 (A.H-V., X.W., and A.J.L.); and the American Heart

Association 14GRNT20480340 and 16IRG27260285 (H.K.A.M.). F. D. L. was supported by the UCLA Quantitative and Computational Biosciences Collaboratory Post-Doctoral Fellowship. All authors reviewed the manuscript prior to publication.

Chapter 5 is a modified version of a published manuscript printed with permission:

Park, S., Ranjbarvaziri, S., Zhao, P., and Ardehali, R. “Cardiac Fibrosis is Associated with Decreased Circulating Levels of Full-Length CILP in Heart Failure” *J Am Coll Cardiol Basic Trans Sci.* Vol. 5, 432-443 (2020). https://doi.org/10.1016/j.jacbts.2020.01.016

S.P., S.R., and R.A. conceived the project and designed the experiments. S.P. performed all experiments, analyzed data and prepared the figures. S.P. and R.A. wrote the manuscript. P.Z. performed all surgeries. All authors reviewed the manuscript. We would like to acknowledge Fides Lay for assisting in the RNA-sequencing analysis and Jasmeet S. Dhaliwal for helping with the trichrome staining. The LTBP2 antibody was a gift from Dr. Marko Hyytiäinen from the University of Helsinki, Finland. We also acknowledge the UCLA Technology Center for Genomics & Bioinformatics, Broad Stem Cell Research Center Flow Cytometry Core, and Confocal Microscopy Core for their expert technical assistance. We acknowledge James L. Engel, Arash Pezhouman, and Ngoc B. Nguyen for their critical reading of this article. This work was supported in part by the National Institute of Health DP2 (HL127728) and AHA Innovative Award (18IPA34170309). All authors reviewed the manuscript prior to publication.

Appendix I is a reprint of a published manuscript printed with permission:

Park, S., Nguyen, N.B., Pezhouman, A., and Ardehali, R. “Cardiac Fibrosis: Potential Therapeutic Targets”. *Translational Research*. Vol. 209, p121-137 (2019). https://doi.org/10.1016/j.trsl.2019.03.001

Nguyen, NB was supported by the Ruth L. Kirschstein NRSA Predoctoral Fellowship (F31HL144057). Pezhouman, A was supported by the Eli & Edythe Broad Center of Regenerative Medicine and Stem Cell Research at UCLA Training Program. Ardehali, R and this publication was supported by the National Institute of Health DP2 (HL127728), California Institute for Regenerative Medicine (RN3-06378) and the American Heart Association Innovative Research Grant (18IPA34170309). All authors reviewed the manuscript prior to publication.

VITA/BIOGRAPHICAL SKETCH

EDUCATION

Ph.D. – Molecular, Cellular, and Integrative Physiology **Sept. 2014 – present**
University of California, Los Angeles (UCLA) Current GPA: 3.962/4.000
B.S. – General Biology **Sept. 2010 - March 2014**
University of California, San Diego (UCSD) GPA: 3.656/4.000 (*cum laude)*

RESEARCH EXPERIENCE

Ph.D. Candidate, Molecular, Cellular, and Integrative Physiology **Sept. 2014 – present**
University of California, Los Angeles (UCLA)
Advisor: Reza Ardehali, M.D., Ph.D.

Laboratory Research Assistant **Feb. 2012 – Aug. 2014**
Sanford-Burnham Prebys Medical Discovery Institute (SBP)
Principal Investigator: Randal Kaufman, Ph.D.

Summer Undergraduate Researcher **June 2011 – Sept. 2011**
University of California, Riverside (UCR)
Principal Investigator: Sean Cutler, Ph.D.

PUBLICATIONS

1. **Shuin Park**, Sara Ranjbarvaziri, Peng Zhao, and Reza Ardehali. *Cardiac Fibrosis is Associated with Decreased Circulating Levels of Full-Length CILP in Heart Failure*. JACC: Basic to Translational Science, 2020. Vol. 5, 432-443.
2. **Shuin Park**, Ngoc B. Nguyen, Arash Pezhouman, and Reza Ardehali. *Cardiac fibrosis: potential therapeutic targets*. Translational Research, 2019. Vol. 209, 121-137. PMC6545256
3. **Shuin Park***, Sara Ranjbarvaziri*, Fides D. Lay, Peng Zhao, Mark J. Miller, Jasmeet S. Dhaliwal, Adriana Huertas-Vazquez, Xiuju Wu, Rong Qiao, Justin M. Soffer, Hanna K.A. Mikkola, Aldons J. Lusis, and Reza Ardehali. *Genetic Regulation of Fibroblast Activation and Proliferation in Cardiac Fibrosis*. Circulation, 2018. Vol. 138, No.12. 1224-1235. PMC6202226
4. Konstantina-Ioanna Sereti*, Ngoc B. Nguyen*, Paniz Kamran*, Peng Zhao, Sara Ranjbarvaziri, **Shuin Park**, Shan Sabri, James L. Engel, Kevin Sung, Rajan P. Kulkarni, Yichen Ding, Tzung K. Hsiai, Kathrin Plath, Jason Ernst, Debashis Sahoo, Hanna K.A. Mikkola, M. Luisa Iruela-Arispe and Reza Ardehali. *Analysis of cardiomyocyte clonal expansion during mouse heart development and injury*. Nature Communications, 2018. Vol. 9, Article number: 754. PMC5821855
5. Sara Ranjbarvaziri*, **Shuin Park***, Ngoc B. Nguyen*, William B. Gilmore, Peng Zhao, and Reza Ardehali. *Generation of Nkx2-5/CreER transgenic mice for inducible Cre expression in developing hearts.* Genesis, 2017. Vol 55, No. 8 e23041. PMC5568924
6. Shiyu Wang, **Shuin Park**, Vamsi K. Kodali, Jaeseok Han, Theresa Yip, Zhouji Chen, Nicholas O.Davidson, and Randal J. Kaufman. *Identification of protein disulfide isomerase 1 as a key isomerase for disulfide bond formation in apolipoprotein B100.* Molecular Biology of the Cell, 2015. Vol. 26, No. 4. 594-604. PMC4325832

*Authors contributed equally

PRESENTATIONS

AHA/UCLA Women's Heart Health **April 2019**
Poster: Enrichment of Pericytes from the Heart

AHA Basic Cardiovascular Sciences (BCVS) Scientific Sessions 2018 **July 2018**

Poster: Exclusion of Major Cell Types in the Murine Heart Enriches for Cardiac Pericytes

Center for DMD at UCLA Annual Retreat **Nov. 2017**
Poster: Exclusion of Major Cell Types in the Murine Heart Enriches for Cardiac Pericytes

AHA Basic Cardiovascular Sciences (BCVS) Scientific Sessions 2017 **July 2018**
Poster: Strain-specific Cardiac Fibroblast Response to ISO-induced Cardiac Fibrosis

UCLA Cardiovascular Symposium 2016 **Sept. 2016**
Poster: Neural crest-derived Cardiac Fibroblasts Become Activated in Response to Acute Myocardial Injury

HONORS AND AWARDS

Vascular Biology Training Grant (T32HL69766) **2018 – 2019**
Ruth L. Kirschstein National Research Service Award **& 2015 - 2017**

AHA BCVS 2018 - Selected Featured Science **2018**
Poster Title: Exclusion of Major Cell Types in the Murine Heart Enriches for Cardiac Pericytes

Center for DMD at UCLA Annual Retreat - Predoctoral Poster Award **2017**
Poster Title: Exclusion of Major Cell Types in the Murine Heart Enriches for Cardiac Pericytes

NIH Institutional Training Grant (5T32GM65823-12) **2014 – 2015**
Ruth L. Kirschstein National Research Service Award

CHAPTER 1

INTRODUCTION

CARDIAC FIBROSIS

Significance of Studying Cardiac Fibrosis

Cardiovascular disease (CVD) is the leading cause of mortality in the world and is exacerbated by the presence of cardiac fibrosis, defined by the accumulation of non-contractile extracellular matrix (ECM) proteins[1]. Upon ischemic injury or pressure overload, the heart undergoes a dynamic remodeling process that results in the formation of scar tissue. As the heart lacks the regenerative capacity to replace fibrotic tissue with healthy myocardium, the presence of scar can have lasting effects on cardiac function. Buildup of ECM proteins can lead to reduced contractility of the heart (lower ejection fraction) and result in arrhythmias, increasing the risk of heart failure and death[2,3]. Despite the prevalence of CVD, there is a lack of therapies targeting the inhibition or reversal of cardiac fibrosis. It has been a challenge to develop novel therapies due to the overall complexity of the process in which cardiac fibrosis is developed. By understanding the various cell types that contribute to scar formation, and the molecular mechanisms that drive these cells, we may unveil promising therapeutic targets for the treatment of cardiac fibrosis.

Types of Cardiac Fibrosis

Cardiac fibrosis can be categorized into three general forms, depending on the etiology of injury[4,5]. First, there is reactive interstitial fibrosis which is fibrosis that develops without loss of healthy cardiomyocytes. The fibrotic tissue is generally more diffuse and is seen in more chronic forms of cardiac injury, such as pressure overload injury or aging. Second, there is infiltrative interstitial fibrosis, which is found in association with infiltrative diseases (such as amyloidosis) or other rare genetic disorders (such as lysosomal storage disease). Anderson-Fabry disease is an example of lysosomal storage disease in which glycoplipid deposits accumulate in different cell types[6,7]. Finally, there is replacement fibrosis, in which fibrotic tissue takes the place of what used to be healthy myocardium. In the event of an acute ischemic injury, such as myocardial infarction, many

cardiomyocytes undergo cell death. The formation of fibrotic tissue to replace this dead tissue is critical in preserving the integrity of the heart, thickening the ventricular wall, and preventing cardiac rupture[8]. Regardless of the type of fibrosis, the long-term presence of cardiac fibrosis can have detrimental effects on overall cardiac function.

Murine Models of Cardiac Fibrosis

Myocardial Infarction

While there are a variety of CVD etiologies, myocardial infarction (MI) is one of the most common, with more than 3 million cases in the United States per year. In MI, a blocked coronary artery restricts blood flow to part of the heart, resulting in the death of cardiomyocytes[9,10]. As cardiomyocytes undergo necrosis and apoptosis, there is a need to clear the dead myocardium, while maintaining stable blood flow throughout the body. An initial inflammatory response becomes activated, driving the release of cytokines and chemokines within the microenvironment[11]. Leukocytes, such as neutrophils, infiltrate the damaged myocardium and phagocytose the dead cardiomyocytes[12]. Pro-inflammatory monocytes also invade the myocardium, release cytokines, differentiate into macrophages, and initiate the expansion of resident macrophages in the heart[12,13]. This inflammatory phase is then followed by a remodeling phase in which large amounts of ECM proteins are produced to replace the dead myocardium, forming fibrotic tissue.

In mice, this process can be experimentally achieved by ligating the left anterior descending (LAD) artery with a suture and effectively blocking blood flow below the ligation[14]. For a permanent occlusion, this ligation is left in the heart, resulting in extensive amounts of cardiac fibrosis that can be seen within days of the injury[15]. By 7 days post-surgery, there is a definite scar replaces the left anterior wall and the left ventricle exhibits a dilated morphology. An alternative to permanent occlusion is to release the LAD ligation after a period of ischemia (typically 45 minutes)

and resume blood flow into the injured area[16]. This simulates ischemic-reperfusion (IR) injury and can be viewed as a more clinically relevant model of MI. However, IR injury does not develop as much fibrosis as permanent occlusion and the fibrotic tissue that forms may take several weeks to become prominent.

β-Adrenergic Stimulation

Long-term activation of the β-adrenergic signaling pathway in the heart has been attributed to the development of cardiac dysfunction, clinically referred to as tachycardiac-induced cardiomyopathy[17]. Various cells in the heart express β-receptors, but this signaling pathway has been mainly studied in cardiomyocytes. Cardiomyocytes express multiple β-receptors (β_1, β_2, and β_3) and the expression of these receptors change under pathological conditions[18]. Downstream effects of altered β-adrenergic signaling include cardiac hypertrophy and fibrosis[19]. There are several β-adrenergic targets that may drive the development of these symptoms, including Ca^{2+} handling proteins (e.g. phospholamban and ryanodine receptors)[17,20,21] and pro-apoptotic proteins[18]. In the clinic, β-adrenergic antagonists are considered standard treatment for the prevention of heart failure. Despite the established link, there are still questions as to how altered β-adrenergic signaling directly causes heart failure.

In rodents, one of the most reproducible models of heart failure is treatment with isoproterenol, a β-adrenergic agonist[22,23]. Isoproterenol can be administered by multiple subcutaneous injections[24] or by osmotic pump[25]. Over time, continuous treatment of isoproterenol results in cardiac hypertrophy, increased blood pressure, and fibrosis. Unlike MI, isoproterenol-induced fibrosis mainly develops within the left ventricle endocardium and the walls do not become dilated[24].

Pressure Overload Injury

Pressure overload in the heart defines a state in which there is increased stress on the ventricular walls, resulting in cardiac remodeling[26]. Chronic pressure overload initially results in compensatory cardiac hypertrophy, which is then followed by dilation and, ultimately, heart failure. Various external factors can induce pressure overload in the heart such as aortic stenosis and hypertension[27]. While pressure overload injury is a form of chronic injury like β-adrenergic modulation, it is mainly driven by mechanical changes in the heart, resulting in a slightly different pathophysiology.

In mice, pressure overload injury can be simulated by transverse aortic constriction (TAC), in which a suture is tied around the aorta to reduce the diameter[28]. This method reproducibly results in cardiac hypertrophy and a gradual progression through heart failure[28]. There is also prominent fibrosis that develops after TAC. Notably, presence of fibrosis can be found in both the interstitial space and the perivascular area[26,29]. Perivascular fibrosis may be a result of increased pressure in the larger coronary vessels, resulting in a need to stabilize the vessels with excess ECM.

CARDIAC PERICYTES

In the heart, there are a multitude of cells that are interacting with one another to form a cohesive, functioning organ. Cardiomyocytes, which make up 30-35% of the cardiac cell population, are well defined in their function to contract and pump blood through the heart in a synchronous manner[30]. However, the development of fibrosis has mainly been attributed to the non-myocyte population of the heart. This 65-70% of the heart is made up of fibroblasts, endothelial cells, immune cells, and mural cells (smooth muscle cells and pericytes)[30,31]. Of these cells, the role of pericytes in the development of cardiac fibrosis has been understudied.

Cardiac Pericyte Function and Interactions with Endothelial Cells

Pericytes are a population of mural cells that surround microvessels in various organs, including the heart. In homeostasis, pericytes are normally found integrated within the endothelial basal membrane of capillaries and post-capillary venules[32]. Their finger-like projections wrap around the vessels, suggesting strong pericyte-endothelial cell interactions[33]. Through these interactions, pericytes serve as regulators of angiogenesis and mediators of vascular stability and contractility[34]. Reduction of pericyte coverage has been attributed to the endothelium degeneration, vessel leakage, and microaneurysms, which can result in various vascular pathologies[35]. There are several signaling pathways that have been implicated in the cross-talk between pericytes and endothelial cells that maintain their tight interactions[32,36]. During angiogenesis, platelet-derived growth factor-B (PDGF-B) signaling is crucial for recruiting pericytes to endothelial tip cells that express high levels of PDGF-B. Loss of PDGF-B reduces pericyte coverage on vessels, leading to vascular defects[37]. Transforming growth factor-β (TGFβ) and Notch signaling have also been implicated in vessel stabilization and maturation. Mutations in either pathway result in hemorrhage or vascular malformations, demonstrating their importance to maintaining vascular health[38,39]. Finally, the angiopoietin-1 (Ang1)/Tie-2 axis, in which Ang1 that is expressed by pericytes interacts with Tie-2 receptors on endothelial cells, further promotes endothelial barrier formation and vessel maturation[34]. Overall, these various signaling pathways outline the importance of pericytes in maintaining vascular health.

Pericyte Heterogeneity

Despite their well-defined role in homeostasis, pericytes have been a challenging cell population to study due to the lack of consensus on how to isolate and label these cells[37]. Most studies refer to this cell-type based on its morphological characteristics and anatomical location due to the lack of established markers for identifying these cells. It is well established that there is heterogeneity between pericytes of different organs as well as heterogeneity within pericytes of the same organ, presenting an additional challenge to studying these cells. In previous studies, a variety of

markers have been used to label pericytes in a wide array of organs, including chondroitin sulfate proteoglycan 4 (NG2)[40], platelet-derived growth factor receptor-β (PDGFRβ)[41], CD146[42], regulator of G-protein signaling 5 (RGS5)[43], and Notch3[44]. However, there are underlying questions as to whether these markers are capable of labeling the entire cardiac pericyte population or if they only label a subpopulation. Future studies on dissecting the heterogeneity of cardiac pericytes are imperative to the complete understanding of this cell type and its function in the heart.

Pericytes in Ischemic Injury

In various organs other than the heart, pericytes have been found to be key players in wound response and disease progression. Given their role in homeostasis, several studies have dissected the vital role of pericytes in regulating angiogenesis in pathological conditions[32,45]. Upon brain injury, pericytes have been found to play key roles in maintaining the blood-brain barrier and constituting a second layer of defense against inflammation[36]. In mouse kidney IR injury models, pericytes expressing TIMP3 were found to stabilize the microvasculature by mediating the activity of various metalloproteinases[46]. It has also been found that pericytes are integral to tumoral angiogenesis - blocking CD146 expression helps to reduce pericyte recruitment to tumor vessels, restricting tumor growth[47–49]. The role of pericytes in regulating angiogenesis makes these cells promising targets for promoting revascularization after ischemic injury.

However, other findings have shown that pericytes may instead be playing a pro-fibrotic role in ischemic injury[50,51]. Pericytes have been reported to be a cellular source for ECM proteins and demonstrate increased collagen production in response to spinal cord injury and stroke[50,52]. Pericytes have also been reported to be progenitor cells that transdifferentiate into fibroblast-like cells and contribute to fibrosis in that manner[53,54]. Furthermore, pericytes have also demonstrated the ability to secrete pro-inflammatory factors that may drive fibrosis[55]. These contradictory results

from other groups suggest that the function of pericytes in ischemic injury may be organ-dependent, thus supporting the need for proper characterization of the cardiac pericyte population.

CARDIAC FIBROBLASTS

Definition and Function of Cardiac Fibroblasts

Cardiac fibroblasts (CFbs) are cells of mesenchymal origin that are commonly defined by their spindle-like shape and lack of a basement membrane[56]. Within the myocardium, they are found interspersed throughout the tissue and consist of a cell body with multiple projections extending outward[56]. There is debate as to how much of the heart consists of CFbs and this number appears to vary by species. The current understanding is that less than 20% of the non-myocyte population of the adult mouse heart are CFbs[31]. Like pericytes, one of the difficulties of studying these cells has been the lack of a common marker. Some of the commonly used markers to label these cells in the heart include CD90 (Thy1)[57], Platelet-derived growth factor receptor alpha (PDGFRα)[58], Discoidin domain receptor 2 (DDR2)[56], and Fibroblast-specific protein (FSP1)[59].

Overall, studies have shown that CFbs play a crucial role in maintaining the structural integrity of the heart throughout development and into adulthood[60]. In development, CFbs contribute to the healthy formation of the chambers that make up the organ. Ablation of CFbs or CFb dysfunction during embryonic development results in hearts with hypoplastic ventricles and other deformities[61–63]. In adult hearts, CFbs mainly function to produce proteins that make up the ECM, such as collagens and fibronectins, as well as the matrix metalloproteinases (MMPs) that degrade the ECM[56]. The ECM itself provides a scaffold for the other cardiac cells and creates a network to distribute the mechanical forces of the contracting heart[64]. Under homeostatic conditions, CFbs are generally quiescent and there are low levels of ECM turnover. However, changes in cell-cell signaling or environmental cues (chemical or mechanical) result in a remodeling of the ECM to ensure that the heart continues to function properly[56]. After cardiac injury, the role of CFbs in

regulating the ECM becomes much more pronounced as they become the major contributing cell type to the development of scar tissue.

Cardiac Fibroblasts in Cardiac Injury

In CVD, resident CFbs are “activated” and become a cell type known as myofibroblasts. The transition of quiescent CFbs to myofibroblasts is not entirely understood, but studies suggest that it is mainly mediated by the transforming growth factor β (TGFβ) superfamily[65,66]. Canonical TGFβ signaling promotes the expression of genes associated with increased proliferation, contractile proteins (e.g. αSMA), and ECM components (collagens, fibronectin, etc.)[2,67]. As major players in the fibrotic process, myofibroblasts have been placed in the spotlight as potential therapeutic targets for reducing cardiac fibrosis. Inhibition of TGFβ signaling or ablation of myofibroblasts has been shown to reduce levels of fibrosis, supporting that myofibroblasts are a viable therapeutic target[67,68]. Understanding the mechanisms that drive the activation of CFbs after injury will provide a foundation for developing these novel therapies.

THIS DISSERTATION

This dissertation is divided into two separate sections (divided into four chapters) investigating the role of pericytes and fibroblasts in the heart after injury. The chapters are divided as such:

Chapter 2: NG2+ Cardiac Pericytes Respond to Myocardial Infarction

This chapter looks specifically at NG2+ cardiac pericytes and how they respond to MI. Transgenic mice were utilized to lineage-trace these NG2+ cardiac pericytes and single cell RNA-sequencing (scRNA-seq) was applied to determine transcriptomic changes across multiple time points after MI. The results show that, after injury, NG2+ pericytes proliferate and express ECM proteins, suggesting that these cells may play a role in the fibrotic process.

Chapter 3: Isolation of Cardiac Pericytes Without Any Previously Established Markers

This chapter outlines a novel method for enriching for cardiac pericytes from the murine heart without using any specific markers. This technique, combined with scRNA-seq, allows for characterization of the entire heterogeneous pericyte cell population, without biasing the results towards a specific subpopulation. This method was applied to both uninjured and injured hearts, allowing for the detection of gene expression changes that occur within the entire pericyte population after injury.

Chapter 4: Genetic Regulation of Fibroblast Activation and Proliferation in Cardiac Fibrosis

This chapter observes how cardiac fibroblast (CFb) responses across three genetically different backgrounds of mice are unique in response to isoproterenol treatment. Despite receiving the same treatment, these mice develop differential levels of fibrosis. Our results showed that while CFbs proliferate to similar levels in all three strains of mice, their levels of activation (determined by their expression of αSMA and periostin) correlate with the levels of fibrosis. This data shows that consideration of mouse strain is crucial for future studies of CFbs.

Chapter 5: Cardiac Fibrosis is Associated with Decreased Circulating Levels of Full-Length CILP in Heart Failure

This chapter is dedicated to the identification of a potential circulating biomarker for cardiac fibrosis that is secreted by CFbs. By using bulk RNA-sequencing data of CFbs from hearts that had undergone sham or TAC, secreted proteins in response to injury were identified. The expression of these proteins was validated *in vitro* and in fibrotic mouse and human tissues. When testing the presence of these markers in the serum of human heart failure samples, expression of the full-length CILP protein was significantly decreased in patients compared to healthy samples.

Appendix I: Cardiac Fibrosis: Potential Therapeutic Targets

This appendix includes a review of promising avenues for therapeutically targeting cardiac fibrosis. It covers approaches that are currently being used in the clinic, as well as novel approaches that have emerged in recent years.

REFERENCES

1. Park, S., Nguyen, N. B., Pezhouman, A. & Ardehali, R. Cardiac Fibrosis: Potential Therapeutic Targets. *Transl. Res.* (2019) doi:10.1016/j.trsl.2019.03.001.
2. Travers, J. G., Kamal, F. A., Robbins, J., Yutzey, K. E. & Blaxall, B. C. Cardiac Fibrosis: The Fibroblast Awakens. *Circ. Res.* **118**, 1021–1040 (2016).
3. de Jong, S., van Veen, T. A. B., van Rijen, H. V. M. & de Bakker, J. M. T. Fibrosis and cardiac arrhythmias. *J. Cardiovasc. Pharmacol.* **57**, 630–638 (2011).
4. Hinderer, S. & Schenke-Layland, K. Cardiac fibrosis – A short review of causes and therapeutic strategies. *Adv. Drug Deliv. Rev.* **146**, 77–82 (2019).
5. Tian, J., An, X. & Niu, L. Myocardial fibrosis in congenital and pediatric heart disease. *Exp. Ther. Med.* **13**, 1660–1664 (2017).
6. Moon, J. C. C. *et al.* Gadolinium enhanced cardiovascular magnetic resonance in Anderson-Fabry disease. Evidence for a disease specific abnormality of the myocardial interstitium. *Eur. Heart J.* **24**, 2151–2155 (2003).
7. Weidemann, F. *et al.* Fibrosis: a key feature of Fabry disease with potential therapeutic implications. *Orphanet J. Rare Dis.* **8**, 116 (2013).
8. Talman, V. & Ruskoaho, H. Cardiac fibrosis in myocardial infarction—from repair and remodeling to regeneration. *Cell Tissue Res.* **365**, 563–581 (2016).
9. Murtha, L. A. *et al.* The Processes and Mechanisms of Cardiac and Pulmonary Fibrosis. *Front. Physiol.* **8**, (2017).
10. Kong, P., Christia, P. & Frangogiannis, N. G. The Pathogenesis of Cardiac Fibrosis. *Cell. Mol. Life Sci. CMLS* **71**, 549–574 (2014).
11. Frangogiannis Nikolaos G. & Rosenzweig Anthony. Regulation of the Inflammatory Response in Cardiac Repair. *Circ. Res.* **110**, 159–173 (2012).
12. Swirski, F. K. & Nahrendorf, M. Leukocyte behavior in atherosclerosis, myocardial infarction, and heart failure. *Science* **339**, 161–166 (2013).

13. Hulsmans, M., Sam, F. & Nahrendorf, M. Monocyte and Macrophage Contributions to Cardiac Remodeling. *J. Mol. Cell. Cardiol.* **93**, 149–155 (2016).
14. Kolk, M. V. V. *et al.* LAD-Ligation: A Murine Model of Myocardial Infarction. *J. Vis. Exp. JoVE* (2009) doi:10.3791/1438.
15. Yang, F. *et al.* Myocardial Infarction and Cardiac Remodelling in Mice. *Exp. Physiol.* **87**, 547–555 (2002).
16. Xu, Z., McElhanon, K. E., Beck, E. X. & Weisleder, N. A Murine Model of Myocardial Ischemia-Reperfusion Injury. *Methods Mol. Biol. Clifton NJ* **1717**, 145–153 (2018).
17. Lohse Martin J., Engelhardt Stefan & Eschenhagen Thomas. What Is the Role of β-Adrenergic Signaling in Heart Failure? *Circ. Res.* **93**, 896–906 (2003).
18. Communal, C., Singh, K., Sawyer, D. B. & Colucci, W. S. Opposing effects of beta(1)- and beta(2)-adrenergic receptors on cardiac myocyte apoptosis : role of a pertussis toxin-sensitive G protein. *Circulation* **100**, 2210–2212 (1999).
19. Rau, C. D. *et al.* Mapping genetic contributions to cardiac pathology induced by Beta-adrenergic stimulation in mice. *Circ. Cardiovasc. Genet.* **8**, 40–49 (2015).
20. Simmerman, H. K. & Jones, L. R. Phospholamban: protein structure, mechanism of action, and role in cardiac function. *Physiol. Rev.* **78**, 921–947 (1998).
21. Marx, S. O. *et al.* PKA phosphorylation dissociates FKBP12.6 from the calcium release channel (ryanodine receptor): defective regulation in failing hearts. *Cell* **101**, 365–376 (2000).
22. Grimm, D. *et al.* Development of heart failure following isoproterenol administration in the rat: role of the renin-angiotensin system. *Cardiovasc. Res.* **37**, 91–100 (1998).
23. Szabó, J., Csáky, L. & Szegi, J. Experimental cardiac hypertrophy induced by isoproterenol in the rat. *Acta Physiol. Acad. Sci. Hung.* **46**, 281–285 (1975).
24. Brooks, W. W. & Conrad, C. H. Isoproterenol-Induced Myocardial Injury and Diastolic Dysfunction in Mice: Structural and Functional Correlates. *Comp. Med.* **59**, 339–343 (2009).

25. Chang, S. C., Ren, S., Rau, C. D. & Wang, J. J. Isoproterenol-Induced Heart Failure Mouse Model Using Osmotic Pump Implantation. *Methods Mol. Biol. Clifton NJ* **1816**, 207–220 (2018).
26. Souders, C. A., Borg, T. K., Banerjee, I. & Baudino, T. A. Pressure Overload Induces Early Morphological Changes in the Heart. *Am. J. Pathol.* **181**, 1226–1235 (2012).
27. Kehat, I. & Molkentin, J. D. Molecular pathways underlying cardiac remodeling during pathophysiologic stimulation. *Circulation* **122**, (2010).
28. deAlmeida, A. C., van Oort, R. J. & Wehrens, X. H. T. Transverse aortic constriction in mice. *J. Vis. Exp. JoVE* (2010) doi:10.3791/1729.
29. Richards, D. A. *et al.* Distinct Phenotypes Induced by Three Degrees of Transverse Aortic Constriction in Mice. *Sci. Rep.* **9**, 1–15 (2019).
30. Nag, A. C. Study of non-muscle cells of the adult mammalian heart: a fine structural analysis and distribution. *Cytobios* **28**, 41–61 (1980).
31. Pinto, A. R. *et al.* Revisiting Cardiac Cellular Composition. *Circ. Res.* **118**, 400–409 (2016).
32. Armulik, A., Abramsson, A. & Betsholtz, C. Endothelial/pericyte interactions. *Circ. Res.* **97**, 512–523 (2005).
33. Dore-Duffy, P. & Cleary, K. Morphology and properties of pericytes. *Methods Mol. Biol. Clifton NJ* **686**, 49–68 (2011).
34. van Dijk, C. G. M. *et al.* The complex mural cell: pericyte function in health and disease. *Int. J. Cardiol.* **190**, 75–89 (2015).
35. Ziemssen, F. & Agostini, H. T. Diabetic Retinopathy. in *Anti-Angiogenic Therapy in Ophthalmology* (ed. Stahl, A.) 89–130 (Springer International Publishing, 2016). doi:10.1007/978-3-319-24097-8_6.
36. Gerhardt, H. & Betsholtz, C. Endothelial-pericyte interactions in angiogenesis. *Cell Tissue Res.* **314**, 15–23 (2003).

37. Armulik, A., Genové, G. & Betsholtz, C. Pericytes: developmental, physiological, and pathological perspectives, problems, and promises. *Dev. Cell* **21**, 193–215 (2011).

38. Gallione, C. J. *et al.* A combined syndrome of juvenile polyposis and hereditary haemorrhagic telangiectasia associated with mutations in MADH4 (SMAD4). *The Lancet* **363**, 852–859 (2004).

39. Gridley, T. Notch signaling in the vasculature. *Curr. Top. Dev. Biol.* **92**, 277–309 (2010).

40. Stallcup, W. B. The NG2 Proteoglycan in Pericyte Biology. *Adv. Exp. Med. Biol.* **1109**, 5–19 (2018).

41. Winkler, E. A., Bell, R. D. & Zlokovic, B. V. Pericyte-specific expression of PDGF beta receptor in mouse models with normal and deficient PDGF beta receptor signaling. *Mol. Neurodegener.* **5**, 32 (2010).

42. Crisan, M. *et al.* A Perivascular Origin for Mesenchymal Stem Cells in Multiple Human Organs. *Cell Stem Cell* **3**, 301–313 (2008).

43. Cho, H., Kozasa, T., Bondjers, C., Betsholtz, C. & Kehrl, J. H. Pericyte-specific expression of Rgs5: implications for PDGF and EDG receptor signaling during vascular maturation. *FASEB J. Off. Publ. Fed. Am. Soc. Exp. Biol.* **17**, 440–442 (2003).

44. Lovschall, H., Mitsiadis, T. A., Poulsen, K., Jensen, K. H. & Kjeldsen, A. L. Coexpression of Notch3 and Rgs5 in the pericyte-vascular smooth muscle cell axis in response to pulp injury. *Int. J. Dev. Biol.* **51**, 715–721 (2007).

45. Birbrair, A. *et al.* Type-2 pericytes participate in normal and tumoral angiogenesis. *Am. J. Physiol. Cell Physiol.* **307**, C25-38 (2014).

46. Schrimpf, C. *et al.* Pericyte TIMP3 and ADAMTS1 modulate vascular stability after kidney injury. *J. Am. Soc. Nephrol. JASN* **23**, 868–883 (2012).

47. Zeng, Q. *et al.* Impaired tumor angiogenesis and VEGF-induced pathway in endothelial CD146 knockout mice. *Protein Cell* **5**, 445–456 (2014).

48. Bergers, G. & Song, S. The role of pericytes in blood-vessel formation and maintenance. *Neuro-Oncol.* **7**, 452–464 (2005).

49. Lei, X., Guan, C.-W., Song, Y. & Wang, H. The multifaceted role of CD146/MCAM in the promotion of melanoma progression. *Cancer Cell Int.* **15**, 3 (2015).

50. Birbrair, A. *et al.* Type-1 pericytes accumulate after tissue injury and produce collagen in an organ-dependent manner. *Stem Cell Res. Ther.* **5**, 122 (2014).

51. Chen, Y.-T. *et al.* Platelet-derived growth factor receptor signaling activates pericyte–myofibroblast transition in obstructive and post-ischemic kidney fibrosis. *Kidney Int.* **80**, 1170–1181 (2011).

52. Kelly, K. K. *et al.* Col1a1+ perivascular cells in the brain are a source of retinoic acid following stroke. *BMC Neurosci.* **17**, 49 (2016).

53. Dulauroy, S., Di Carlo, S. E., Langa, F., Eberl, G. & Peduto, L. Lineage tracing and genetic ablation of ADAM12(+) perivascular cells identify a major source of profibrotic cells during acute tissue injury. *Nat. Med.* **18**, 1262–1270 (2012).

54. LeBleu, V. S. *et al.* Origin and function of myofibroblasts in kidney fibrosis. *Nat. Med.* **19**, 1047–1053 (2013).

55. Leaf, I. A. *et al.* Pericyte MyD88 and IRAK4 control inflammatory and fibrotic responses to tissue injury. *J. Clin. Invest.* **127**, 321–334 (2017).

56. Souders, C. A., Bowers, S. L. K. & Baudino, T. A. Cardiac Fibroblast: The Renaissance Cell. *Circ. Res.* **105**, 1164–1176 (2009).

57. Hudon-David, F., Bouzeghrane, F., Couture, P. & Thibault, G. Thy-1 expression by cardiac fibroblasts: Lack of association with myofibroblast contractile markers. *J. Mol. Cell. Cardiol.* **42**, 991–1000 (2007).

58. Smith, C. L., Baek, S. T., Sung, C. Y. & Tallquist, M. D. Epicardial-derived cell epithelial-to-mesenchymal transition and fate specification require PDGF receptor signaling. *Circ. Res.* **108**, e15-26 (2011).

59. Strutz, F. *et al.* Identification and characterization of a fibroblast marker: FSP1. *J. Cell Biol.* **130**, 393–405 (1995).

60. Fan, D., Takawale, A., Lee, J. & Kassiri, Z. Cardiac fibroblasts, fibrosis and extracellular matrix remodeling in heart disease. *Fibrogenesis Tissue Repair* **5**, 15 (2012).

61. Acharya, A. *et al.* The bHLH transcription factor Tcf21 is required for lineage-specific EMT of cardiac fibroblast progenitors. *Dev. Camb. Engl.* **139**, 2139–2149 (2012).

62. Furtado, M. B., Nim, H. T., Boyd, S. E. & Rosenthal, N. A. View from the heart: cardiac fibroblasts in development, scarring and regeneration. *Development* **143**, 387–397 (2016).

63. Furtado Milena B. *et al.* Cardiogenic Genes Expressed in Cardiac Fibroblasts Contribute to Heart Development and Repair. *Circ. Res.* **114**, 1422–1434 (2014).

64. Bowers, S. L. K., Banerjee, I. & Baudino, T. A. The extracellular matrix: at the center of it all. *J. Mol. Cell. Cardiol.* **48**, 474–482 (2010).

65. Sigel, A. V., Centrella, M. & Eghbali-Webb, M. Regulation of proliferative response of cardiac fibroblasts by transforming growth factor-beta 1. *J. Mol. Cell. Cardiol.* **28**, 1921–1929 (1996).

66. Leask, A. TGFbeta, cardiac fibroblasts, and the fibrotic response. *Cardiovasc. Res.* **74**, 207–212 (2007).

67. Khalil, H. *et al.* Fibroblast-specific TGF-β-Smad2/3 signaling underlies cardiac fibrosis. *J. Clin. Invest.* **127**, 3770–3783 (2017).

68. Kanisicak, O. *et al.* Genetic lineage tracing defines myofibroblast origin and function in the injured heart. *Nat. Commun.* **7**, 12260 (2016).

CHAPTER 2

NG2+ Cardiac Pericytes Respond to Myocardial Infarction

ABSTRACT

Myocardial infarction (MI) is a form of acute ischemic injury to the heart in which a blocked coronary artery results in extensive cardiomyocyte death and large areas of fibrosis. There are many cell types that respond to MI, including immune cells and fibroblasts, that make this process extremely dynamic. Pericytes are an understudied cell population that may also potentially participate in this process. Pericytes are defined as mural cells present in a variety of organs that share a basement membrane with microvascular endothelial cells. This interaction is crucial in regulating vessel contractility and maintaining vessel integrity. Studies in the kidney and brain have shown that pericytes play a significant role after ischemic injury by transdifferentiating into myofibroblasts or producing extracellular matrix (ECM) proteins, respectively. Whether pericytes in the heart also play a similar role after MI has not been thoroughly examined. Based on the functional role of pericytes in other organs, we hypothesized that cardiac pericytes also participate in the fibrotic process after MI. In this study, we used Chondroitin sulfate proteoglycan 4 (NG2) as a marker for pericytes in the heart, as it has been used as a surrogate marker for pericytes in multiple organs. By using *NG2*$^{CreER/+}$;*Rosa26*$^{tdT/+}$ to lineage trace NG2-expressing pericytes, we show that at least a subset of this cell population preferentially accumulates in the injury area, proliferates, and upregulates ECM proteins in response to MI. This response was specifically localized to the infarcted areas in the hearts and appeared to peak at later time points after injury (day 7). Single cell RNA-sequencing (scRNA-seq) confirmed an increased enrichment of pro-fibrotic genes at 7 days post-MI, which persisted through 14 days post-MI. Our data shows that pericytes participate in the post-fibrotic response after an acute injury such as MI and that their role may be most pronounce at later stages of remodeling. Future studies are warranted to investigate the spatiotemporal contribution of pericytes to the development of the mature scar.

INTRODUCTION

Heart disease is the leading cause of mortality in western countries[1]. Pathological stress from injury leads to irreversible loss of cardiomyocytes with subsequent replacement of healthy myocardium with fibrous scar tissue[2,3]. The development of cardiac fibrosis is a dynamic process that involves an array of different cell types that interact with one another[1,2]. In response to an acute ischemic event, such as myocardial infarction (MI), cardiomyocytes undergo apoptosis and necrosis[4]. This event triggers an inflammatory response that recruits immune cells, such as neutrophils and macrophages, to the site of injury[5]. These immune cells function to remove dead and dying cardiac cells whilst secreting factors that initiate a remodeling phase in which cardiac fibroblasts produce various extracellular matrix (ECM) proteins that result in the formation of scar tissue[2,6]. Initially the formation of scar tissue is critical in preserving the integrity of the heart and preventing myocardial rupture[7]. However, the heart lacks the regenerative capacity to replace scar tissue with healthy myocardium, leading to long-term effects such as reduced ejection fraction, arrhythmias, and ultimately heart failure. Targeting cardiac fibroblasts as the main contributor to the fibrotic process has been a therapeutic goal for treating heart disease, but it is unknown whether other cell types, such as pericytes, may also play a role in the development of cardiac fibrosis.

Cardiac pericytes are an understudied population of mural cells that have been garnering attention in recent years. Under homeostatic conditions, they remain tightly associated with endothelial cells of the microvasculature[8] to maintain vascular integrity and regulate vessel contractility[9,10]. Loss of pericyte coverage results in reduced number of capillaries and increased vessel leakage[11]. Beyond this function, pericytes have also been reported to exhibit characteristics of mesenchymal stem cells, such as having the potential to differentiate into various cell types *in vitro*[12]. While the capabilities of pericytes to differentiate into other cell types *in vivo* has been questioned, some studies have suggested that pericytes may instead be capable

of demonstrating unique functions in response to specific stimuli. Indeed, studies in other organs have suggested that pericytes play crucial roles in responding to ischemic injury. In spinal cord injury, pericytes are the major cellular source of ECM proteins[13] and in kidney ischemia, pericytes transdifferentiate into myofibroblasts[14,15]. These pro-fibrotic roles appear to be organ-specific, creating a need to determine the contribution of pericytes in the heart to cardiac fibrosis after ischemic injury[16].

In this study, we hypothesized that cardiac pericytes respond to MI and participate in the injury response. We utilized the *NG2*$^{CreER/+}$ mouse strain to lineage-trace cells in the heart that express NG2 and demonstrated that pericytes contribute to cardiac fibrosis in a distinct spatiotemporal pattern[17]. During later timepoints after MI, NG2+ pericytes begin to proliferate and accumulate in the injury region, where they also begin to express ECM proteins. Single cell RNA-sequencing (scRNA-seq) also revealed an enrichment of ECM genes and pro-fibrotic pathways in NG2+ cardiac pericytes after MI, confirming their dynamic response to ischemic injury.

RESULTS

NG2 marks a population of cardiac pericytes

We first validated that NG2 expression is largely restricted to pericytes in the heart. Immunofluorescence (IF) staining and flow analysis demonstrated that NG2 is expressed in the murine heart and is co-expressed with other pericyte markers such as CD146 and PDGFRβ **(Supplementary Figure IA-D)**. To identify pericytes in the heart without the need for immunostaining, we used the *Cspg4*-DsRed.T1 transgenic mouse strain (hereby referred to as *NG2*$^{DsRed/+}$), in which DsRed.T1 protein is expressed under the promoter of *Cspg4*[18]. DsRed+ cells in isolated *NG2*$^{DsRed/+}$ hearts did not express markers of endothelial cells, cardiomyocytes, fibroblasts, and leukocytes **(Supplementary Figure IE)**, but co-expressed pericyte markers **(Figure 1A)**. In addition, we observed that few NG2+ cells also expressed smooth muscle cell

markers such as α-smooth muscle actin (αSMA) and calponin 1 (CNN1) **(Supplementary Figure IF)**. The gene expression profile of sorted DsRed+ cells confirmed that *NG2*$^{DsRed/+}$ labels pericytes in the heart **(Figure 1B)**. Detailed microscopic analysis of the myocardium revealed DsRed+ cells to be diffusely present in the myocardium and closely associated with microvasculature **(Figure 1C)**.

NG2 marks cardiac pericytes that express collagen after MI

To determine whether NG2+ cells express ECM components in response to MI, we generated a double transgenic mouse model by crossing *NG2*$^{DsRed/+}$ mice with *Col1a1*$^{GFP/+}$ mice, in which Collagen1a1 (Col1a1) expression would drive the expression of GFP (hereby referred to as *NG2*$^{DsRed/+}$;*Col1a1*$^{GFP/+}$)[19] **(Figure 1D)**. *NG2*$^{DsRed/+}$;*Col1a1*$^{GFP/+}$ mice were subjected to sham or MI injury and the hearts were analyzed 7 days later. Flow cytometry analysis showed that the percentage of cells expressing *Col1a1* (GFP+) within the NG2+ population (DsRed+) significantly increased after injury **(Figure 1E)**. These double-positive cells were more abundant in hearts that had undergone MI and could be seen mainly at the border zone and infarct areas **(Figure 1F, Supplementary Figure IIA-B)**. Our data demonstrates that pericytes marked by NG2 begin to express collagen after injury and thus may participate in the fibrotic response.

Lineage-traced NG2+ cells accumulate in the infarct zone after injury

We next generated a double transgenic mouse model, *NG2*$^{CreER/+}$;*Rosa26*$^{tdT/+}$, to lineage trace pericytes that express NG2 and interrogate their fate, location and gene expression profiles at a single-cell resolution during homeostasis and in response to cardiac injury **(Figure 2A)**. In these mice, tamoxifen administration induces Cre recombination in NG2+ cells, resulting in permanent labeling with tdTomato (tdT) fluorescent protein[20]. tdT+ cells in *NG2*$^{CreER/+}$;*Rosa26*$^{tdT/+}$ hearts expressed NG2 and other pericyte markers **(Figure 2B)**. In order to lineage-trace NG2+ pericytes after injury, we injected *NG2*$^{CreER/+}$;*Rosa26*$^{tdT/+}$ mice with tamoxifen for 4 consecutive days,

allowed for a one week washout period, induced MI injury, and analyzed the hearts 2, 4, and 7 days after injury **(Figure 2C)**. We quantified the number of tdT+ cells present in the hearts and found that the number of tdT+ cells in the fibrotic area increased as more days passed after injury **(Figure 2D-E)**. Whether this was the result of migration of NG2+ cells from the remote area or proliferation of NG2+ cells within and near the injury site could not be concluded from these experiments. At 7 days post-MI, the infarct area was mostly replaced with scar tissue with sparse live cells. However, tdT+ cells had a definite presence even within the mature scar at 7 days post-MI **(Figure 2F)**, suggesting that these cells play a role during this later timepoint after injury. These results suggest that NG2+ pericytes appear to be more abundant in fibrotic areas and their accumulation intensifies with time in the first 7 days after MI.

NG2+ pericytes do not transdifferentiate into other cardiac cell types after MI

Despite evidence demonstrating the *in vitro* capabilities of pericytes to differentiate into other cell types[21], whether this ability is preserved *in vivo* has been questioned. Guimarães-Camboa, N. et al. demonstrated that pericytes in the heart do not transdifferentiate into other cell types after transverse aortic constriction (TAC), challenging the idea that pericytes may be progenitors for other cell types[22]. However, the model of TAC has a different pathophysiology that results in diffuse fibrosis, which differs from the larger replacement fibrosis seen in MI[23]. We sought to determine whether pericytes have inherent stem cell-like qualities *in vivo* that are triggered with an acute ischemic event by lineage tracing NG2+ pericytes using *NG2*$^{CreER/+}$;*Rosa26*$^{tdT/+}$ mice that had undergone MI. In this model, if lineage traced NG2+ pericytes transdifferentiated into another cardiac cell type, they would retain their tdT fluorescent label but express markers of other cell types. Hearts were analyzed 2, 4, and 7 days after MI to determine whether injury induces cardiac pericytes to transdifferentiate into other cardiac cell types at various time points. IF staining confirmed that NG2+ cardiac pericytes maintain their pericyte identity and do not express markers of fibroblasts, cardiomyocytes, hematopoietic cells, or endothelial cells **(Figure 3)**. These results

confirm the previously published findings that endogenous pericytes are not multipotent tissue resident progenitors and their observed *in vitro* plasticity is not translatable to an *in vivo* injury setting.

NG2+ cardiac pericytes proliferate after MI

Our data showed that after injury, there appears to be a gradual increase in the percentage of tdT+ cells within the infarct area **(Figure 2D-F)**. In order to determine whether this is due to NG2+ pericytes proliferating after injury, we treated the mice with 5-bromo-2'-deoxyuridine (BrdU) to label cells that are undergoing DNA replication[24,25]. *NG2*$^{CreER/+}$;*Rosa26*$^{tdT/+}$ mice were given a single injection of BrdU immediately after surgery and then provided water containing diluted BrdU until the day of analysis **(Figure 4A)**. Flow cytometry analysis demonstrated that in uninjured hearts, the percentage of proliferating tdT+ cells was very low **(Figure 4B)**. This low level of proliferation was maintained at 2 and 4 days after injury. However, there was a significant increase in the percentage of BrdU+ pericytes at 7 days post-MI, suggesting that pericytes begin to proliferate at later stages after injury **(Figure 4B)**. We then used 5-ethynyl-2'-deoxyuridine (EdU) to localize where proliferating pericytes are in relation to the infarct region[26,27]. In uninjured hearts, there were very few proliferating cells and no visible proliferating pericytes **(Figure 4C)**. We also observed no appreciable level of proliferating NG2+ pericytes in the remote areas of infarcted heart at different time points **(Figure 4C)**. While low levels of proliferating pericytes were found in the infarct areas at days 2 and 4 post MI, we observed an abundance of EdU+NG2+ pericytes 7 days after MI, suggesting a spike in proliferating pericytes at the later phases of injury **(Figure 3D)**. Proliferating pericytes could be found both at the border zone and within the infarct area of injured hearts, supporting that these cells are proliferating in response to the injury.

NG2+ cells express Col1a1 after MI

Our results so far show that expression of collagen is induced in NG2+ pericytes after MI. However, the use of *NG2*$^{DsRed/+}$;*Col1a1*$^{GFP/+}$ transgenic mice could not define the identity of these cells. There remained the question of whether other cell types such as collagen-producing fibroblasts begin to upregulate NG2 expression after injury, thus contaminating our results. To address this question, we sought to determine whether NG2 lineage-traced cells (most of which don't express collagen) can be induced by injury to express collagen. We generated triple transgenic *NG2*$^{CreER/+}$;*Rosa26*$^{tdT/+}$;*Col1a1*$^{GFP/+}$ mice, in which lineage-derived pericytes can be examined after injury for their expression of collagen. These mice received tamoxifen injection for 4 days a week prior to sham or MI surgery, and hearts were harvested after 7 days for analysis **(Figure 5A, 2B)**. In sham hearts, we did not observe many double positive cells (NG2-derived pericytes expressing collagen) **(Figure 4B)**. After injury, we could see significant double positive cells were diffusely dispersed within the border zone and infarct at 7 days post-surgery **(Figure 5C)**. The remote areas were similar to sham hearts in that there were few double positive cells (data not shown). We conducted flow cytometry analysis to quantify NG2+ cells that begin to express Col1a1 and found that the percentage of tdT+GFP+ cells significantly increased after injury **(Figure 5D)**. These data strongly support that MI induces NG2+ pericytes to express Col1a1 and this expression is specific to the fibrotic area.

Single cell RNA-seq of NG2+ pericytes reveals enrichment of ECM genes/pathways

In order to further elucidate the molecular mechanisms in which pericytes are responding to MI, we isolated tdT+ cells from *NG2*$^{CreER/+}$;*Rosa26*$^{tdT/+}$ mice that had undergone sham or MI for 4, 7, or 14 days and subjected them to scRNA-seq via the 10x Genomics platform. We chose to include the 14 day post-MI timepoint to capture changes that were occurring in pericytes in later stages after MI. We processed and analyzed a total of 5311 cells using the Seurat R package[28]. Although we sorted for tdT+ cells, our liberal gating approach to capture as many NG2+ cells resulted in slight contamination with other cell types **(Supplementary Figure IIIA)**. Cluster analysis revealed

several distinct populations with a major pericyte population and other minor clusters corresponding to fibroblasts (*Pdgfra*+)[29], endothelial cells (*Pecam1*+)[30], Schwann cells (*Plp1*+)[31], and smooth muscle cells (*Acta2*+)[32] **(Supplementary Figure IIIB-C)**. We subset only pericytes for further downstream analysis by identifying a cluster of cells that had high enrichment of pericyte markers *Cspg4, Mcam, Pdgfrb,* and *Notch3* and but was also negative for the smooth muscle marker *Acta2* **(Figure 6A, Supplementary Figure IIIC-D)**. From the uniform manifold approximation and projection (UMAP) plot, we observed that pericytes from all conditions (sham and MI at different timepoints) still form a single cluster, but there was a noticeable shift in the transcriptomic profiles of pericytes from injured conditions when compared to sham **(Figure 6A)**. However, there were no significant changes to expression of major known pericyte markers across the conditions, supporting our previous results that pericytes after injury maintain their pericyte profile **(Supplementary Figure IIIE)**. Instead, we noted that the visible shift in the cells on the UMAP plot may be associated with transcriptomic changes that occur in response to injury.

To determine biological processes that may be enriched at each timepoint, we identified upregulated and downregulated genes in cells from 4, 7, and 14 days after MI compared to cells from sham hearts and conducted gene ontology (GO) analysis **(Figure 6B)**. Notably, at 7 days after MI, pathways associated with supramolecular fiber organization and extracellular structure were positively enriched while at 14 days after MI, there was significant enrichment of pathways related with ECM production (protein heterotrimerization and collagen fibril organization) **(Figure 6B)**. Furthermore, translation was the most significantly enriched biological process at both 7 and 14 days after MI, which supports the finding that these cells are proliferating and secreting ECM proteins at these timepoints **(Figure 6B)**. In order to confirm the *in vivo* responses that our data has shown, we looked at gene expression of specific genes that regulate proliferation and encode for ECM proteins. Expression in these categories peaked at 7 days post-MI, aligning with our *in vivo* characterization **(Figure 6C)**. These genes continued to have increased expression through

14 days post-MI, further suggesting that pericytes may have a continued role in the later scar maturation phase.

Finally, there have been many studies that demonstrate the importance of various signaling pathways in pericytes. Transforming growth factor-β (TGFβ) signaling and PDGFR signaling in pericytes have both been attributed to the activation of pericytes in fibrosis[14,33]. When we looked at the expression of downstream effectors of both TGFβ and PDGFR signaling, we saw that expression significantly increased after injury **(Figure 6A-B)**.

DISCUSSION

The role of pericytes in cardiac ischemic injury has been an underexplored topic in understanding the importance of these cells. We hypothesized that pericytes respond to MI and participate in the fibrotic response. By lineage-tracing NG2+ pericytes, our results demonstrated that at later stages after MI (7 days post-injury), pericytes proliferate and express prominent levels of Col1a1. scRNA-seq confirms this response, even showing a continued upregulation of pro-fibrotic genes at 14 days post-MI. These results not only highlight that pericytes do have a significant response to ischemic cardiac injury, but also suggest that pericytes may play a role in the later scar maturation phase of cardiac fibrosis.

Pericytes have been attributed to be the major cell type involved in the development of fibrosis in other organ systems. There is strong evidence suggesting that pericytes in the kidney are the major source of activated fibroblasts upon ischemia[15,34] and that pericytes are the main cellular source of ECM proteins in spinal cord injury[35]. However, the cellular composition of the heart is different from other organs in that cardiac fibroblasts are already established to be the major cell type to contribute to fibrosis[6]. In mice, cardiac fibroblasts become activated within a couple of days of MI, secrete large amounts of ECM proteins 4-7 days post-injury, and then lose their

proliferative capacity by 7-10 days post-injury[36]. This behavior differs from the NG2+ pericytes in our studies, which appear to be proliferative and significantly express ECM proteins at 7 days post-injury. Our scRNA-seq data also suggests that NG2+ pericytes maintain this “activated” state through 14 days post-injury. These results demonstrate that pericytes may be playing a unique role from fibroblasts in the development of fibrosis. There require more studies to determine the significance of NG2+ cardiac pericytes in these later stages after MI.

The findings of our study supplement the growing literature on pericyte function in cardiac ischemic injury. However, it is important to note the key differences between our findings and what others have reported. Initial studies conducted by Birbrair, A. et al. first suggested that pericytes in the heart do not produce collagen after injury[16]. While this study identified Col1a1 expression by IF staining, we utilized the *Col1a1*$^{GFP/+}$ mouse strain to reliably visualize Col1a1 expression, which was further corroborated by our scRNA-seq data. Guimarães-Camboa, N. et al. also demonstrated minimal levels of Col1a1 expression in cardiac pericytes after injury[22]. However, their findings used a different pericyte marker to lineage-trace their cells and were in a pressure overload injury model, which differs greatly in pathophysiology to MI. These differences highlight that our findings may be specific to a subpopulation of NG2+ cardiac pericytes and within the context of MI. There is a need to further study this population of cells in other models of cardiac injury (e.g. pressure overload, aging, dilated cardiomyopathy) to determine their complete function in cardiac fibrosis. Furthermore, there is a possibility that other subpopulations of pericytes with varying functions in MI exist. As we did not explore the heterogeneity of cardiac pericytes in injury, this is a question that may need to be addressed in future studies.

Overall, our findings demonstrate that cardiac pericytes exhibit a significant response in the event of MI and may play a role in later stages of injury response. This study brings to light the need to further study this population of cells to determine their therapeutic potential.

METHODS

Mice

NG2$^{DsRed/+}$ mice (Stock No. 008241) and *Rosa26*$^{tdT/+}$ mice were acquired from The Jackson Lab. *Col1a1*$^{GFP/+}$ were a gift from the Evans lab at the University of California, San Diego. *NG2*$^{CreER/+}$ were provided by the Carmichael lab at the University of California, Los Angeles (UCLA). For all experiments, adult (8-12 weeks) male and female mice were used. All procedures were carried out with the approval of the UCLA Animal Research Committee.

Myocardial Infarction and Aftercare

Mice were initially anesthetized by intraperitoneal injection of ketamine/Xylazine and then intubated for positive pressure ventilation with a mixture of oxygen and 2-3% isoflurane throughout the surgical procedure. The pericardium was opened after left thoracotomy between the fourth and fifth rib and an 8-0 suture was placed around the left anterior descending artery. The suture was tightened around the vessel to simulate myocardial infarction and the chest was closed in layers by using 5-0 Vicryl suture. Ventilation was maintained until sufficient spontaneous breathing occurs and post-operative analgesia (0.1mg/kg buprenorphine and 5mg/kg carprofen) was provided immediately after the procedure. Mice were left to recover in a temperature-controlled chamber until they resumed full mobility.

Section Preparation and Immunofluorescence Staining

Mice were injected with heparin and euthanized 20 minutes afterwards. The hearts were perfused with 30 mL of PBS and then fixed in 4% PFA for 2 hours at 4°C. After a quick wash in PBS, the hearts were stored in 30% sucrose overnight at 4°C. The hearts were then embedded in Optimal cutting temperature compound (OCT) and stored at -80°C. The blocks were sectioned using a Leica cryostat at a thickness of 8μm or 100μm and the sections were mounted on Colorfrost Plus microscope slides (Fisher) and stored at -20°C until imaging.

For immunofluorescence staining, slides with 8μm sections were left at room temperature for 10 minutes, washed 3 times with PBS, and permeabilized with 0.25% Triton X-100 (prepared in PBS) for 10 minutes. The slides were then blocked with blocking buffer (10% NGS, PBS-0.1%Tween 20) for 1 hour at room temperature, followed by incubation with primary antibodies (diluted in blocking buffer) overnight at 4°C in the dark. Slides were subsequently washed 3 times with PBS-0.1%Tween 20 and incubated with secondary antibodies (Thermo Fisher Scientific) diluted in blocking buffer for 1 hour at room temperature. Antibodies and dilutions are shown in **Supplementary Table 1**. After another 3 washes with PBS-0.1%Tween 20, coverslips were mounted on the slides using mounting medium containing DAPI (Vector). The slides were imaged by a Zeiss confocal microscope (LSM880) and image processing was done through the ZEN 2 (blue edition) software.

Flow Cytometry/Fluorescence-Activated Cell Sorting (FACS)

Mice were injected with heparin and euthanized 20 minutes afterwards. Hearts were dissected and cannulated for perfusion with 30mL of phosphate-buffered saline (PBS). The hearts were then perfused with 5mL of digestion enzyme (recipe in table below) and chopped into small pieces. The pieces were collected and incubated in 10mL of digestion enzyme on a rotator at 37°C for one hour with periodic pipetting to ensure complete digestion. The digested cells were passed through a 40μm filter and centrifuged (350xg, 10 minutes) to collect all cells. Debris were removed using a Debris Removal Kit (Miltenyi) and cells were resuspended in FACS buffer. If antibody staining was necessary, resuspended cells were incubated with antibodies for 30 minutes on ice. For staining with biotinylated antibodies, streptavidin-APC-eFluor780 conjugate was added for an additional 30 minute incubation on ice after washing with FACS buffer. Antibodies and dilutions are shown in **Supplementary Table 2**. Cells were analyzed or sorted using a BD FACSAria™ II cell sorter. All data was analyzed using FlowJo software.

RNA Extraction and Reverse Transcription qPCR (RT-qPCR)

If collecting RNA from sorted cells, cells were sorted directly into TRIzol™ LS Reagent (Thermo Fisher Scientific). RNA was extracted from sorted cells or whole heart samples using TRIzol™ LS Reagent and following the manufacturer's protocol. Extracted RNA was quantified by NanoDrop™ (Thermo Fisher Scientific) and then converted into complementary DNA (cDNA) by using the iScript™ cDNA Synthesis Kit (Bio-Rad) and following the manufacturer's instructions. RT-qPCR reactions were prepared with SYBR Green Master Mix (Bio-Rad) and specific primers designed for each target gene (sequences shown in **Supplementary Table 3**). The reactions were run on a CFX96 Touch™ Real-Time PCR Detection System (Bio-Rad) and analysis was done using the double ΔCT method.

Cell Counting

Tilescan images were taken of 3-5 slides per heart. The fibrotic area was determined by either lack of live tissue or *Col1a1* (GFP) expression. The number of tdT+ cells and the number of pixels per region were counted and calculated respectively using ImageJ.

Proliferation – BrdU and EdU

To label proliferating cells in the heart, mice were injected with 100µg of BrdU immediately after sham or MI surgery. The mice were then given water containing BrdU (1mg/mL) to continuously label proliferating cells. This water was changed every other day. BrdU labeling was then analyzed by flow cytometry by using the APC BrdU Flow Kit (BD Pharmingen™). For EdU experiments, we intraperitoneally injected 1 mg of EdU (prepared in DMSO and diluted in saline) and sacrificed the mice after 4 hours. Hearts were processed as described above and the Click-it (Plus) EdU Imaging Assay (Thermo Fisher Scientific) was used to fluorescently mark EdU labeling as per the manufacturer's instructions.

Single Cell RNA-sequencing and Analysis

Cells were sorted from *NG2*$^{CreER/+}$;*Rosa26*$^{tdT/+}$ hearts that had undergone sham or MI (4, 7, and 14 days post-injury) (2 hearts per sample) as described above into Dulbecco's Modified Eagle Medium without calcium (Gibco) and 10%FBS. Afterwards, the cell suspension was centrifuged and all media except for roughly 40µl was removed. The number of cells was counted using a hemocytometer. Cells were then prepared for scRNA-seq by using the 10x Genomics Chromium Controller and the Chromium Single Cell 3' GEM, Library & Gel Bead Kit, v3. Libraries were sequenced on a NovaSeq Sequencer (Illumina) and with an average of 150,000,000 million reads sequenced per sample. Data was processed using the 10x Cell Ranger pipeline and further analyzed using Seurat[28]. Gene Ontology analysis was done through the Metascape web portal[37] (http://metascape.org).

Statistical Analysis

All quantification data are presented as mean ± standard error of the mean (SEM) and significance was determined by using Student's t-test or Two-way ANOVA. A p-value < 0.05 was considered statistically significant and data were analyzed using GraphPad Prism 8.

Figure 1

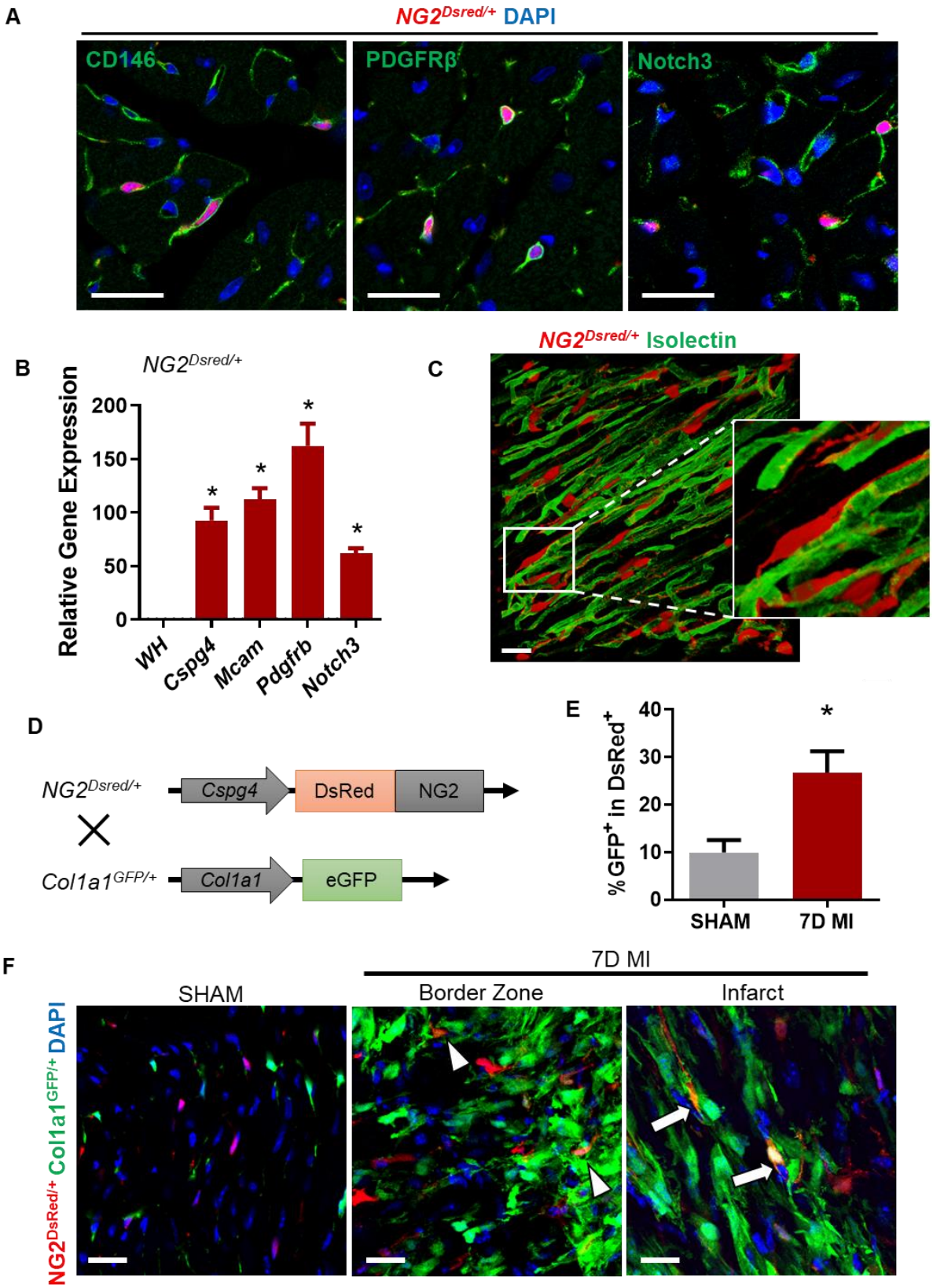
A
NG2Dsred/+ DAPI
CD146
PDGFRβ
Notch3
B
NG2Dsred/+
Relative Gene Expression
200
150
100
50
0
WH
Cspg4
Mcam
Pdgfrb
Notch3
C
NG2Dsred/+ Isolectin
D
NG2Dsred/+
Cspg4
DsRed
NG2
Col1a1GFP/+
Col1a1
eGFP
E
%GFP+ in DsRed+
40
30
20
10
0
SHAM
7D MI
F
7D MI
SHAM
Border Zone
Infarct
NG2DsRed/+ Col1a1GFP/+ DAPI

Figure 1: NG2 labels cardiac pericytes that express Col1a1 after MI

(A) DsRed+ cells (red) in *NG2*$^{DsRed/+}$ hearts express pericyte markers CD146, PDGFRβ, and Notch3 (green). **(B)** Sorted DsRed+ cells had higher expression of pericyte genes compared to unsorted whole heart (WH) samples. **(C)** High magnification images demonstrate that DsRed+ cells are closely associated with isolectin-labeled vessels. **(D)** Breeding schematic to develop *NG2*$^{DsRed/+}$;*Col1a1*$^{GFP/+}$ double transgenic mice. **(E)** Flow cytometry analysis of *NG2*$^{DsRed/+}$;*Col1a1*$^{GFP/+}$ hearts 7 days after sham or myocardial infarction (7D MI) surgery. After injury, the percentage of GFP+ cells that are present within the DsRed+ population significantly increases. **(F)** In *NG2*$^{DsRed/+}$;*Col1a1*$^{GFP/+}$ hearts, DsRed+GFP+ double positive cells are present mainly by the border zone and infarct area. Arrowheads indicate DsRed+ cells with low GFP expression and arrows show high expression of both DsRed and GFP. DAPI is used to label nuclei (blue) in all stainings. Scale bar: 20μm. *p-value < 0.05.

Figure 2

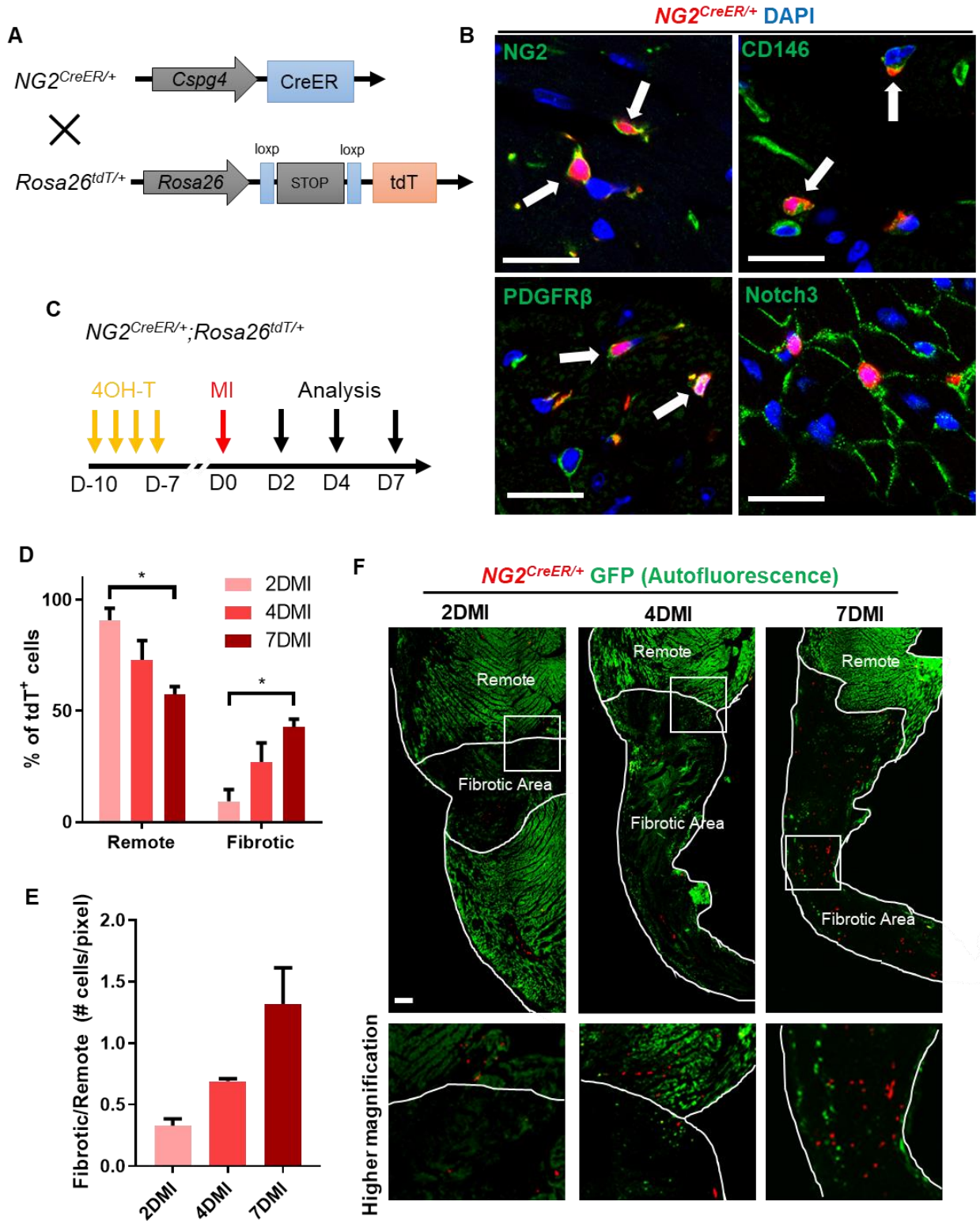
A
NG2CreER/+
Cspg4
CreER
Rosa26tdT/+
Rosa26
loxp
STOP
loxp
tdT
B
NG2CreER/+ DAPI
NG2
CD146
PDGFRβ
Notch3
C
NG2CreER/+;Rosa26tdT/+
4OH-T
MI
Analysis
D-10
D-7
D0
D2
D4
D7
D
% of tdT+ cells
100
50
0
2DMI
4DMI
7DMI
Remote
Fibrotic
E
Fibrotic/Remote (# cells/pixel)
2.0
1.5
1.0
0.5
0.0
2DMI
4DMI
7DMI
F
NG2CreER/+ GFP (Autofluorescence)
2DMI
4DMI
7DMI
Remote
Fibrotic Area
Higher magnification

Figure 2: NG2 lineage-traced pericytes accumulate in the infarct area after MI

(A) Breeding schematic to generate *NG2*$^{CreER/+}$;*Rosa26*$^{tdT/+}$ double transgenic mice. **(B)** NG2 lineage-traced tdTomato+ (tdT+) cells (red) express NG2 and other pericyte markers. DAPI is used to label nuclei (blue). Scale bar: 20μm. **(C)** Schematic for tamoxifen injection in relation to myocardial infarction (MI) surgery. Hearts were analyzed 2, 4, and 7 days after injury (2DMI, 4DMI, and 7DMI). **(D)** Sections of *NG2*$^{CreER/+}$;*Rosa26*$^{tdT/+}$ hearts were imaged and the total number of tdT+ cells per section was counted. The percentage of tdT+ cells per section in the remote area and the fibrotic areas were quantified. **(E)** The number of tdT+ cells/pixel of tissue was quantified for the remote and fibrotic areas. The ratio of these values was plotted. **(F)** Representative images of the left ventricular free wall of *NG2*$^{CreER/+}$;*Rosa26*$^{tdT/+}$ hearts 2, 4, and 7 days after MI. The autofluorescence of the healthy tissue is in green and tdT+ cells can be seen throughout the heart. At 2DMI and 4DMI, there are not as many tdT+ cells in the fibrotic area compared to 7DMI. Scale bar: 250μm. *p-value < 0.05.

Figure 3

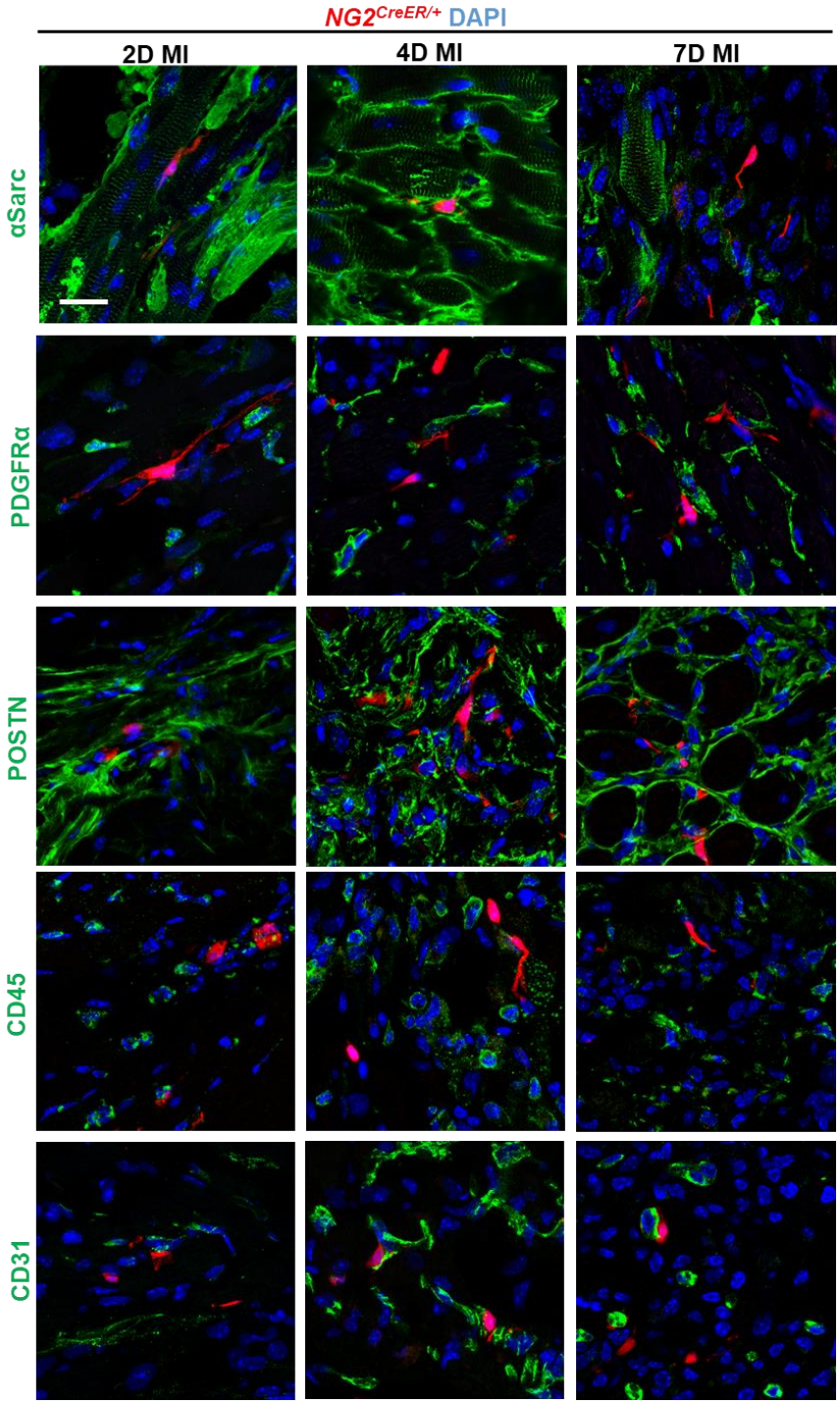

Figure 3: NG2+ cells do not transdifferentiate into other cell types after injury

NG2$^{CreER/+}$;*Rosa26*$^{tdT/+}$ hearts 2, 4, and 7 days after MI were stained for cardiomyocyte (α-sarcomeric actinin, αSarc), fibroblast (PDGFRα), myofibroblast (periostin, POSTN), hematopoietic cells (CD45), and endothelial cells (CD31). Double positive cells could not be found at any time point. DAPI is used to label nuclei (blue). Scale bar: 20μm.

Figure 4

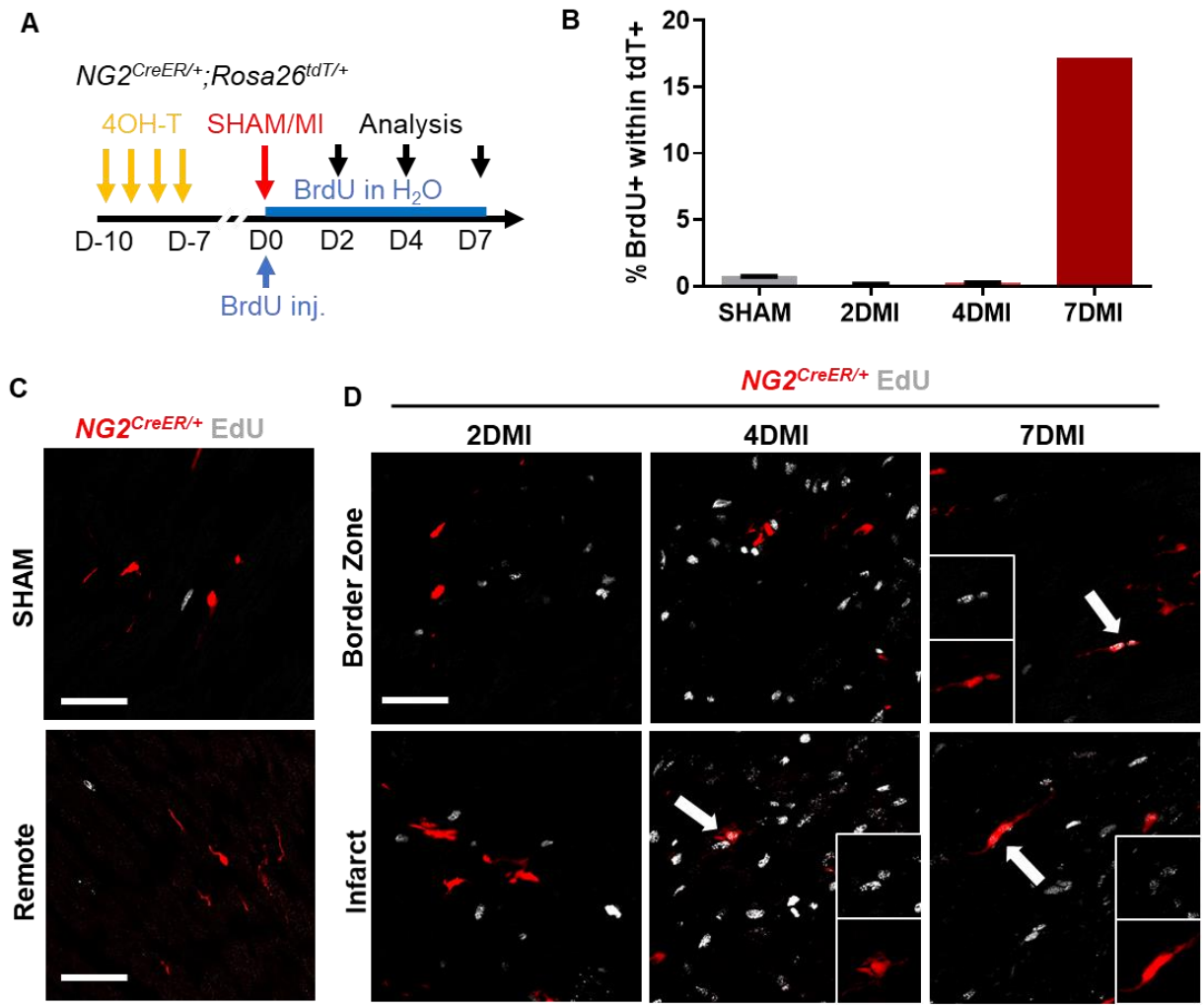
A
NG2CreER/+;Rosa26tdT/+
4OH-T
SHAM/MI
Analysis
BrdU in H2O
D-10
D-7
D0
D2
D4
D7
BrdU inj.
B
% BrdU+ within tdT+
20
15
10
5
0
SHAM
2DMI
4DMI
7DMI
C
NG2CreER/+ EdU
SHAM
Remote
D
NG2CreER/+ EdU
2DMI
4DMI
7DMI
Border Zone
Infarct

Figure 4: NG2+ cardiac pericytes proliferate in the infarcted area

(A) Schematic of BrdU treatment. After surgery, *NG2*$^{CreER/+}$;*Rosa26*$^{tdT/+}$ mice receive a single injection of BrdU and then are given water containing BrdU until analysis. **(B)** Flow cytometry analysis of percentage of BrdU+tdT+ cells in *NG2*$^{CreER/+}$;*Rosa26*$^{tdT/+}$ that have undergone sham or myocardial infarction (MI) surgery. There is a sudden increase in proliferating tdt+ cells at 7DMI. **(C)** *NG2*$^{CreER/+}$;*Rosa26*$^{tdT/+}$ mice were injected with EdU prior to euthanasia. SHAM hearts and remote areas of injured hearts had low levels of proliferating tdT+ cells. **(D)** After MI, proliferating tdT+ cells could be found mainly within the border zone and infarct area (arrows). Scale bar: 50μm.

Figure 5

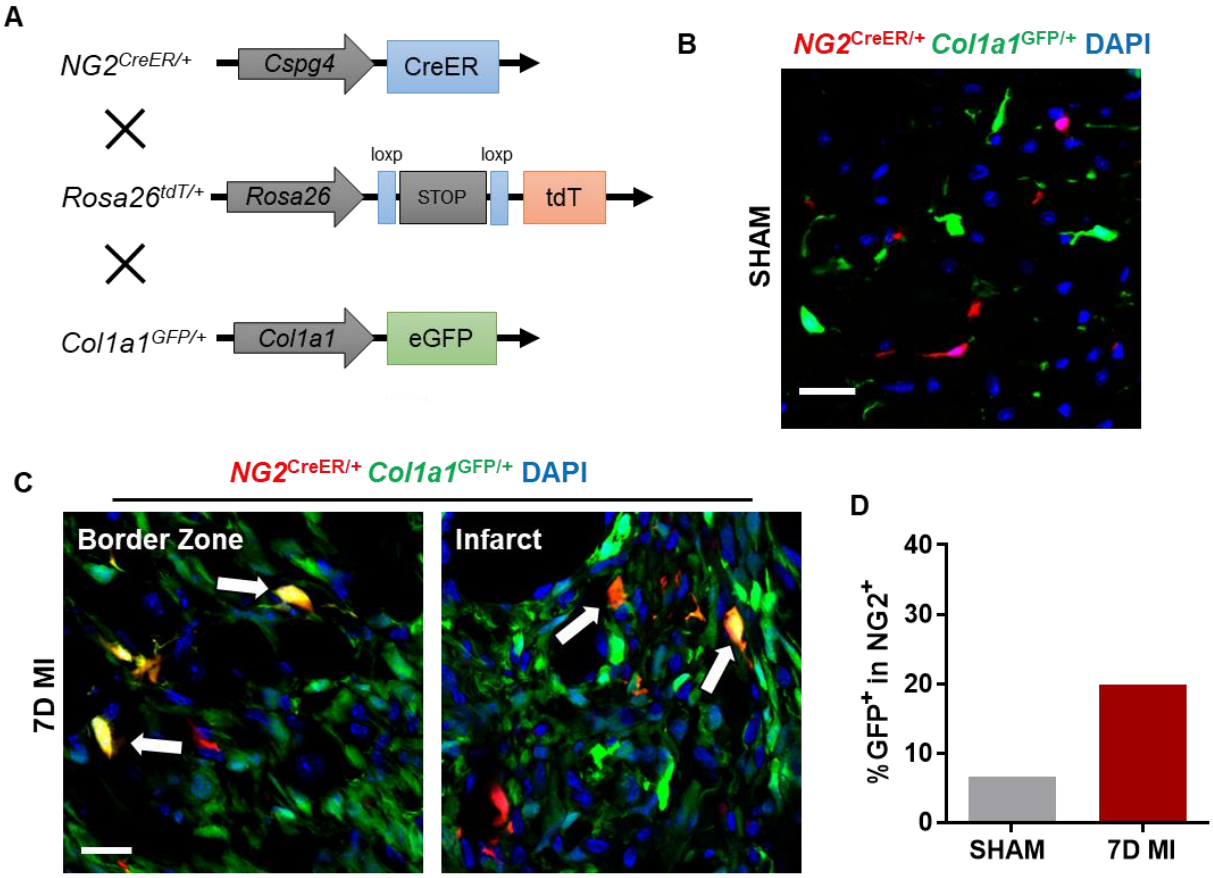

Figure 5: NG2 lineage-traced cardiac pericytes express Col1a1 after MI

(A) Breeding schematic to generate *NG2*$^{CreER/+}$;*Rosa26*$^{tdT/+}$;*Col1a1*$^{GFP/+}$ mice. **(B)** In sham hearts, there were little to no tdT+GFP+ cells. **(C)** 7 days after MI, there are a significant number of tdT+GFP+ cells at the border zone and infarct area. **(D)** Flow cytometry analysis confirms the increase in tdT+GFP+ cells after injury. DAPI is used to label nuclei (blue). Scale bar: 20μm.

Figure 6

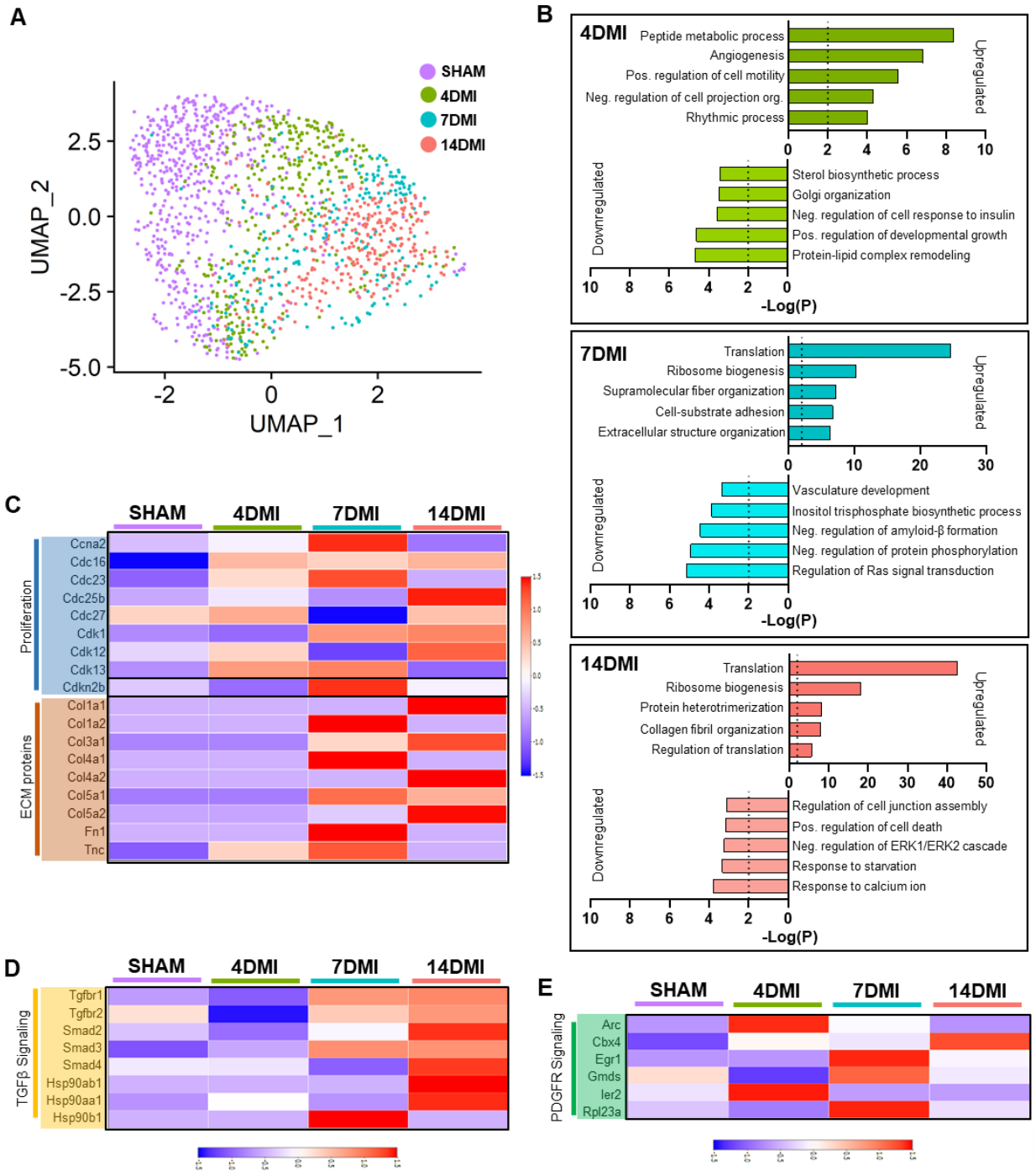
A
SHAM
4DMI
7DMI
14DMI
UMAP_2
UMAP_1
B
4DMI
Peptide metabolic process
Angiogenesis
Pos. regulation of cell motility
Neg. regulation of cell projection org.
Rhythmic process
Upregulated
Sterol biosynthetic process
Golgi organization
Neg. regulation of cell response to insulin
Pos. regulation of developmental growth
Protein-lipid complex remodeling
Downregulated
-Log(P)
7DMI
Translation
Ribosome biogenesis
Supramolecular fiber organization
Cell-substrate adhesion
Extracellular structure organization
Vasculature development
Inositol trisphosphate biosynthetic process
Neg. regulation of amyloid-β formation
Neg. regulation of protein phosphorylation
Regulation of Ras signal transduction
14DMI
Protein heterotrimerization
Collagen fibril organization
Regulation of translation
Regulation of cell junction assembly
Pos. regulation of cell death
Neg. regulation of ERK1/ERK2 cascade
Response to starvation
Response to calcium ion
C
SHAM
4DMI
7DMI
14DMI
Proliferation
Ccna2
Cdc16
Cdc23
Cdc25b
Cdc27
Cdk1
Cdk12
Cdk13
Cdkn2b
ECM proteins
Col1a1
Col1a2
Col3a1
Col4a1
Col4a2
Col5a1
Col5a2
Fn1
Tnc
D
TGFβ Signaling
Tgfbr1
Tgfbr2
Smad2
Smad3
Smad4
Hsp90ab1
Hsp90aa1
Hsp90b1
E
PDGFR Signaling
Arc
Cbx4
Egr1
Gmds
Ier2
Rpl23a

Figure 6: Single cell RNA-sequencing of NG2-lineage traced cardiac pericytes

(A) UMAP plot of pericytes that have subset from the single cell RNA-sequencing (scRNA-seq) of *NG2*$^{CreER/+}$;*Rosa26*$^{tdT/+}$ hearts that had undergone sham or MI for 4, 7, and 14 days. **(B)** Gene Ontology analysis on genes that were upregulated and downregulated at each time point after injury compared to sham cells. **(C)** Genes associated with proliferation and extracellular matrix (ECM) proteins were upregulated at later stages after injury. Genes associated with the TGFβ **(D)** and the PDGFR signaling pathway **(E)** are upregulated after injury, suggestive of their role in injury response.

Supplementary Figure I

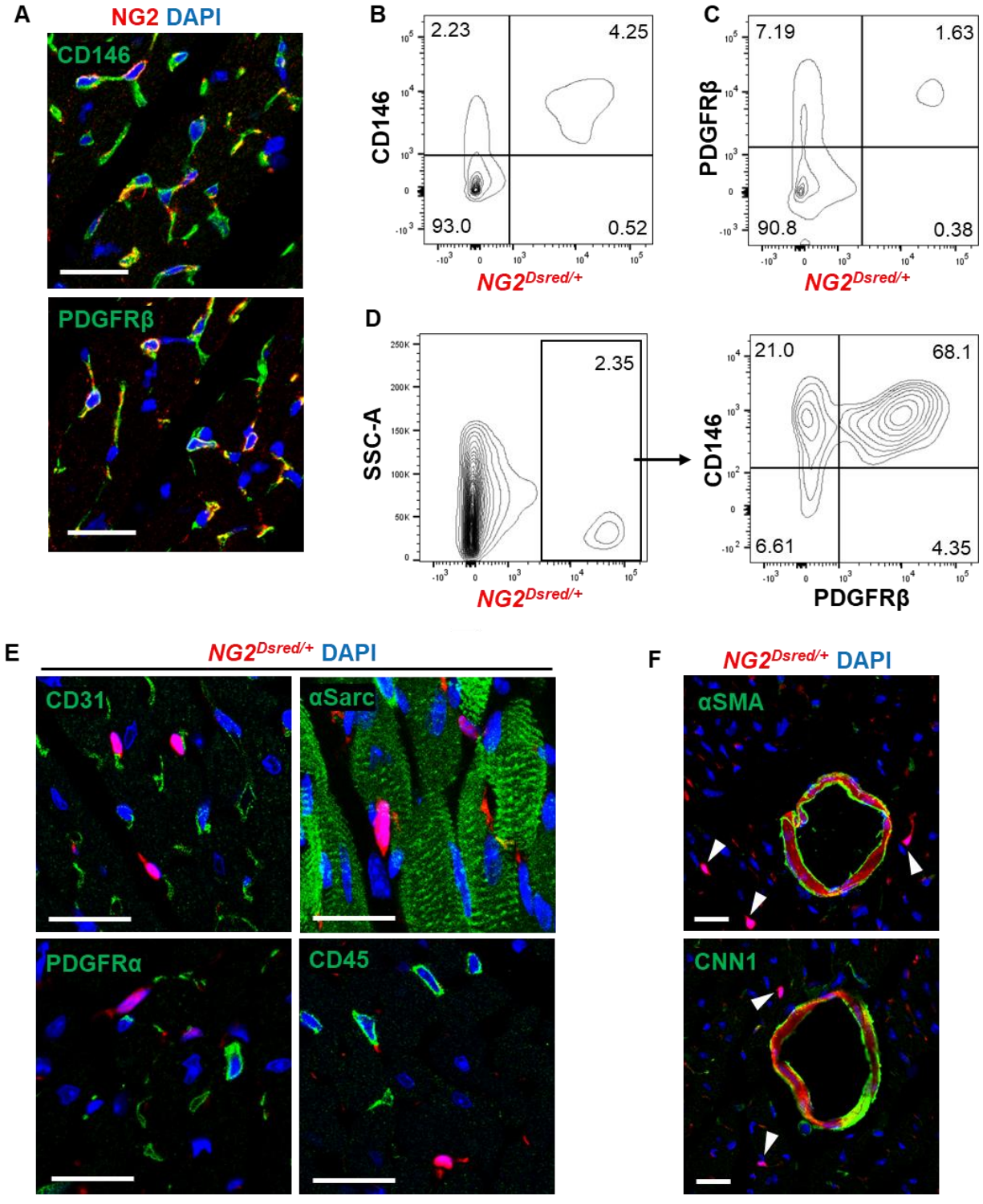

Supplementary Figure I: *NG2*$^{DsRed/+}$ mouse strain labels cardiac pericytes

(A) Co-staining of NG2 with pericyte markers CD146 and PDGFRβ confirms that NG2 marks cardiac pericytes. **(B-D)** Flow cytometry shows that the majority of DsRed+ cells in *NG2*$^{DsRed/+}$ hearts express both CD146 and PDGFRβ. **(E)** *NG2*$^{DsRed/+}$ hearts do not label endothelial cells, cardiomyocytes, fibroblasts or hematopoietic cells (markers in green). **(F)** Smooth muscle cells around larger vessels are labeled with *NG2*$^{DsRed/+}$ but can be clearly differentiated from NG2+ pericytes, which reside in single cells (arrowheads). DAPI is used to label nuclei (blue). Scale bar: 20μm.

Supplementary Figure II

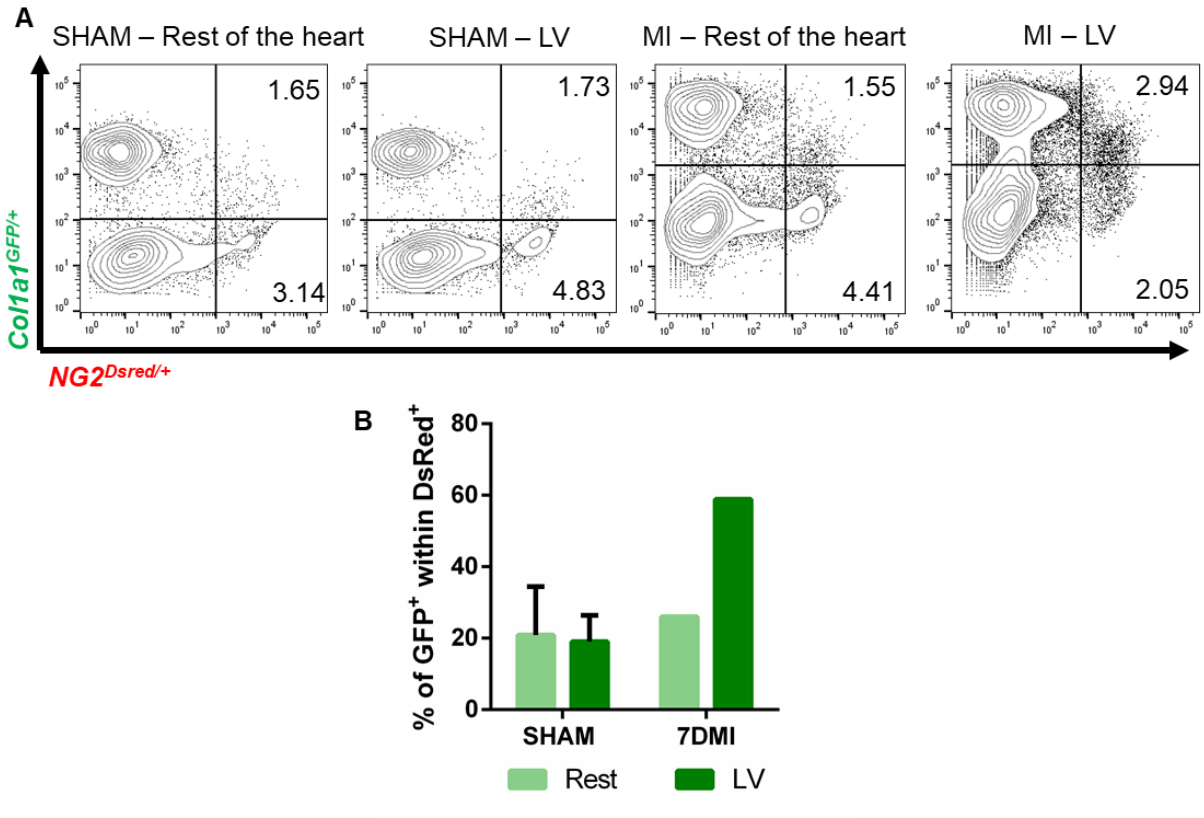

Supplementary Figure II: Col1a1 expression in NG2+ cells is localized to the infarct area

(A) Representative flow cytometry plots of hearts 7 days after sham or MI surgery. The left ventricle (LV) was separated from the rest of the heart and analyzed separately. Increase in the percentage of DsRed+GFP+ cells was specific to the LV in MI samples. **(B)** Quantification of DsRed+GFP+ cells.

Supplementary Figure III

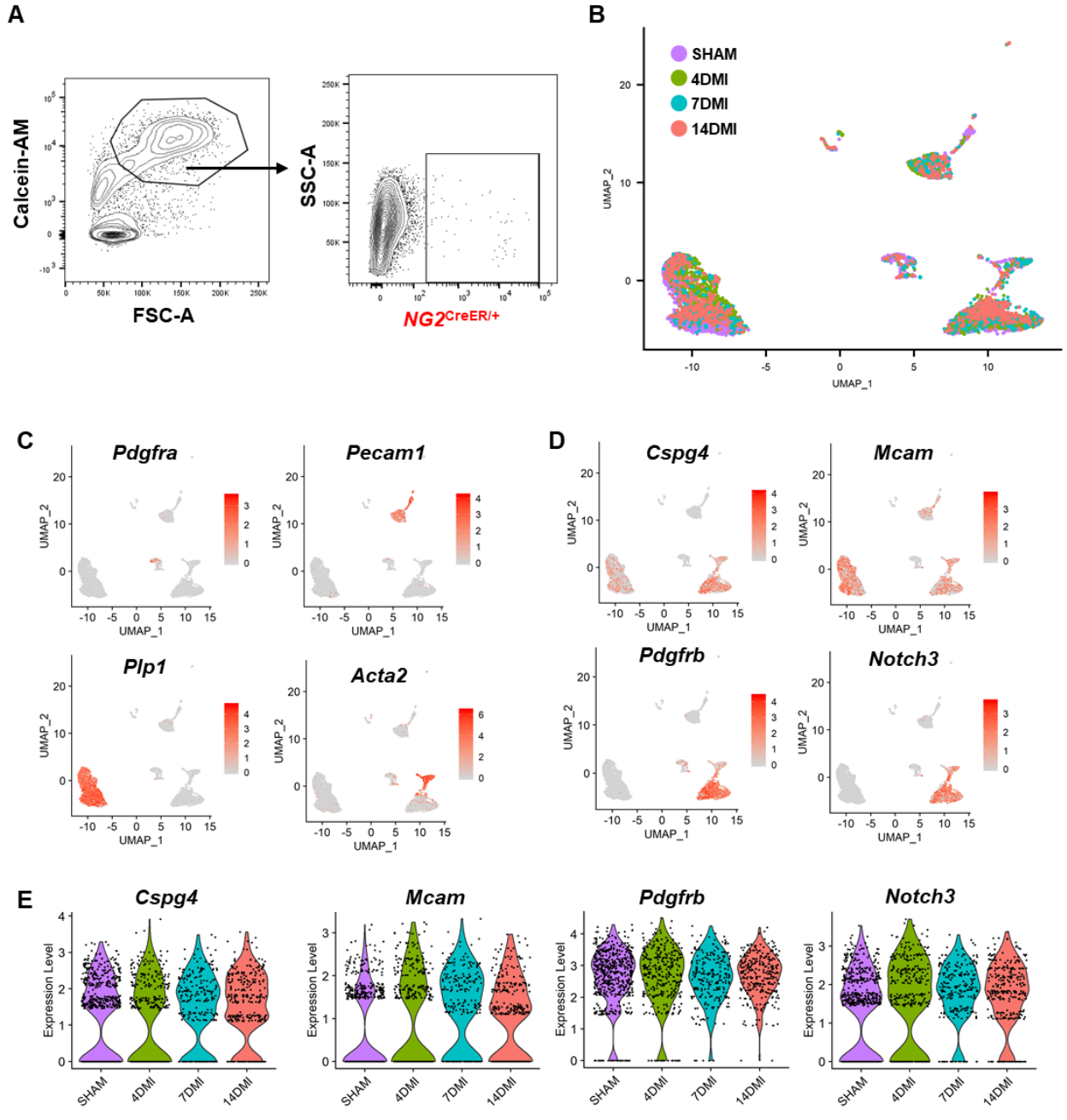

Supplementary Figure III: Single cell RNA-sequencing of NG2-lineage traced cardiac pericytes

(A) Representative FACS plots for sorting viable tdT+ cells from *NG2*$^{CreER/+}$;*Rosa26*$^{tdT/+}$ hearts that had undergone sham or MI for single cell RNA-sequencing (scRNA-seq). **(B)** UMAP plot of all cells collected for single cell RNA-seq (scRNA-seq). **(C)** Other cardiac cell types that were sequenced were identified by expression of specific markers. **(D)** Expression of pericyte markers across the UMAP dictates a major cluster to be enriched for pericytes. **(E)** Expression of pericyte markers after MI does not change significantly, confirming that these cells maintain their pericyte identity after injury.

Supplementary Table 1

IF Staining Antibodies

Target Protein	Manufacturer (catalog no.)	Dilution
NG2	Millipore Sigma (AB5320)	1:50
CD146	Abcam (ab75769)	1:100
PDGFRβ	Abcam (ab32570)	1:100
PDGFRβ	eBioscience (14-1402-82)	1:50
Notch3	ABClonal (A3115)	1:50
CD31	Abcam (ab28364)	1:100
CD31	eBioscience (14-0311-82)	1:50
αSarc	Sigma-Aldrich (A7811)	1:400
PDGFRα	R&D Systems (AF1062)	1:100
CD45	eBioscience (14-0451-82)	1:50
αSMA	Sigma-Aldrich (A2547)	1:100
CNN1	Atlas Antibodies (HPA014263)	1:100
POSTN	R&D Systems (AF2955)	1:100

Supplementary Table 2

Flow Cytometry/FACS Antibodies

Target Protein – Conjugate	Manufacturer (catalog no.)	Dilution
CD146 – APC	Biolegend (134712)	1:100
PDGFRβ – Biotin	Miltenyi Biotec (130-109-866	1:10
Streptavidin, APC-eFluor 780	eBioscience (47-4317-82)	1:200

Supplementary Table 3

RT-qPCR Primers

Gene	Sequence
Gapdh	F: 5'- AGGTCGGTGTGAACGGATTTG
	R: 5'- TGTAGACCATGTAGTTGAGGTCA
Cspg4	F: 5'- GCTGTCTGTTGACGGAGTGTT
	R: 5'- CGGCTGATTCCCTTCAGGTAAG
Mcam	F: 5'- CCCAAACTGGTGTGCGTCTT
	R: 5'- GGAAAATCAGTATCTGCCTCTCC
Pdgfrb	F: 5'- TTCCAGGAGTGATACCAGCTT
	R: 5'- AGGGGGCGTGATGACTAGG
Notch3	F: 5'- AGTGCCGATCTGGTACAACTT
	R: 5'- CACTACGGGGTTCTCACACA

REFERENCES

1. Savarese, G. & Lund, L. H. Global Public Health Burden of Heart Failure. *Card Fail Rev* **3**, 7–11 (2017).
2. Fan, D., Takawale, A., Lee, J. & Kassiri, Z. Cardiac fibroblasts, fibrosis and extracellular matrix remodeling in heart disease. *Fibrogenesis Tissue Repair* **5**, 15 (2012).
3. Kong, P., Christia, P. & Frangogiannis, N. G. The Pathogenesis of Cardiac Fibrosis. *Cell Mol Life Sci* **71**, 549–574 (2014).
4. Yang, F. *et al.* Myocardial Infarction and Cardiac Remodelling in Mice. *Experimental Physiology* **87**, 547–555 (2002).
5. Frangogiannis Nikolaos G. & Rosenzweig Anthony. Regulation of the Inflammatory Response in Cardiac Repair. *Circulation Research* **110**, 159–173 (2012).
6. Travers, J. G., Kamal, F. A., Robbins, J., Yutzey, K. E. & Blaxall, B. C. Cardiac Fibrosis: The Fibroblast Awakens. *Circ. Res.* **118**, 1021–1040 (2016).
7. Oka, T. *et al.* Genetic manipulation of periostin expression reveals a role in cardiac hypertrophy and ventricular remodeling. *Circ. Res.* **101**, 313–321 (2007).
8. Armulik, A., Abramsson, A. & Betsholtz, C. Endothelial/pericyte interactions. *Circ. Res.* **97**, 512–523 (2005).
9. Bergers, G. & Song, S. The role of pericytes in blood-vessel formation and maintenance. *Neuro-oncology* **7**, 452–464 (2005).
10. van Dijk, C. G. M. *et al.* The complex mural cell: pericyte function in health and disease. *Int. J. Cardiol.* **190**, 75–89 (2015).
11. Hammes, H.-P. *et al.* Pericytes and the Pathogenesis of Diabetic Retinopathy. *Diabetes* **51**, 3107–3112 (2002).
12. A Perivascular Origin for Mesenchymal Stem Cells in Multiple Human Organs: Cell Stem Cell. https://www.cell.com/cell-stem-cell/fulltext/S1934-5909(08)00337-

8?_returnURL=https%3A%2F%2Flinkinghub.elsevier.com%2Fretrieve%2Fpii%2FS1934590908003378%3Fshowall%3Dtrue.

13. Picoli, C. C. *et al.* Pericytes Act as Key Players in Spinal Cord Injury. *The American Journal of Pathology* **189**, 1327–1337 (2019).
14. Chen, Y.-T. *et al.* Platelet-derived growth factor receptor signaling activates pericyte–myofibroblast transition in obstructive and post-ischemic kidney fibrosis. *Kidney International* **80**, 1170–1181 (2011).
15. LeBleu, V. S. *et al.* Origin and function of myofibroblasts in kidney fibrosis. *Nat. Med.* **19**, 1047–1053 (2013).
16. Birbrair, A. *et al.* Type-1 pericytes accumulate after tissue injury and produce collagen in an organ-dependent manner. *Stem Cell Res Ther* **5**, 122 (2014).
17. Stallcup, W. B. The NG2 Proteoglycan in Pericyte Biology. *Adv. Exp. Med. Biol.* **1109**, 5–19 (2018).
18. Zhu, X., Bergles, D. E. & Nishiyama, A. NG2 cells generate both oligodendrocytes and gray matter astrocytes. *Development* **135**, 145–157 (2008).
19. Moore-Morris, T. *et al.* Resident fibroblast lineages mediate pressure overload-induced cardiac fibrosis. *J. Clin. Invest.* **124**, 2921–2934 (2014).
20. Huang, W. *et al.* Novel NG2-CreERT2 knock-in mice demonstrate heterogeneous differentiation potential of NG2 glia during development. *Glia* **62**, 896–913 (2014).
21. Crisan, M. *et al.* A Perivascular Origin for Mesenchymal Stem Cells in Multiple Human Organs. *Cell Stem Cell* **3**, 301–313 (2008).
22. Guimarães-Camboa, N. *et al.* Pericytes of Multiple Organs Do Not Behave as Mesenchymal Stem Cells In Vivo. *Cell Stem Cell* **20**, 345-359.e5 (2017).
23. Lygate, C. Surgical models of hypertrophy and heart failure: Myocardial infarction and transverse aortic constriction. *Drug Discovery Today: Disease Models* **3**, 283–290 (2006).

24. Gratzner, H. G. Monoclonal antibody to 5-bromo- and 5-iododeoxyuridine: A new reagent for detection of DNA replication. *Science* **218**, 474–475 (1982).
25. Park Shuin *et al.* Genetic Regulation of Fibroblast Activation and Proliferation in Cardiac Fibrosis. *Circulation* **138**, 1224–1235 (2018).
26. Salic, A. & Mitchison, T. J. A chemical method for fast and sensitive detection of DNA synthesis in vivo. *Proc. Natl. Acad. Sci. U.S.A.* **105**, 2415–2420 (2008).
27. Mead, T. J. & Lefebvre, V. Proliferation Assays (BrdU and EdU) on Skeletal Tissue Sections. *Methods Mol Biol* **1130**, 233–243 (2014).
28. Stuart, T. *et al.* Comprehensive Integration of Single-Cell Data. *Cell* **177**, 1888-1902.e21 (2019).
29. Pinto Alexander R. *et al.* Revisiting Cardiac Cellular Composition. *Circulation Research* **118**, 400–409 (2016).
30. Mourik, J. A. van, Leeksma, O. C., Reinders, J. H., Groot, P. G. de & Zandbergen-Spaargaren, J. Vascular endothelial cells synthesize a plasma membrane protein indistinguishable from the platelet membrane glycoprotein IIa. *J. Biol. Chem.* **260**, 11300–11306 (1985).
31. Farbehi, N. *et al.* Single-cell expression profiling reveals dynamic flux of cardiac stromal, vascular and immune cells in health and injury. *eLife* **8**,.
32. Yuan, S.-M. α-Smooth Muscle Actin and ACTA2 Gene Expressions in Vasculopathies. *Braz J Cardiovasc Surg* **30**, 644–649 (2015).
33. Wu, C.-F. *et al.* Transforming Growth Factor β-1 Stimulates Profibrotic Epithelial Signaling to Activate Pericyte-Myofibroblast Transition in Obstructive Kidney Fibrosis. *Am J Pathol* **182**, 118–131 (2013).
34. Lin, S.-L., Kisseleva, T., Brenner, D. A. & Duffield, J. S. Pericytes and perivascular fibroblasts are the primary source of collagen-producing cells in obstructive fibrosis of the kidney. *Am. J. Pathol.* **173**, 1617–1627 (2008).

35. Hesp, Z. C. *et al.* Proliferating NG2-Cell-Dependent Angiogenesis and Scar Formation Alter Axon Growth and Functional Recovery After Spinal Cord Injury in Mice. *J. Neurosci.* **38**, 1366–1382 (2018).
36. Fu, X. *et al.* Specialized fibroblast differentiated states underlie scar formation in the infarcted mouse heart. *J Clin Invest* **128**, 2127–2143 (2018).
37. Zhou, Y. *et al.* Metascape provides a biologist-oriented resource for the analysis of systems-level datasets. *Nat Commun* **10**, 1523 (2019).

CHAPTER 3

Isolation of Cardiac Pericytes Without Any Previously Established Markers

ABSTRACT

The vascular system is critical for the delivery of oxygen and nutrients to all organs of the body. Within the vessels that make up this circulatory network, pericytes are a subset of mural cells that function to maintain vessel integrity and regulate contraction in the microvasculature. Despite their importance to vascular health, there have been challenges to studying this cell type in a collective manner. For one, there appears to be heterogeneity between pericytes of different organs as well as in pericytes within the same organ. Therefore, using previously established markers may not accurately label the entire pericyte population. This has made it difficult to view previously published data regarding the function and the role of pericytes in a holistic manner. To circumvent this, we sought to identify a method to enrich for the entire pericyte population in the murine heart for future downstream analysis. To do this, we developed a protocol using cell filtration, transgenic mice, and FACS to exclude other cardiac cell types. We then took advantage of recent developments in single cell transcriptomics to observe the heterogeneity of the enriched cells, which were majority cardiac pericytes. As we expected, the expression of commonly used markers did not encompass all of the pericytes in our data, supporting that this population is quite heterogeneous. This protocol was also applied to mice that had undergone myocardial infarction, demonstrating the utility of our protocol to study cardiac pericytes in injury. We believe that our results can provide a foundation for identification of novel markers and other future studies on this cell population.

INTRODUCTION

The vascular system is composed of blood vessels that play a crucial role in the delivery of oxygen and nutrients to various organs[1]. The walls of blood vessels are made up of two cell types: 1) endothelial cells that line the vessel walls and 2) mural cells – smooth muscle cells or pericytes – that directly associate with endothelial cells. While both smooth muscle cells and pericytes have similar functions in regulating blood flow and maintaining vessel integrity, these cells are still distinct from one another[2]. Smooth muscle cells typically reside in the tunica media of larger vessels and form multiple layers that wrap around the endothelial cells, but pericytes have small cell bodies with cellular projections that are embedded within the basement membrane of the microvasculture[1,3]. In recent years, pericytes have begun to garner attention due to their functions in regulating angiogenesis and potentially responding to ischemic injury[4,5]. Loss of pericyte-endothelial cell interactions or aberrant pericyte behavior has been associated with a variety of diseases, including diabetic retinopathy and tumor angiogenesis[4,6,7]. However, it has been a challenge to study this cell type as they are mainly defined by their morphological characteristics and anatomical location. To-date, there lacks a marker that can be used to specifically identify and isolate this cell type for further studies due to the high level of heterogeneity within the population. This has prevented in-depth studies on pericyte function in injury and whether they can be therapeutically targeted.

There have been several markers used to target these cells in various studies. Some of the most common markers to singly label pericytes include chondroitin sulfate proteoglycan 4 (NG2)[8], platelet-derived growth factor receptor-β (PDGFRβ)[9], CD146[10], regulator of G-protein signaling 5 (RGS5)[11], and Notch3[12]. NG2 is a transmembrane proteoglycan that has been shown to be necessary for pericyte recruitment to endothelial cells during angiogenesis[13–15]. CD146 is a junctional protein that has also been shown to be expressed on endothelial cells and may participate in promoting pathological angiogenesis via the VEGF/VEGFR2 pathway[16]. PDGFRβ

is a tyrosine kinase receptor that mitigates platelet-derived growth factor signaling which, depending on the external stimuli, can participate in a multitude of cellular functions such as survival, proliferation, and cellular differentiation[17]. Loss of RGS5 has been reported to lead to vascular leakage, suggesting that this G protein-coupled receptor modulator plays a role in pericyte-endothelial interactions[18]. Notch3 plays an important role in pericyte development and Notch deficiency results in loss of vessel stability[19]. Despite the number of studies using these markers, their specificity appears to depend on the organ of interest[6]. Additionally, the use of a single marker may only label a subpopulation of pericytes that have a distinct role in homeostasis and disease. Therefore, several studies use panels of markers to exclude other cell types and purify for the pericyte population[10,20]. This process can involve using more than one of the markers listed above or including negative selection markers to exclude other cell types. However, the use of different marker panels makes it difficult to review the previous studies regarding pericytes in a collective manner and apply the findings from one organ to another. There is a need to properly characterize this heterogeneous population of cells in an organ-specific manner to develop a common foundation for future studies.

With the advent of technologies to examine a population of cells at a single cell resolution, studies on heterogeneous cell types have become recently possible. Notably, single cell RNA-sequencing (scRNA-seq) has become an accessible technique to analyze the transcriptomic profiles of thousands of cells[21,22]. We sought to harness this technology to dissect the heterogeneity of pericytes in the murine heart. However, when we observed a publicly available dataset of scRNA-seq of the whole murine heart, the enrichment of pericytes was very low. We thus aimed to develop a protocol to enrich for pericytes prior to downstream analysis via scRNA-seq. While this could be done using any of the markers discussed, there was concern that utilizing any combination of markers could result in capturing only a subpopulation of cardiac pericytes. Therefore, we developed a protocol that could enrich for pericytes in the murine heart without

using any specific markers. This protocol could be applied to healthy and injured hearts, thus developing a foundation for future studies on the heterogeneity of this cell population and their functional roles under different conditions.

RESULTS

Single cell RNA-sequencing of the whole heart results in low enrichment of pericytes

With the plethora of scRNA-seq data that has been published, we first sought to identify publicly available databases that would include cardiac pericytes. The Tabula Muris is a collection of single cell transcriptomic data spanning multiple organs from mice[23]. When we looked at expression of pericyte markers in the hearts collected by this consortium, we saw that there was very low enrichment of pericytes in these data (cluster 6) **(Figure 1A-B)**. This data demonstrated that conducting scRNA-seq on the whole heart would yield a low percentage of pericytes. Therefore, there was a need to develop a way to enrich for pericytes to capture more of these cells for further downstream analysis.

Exclusion of other cardiac cells can enrich for cardiac pericytes

While there are several pericyte markers being used in other studies, the heterogeneity of the cell population questions whether the findings of these studies may only be applicable to a subpopulation of pericytes. We aimed to address this issue by enriching for cardiac pericytes prior to scRNA-seq without using any known markers. We optimized a protocol that consisted of excluding other major cardiac cell types, included cardiomyocytes, fibroblasts, endothelial cells, immune cells, vascular smooth muscle cells, and cardiac neurons. We generated a double transgenic mouse by crossing *Myh6*$^{GFP/+}$ mice with *Col1a1*$^{GFP/+}$ to label the majority of cardiomyocytes and fibroblasts with GFP[24,25] **(Figure 2A)**. After digesting the hearts from *Myh6*$^{GFP/+}$;*Col1a1*$^{GFP/+}$ adult mice into single cells, the cell suspension was passed through a 70μm filter to exclude larger cells such smooth muscle and neurons. The cells were treated with calcein-

AM[26] for viability and stained with antibodies targeting endothelial cells (CD31)[27] , erythrocytes (Ter119)[28], leukocytes (CD11b)[29] and other hematopoietic cells (CD45)[30]. Cells that were positive for calcein-AM, but negative for all other markers (i.e. GFP, CD31, CD45, Ter119, and CD11b) were sorted **(Figure 2B-C)**. RT-qPCR confirmed that this population had high expression of pericyte markers and minimal expression of other cell type markers **(Figure 2D)**. The cells were also cytospun and stained, confirming protein expression of pericyte markers **(Figure 2E)**. Using this protocol, we were able to enrich for cardiac pericytes in a manner that can be used for downstream scRNA-seq.

Single cell RNA-sequencing of enriched pericyte population

Cells were collected in the protocol described above and subjected to scRNA-seq through the 10x Genomics capture platform[22]. We sequenced a total of 5972 cells that formed unique clusters on the uniform manifold approximation and projection (UMAP) plot[31] **(Figure 3B)**. By looking at the expression of various cell type markers, we could identify clusters of cells that corresponded to fibroblasts (*Pdgfra*+)[32], cardiomyocytes (*Tnnt2*+)[33], and Schwann cells (*Plp1*+)[34] **(Figure 3C)**. There were very few endothelial cells or macrophages, suggesting that antibody-based exclusion is more reliable than fluorescent labeling by transgenic mice **(Figure 3C)**. Also, unlike the previously published scRNA-seq data on whole heart samples, the largest cluster in our data was enriched for pericyte markers *Cspg4, Mcam, Pdgfrb, Rgs5,* and *Notch3* **(Figure 3D)**. We subset the 2818 cells from this pericyte cluster and observed the distribution of pericyte marker expression. Of 2818 total cells, only 110 expressed all five markers, and the rest expressed varying combinations of these markers **(Figure 3D)**. These results further support that cardiac pericytes are a heterogeneous population and that individual markers may only be marking specific subpopulations of pericytes.

Single cell RNA-sequencing of enriched pericytes after myocardial infarction

Myocardial infarction (MI) is an acute ischemic injury to the heart that results in cardiomyocyte death and the development of fibrotic tissue[35]. As pericytes have been associated with participating in the ischemic injury response in other organs[5,36], we wondered if our enrichment protocol could be applied to hearts that had undergone MI. *Myh6*$^{GFP/+}$;*Col1a1*$^{GFP/+}$ adult mice underwent MI by permanent ligation of the left anterior descending artery and the hearts were collected 7 days later. Pericytes were collected from these hearts using the enrichment protocol and subjected to scRNA-seq. The two sets of cells were merged together for analysis **(Figure 4A)**. The largest cluster of cells was enriched in pericyte markers and was subset out for further analysis **(Figure 4B-C)**. As the pericytes formed 3 unique clusters **(Figure 4C)**, we were curious as to whether any of the clusters were representative of "pro-fibrotic" pericytes. We first looked at the percentage of cells from uninjured and injured hearts that make up each cluster. After injury, there was significant expansion of cells in cluster 3 **(Figure 4D)** and the majority of cells that made up cluster 3 were derived from the injured hearts **(Figure 4E)**. Pericytes in cluster 3 had high enrichment of genes associated with wound healing, extracellular matrix (ECM) proteins and response to ischemia **(Figure 4F, Supplementary Table 1)**. These results strongly suggest that pericytes found in cluster 3 may be pericytes that are responsive to MI.

When looking at highly expressed genes in cluster 3, we identified the gene *Vtn*, which encodes for vitronectin (VTN). VTN is a glycoprotein that binds to components within the ECM, such as collagens[37]. The expression of *Vtn* was specific to cluster 3 of pericytes **(Figure 5A)**, suggesting that its expression is associated with the injury response by pericytes. Immunofluorescence staining for VTN in hearts 7 days post-MI confirmed that expression was specific to the fibrotic area (data not shown) and was co-expressed with the pericyte marker PDGFRβ **(Figure 5B)**. These results suggest that VTN may be a promising target for observing pro-fibrotic pericytes.

DISCUSSION

Cardiac pericytes are an understudied cell population that have been difficult to characterize in-depth, due to the lack of specific markers for identifying and isolating these cells. Markers used in other organ systems either label other cell types or only label a subpopulation of pericytes in the heart. In order to conduct analysis on the heterogeneity of cardiac pericytes while including the entire population, we sought to develop a protocol that could enrich for pericytes for scRNA-seq. By excluding other major cell types using a combination of transgenic mice, cell filtration, and FACS, we optimized a protocol in which pericytes could be highly enriched. We took this enriched population, conducted scRNA-seq and was able to capture a high number of pericytes in our data. When we looked at expression of commonly used pericyte markers and could see that the expression of each marker varied within this population, supporting that this is a heterogeneous cell type. This protocol could also be applied to hearts that had undergone MI, allowing for studies on pericyte subpopulations and their roles in cardiac injury. By using scRNA-seq, we identify a cluster of pericytes that express genes associated with wound healing., ECM proteins, and response to ischemia. This cluster was highly specific in its expression of VTN and the expression of VTN was found to be specific to the fibrotic areas of the heart. Overall, our data provides a foundation for future studies on cardiac pericyte markers and function in injury.

Though the protocol we have developed can be useful in future studies of cardiac pericytes, there are several limitations to its widespread use. One, our protocol uses transgenic mice to label cardiomyocytes and fibroblasts, limiting the use of this protocol with other transgenic mouse models. In order to apply this protocol to other strains of mice, one would have to modify the protocol to somehow exclude these two major cell types. Two, as seen from the scRNA-seq data, the purity of pericytes collected using our protocol is not very high. There is still a significant number of other cell types that could be seen in the UMAP plot. Because we utilized a technique to look at single cells, we were able to exclude extraneous cells and focus on the pericytes. However, using this protocol for other types of bulk analysis would have to be considered carefully,

as other cell types may contaminate downstream analysis. Though there are limitations to our developed protocol, the data that we receive can still be utilized in other studies, particularly in the identification of novel markers.

METHODS

Public Databases

Single cell RNA-sequencing data of whole murine heart was downloaded from the Tabula Muris compendium[23] (https://tabula-muris.ds.czbiohub.org/) and processed using Seurat[38].

Mice and Myocardial Infarction

Myh6$^{GFP/+}$ mice were purchased from Jackson Laboratory and *Col1a1*$^{GFP/+}$ mice were provided from the Sylvia Evans lab. Adult (2-3 months old) male and female mice were used in all experiments. There were no sex-related differences in our data.

To induce myocardial infarction, mice were first anesthetized by injection of ketamine/Xylazine. Throughout the surgery, the mice were intubated for positive pressure ventilation with a mixture of oxygen and 2-3% isoflurane. Left thoracotomy between the fourth and fifth rib was conducted, and the pericardium was opened. An 8-0 suture was placed around the left anterior descending artery and tightened to simulate myocardial infarction. The chest was then closed by using 5-0 Vicryl suture and ventilation was maintained until sufficient spontaneous breathing. 0.1mg/kg buprenorphine and 5mg/kg carprofen was provided immediately after the surgery and the mice were left to recover in a temperature-controlled chamber until they were fully mobile. All procedures were carried out with the approval of the University of California, Los Angeles Animal Research Committee.

Fluorescence-Activated Cell Sorting (FACS)

Mice were injected with heparin 20 minutes prior to euthanasia by isoflurane. The hearts were dissected out, cannulated, and perfused with 20mL of Phosphate-buffered saline (PBS) followed by 5 mL of warmed digestion enzyme (PBS with Collagenase II, Dispase I, and DNase). The hearts were then chopped into small pieces and incubated in digestion enzyme at 37°C for an hour with periodic pipetting to ensure complete digestion. The digested cells were then filtered through a 70μm filter, centrifuged, and resuspended in cold PBS for debris removal. The Debris Removal Kit (Miltenyi) was used as per manufacturer's instructions. Afterwards, the cells were treated with calcein-AM (Thermo Fisher Scientific) and then stained with anti-CD31-PE-Cy7, anti-CD11b-PE-Cy7, anti-Ter119-PE-Cy7, and anti-CD45-PE-Cy7 antibodies diluted in FACS buffer for 30 minutes at room temperature. Cells were then washed and resuspended in FACS buffer for sorting on an BD FACSAria sorter. For downstream RT-qPCR, cells were collected in TRIzol™ LS Reagent (Thermo Fisher Scientific) and for downstream scRNA-seq, cells were collected in DMEM media + 10%FBS without calcium.

RNA Extraction and Real-Time qPCR (RT-qPCR)

Cells in TRIzol™ LS Reagent (Thermo Fisher Scientific) after sorting were stored in -80°C. After thawing, RNA was extracted by a series of chloroform additions and isopropanol precipitation. RNA quality and quantity were measured by NanoDrop™ (Thermo Fisher Scientific). RNA was then reverse transcribed into cDNA by using an iScript™ cDNA Synthesis Kit (Bio-Rad) and following the manufacturer's instructions. RT-qPCR reactions were prepared with SYBR Green Master Mix (Bio-Rad) and primers designed for each target gene **(Suppelementary Table 2)**. The reactions were run on a CFX96 Touch™ Real-Time PCR Detection System (Bio-Rad) and analysis was done via the double ΔCT method.

Cytospinning

Cells were sorted as described above into PBS containing EDTA and centrifuged in a Cytospin™ 4 Cytocentrifuge (Thermo Fisher Scientific) at 800rpm for 4 minutes. Cells were spun onto Colorfrost Plus microscope slides (Fisher) and fixed with 4% paraformaldehyde (PFA).

Immunofluorescence staining

Murine hearts were dissected after injection with heparin and proper euthanasia. The hearts were perfused with PBS, fixed with 4% PFA overnight, and incubated in 30% sucrose for another day. The tissues were embedded in Optimal cutting temperature compound and sectioned into 8μm thick sections using a Leica cryostat. Sections were mounted on Colorfrost Plus microscope slides (Fisher) and stored at -20°C until stained.

For staining, slides were washed with PBS and incubated with 0.25%TritonX-100 to permeabilize. Cytospun cells were not permeabilized. Slides were then incubated in blocking buffer (10% goat serum in PBS-0.1%Tween) for 1 hour at room temperature. Slides were then incubated with primary antibodies (overnight at 4°C), washed, and then incubated with secondary antibodies (1 hour at room temperature). Antibodies and dilutions are presented in **Supplementary Table 3**. Coverslips were mounted with mounting medium containing DAPI (Vector). Slides were images using a Leica LEICACTR6500 microscope or a Zeiss LSM880 confocal microscope.

Single Cell RNA-sequencing Analysis

Enriched cardiac pericytes were sorted into DMEM media + 10%FBS without calcium and prepared for single cell RNA-sequencing using the 10x Genomics Chromium Controller. Libraries were prepared using the Chromium Single Cell 3' GEM, Library & Gel Bead Kit, v2 and sequenced on Nextseq 500 sequencer (Illumina). Data was processed through the Cell Ranger pipeline (10x) and analyzed using Seurat[38].

Figure 1

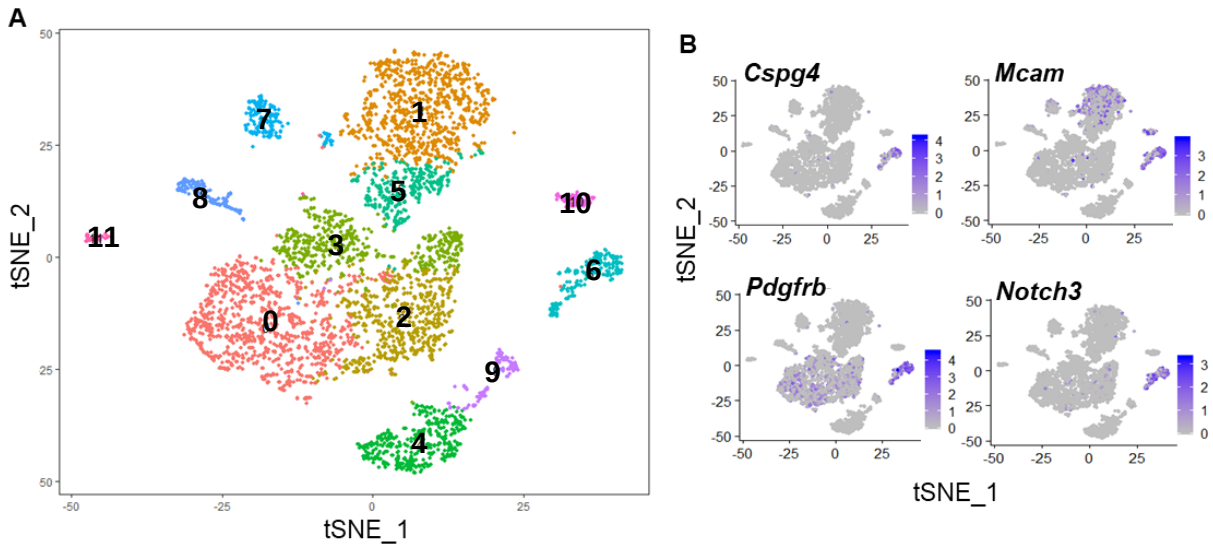

Figure 1: Single cell RNA-sequencing of the whole heart results in low enrichment of cardiac pericytes

(A) T-distributed Stochastic Neighbor Embedding (tSNE) plot of sorted murine heart cells downloaded from the Tabula Muris compendium. **(B)** Expression of pericyte markers is limited to cluster 6, which is a very small percentage of total cells.

Figure 2

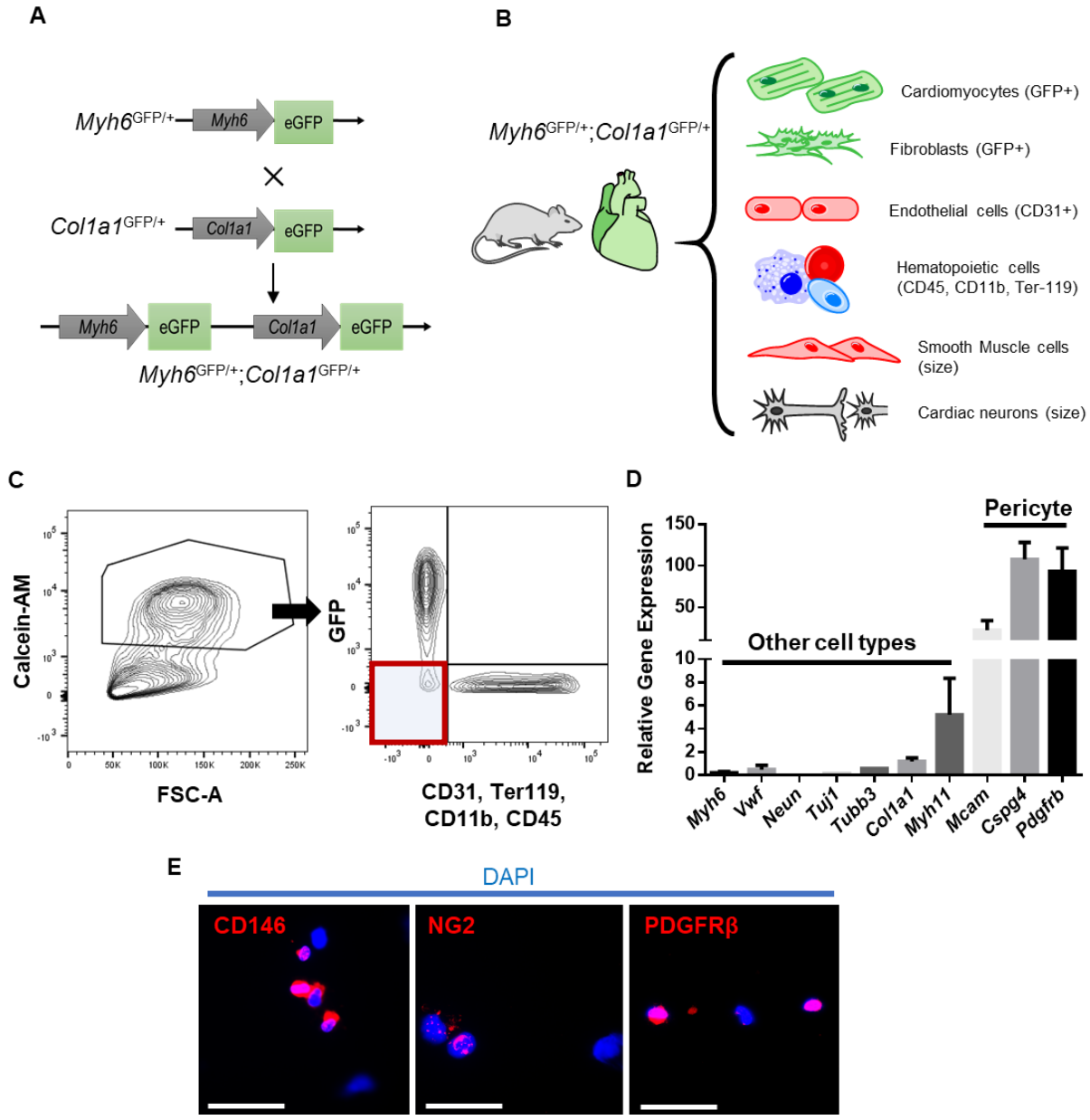
A
Myh6GFP/+
Myh6
eGFP
Col1a1GFP/+
Col1a1
eGFP
Myh6
eGFP
Col1a1
eGFP
Myh6GFP/+;Col1a1GFP/+
B
Myh6GFP/+;Col1a1GFP/+
Cardiomyocytes (GFP+)
Fibroblasts (GFP+)
Endothelial cells (CD31+)
Hematopoietic cells (CD45, CD11b, Ter-119)
Smooth Muscle cells (size)
Cardiac neurons (size)
C
Calcein-AM
FSC-A
GFP
CD31, Ter119, CD11b, CD45
D
Relative Gene Expression
Pericyte
Other cell types
Myh6
Vwf
Neun
Tuj1
Tubb3
Col1a1
Myh11
Mcam
Cspg4
Pdgfrb
E
DAPI
CD146
NG2
PDGFRβ

Figure 2: Exclusion-based approach to enrich for cardiac pericytes

(A) Breeding schematic for generating *Myh6*$^{GFP/+}$;*Col1a1*$^{GFP/+}$ mice. **(B)** Schematic describing the methods of excluding all of the different cardiac cell types to enrich for cardiac pericytes. **(C)** Representative FACS plots depicting the sort protocol. Calcein-AM+ cells were gated on and within the viable cells, the population that was negative for all markers was sorted for analysis (red box). **(D)** Gene expression profile of the cells collected after pericyte enrichment have high levels of expression of pericyte markers and have low levels of expression of other cell type markers. **(E)** After sorting, the cells were cytospun and stained for pericyte markers, confirming that collected cells are pericytes. DAPI was used to stain nuclei (blue). Scale bar: 20μm.

Figure 3

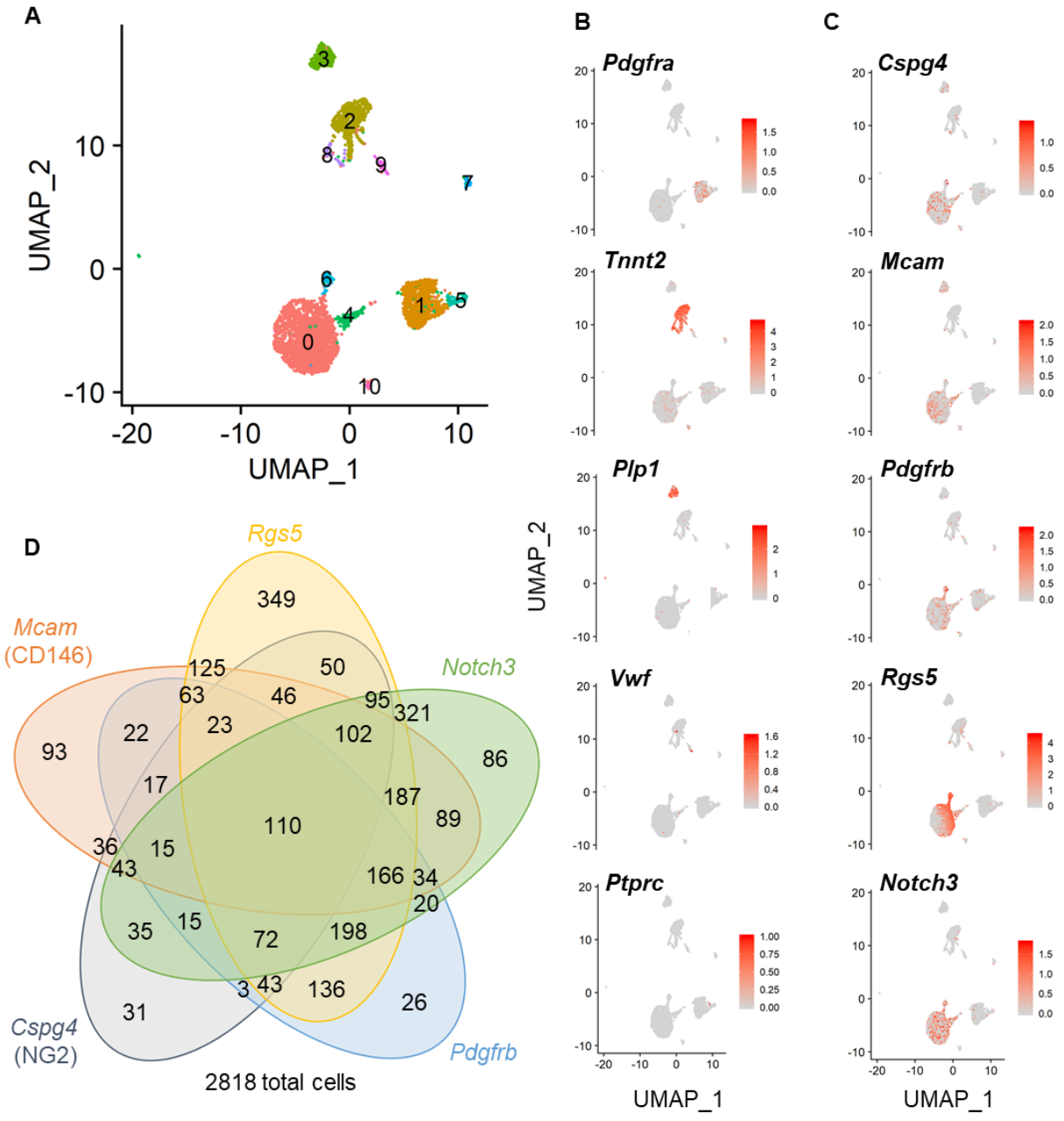
A
UMAP_2
UMAP_1
B
C
Pdgfra
Cspg4
Tnnt2
Mcam
Plp1
Pdgfrb
Vwf
Rgs5
Ptprc
Notch3
UMAP_2
UMAP_1
UMAP_1
D
Rgs5
Mcam
(CD146)
Notch3
Cspg4
(NG2)
Pdgfrb
2818 total cells

Figure 3: Single cell RNA-sequencing of enriched cardiac pericyte population confirms cellular heterogeneity

(A) UMAP plot of enriched cardiac pericyte population shows multiple clusters of cells that were sequenced. **(B) O**ther cell type markers can be used to identify cardiomyocytes, fibroblasts, glial cells, endothelial cells, and hematopoietic cells that made it through out enrichment protocol. **(C)** The largest cluster of cells express pericyte markers. **(D)** Venn diagram showing the heterogeneity of expression of the 5 pericyte markers. This suggests that studies that singly label pericytes may only be observing a subpopulation of the pericyte population.

Figure 4

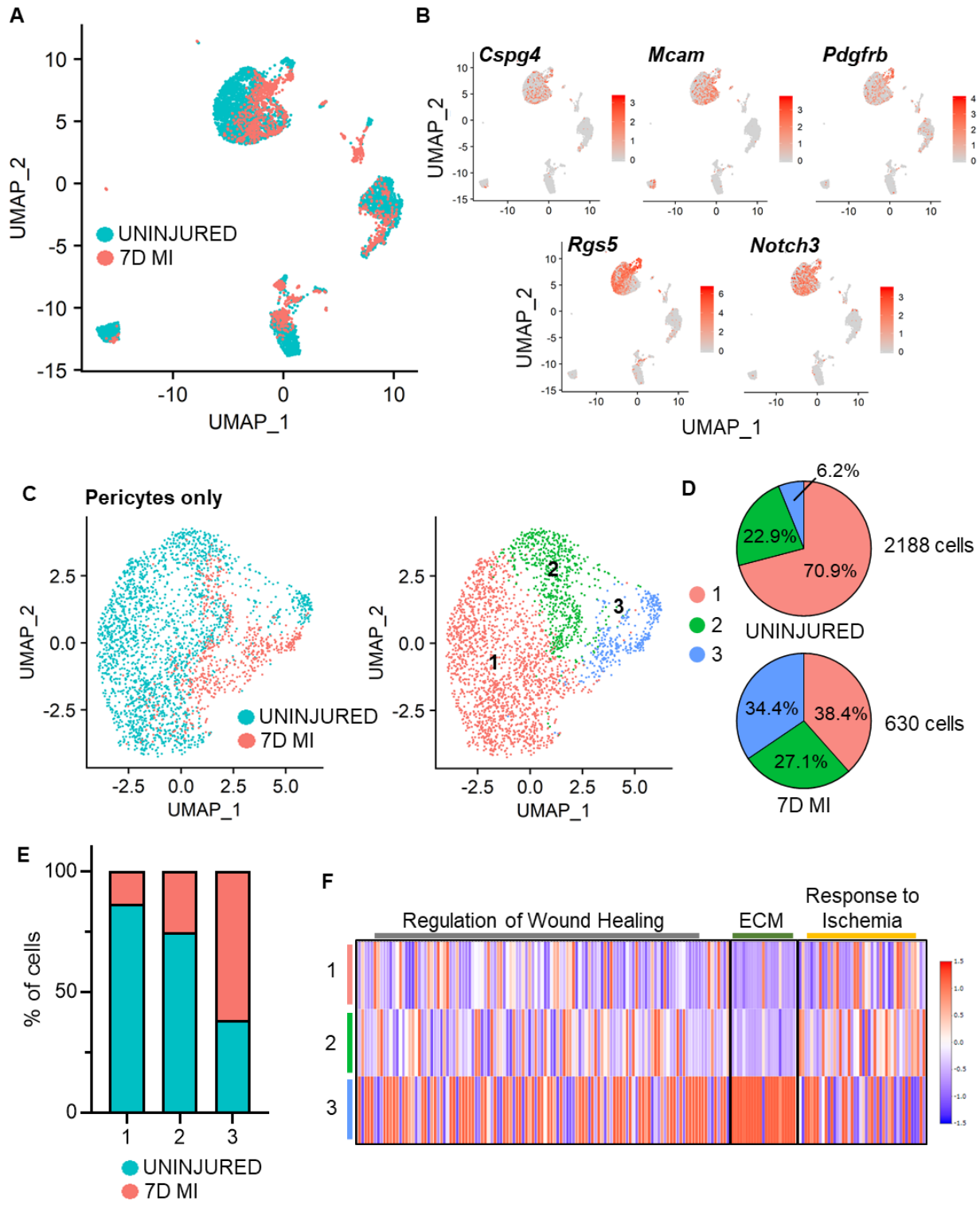
A
UMAP_2
UMAP_1
UNINJURED
7D MI
B
Cspg4
Mcam
Pdgfrb
Rgs5
Notch3
UMAP_2
UMAP_1
C
Pericytes only
UMAP_2
UMAP_1
UNINJURED
7D MI
1
2
3
D
6.2%
22.9%
70.9%
2188 cells
UNINJURED
34.4%
38.4%
27.1%
630 cells
7D MI
E
% of cells
UNINJURED
7D MI
F
Regulation of Wound Healing
ECM
Response to Ischemia

Figure 4: Identification of a pro-fibrotic subpopulation of cardiac pericytes

(A) UMAP of cells from uninjured hearts and hearts 7 days post-myocardial infarction (7DMI). **(B)** Pericyte marker expression across all cells that were sequenced. **(C)** Largest cluster that was enriched for pericyte markers were subset and re-analyzed, creating a new UMAP plot. The cells formed three unique clusters. **(D)** Of all the pericytes collected from uninjured and 7DMI, the distribution of these cells into each of the three clusters is shown. Between uninjured and 7DMI samples, there was an increase in the number of cells that fall into cluster 3 (blue). **(E)** Within the cells that make up each cluster, the percentage of cells that came from uninjured and 7DMI hearts are shown. Unlike cluster 1 and 2, cluster 3 is made up of mostly cells from 7DMI hearts. **(F)** Heatmap showing average expression of genes associated with wound healing, extracellular matrix (ECM) proteins, and response to ischemia in each cluster. Cluster 3 shows the highest enrichment of genes in all three categories, suggesting that this population may be responsive to injury.

Figure 5

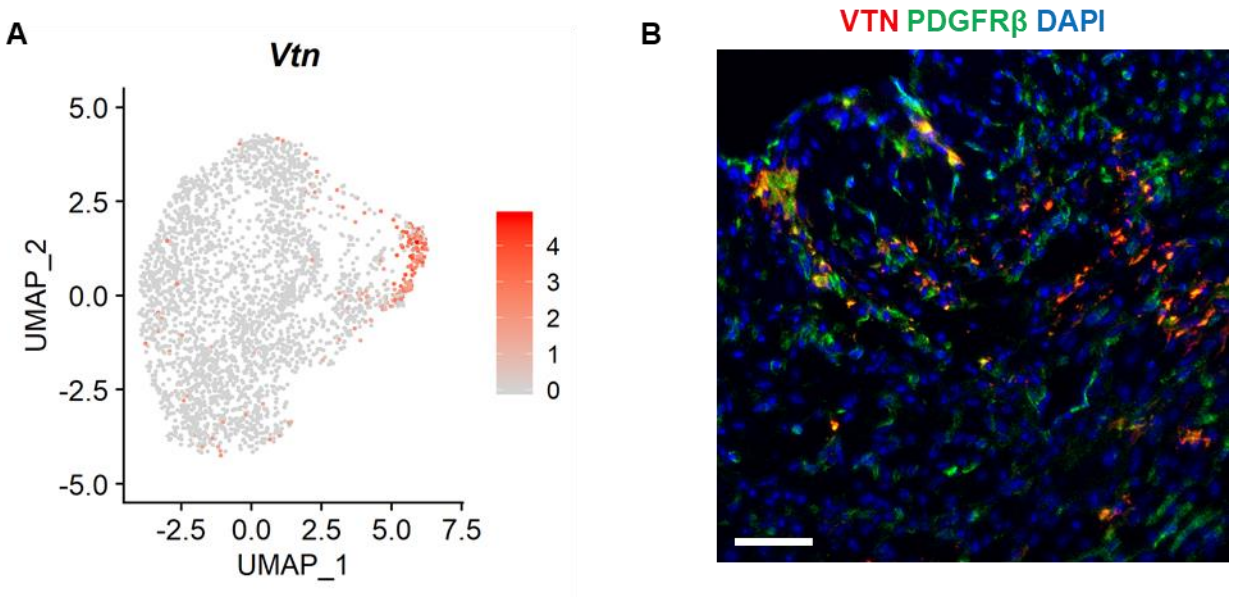

Figure 5: Vitronectin is upregulated in a pro-fibrotic subpopulation of cardiac pericytes

(A) *Vtn* expression across the pericyte cluster shows specific expression in cluster 3. **(B)** Staining for vitronectin (VTN) (red) and PDGFRβ (green) in the fibrotic area of hearts 7 days post-MI. DAPI was used to stain nuclei (blue). Scale bar: 50μm.

Supplementary Table 1

Heatmap Genes

Regulation of Wound Healing			ECM	Response to Ischemia	
Abat	*Foxc2*	*Serpinb2*	*Col12a1*	*Aifm1*	*Ppib*
Adamts10	*Gja1*	*Serpinc1*	*Col15a1*	*Bcl2*	*Ppic*
Adamts12	*Gja6*	*Serpine1*	*Col16a1*	*Camk2a*	*Rnls*
Adamts6	*Gsn*	*Serpine2*	*Col1a1*	*Camk2d*	*Uchl1*
Adra2a	*Hbegf*	*Serping1*	*Col1a2*	*Camk2g*	
Adrb2	*Hmgb1*	*Smad2*	*Col27a1*	*Camk2b*	
Alox12	*Hmgcr*	*Smad3*	*Col3a1*	*Cav1*	
Alox15	*Hopx*	*Sox12*	*Col4a1*	*Cib1*	
Ano3	*Hpse*	*Sox8*	*Col4a2*	*Cpeb4*	
Ano6	*Hras*	*Sox9*	*Col4a3*	*Cpeb2*	
Anxa1	*Kank1*	*Srsf4*	*Col4a4*	*Cpeb3*	
Anxa2	*Krt1*	*Srsf6*	*Col4a5*	*Eef2*	
Anxa5	*Lbh*	*Stab1*	*Col5a1*	*Eftud2*	
Apoe	*Lyn*	*Stx2*	*Col5a2*	*Eef2k*	
Arfgef1	*Mylk*	*Stxbp5*	*Col5a3*	*Eif4ebp1*	
Arfgef2	*Nfe2l2*	*Tc2n*	*Col6a1*	*Eif4ebp2*	
Avil	*Nos3*	*Tec*	*Col6a2*	*Fn1*	
C1qtnf1	*Pdgfa*	*Tgfbr2*	*Col6a3*	*Hk2*	
C1qtnf6	*Pdgfb*	*Thbd*	*Col8a1*	*Hk1*	
Capn1	*Pdgfra*	*Thbs1*	*Fbn1*	*Hyou1*	
Capn11	*Pdgfrb*	*Thbs3*	*Fbn2*	*Map2k6*	
Capn2	*Phldb2*	*Thbs4*	*Fn1*	*Map2k3*	
Capn3	*Plat*	*Tlr4*	*Tnc*	*Nek1*	
Cask	*Plau*	*Tnfaip3*		*Map3k5*	
Cav1	*Plaur*	*Tnfrsf12a*		*Map3k15*	
Cd109	*Plek*	*Txk*		*Map3k6*	
Cd34	*Ppard*	*Ubash3b*		*Mlycd*	
Cd36	*Prkca*	*Usf1*		*Nol3*	
Clasp1	*Prkcd*	*Vav1*		*Panx1*	
Clasp2	*Prkce*	*Vav2*		*Per2*	
Comp	*Prkcg*	*Vav3*		*Per1*	
Dpp4	*Prkch*	*Vegfb*		*Ppargc1a*	
Edn1	*Prkg1*	*Vil1*		*Ppif*	
Enpp4	*Prkg2*	*Vill*		*Ppih*	
F2r	*Pros1*	*Vps33b*		*Ppid*	
F3	*Ptger3*	*Vtn*		*Ppie*	
Fap	*Ptger4*	*Wfdc1*		*Ppig*	
Fcer1g	*Reg3g*	*Wnt4*		*Gm5160*	
Fgf2	*Rreb1*			*Nktr*	
Foxc1	*Scara5*			*Ppia*	

Supplementary Table 2

RT-qPCR Primers

Gene	Sequence
Myh6	F: 5'- ACATGAAGGAGGAGTTTGGG
	R: 5'- GCACTTGGAGCTGTAGGTCA
Vwf	F: 5'- GCTCCAGCAAGTTGAAGACC
	R: 5'- GCAAGTCACTGTGTGGCACT
Neun	F: 5'- ATCGTAGAGGGACGGAAAATTGA
	R: 5'- GTTCCCAGGCTTCTTATTGGTC
Tuj1	F: 5'- TAGACCCCAGCGGCAACTAT
	R: 5'- GTTCCAGGTTCCAAGTCCACC
Tubb3	F: 5'- TAGACCCCAGCGGCAACTAT
	R: 5'- GTTCCAGGTTCCAAGTCCACC
Col1a1	F: 5'- GCCAAGAAGACATCCCTGAAG
	R: 5'- TGTGGCAGATACAGATCAAGC
Myh11	F: 5'- CGGCAATGCGAAAACCGTC
	R: 5'- AGTGACATCGAAGTTGATGCG
Mcam	F: 5'- CCCAAACTGGTGTGCGTCTT
	R: 5'- GGAAAATCAGTATCTGCCTCTCC
Cspg4	F: 5'- GCTGTCTGTTGACGGAGTGTT
	R: 5'- CGGCTGATTCCCTTCAGGTAAG
Pdgfrb	F: 5'- TTCCAGGAGTGATACCAGCTT
	R: 5'- AGGGGGCGTGATGACTAGG
Gapdh	F: 5'- AGGTCGGTGTGAACGGATTTG
	R: 5'- TGTAGACCATGTAGTTGAGGTCA

Supplementary Table 3

Immunofluorescence Staining Antibodies

Target Protein	**Manufacturer (catalog no.)**	**Dilution**
NG2	Millipore Sigma (AB5320)	1:50
CD146	Abcam (ab75769)	1:100
PDGFRβ	Abcam (ab32570)	1:100
PDGFRβ	eBioscience (14-1402-82)	1:50
VTN	ABClonal (A1667)	1:50

REFERENCES

1. Bergers, G. & Song, S. The role of pericytes in blood-vessel formation and maintenance. *Neuro-oncology* **7**, 452–464 (2005).
2. Hughes, S. & Chan-Ling, T. Characterization of Smooth Muscle Cell and Pericyte Differentiation in the Rat Retina In Vivo. *Invest. Ophthalmol. Vis. Sci.* **45**, 2795–2806 (2004).
3. Bacakova, L. *et al.* The Role of Vascular Smooth Muscle Cells in the Physiology and Pathophysiology of Blood Vessels. *Muscle Cell and Tissue - Current Status of Research Field* (2018) doi:10.5772/intechopen.77115.
4. Birbrair, A. *et al.* Type-2 pericytes participate in normal and tumoral angiogenesis. *Am. J. Physiol., Cell Physiol.* **307**, C25-38 (2014).
5. Birbrair, A. *et al.* Type-1 pericytes accumulate after tissue injury and produce collagen in an organ-dependent manner. *Stem Cell Res Ther* **5**, 122 (2014).
6. Armulik, A., Genové, G. & Betsholtz, C. Pericytes: developmental, physiological, and pathological perspectives, problems, and promises. *Dev. Cell* **21**, 193–215 (2011).
7. Hammes, H.-P. *et al.* Pericytes and the Pathogenesis of Diabetic Retinopathy. *Diabetes* **51**, 3107–3112 (2002).
8. Stallcup, W. B. The NG2 Proteoglycan in Pericyte Biology. *Adv. Exp. Med. Biol.* **1109**, 5–19 (2018).
9. Winkler, E. A., Bell, R. D. & Zlokovic, B. V. Pericyte-specific expression of PDGF beta receptor in mouse models with normal and deficient PDGF beta receptor signaling. *Mol Neurodegener* **5**, 32 (2010).
10. Crisan, M. *et al.* A Perivascular Origin for Mesenchymal Stem Cells in Multiple Human Organs. *Cell Stem Cell* **3**, 301–313 (2008).
11. Cho, H., Kozasa, T., Bondjers, C., Betsholtz, C. & Kehrl, J. H. Pericyte-specific expression of Rgs5: implications for PDGF and EDG receptor signaling during vascular maturation. *FASEB J.* **17**, 440–442 (2003).

12. Lovschall, H., Mitsiadis, T. A., Poulsen, K., Jensen, K. H. & Kjeldsen, A. L. Coexpression of Notch3 and Rgs5 in the pericyte-vascular smooth muscle cell axis in response to pulp injury. *Int. J. Dev. Biol.* **51**, 715–721 (2007).
13. Fukushi, J., Makagiansar, I. T. & Stallcup, W. B. NG2 proteoglycan promotes endothelial cell motility and angiogenesis via engagement of galectin-3 and alpha3beta1 integrin. *Mol. Biol. Cell* **15**, 3580–3590 (2004).
14. A, N., Kj, D., Jt, P., Sr, J. & Wb, S. The primary structure of NG2, a novel membrane-spanning proteoglycan. *J Cell Biol* **114**, 359–371 (1991).
15. Ozerdem, U. & Stallcup, W. B. Pathological angiogenesis is reduced by targeting pericytes via the NG2 proteoglycan. *Angiogenesis* **7**, 269–276 (2004).
16. Zeng, Q. *et al.* Impaired tumor angiogenesis and VEGF-induced pathway in endothelial CD146 knockout mice. *Protein Cell* **5**, 445–456 (2014).
17. Sweeney, M. D., Ayyadurai, S. & Zlokovic, B. V. Pericytes of the neurovascular unit: key functions and signaling pathways. *Nat. Neurosci.* **19**, 771–783 (2016).
18. Özen, I. *et al.* Loss of Regulator of G-Protein Signaling 5 Leads to Neurovascular Protection in Stroke. *Stroke* **49**, 2182–2190 (2018).
19. Kofler, N. M., Cuervo, H., Uh, M. K., Murtomäki, A. & Kitajewski, J. Combined deficiency of Notch1 and Notch3 causes pericyte dysfunction, models CADASIL and results in arteriovenous malformations. *Scientific Reports* **5**, 1–13 (2015).
20. Lee, L. L., Khakoo, A. Y. & Chintalgattu, V. Isolation and Purification of Murine Cardiac Pericytes. *J Vis Exp* (2019) doi:10.3791/59571.
21. Hwang, B., Lee, J. H. & Bang, D. Single-cell RNA sequencing technologies and bioinformatics pipelines. *Experimental & Molecular Medicine* **50**, 1–14 (2018).
22. Zheng, G. X. Y. *et al.* Massively parallel digital transcriptional profiling of single cells. *Nature Communications* **8**, 1–12 (2017).

23. Schaum, N. *et al.* Single-cell transcriptomics of 20 mouse organs creates a Tabula Muris. *Nature* **562**, 367–372 (2018).
24. Ieda, M. *et al.* Direct Reprogramming of Fibroblasts into Functional Cardiomyocytes by Defined Factors. *Cell* **142**, 375–386 (2010).
25. Moore-Morris, T. *et al.* Resident fibroblast lineages mediate pressure overload-induced cardiac fibrosis. *J. Clin. Invest.* **124**, 2921–2934 (2014).
26. Bratosin, D., Mitrofan, L., Palii, C., Estaquier, J. & Montreuil, J. Novel fluorescence assay using calcein-AM for the determination of human erythrocyte viability and aging. *Cytometry Part A* **66A**, 78–84 (2005).
27. Mourik, J. A. van, Leeksma, O. C., Reinders, J. H., Groot, P. G. de & Zandbergen-Spaargaren, J. Vascular endothelial cells synthesize a plasma membrane protein indistinguishable from the platelet membrane glycoprotein IIa. *J. Biol. Chem.* **260**, 11300–11306 (1985).
28. Kina, T. *et al.* The monoclonal antibody TER-119 recognizes a molecule associated with glycophorin A and specifically marks the late stages of murine erythroid lineage. *Br. J. Haematol.* **109**, 280–287 (2000).
29. Kubo, N., Boisvert, W. A., Ballantyne, C. M. & Curtiss, L. K. Leukocyte CD11b expression is not essential for the development of atherosclerosis in mice. *J. Lipid Res.* **41**, 1060–1066 (2000).
30. Nakano, A., Harada, T., Morikawa, S. & Kato, Y. Expression of leukocyte common antigen (CD45) on various human leukemia/lymphoma cell lines. *Acta Pathol. Jpn.* **40**, 107–115 (1990).
31. McInnes, L., Healy, J. & Melville, J. UMAP: Uniform Manifold Approximation and Projection for Dimension Reduction. *arXiv:1802.03426 [cs, stat]* (2018).
32. Pinto Alexander R. *et al.* Revisiting Cardiac Cellular Composition. *Circulation Research* **118**, 400–409 (2016).

33. Wu, B. *et al.* Inducible Cardiomyocyte-Specific Gene Disruption Directed by the Rat Tnnt2 Promoter in the Mouse. *Genesis* **48**, 63–72 (2010).
34. Farbehi, N. *et al.* Single-cell expression profiling reveals dynamic flux of cardiac stromal, vascular and immune cells in health and injury. *eLife* **8**,.
35. Talman, V. & Ruskoaho, H. Cardiac fibrosis in myocardial infarction—from repair and remodeling to regeneration. *Cell Tissue Res* **365**, 563–581 (2016).
36. Lin, S.-L., Kisseleva, T., Brenner, D. A. & Duffield, J. S. Pericytes and perivascular fibroblasts are the primary source of collagen-producing cells in obstructive fibrosis of the kidney. *Am. J. Pathol.* **173**, 1617–1627 (2008).
37. Schvartz, I., Seger, D. & Shaltiel, S. Vitronectin. *Int. J. Biochem. Cell Biol.* **31**, 539–544 (1999).
38. Stuart, T. *et al.* Comprehensive Integration of Single-Cell Data. *Cell* **177**, 1888-1902.e21 (2019).

CHAPTER 4

Genetic Regulation of Fibroblast Activation and Proliferation in Cardiac Fibrosis

Genetic Regulation of Fibroblast Activation and Proliferation in Cardiac Fibrosis

Shuin Park, BS*[1, 2, 3]; Sara Ranjbarvaziri, PhD*[1, 2, 3]; Fides D. Lay, PhD[2, 4,]; Peng Zhao, MD, PhD[1, 2]; Mark J. Miller, BA[1, 2]; Jasmeet S. Dhaliwal[1, 2]; Adriana Huertas-Vazquez, PhD[1]; Xiuju Wu, MD, PhD[1]; Rong Qiao, MD[1, 2]; Justin M. Soffer, BS[1, 2]; Hanna K.A. Mikkola, MD, PhD[2, 4, 6]; Aldons J. Lusis, PhD[1, 5, 6, 7]; Reza Ardehali, MD, PhD[#1, 2, 3, 6]

[1]Division of Cardiology, Department of Medicine, David Geffen School of Medicine, University of California, Los Angeles, CA

[2]Eli and Edythe Broad Center of Regenerative Medicine and Stem Cell Research, University of California, Los Angeles, CA

[3]Molecular, Cellular, and Integrative Physiology Graduate Program, University of California, Los Angeles, CA

[4]Department of Molecular, Cell, and Developmental Biology, University of California, Los Angeles, CA

[5]Department of Microbiology, Immunology and Molecular Genetics, University of California, Los Angeles, CA

[6]Molecular Biology Institute, University of California, Los Angeles, CA

[7]Department of Human Genetics, University of California, Los Angeles, CA

*These authors contributed equally to this article.

#corresponding author

DISCLOSURES

None

ABSTRACT

Background: Genetic diversity and the heterogeneous nature of cardiac fibroblasts (CFbs) have hindered characterization of the molecular mechanisms that regulate cardiac fibrosis. The Hybrid Mouse Diversity Panel (HMDP) offers a valuable tool to examine genetically diverse cardiac fibroblasts and their role in fibrosis.

Methods: Three strains of mice (C57BL/6J, C3H/HeJ, and KK/HlJ) were selected from the HMDP and treated with either isoproterenol (ISO) or saline by an intraperitoneally implanted osmotic pump. After 21 days, cardiac function and levels of fibrosis were measured by echocardiography and trichrome staining, respectively. Activation and proliferation of CFbs were measured by *in vitro* and *in vivo* assays under normal and injury conditions. RNA-sequencing was done on isolated CFbs from each strain and results were analyzed by Ingenuity Pathway Analysis (IPA) and validated by reverse transcription-qPCR, immunohistochemistry, and ELISA.

Results: ISO treatment in C57BL/6J, C3H/HeJ, and KK/HlJ mice resulted in minimal, moderate, and extensive levels of fibrosis, respectively (n = 7-8 hearts/condition). Isolated CFbs treated with ISO exhibited strain-specific increases in the levels of activation but showed comparable levels of proliferation. Similar results were found *in vivo*, with fibroblast activation, and not proliferation, correlating with the differential levels of cardiac fibrosis after ISO treatment. RNA-sequencing revealed that CFbs from each strain exhibit unique gene expression changes in response to ISO. We identified *Ltbp2* as a commonly upregulated gene after ISO treatment. Expression of LTBP2 was elevated and specifically localized in the fibrotic regions of the myocardium after injury in mice and in human heart failure patients.

Conclusions: This study highlights the importance of genetic variation in cardiac fibrosis by using multiple inbred mouse strains to characterize CFbs and their response to ISO treatment. Our data

suggest that, while fibroblast activation is a response that parallels the extent of scar formation, proliferation may not necessarily correlate with levels of fibrosis. Additionally, by comparing CFbs from multiple strains, we identified pathways as potential therapeutic targets and LTBP2 as a marker for fibrosis, with relevance to patients with underlying myocardial fibrosis.

INTRODUCTION

Acute myocardial injury or elevated pressure in the heart results in a multitude of cardiac pathologies, particularly cardiac fibrosis. It has been reported that such injury leads to activation and proliferation of cardiac fibroblasts (CFbs), some of which deposit excessive extracellular matrix (ECM) components that compromise myocardial structure and function[1, 2]. Despite the significant role that CFbs play in injury response, characterization of this cell type has been challenging due to their heterogeneous nature and lack of fibroblast-specific markers[2, 3]. Furthermore, detailed knowledge of the molecular mechanisms that regulate their specific contributions to scar development is lacking.

The Hybrid Mouse Diversity Panel (HMDP) is a collection of over 100 genotyped inbred strains of mice that allow for identification of genetic factors that contribute to various common disease traits[4]. In a comprehensive study by Rau et al., mice within the HMDP were phenotypically characterized following chronic treatment with isoproterenol (ISO), a β-adrenergic agonist [5]. Excessive stimulation of β-adrenergic receptors in the heart has been linked to increased CFb proliferation and collagen synthesis[5]. Chronic treatment of the HMDP with ISO resulted in a wide range of severity in cardiac hypertrophy and associated fibrosis across the different strains. These findings support the hypothesis that genetic variation influences the development and progression of cardiac dysfunction and pathological fibrosis. However, these studies evaluated changes at the cardiac tissue level and did not delineate the roles of specific cell types to each strain's respective phenotype.

In the present study, we utilized three HMDP strains with varying responses to ISO treatment to investigate the mechanisms by which their respective CFbs may regulate the process of cardiac fibrosis. We demonstrated that CFbs respond to ISO in a strain-specific manner both *in vitro* and *in vivo*. Notably, CFbs from all three strains exhibited significant differences in levels of

activation in response to ISO but had similar rates of proliferation. Additionally, we performed RNA-sequencing and identified various molecular pathways that were differentially enriched across the three strains in response to ISO. RNA-sequencing further unveiled genes that were commonly upregulated in CFbs from all three strains. Within these genes, we validated *Ltbp2* as a potential marker of fibrosis that can be applied to a genetically diverse population. Overall, our findings contribute to the understanding of cardiac fibroblast function in the context of ISO-induced cardiac fibrosis and further highlight the importance of genetic variation in complex diseases and cellular functions.

RESULTS

Pathological analysis of ISO-induced cardiac function and fibrosis in selected mouse strains

The entire HMDP was characterized at baseline and in response to ISO treatment to determine the extent of cardiac fibrosis **(Figure 1A)**. The survey revealed significant variations in cardiac pathophysiology and fibrosis under baseline conditions and in response to ISO administration[5, 6]. Based on this considerable variability, we selected three representative strains that exhibited distinct pathological phenotypes: C57BL/6J, C3H/HeJ, and KK/HIJ, showing minimal, moderate, and substantial myocardial fibrosis after ISO injury, respectively. Adult female mice (8-10 weeks, 20-28 grams) from each strain were intraperitoneally implanted with an Alzet micro-osmotic pump containing saline or ISO. Mice from all strains were of similar size **(Supplementary Figure IA)** and body weight (data not shown). Throughout the course of treatment, the mice did not display adverse physical symptoms in response to ISO. After 21 days of treatment, animals were sacrificed and hearts were harvested for analysis. Masson's trichrome staining demonstrated minimal to no visible fibrotic areas in all mice treated with saline **(Figure 1B)**. After ISO treatment, both C3H/HeJ and KK/HlJ hearts exhibited clear fibrotic areas (blue), while C57BL/6J hearts had minimal amounts of fibrosis. Consistent with the histological observations, quantitative analysis

of the fibrotic areas showed significant differences across the selected strains, with KK/HIJ hearts consistently exhibiting the greatest area of fibrosis in response to ISO (C57BL/6J: Saline=0.1±0.1% ISO=1.2±0.1%, C3H/HeJ: Saline=0.3±0.1% ISO=2.4±0.4%, KK/HlJ: Saline=0.3±0.1% ISO=6.4±0.7%) **(Figure 1C)**. Additionally, ISO treatment caused observable increases in heart size **(Supplementary Figure IB)** and heart weight/tibia length ratios **(Supplementary Figure IC)** in both KK/HIJ and C3H/HeJ strains, while C57BL/6J mice showed minimal signs of cardiac hypertrophy.

Functional echocardiography analysis demonstrated increased left ventricle end-diastolic dimension (EDD) and end-systolic dimension (ESD) in the C3H/HeJ and KK/HIJ strains 21 days after ISO treatment **(Supplementary Figure ID)**. Furthermore, these strains exhibited significant decreases in ejection fraction (C57BL/6J: Saline=+1.2±2.3% ISO=+0.15±3.13%, C3H/HeJ: Saline=+2.0±5.0% ISO=-15.9±5.2%, KK/HlJ: Saline=+2.2±3.2% ISO=-17.9±6.6%) **(Figure 1D)** and fractional shortening **(Supplementary Figure IE)** after ISO treatment. In contrast, C57BL/6J mice had preserved cardiac function in ISO-treated compared to saline-treated hearts **(Figure 1D and Supplementary Figure IE)**.

These results confirm that chronic β-adrenergic stimulation in different mouse strains leads to varying severity of cardiac fibrosis. These phenotypical differences were used to further characterize the contributions of CFbs to ISO-induced fibrosis.

***In vitro* characterization of strain-specific cardiac fibroblasts in response to ISO**

Based on the varying levels of fibrosis exhibited by the three selected strains, we focused on characterizing strain-specific CFbs and their potential role in generating the observed patterns of cardiac fibrosis. Initially, CFbs from each strain were isolated and cultured as described in the Methods[2]. While our isolation protocol does not purify the entire CFb population, it ensures that

the same population of cells will be compared across the three strains. Phase contrast images and immunocytochemistry (ICC) confirmed that CFbs from all strains exhibit similar mesenchymal morphology **(Supplementary Figure IIA)** and express fibroblast markers collagen 1 (Col1) and PDGFRα **(Supplementary Figure IIB and IIC)**. We then sought to determine whether these fibroblasts exhibited similar patterns of activation and proliferation in culture. CFbs were stained for the expression of α-smooth muscle actin (αSMA), a marker associated with activated fibroblasts[7], and Phospho-Histone H3 (pHH3)[8], for proliferation analysis. We observed very low expression of αSMA within Col1$^+$ CFbs from all strains **(Supplementary Figure IID and IIE)**, indicating that these cells do not become activated without stimuli, and have similar rates of proliferation (%pHH3$^+$ nuclei) at the basal level **(Supplementary Figure IIF and IIG)**.

We next examined whether strain-specific CFbs may have differential responses to ISO *in vitro*. CFbs from each strain were isolated, expanded, and passaged prior to being treated with culture media containing ISO **(Figure 2A)**. Cells were then fixed and characterized by phase contrast microscopy **(Figure 2B)** and ICC. A significant percentage of CFbs from C3H/HeJ and KK/HlJ began to co-express αSMA and Col1, while CFbs from C57BL/6J exhibited minimal αSMA expression in the presence of ISO (C57BL/6J: No ISO=0.8±0.5% ISO=1.9±1.8%, C3H/HeJ: No ISO=1.0±0.5% ISO=12.3±1.7%, KK/HlJ: No ISO=1.1±0.5% ISO=7.5±1.6%) **(Figure 2C and 2D)**. Immunostaining for pHH3 revealed that the rate of proliferation was significantly increased across all three strains to similar levels when compared to their respective untreated control groups (C57BL/6J: No ISO=5.6±1.2% ISO=20.9±3.5%, C3H/HeJ: No ISO=4.9±1.4% ISO=16.9±4.8%, KK/HlJ: No ISO=3.4±1.4% ISO=20.0±2.9%) **(Figure 2E and 2F)**. CFbs isolated from mice pre-treated with implanted ISO osmotic pumps **(Supplementary Figure IIIA)** did not exhibit significant changes in activation or proliferation in response to additional *in vitro* ISO treatment **(Supplementary Figure IIIB and IIIC)**. This may be attributed to an already stimulated state of cells before culture, resulting in minimal response to ISO *in vitro*[9].

We additionally treated CFbs *in vitro* with TGFβ, a pro-fibrotic cytokine, for 72 hours **(Supplementary Figure IVA)**[10]. The morphology of the cells appeared grossly similar across all three strains **(Supplementary Figure IVB)**. CFbs from all three strains exhibited significant increases in the level of activation from baseline, although the levels in KK/HlJ were significantly higher than in C57BL/6J **(Supplementary Figure IVC and IVD)**. The proliferation rates of CFbs from all strains increased similarly in response to TGFβ **(Supplementary Figure IVE)**.

Together, these data suggest that cultured CFbs respond to ISO in a strain-specific manner. While ISO treatment resulted in differing levels of activation in cultured CFbs, their levels of proliferation were similar.

Cardiac fibroblasts demonstrate strain-specific responses to ISO treatment *in vivo*

While other studies have viewed fibroblast activation and proliferation to be interdependent responses to stimulation, our *in vitro* results suggest otherwise. To determine whether a similar behavior is observed *in vivo*, we investigated CFb activation and proliferation after ISO stimulation in the three selected strains.

First, we observed the presence of activated fibroblasts in C57BL/6J, C3H/HeJ, and KK/HlJ mice in response to ISO treatment. Immunohistochemistry (IHC) was used to observe co-localization of Col1 with αSMA or periostin for the identification of activated CFbs[11, 12]. In all saline-treated groups, Col1 staining was mainly present around larger vessels and co-localization with αSMA was exceedingly rare **(Figure 3A)**. However, after ISO treatment, there was an increase in Col1 staining, particularly in C3H/HeJ and KK/HlJ hearts **(Supplementary Figure VA)**. Many $Col1^{+}$ cells co-expressed αSMA in both perivascular and interstitial regions of the myocardium in C3H/HeJ and KK/HlJ hearts, indicating the presence of activated CFbs **(Figure 3A)**. This increase

was quantified as the area of $Col1^{+}\alpha SMA^{+}$ staining normalized to the total area of each heart section (C57BL/6J: Saline=0.5±0.2 ISO=5.2±1.0, C3H/HeJ: Saline=2.2±0.6 ISO=12.4±2.2, KK/HlJ: Saline=4.8±1.5 ISO=42.0±4.7) **(Figure 3B)**. IHC for periostin also confirmed the differential levels of activated CFbs observed across the three strains **(Supplementary Figure VB)**. Consistent with our *in vitro* results, the levels of CFb activation corresponded with the amount of fibrosis seen within each strain.

Next, we sought to assess the proliferative behavior of CFbs *in vivo* after ISO injury. Mice were injected with Bromodeoxyuridine (BrdU) at the time of micro-osmotic pump implantation for saline/ISO and exposed to BrdU diluted in drinking water throughout the 21 days of treatment **(Figure 3C)**. IHC of the control hearts demonstrated low levels of $BrdU^{+}$ proliferating CFbs throughout the myocardium. However, with ISO treatment, we observed a significantly higher number of $BrdU^{+}$ cells throughout the perivascular and interstitial $Col1^{+}$ regions in all three strains **(Figure 3D)**. Flow cytometry demonstrated similar percentages of $BrdU^{+}$ CFbs in the control groups for all three strains. The proportion of $BrdU^{+}$ CFbs significantly increased to a similar amount after ISO treatment in all three strains (C57BL/6J: Saline=5.8±1.5% ISO=20.9±0.6%, C3H/HeJ: Saline=7.1±0.8% ISO=32.7±5.3%, KK/HlJ: Saline=6.2±0.8% ISO=23.4±1.4%) **(Figure 3E and Supplementary Figure VC)**.

These results demonstrate that while a similar pattern of CFb proliferation was observed in all three strains after ISO treatment, the extent of cardiac fibrosis directly correlated with the number of activated CFbs.

Inhibition of cardiac fibroblast proliferation *in vitro* does not affect their activation levels

Our results suggest that CFb proliferation and activation may be distinct responses to ISO treatment with different phenotypic presentation depending on genetic background. To confirm

this, we sought to inhibit CFb proliferation *in vitro* and determine whether it would affect the activation of these cells.

CFbs from each strain were isolated, cultured, and subjected to one of three conditions: (i) culture in normal media, (ii) treatment with mitomycin-C (mito-C) for 2 hours, or (iii) irradiation (IR) for 2 minutes. We chose treatment with mito-C or irradiation as two independent methods to inhibit CFb proliferation[13]. We then exposed the cells to ISO and conducted ICC for pHH3 and αSMA **(Figure 4A)**. In all three strains, the percentages of $pHH3^{+}$ nuclei were significantly reduced following mito-C and IR treatment (C57BL/6J: Control=17.38±6.1% Mito-C=0.5±0.3% IR=3.5±1.3%, C3H/HeJ: Control=11.69±1.5% Mito-C=2.2±0.9% IR=3.7±1.6%, KK/HlJ: Control=14.8±0.5% Mito-C=0.3±0.3% IR=2.7±1.8%) **(Figure 4B)**. However, we did not observe significant differences in the percentage of CFbs that expressed markers for CFb activation such as αSMA (C57BL/6J: Control=0.2±0.1% Mito-C=0.1±0.1% IR=1.5±0.7%, C3H/HeJ: Control=5.0±0.7% Mito-C=4.1±1.6% IR=2.5±0.8%, KK/HlJ: Control=18.5±8.5% Mito-C=13.11±2.06%, IR=8.1±0.7%) **(Figure 4C)**. These results confirm that CFb proliferation and activation do not necessarily correlate with each other and may contribute to fibrosis in unique manners.

Strain-specific cardiac fibroblasts have unique transcriptional profiles in response to *in vivo* ISO treatment

The use of multiple genetic strains for transcriptome analysis allows for a comprehensive approach to determine potential genetic contributors of specific phenotypes. To further characterize CFbs within the three selected strains, we performed RNA-sequencing on isolated CFbs from C57BL/6J, C3H/HeJ, and KK/HlJ mice that underwent saline or ISO treatment for 21 days. The effects of ISO on each strain's transcriptome was unique, as seen by the global heatmap of differential gene expression of all three strains, further justifying the need to study

strain-specific phenotypes **(Figure 5A)**. Based on the *in vitro* and *in vivo* results, we focused on genes mainly associated with fibrosis and proliferation. We observed that genes related to fibroblast activation and fibrosis were highly upregulated in KK/HIJ CFbs in response to ISO compared to C3H/HeJ and C57BL/6J CFbs **(Figure 5B)**. In contrast, we observed comparable expression levels of select cell cycle and proliferation genes across the three strains **(Figure 5C)**. Furthermore, we used Ingenuity Pathway Analysis (IPA) to identify enriched pathways which may be involved in regulating such differences within each strain **(Supplementary Figure VIA)**. Overall, C3H/HeJ and KK/HlJ CFbs exhibited higher activation scores for several pro-fibrotic pathways when compared to C57BL/6J, such as the TGFβ signaling[14], β-adrenergic signaling[5], and Endothelin-1 signaling pathways[15] **(Supplementary Figure VIB)**. The GP6 signaling pathway was of particular interest as it showed the highest activation scores in KK/HlJ CFbs and was one of the more significantly enriched pathways identified by IPA **(Supplementary Figure VIA and VIB)**.

To identify changes that occurred throughout the course of injury, we additionally isolated CFbs from ISO-treated mice 14 days after pump implantation for RNA-sequencing. Compared to saline-treated groups, CFbs from all strains exhibited an extensive number of differentially expressed genes **(Supplementary Figure VIIA)** and enriched pathways **(Supplementary Figure VIIB)** between days 14 and 21 of injury, suggesting that changes continue to occur at the transcriptome level in CFbs up until the final week of treatment. Between days 14 and 21, C57BL/6J CFbs exhibited negative activation scores of various pro-fibrotic pathways **(Supplementary Figure VIIC)**. On the other hand, C3H/HeJ CFbs exhibited higher levels of activation of several pro-fibrotic pathways, suggesting that CFbs are continuing to respond to ISO treatment **(Supplementary Figure VIIC)**. Finally, KK/HlJ CFbs did not exhibit significant changes in pathway activation between 14 and 21 days of treatment. **(Supplementary Figure VIIC)**. According to our IPA analysis, each strain demonstrated distinct differences in pathway activation

at different time points of ISO treatment. Further exploration of these pathways is required to delineate the mechanisms by which they alter ISO-induced cardiac fibrosis.

Ltbp2 is upregulated in response to cardiac fibrosis

Like genome-wide association studies (GWAS), the HMDP facilitates identification of unique genes that may be associated with complex phenotypic traits. To account for diversity seen in heart failure pathologies, we sought to identify genes that can be associated with fibrosis regardless of genetic background. From the RNA-sequencing data, we focused on genes that were upregulated within each strain in response to ISO. Several of these genes overlapped across two strains, but the majority of the genes were unique to each strain **(Figure 6A)**. We focused on genes that were upregulated in all three strains in response to ISO and identified *Ltbp2* to be of interest **(Figure 6B and Supplementary Figure VIIIA)**. Reverse transcription-qPCR (RT-qPCR) for *Ltbp2* within CFbs confirmed the trends seen within the RNA-sequencing data (C57BL/6J: 2.0±0.5, C3H/HeJ: 3.6±0.7, KK/HlJ: 3.2±0.8) **(Figure 6C and Supplementary Table II)**.

To confirm the presence of LTBP2 protein in fibrosis, we conducted IHC on cardiac sections from all three strains after ISO treatment. In saline-treated hearts, there was minimal expression of LTBP2 throughout the myocardium **(Figure 6D)**. However, in response to ISO, LTBP2 co-localized with DDR2, a marker for fibroblasts, and αSMA **(Figure 6D)**. The expression of LTBP2 was specifically localized to the fibrotic regions, even in C57BL/6J hearts, where there was minimal fibrosis **(Figure 6D)**. As it is a secreted protein, we additionally sought to determine whether ISO treatment elevates LTBP2 levels in circulation. We found that LTBP2 levels were significantly increased in plasma of KK/HlJ mice, with upward trents in C57BL/6J and C3H/HeJ mice, after ISO treatment **(Supplementary Figure VIIIB and Supplementary Table III)**.

To determine whether LTBP2 expression is also present in other models of fibrosis, we performed transverse aortic constriction (TAC) surgery on the three mouse strains[16]. We observed cardiac hypertrophy and the presence of myocardial fibrosis in the three strains after TAC (data not shown). In C57BL/6J mice, RNA-sequencing and RT-qPCR demonstrated significant increases in *Ltbp2* expression in CFbs 7 days after TAC surgery compared to sham **(Supplementary Figure VIIIC and VIIID)**. Additionally, IHC showed that LTBP2 was preferentially localized in the fibrotic areas within the myocardium of mice that underwent TAC **(Figure 6D)**.

Finally, we investigated whether LTBP2 is upregulated in human plasma with underlying heart failure. We found that average LTBP2 levels were mildly increased in patients with heart failure with reduced ejection fraction (HFrEF) when compared to healthy individuals. **(Supplementary Figure IXA and Supplementary Table IV)**. Furthermore, IHC staining of human myocardial tissue from heart failure patients revealed LTBP2 expression to be significantly increased compared to expression in the healthy human myocardium **(Supplementary Figure IXB)**.

Taken together, our results suggest that the expression of LTBP2 may be indicative of the development of cardiac fibrosis, but its specific role in fibrosis requires further exploration.

DISCUSSION

Despite the functional significance of CFbs in cardiovascular disease, the specific contributions of these cells to cardiac fibrosis are not completely understood. Previous studies revealed a wide spectrum of cardiac pathology across various inbred strains of mice when subjected to chronic β-adrenergic stimulation by ISO[5, 6]. We hypothesized that characterizing fibroblasts of multiple strains with different severities of ISO-induced cardiac fibrosis would allow us to dissect the contributions of these cells to scar development. Our results show that fibroblast activation, not proliferation, correlates with the striking differences in fibrosis among the divergent strains.

Moreover, comparisons of gene expression profiles across the strains revealed differences in underlying mechanistic pathways and led to the identification of a potential marker of fibrosis.

While recent research has focused on how CFbs become activated and proliferate in response to injury[17], the mechanisms by which these processes dictate scar development have yet to be elucidated. Prior to this study, CFb activation and proliferation were generally considered to be interconnected responses that contribute to fibrosis[17, 18]. Here, by comparing CFbs from three selected strains of the HMDP – C57BL/6J, C3H/HeJ, and KK/HlJ – we discovered that there is a direct correlation of CFb activation with the severity of fibrosis, while CFbs from all strains exhibited similar proliferative capacity in response to ISO. These results suggest that CFb proliferation may be an independent response from CFb activation and that levels of proliferation do not necessarily correlate with the extent of scar formation. It is possible that CFb proliferation is an indicator of CFb stimulation, but the functional roles of this phenomenon require further studies.

Myocardial injury evokes multiple signaling pathways in cardiac fibroblasts that ultimately lead to the activation of genes that regulate cardiac fibrosis[19]. To delineate gene expression differences between CFbs from each select strain, we conducted RNA-sequencing on sorted CFbs after saline and ISO treatment. After ISO treatment, CFbs from each strain responded with distinct changes in their gene expression profiles. Our results revealed many genes with small fold changes and the analysis was conducted to be inclusive of these changes. We observed enrichment of fibroblast activation genes that paralleled the extent of fibrosis observed in each strain, while the upregulation of proliferation genes was comparable across all strains. IPA analysis identified the GP6 signaling pathway as exhibiting activation scores that corresponded with the levels of fibrosis seen across the three selected strains. GP6 is a collagen receptor abundantly expressed on platelets that activates a downstream signaling cascade promoting

platelet aggregation and thrombus formation[20]. The role of this signaling pathway in fibroblasts has yet to be explored, but our results suggest that modulation of this signaling cascade may regulate the formation of fibrosis. Our RNA-sequencing data also revealed that genetic differences may influence the timely progression of scar formation. In C57BL/6J mice, CFbs were not immune to ISO treatment, but rather exhibited a downregulation of pro-fibrotic pathways between day 14 and day 21 of treatment. On the contrary, C3H/HeJ mice appeared to display a slow progression towards the formation of fibrosis, evidenced by the continuing changes in gene expression profiles between day 14 and day 21. Finally, KK/HlJ mice, as the most sensitive strain, exhibited surprisingly few changes in canonical pathway activation between day 14 and day 21 of treatment, suggesting that CFbs may have already undergone transcriptional changes in response to ISO prior to the time of analysis. Ultimately, these findings raise questions regarding whether phenotypic and/or transcriptomic changes observed after cardiac injury within a single mouse strain can be applicable to other strains. It is important to interrogate these pathways to gain insight into mechanisms of CFb activation, explore how cardiac fibrosis is regulated, and perhaps design novel anti-fibrotic therapies.

Heart failure resulting from prolonged interstitial fibrosis is a highly heterogeneous disorder influenced by many environmental and genetic factors. GWAS allows for the identification of genetic variations on complex traits such as heart failure[21]. However, multiple large-scale GWAS studies have provided limited success in identifying genetic signals driving heart failure[22]. This is partly due to the paucity of quantitative phenotypic data as well as diverse environmental factors. Therefore, there have been challenges in developing treatments for heart failure and cardiac fibrosis that are applicable to a diverse population. The HMDP is a unique tool to mimic in mice the genetic variance and substantial diversity of heart failure development seen in humans. While previous studies have sought to identify genetic markers uniquely associated with heart failure in a specific genetic background, we sought to investigate common markers that are associated with

cardiac fibrosis in a panel of genetically diverse mouse strains. Our results revealed *Ltbp2* to be upregulated in CFbs from all three strains and that the expression of LTBP2 was primarily localized in the fibrotic regions. LTBP2 is part of the Latent TGFβ1-Binding Protein family, which have been shown to participate in the regulation of TGFβ signaling and display high affinity binding sites for extracellular matrix proteins. However, while the functions of LTBP1[23], LTBP3[24], and LTBP4[25] in disease have been extensively characterized, the role of LTBP2 in cardiac injury is still unclear. Whether LTBP2 is merely a surrogate for cardiac fibrosis or is involved in its pathogenesis is not entirely known. Furthermore, the specificity of LTBP2 to cardiac fibrosis, and its potential role in the manifestation of other types of organ fibrosis cannot be disregarded. However, our results in both mice and human heart failure patients support the possibility of LTBP2 being used as a marker for fibrosis that can be used across a genetically diverse population.

Our data demonstrates the importance of considering genetic backgrounds when conducting studies on CFbs that reflect changes in cardiac phenotype in response to injury. The comparisons conducted across multiple strains allowed for a unique approach in associating CFbs with a spectrum of ISO-induced fibrosis, rather than just the presence of fibrosis itself. This form of analysis allowed us to determine significant factors that directly correlate with the development of scar tissue, which may have not been recognized if the study was done within a single strain. This multiple-strain approach, when combined with molecular and cell-based characterizations, serves as an important tool for future work delineating the functions not only of CFbs, but also of a variety of cardiac cell types.

METHODS

The data, analytic methods, and study materials will be made available to other researchers for purposes of reproducing the results or replicating the procedure. The authors declare that all

supporting data are available within the article and its online supplementary files. The transcriptomics data is available under the GEO accession ID GSE109376.

Mice

Adult female C57BL/6J, C3H/HeJ, and KK/HlJ mice (8-10 weeks) were obtained from Jackson Laboratory. All procedures were carried out with the approval of the University of California, Los Angeles (UCLA) Animal Research Committee or the Institutional Animal Care. Two operators blinded to the experimental designs performed all animal surgeries and *in vivo* analyses.

Isoproterenol treatment

Isoproterenol (ISO) treatment was performed by implantation of Alzet osmotic pumps (Cupertino, CA) in C57B/6J, C3H/HeJ, and KK/HlJ mice (n=20). Pumps were filled with ISO (Sigma, CA) (30mg/kg body weight/per day) and implanted in the abdominal cavity under anesthesia with isoflurane. Mice were treated pre- and post-operatively with Sulfamethoxazole and Trimethoprim oral suspension (Hi-Tech Pharmacal, NY). Mice in control groups were implanted with pumps filled with saline. Mice were sacrificed and hearts were harvested 14 or 21 days post-implantation for further analysis (n=52).

Echocardiography

Transthoracic echocardiography was performed on both saline and ISO treated mice before treatment and 21 days after pump implantation. Echocardiography was performed by a single operator who was blinded to the mouse strains and treatment groups using the Vevo 770 high-resolution ECHO system equipped with a 35 MHz transducer. First, chest fur was removed using a depilatory lotion (Nair). Mice were lightly anesthetized with vaporized isoflurane (2.5% for induction, 1.0% for maintenance) in oxygen and lightly restrained in a supine position on a heated pad to maintain body temperature at 37° C. Continuous EKG monitoring was done throughout the

imaging studies and heart rates were maintained between 500 and 600 beats per minute. The probe was placed along the short axis of the left ventricle with the papillary muscles providing a guide for the proper depth. 2D images were captured to measure internal wall dimensions during both systole and diastole, as well as providing another measure of the heart rate. Saved images were analyzed by a single operator who was blinded to the experimental design using the Vevo 2100 software. The LV chamber dimensions and posterior wall thickness (PWT) were obtained from M-mode images; LV systolic function was also assessed from these measurements by calculating ejection fraction (EF) and fractional shortening (FS).

Heart weight, body weight, and tibia length collection

After 21 days of saline or isoproterenol treatment, mice from each strain (n=20 per strain) were sacrificed and their body weights were recorded. The heart was removed and, after PBS perfusion, weighed. Additionally, the right tibia of each mouse was removed and measured with a caliper.

Histological analyses (Trichrome staining, scar size measurement, immunohistochemistry)

Freshly isolated tissues were fixed in 4% paraformaldehyde (Electron Microscopy Sciences) in PBS (Fisher Scientific) overnight in 4°C. Afterwards, the tissues were washed with PBS and immersed in a 30% sucrose solution (Sigma) in PBS in 4°C overnight. The hearts were then embedded in Tissue- Tek OCT Compound (Sakura) and transferred to a bath of 2-Methylbutane (Fisher Scientific) on dry ice. Frozen tissues were sectioned at 7 μm thickness using a cryostat (Leica) and stored at -80°C.

Masson's trichrome staining (Sigma) was performed according to the manufacturer's instructions and images were taken of the entire cross-section of the heart using bright-field microscopy (Leica). To assess the degree of cardiac fibrosis, NIH ImageJ software was used by comparing

the area of tissue stained blue (collagen) to the total tissue area (10-12 randomly chosen sections per heart, n=7-8 hearts per strains).

For immunohistochemistry, slides were dried at room temperature for 20 minutes, washed 3 times for 10 minutes each in PBS, permeabilized in PBS containing 0.25% Triton X-100 (Fisher Scientific) for 10 minutes at room temperature followed by washing in PBS-T (PBS containing 0.05% Tween-20 (Fisher)) twice for 5 minutes. The tissue slides were incubated with blocking buffer (10% normal goat serum (Sigma) in PBS-T) for 30 minutes at room temperature. The tissue slides were then incubated with primary antibodies **(Supplementary Table I)** diluted in blocking buffer overnight at 4 °C followed by 1 hour at room temperature. After washing three times for 10 minutes with PBS-T, the tissue slides were incubated with the secondary antibody **(Supplementary Table I)** for 1 hour at room temperature, washed three times for 10 minutes with PBS-T, and then mounted with DAPI-containing mounting media (Vector). The immunostained slides were observed and analyzed using a fluorescent microscope (LEICACTR6500, Leica) and a confocal microscope (LSM880, Zeiss).

Isolation of cardiac fibroblasts from murine hearts

Mice were injected with heparin (SAGENT Pharmaceuticals) prior to being euthanized. After euthanasia, the hearts were dissected and perfused with Hanks' Balanced Salt Solution (HBSS). They were cut into small pieces and digested with Liberase Blendzyme TH and TM (Roche) in Medium 199 with DNAse I (Invitrogen) and polaxamer in 37°C for 1h. Cells were passed through a 70µm cell strainer (BD Falcon) and centrifuged. The cell pellet was re-suspended in staining buffer (3% FBS in HBSS) containing antibodies targeting an established panel of surface markers: exclusion of hematopoietic ($CD45^-$[1:200], $Ter119^-$ [1:400]), macrophage ($CD11b^-$ [1:400]), and endothelial ($CD31^-$ [1:400]) lineages, followed by the inclusion of $Thy1^+$ (1:200) cells (hereafter referred to as $Thy1^+HE^-$) **(Supplementary Table I)**. The cells were incubated in the dark for 30 minutes at room temperature. The cells were then sorted by a BD FACSAria II flow cytometer.

Primary cardiac fibroblast culture and characterization

Cardiac fibroblast isolation was prepared as described in the Supplementary Methods **(Supplementary Table I)**. After sorting (BD FACSAria II), $Thy1^+/CD45^-/Ter119^-/CD11b^-/CD31^-$ cardiac fibroblasts (hereafter referred to as $Thy1^+HE^-$ CFbs) were cultured on 0.1% gelatin-coated 12-well plates in DMEM supplemented with 15% FBS and antibiotics ($5x10^4$ cells/well). Media was changed 24 hours after the primary culture, followed by changes every 48 hours. Cells were passaged upon 80% confluency. After the first passage, cells were washed and cultured in serum-free culture medium supplemented with 0.5 mg/mL insulin and 0.5 mg/mL transferrin. At confluence, cells were treated with 100µm/L ISO (Sigma) or 50ng/mL TGFβ (Cell Signaling). After 72 hours, cells were washed, fixed in 4% paraformaldehyde, and stained for analysis. Cell counts were performed on ImageJ using the 'Cell Counter' plug-in by two people blind to the conditions.

Inhibition of *in vitro* cell proliferation

Cells were isolated, expanded, and passaged upon 80% confluency with serum-free culture media ($2.5x10^4$ cells/well). Prior to treatment with ISO, cells were treated with mitomycin-C (10µg/mL) (Acros Organics) for 2 hours or irradiated for 2 minutes at 3 Gy.

BrdU detection by flow cytometry and immunohistochemistry

BrdU (1mg) was injected intraperitoneally on the day of pump implantation. Mice were supplied BrdU in their drinking water (1 mg/mL) for 21 days. The water was changed every two days. Intracellular staining for BrdU was performed in accordance to the instructions of the BD Pharmingen™ BrdU Flow Kit. In short, cells were fixed and permeabilized in Cytofix/Cytoperm Buffer (BD), followed by incubation in Cytoperm Permeabilization Buffer plus (BD) and DNase treatment (BD). The cells were then exposed to fluorescent anti-BrdU antibody, washed, resuspended in staining buffer, and analyzed using a BD FACSAria II flow cytometer. For

immunohistochemistry, slides were dried at room temperature for 20 minutes, washed 3 times for 10 minutes each in PBS, permeabilized in PBS containing 0.5% Triton X-100 (Fisher Scientific) for 10 minutes at room temperature, and pre-treated with 2M HCl for 30 minutes at 37°C. After brief washing with PBS, the slides were incubated with blocking buffer (10% normal goat serum (Sigma) in PBS) for 30 minutes at room temperature. The slides were then incubated with anti-BrdU antibody (Abcam) and primary antibodies to mark fibroblasts and activated fibroblasts **(Supplementary Table I)** in 4°C overnight, followed by 15 minutes in 37°C. After washing three times for 10 minutes with PBS-T, the tissue slides were incubated with the secondary antibody **(Supplementary Table I)** for 1 hour at room temperature, washed three times for 10 minutes with PBS-T, and then mounted with mounting media (Vector). The slides were then imaged by an LSM880 confocal microscope (Zeiss).

RNA-sequencing

$Thy1^{+}HE^{-}$ CFbs were isolated from saline and ISO-treated hearts 14 or 21 days after pump implantation (n=2 per strain/condition), and then sorted directly into TRIzol® LS Reagent (Ambion). Total RNA was extracted using the RNeasy miniElute Cleanup Kit (Qiagen), according to manufacturer's instructions. Complementary DNA (cDNA) libraries were generated using reagents provided in the KAPA mRNA Hyperprep kit. The amplified cDNA library was sequenced on an Illumina HiSeq 3000 according to manufacturer's instructions. Libraries were sequenced using 50 single-end read protocol, which yielded approximately 20 million raw reads per sample. Read quality was assessed using FastQC and reads were subsequently trimmed 5bp from the start of the reads up and 2 bp from the end of the reads. Alignment to the mm10 mouse genome were performed using STAR v2.5.3a with –twopassMode Basic option. Gene counts were generated using --quantMode GeneCounts option. Raw gene counts were transformed to counts per million (CPM) and log2-counts per million (log2-CPM) data matrix and further normalized by trimmed mean of M-values (TMM) method in the edgeR Bioconductor package. Genes with

CPM<1 across all samples were excluded from further analysis. To determine differentially expressed genes, the *voom* method of *limma* was applied, accommodating the mean-variance in the linear model using precision weight, and significant gene set was selected with nominal p-value<0.05 threshold. Global functional analyses, network analyses, and canonical pathway analyses were performed using Ingenuity Pathway Analysis (Ingenuity® Systems, www.ingenuity.com).

Quantitative RT-qPCR

Total RNA from $Thy1^{+}HE^{-}$ cells from control and ISO-treated hearts were extracted using TRIzol® LS Reagent (Ambion) and RNeasy MinElute Cleanup Kit (Qiagen) according to the manufacturers' instructions. The concentration and quality of extracted RNA were measured using a NanoDrop ND-1000 Spectrophotometer (Thermo Scientific). cDNA was synthesized using an *iScript*™ cDNA Synthesis Kit (Bio-Rad). For quantitative RT-qPCR, we used an *iTaq*™ *Universal SYBR® Green supermix* (Bio-RAD), amplified cDNA and gene-specific primers **(Supplementary Table IV)** on a *CFX96 real-time* PCR detection system (Bio-Rad). PCR conditions included initial denaturation at 95°C for 2 minutes and 10 seconds, 39 cycles of denaturation at 95°C for 15 seconds, annealing at 60°C for 30 seconds, extension at 72 °C for 30 seconds, followed by a final extension at 72°C for 10 minutes. The mean cycle threshold (Ct) values from triplicate measurements were used to calculate relative gene expressions, with normalizations to GAPDH as an internal control. We used the $\Delta\Delta$CT method to analyze relative gene expression in treated samples compared to non-treated samples. Technical replicates (n=3) and biological replicates (n=7-9) were performed for each strain and condition.

Transverse Aortic Constriction (TAC)

Adult mice weighing 25±5 g were randomly divided into sham and TAC groups (n=4-6 per group) Animals were anesthetized by an intraperitoneal injection of ketamine/xylazine (100 mg/10

mg/kg). Endotracheal intubation was performed using a blunt 20-gauge needle that was then connected to a volume-cycled rodent ventilator (SAR-830/P; CWE, Inc.) with a tidal volume of 0.2 ml and a respiratory rate of 120/min. The chest was entered in the second intercostal space at the top left aortic arch, the transverse aorta was isolated, and aortic constriction was performed by tying a 7-0 nylon suture ligature against a 27-gauge blunt needle. The needle was then removed to yield a constriction 0.4 mm in diameter. In sham-operated control mice, the entire procedure was identical except that aortic constriction was not performed. The chest tube was used to evacuate the pneumothorax, and it was removed once negative pressure was re-established. The chest was closed in layers using 5-0 Vicryl sutures. Ventilation was maintained until sufficient spontaneous breathing occurred, followed by extubation and removal of the chest tube. The whole surgical procedure was performed under aseptic conditions.

Plasma collection and Enzyme-linked immunosorbent assay (ELISA)

Blood was collected from euthanized mice after saline and ISO treatment into Lithium Heparin Blood Collection Tubes (BD). Plasma was separated from blood using Ficoll-Paque PLUS (GE Healthcare), following the manufacturer's instructions. ELISAs were conducted following the manufacturer's instructions. All samples were measured in duplicate and the calculated concentrations were multiplied by the dilution factor to determine the final concentration. The study was approved by an IRB (12-001164) and participants gave written informed consent.

Statistical analysis

Statistical testing was performed with GraphPad Prism 6. Results are presented as mean ± SEM and were analyzed using one-way ANOVA, two-way ANOVA or Student t-test (significance was assigned for $P<0.05$). Multiple comparisons were considered by Tukey's multiple comparison test, the Sidak method, or the Holm-Sidak method.

ACKNOWLEDGEMENTS

S.R., S.P., and R.A. conceived the project and designed the experiments. X.W. and A. J. L. assisted with the initial design. S.P. and S.R. performed all experiments, analyzed data and prepared the figures. S.P. and S.R. had full access to all the data in the study and take responsibility for the integrity of the data and the accuracy of the data analysis. S.P., S.R., and R.A. wrote the manuscript. H.K.A.M. and F.D. L. helped with the analysis of RNA-sequencing data and acknowledge support the Quantitative and Computational Biosciences Community directed by Matteo Pellegrini. A.H-V. assisted with obtaining human serum samples. M.J.M., J.S.D., R.Q., and J.M.S. assisted with all stainings. P.Z. performed all surgeries. All authors reviewed the manuscript. Echocardiograms were performed in Dr. Yibin Wang's lab. We would like to acknowledge Shuxun Ren with his assistance in the initial surgeries. The LTBP2 antibody was a generous gift from Dr. Marko Hyytiäinen from the University of Helsinki, Finland. We are grateful for the expert technical assistance from the UCLA Broad Stem Cell Research Center Flow Cytometry Core, Confocal Microscopy Core, and Clinical Microarray Core. We acknowledge Ngoc B. Nguyen and James L. Engel for their critical reading of this article.

SOURCES OF FUNDING

This work was supported by the NIH DP2 HL127728 (R.A); UCLA Broad Stem Cell Research Center-Rose Hills Foundation Research Award (R.A.); the Eli & Edythe Broad Center of Regenerative Medicine and Stem Cell Research Center at UCLA Research Award (R.A. and H.K.A.M.); NIH HL28481 (A.H-V., X.W., and A.J.L.); NIH HL123295 (A.H-V., X.W., and A.J.L.); and the American Heart Association 14GRNT20480340 and 16IRG27260285 (H.K.A.M.). S.P. was supported by the Ruth L. Kirschstein National Research Service Award T32HL69766. S. R. was supported by the UCLA Graduate Programs in Bioscience. F. D. L. was supported by the UCLA Quantitative and Computational Biosciences Collaboratory Post-Doctoral Fellowship.

Figure 1

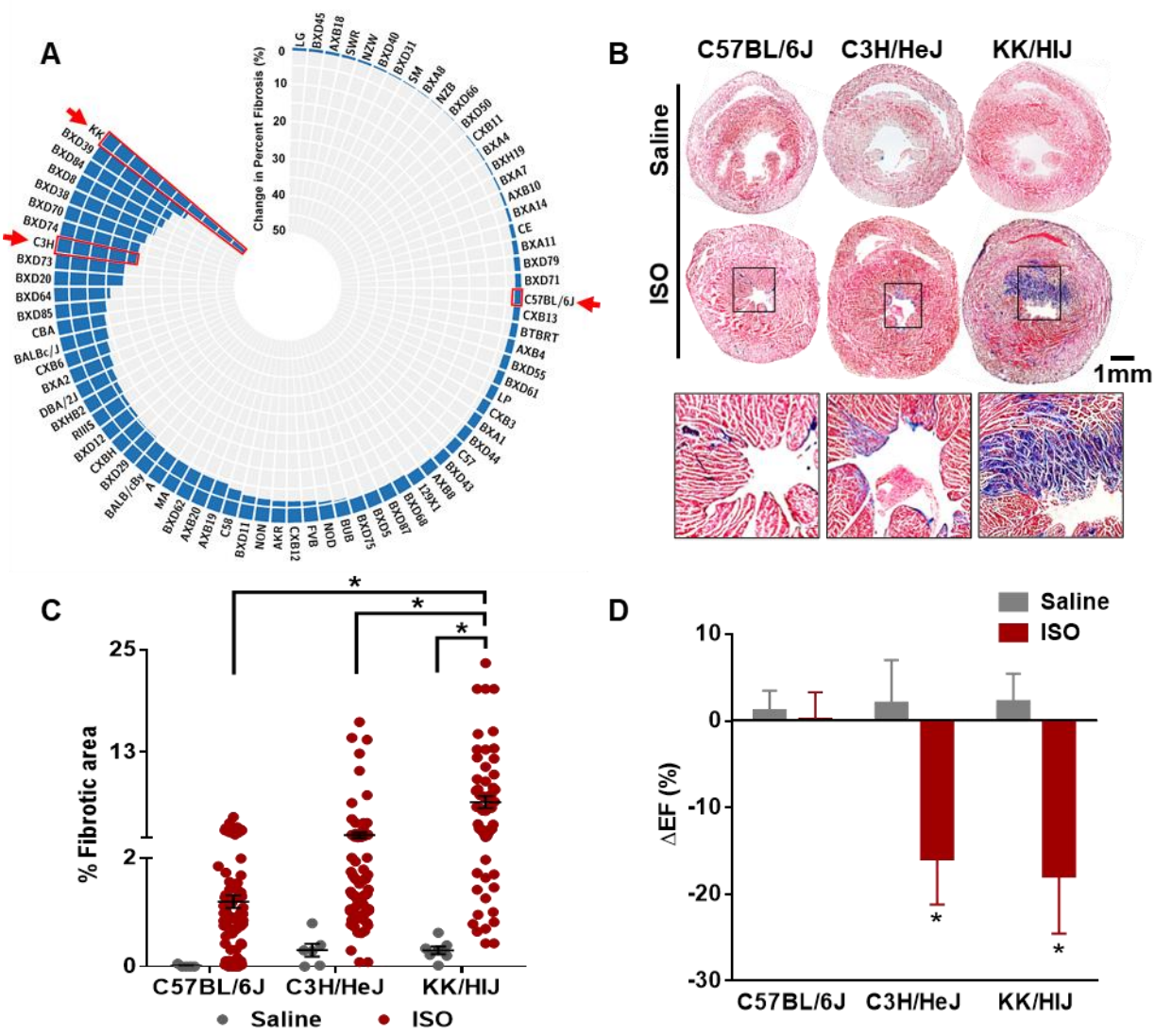
A
Change in Percent Fibrosis (%)
0
10
20
30
40
50
LG
BXD45
AXB18
SWR
NZW
BXD40
BXD31
SM
BXA8
NZB
BXD66
BXD50
CXB11
BXA4
BXH19
BXA7
AXB10
BXA14
CE
BXA11
BXD79
BXD71
C57BL/6J
CXB13
BTBRT
AXB4
BXD55
BXD61
LP
CXB3
BXA1
BXD44
C57
BXD43
AXB8
129X1
BXD68
BXD87
BXD5
BUB
NOD
FVB
CXB12
AKR
NON
BXD11
C58
AXB19
AXB20
BXD62
MA
A
BALB/cBy
BXD29
CXBH
BXD12
RIIIS
BXHB2
DBA/2J
BXA2
CXB6
BALBc/J
CBA
BXD85
BXD64
BXD20
BXD73
C3H
BXD74
BXD70
BXD38
BXD8
BXD84
BXD39
KK
B
C57BL/6J
C3H/HeJ
KK/HIJ
Saline
ISO
1mm
C
% Fibrotic area
25
13
2
0
*
*
*
C57BL/6J
C3H/HeJ
KK/HIJ
Saline
ISO
D
Saline
ISO
ΔEF (%)
10
0
-10
-20
-30
*
*
C57BL/6J
C3H/HeJ
KK/HIJ

Figure 1: Severity of fibrosis varies across different mouse strains (C57BL/6J, C3H/HeJ, KK/HlJ) in response to ISO treatment

(A) Wide variation in percentage of fibrosis was observed between the strains of the hybrid mouse diversity panel (HMDP) after ISO treatment. **(B)** Masson's Trichrome stained sections of hearts from the three selected strains after 21 days of saline/ISO treatment (n=7-8 mice per condition). **(C)** Quantification of fibrotic area as a percentage of total section area (n=10-12 sections per heart). **(D)** Left ventricular ejection fractions (EF) were measured by echocardiography in both saline- and ISO-treated groups across the different strains at day 0 and day 21 of treatment. Changes in ejection fraction between these two timepoints were determined as the ΔEF for each mouse (n=20 mice per strain). Data presented as mean ± SEM. Two-way ANOVA, *P < 0.05. Scale bar: 1mm

Figure 2

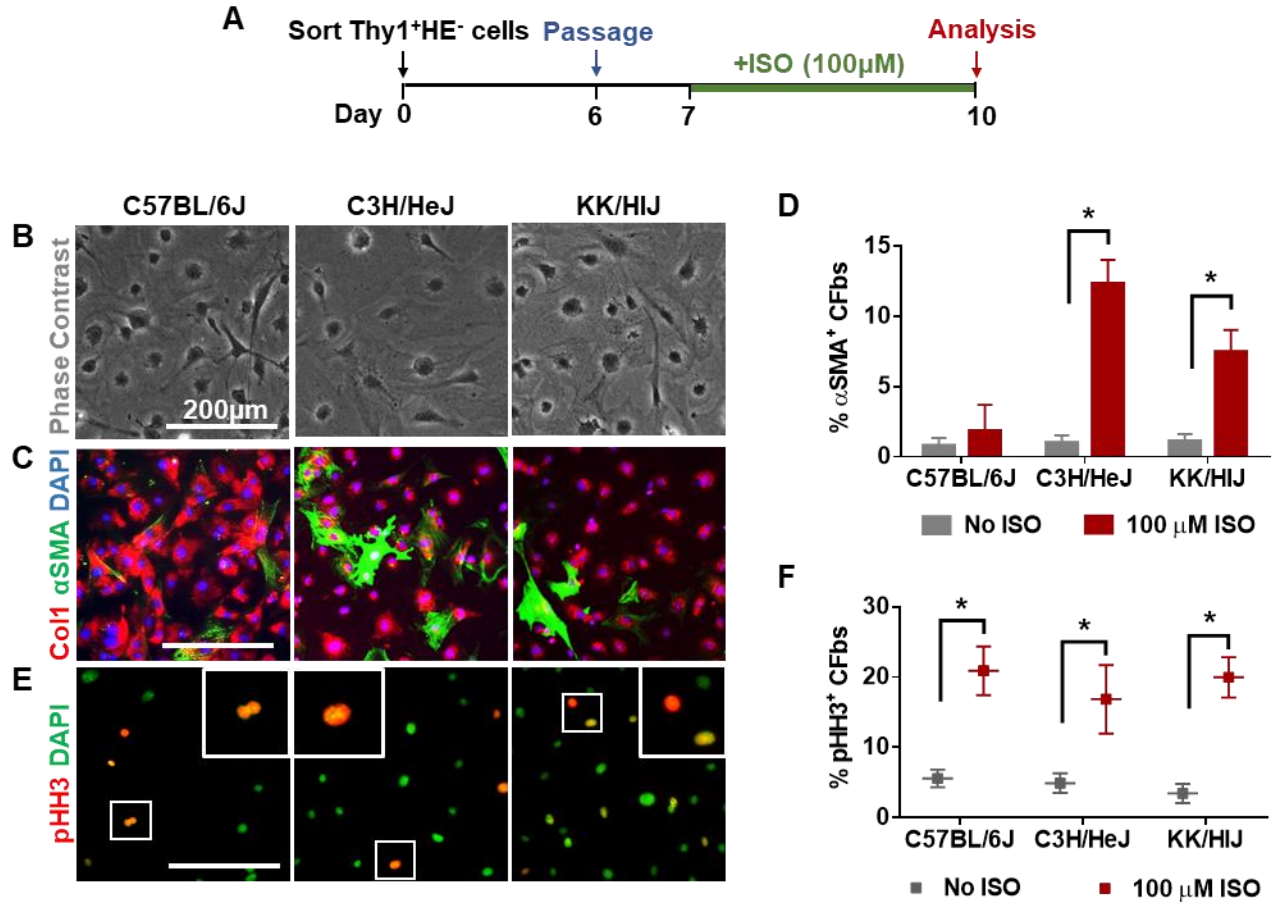
A
Sort Thy1+HE- cells
Passage
Analysis
+ISO (100μM)
Day 0
6
7
10
B
C57BL/6J
C3H/HeJ
KK/HlJ
Phase Contrast
200μm
C
Col1 αSMA DAPI
E
pHH3 DAPI
D
% αSMA+ CFbs
15
10
5
0
C57BL/6J
C3H/HeJ
KK/HlJ
No ISO
100 μM ISO
F
% pHH3+ CFbs
30
20
10
0
C57BL/6J
C3H/HeJ
KK/HlJ
No ISO
100 μM ISO

Figure 2: *In vitro* ISO treatment affects CFb activation and proliferation in a strain-specific manner

(A) Schematic diagram outlining the *in vitro* experiments. Cells were isolated by FACS, expanded, and passaged prior to exposure to ISO for 72 hours. **(B)** Phase contrast images of CFbs after ISO treatment. **(C)** Activated fibroblasts were identified by co-expression of Col1 (red) and αSMA (green) after ISO treatment. **(D)** Quantification of activated CFbs ($Col1^{+}\alpha SMA^{+}$ cells) is shown as a percentage of double-positive cells relative to all fibroblasts ($Col1^{+}$ cells) (n=5 wells/strain/condition). **(E)** Staining for mitotic marker phospho-Histone H3 (pHH3) was used to identify proliferating CFs in response to ISO. **(F)** Proliferation of CFbs after ISO treatment was measured by comparing the number of $pHH3^{+}$ nuclei relative to total nuclei (n=5 wells/strain/condition). DAPI was used to stain nuclei. Data presented as mean ± SEM. Student t-test, *P < 0.05. Scale bar: 200μm.

Figure 3

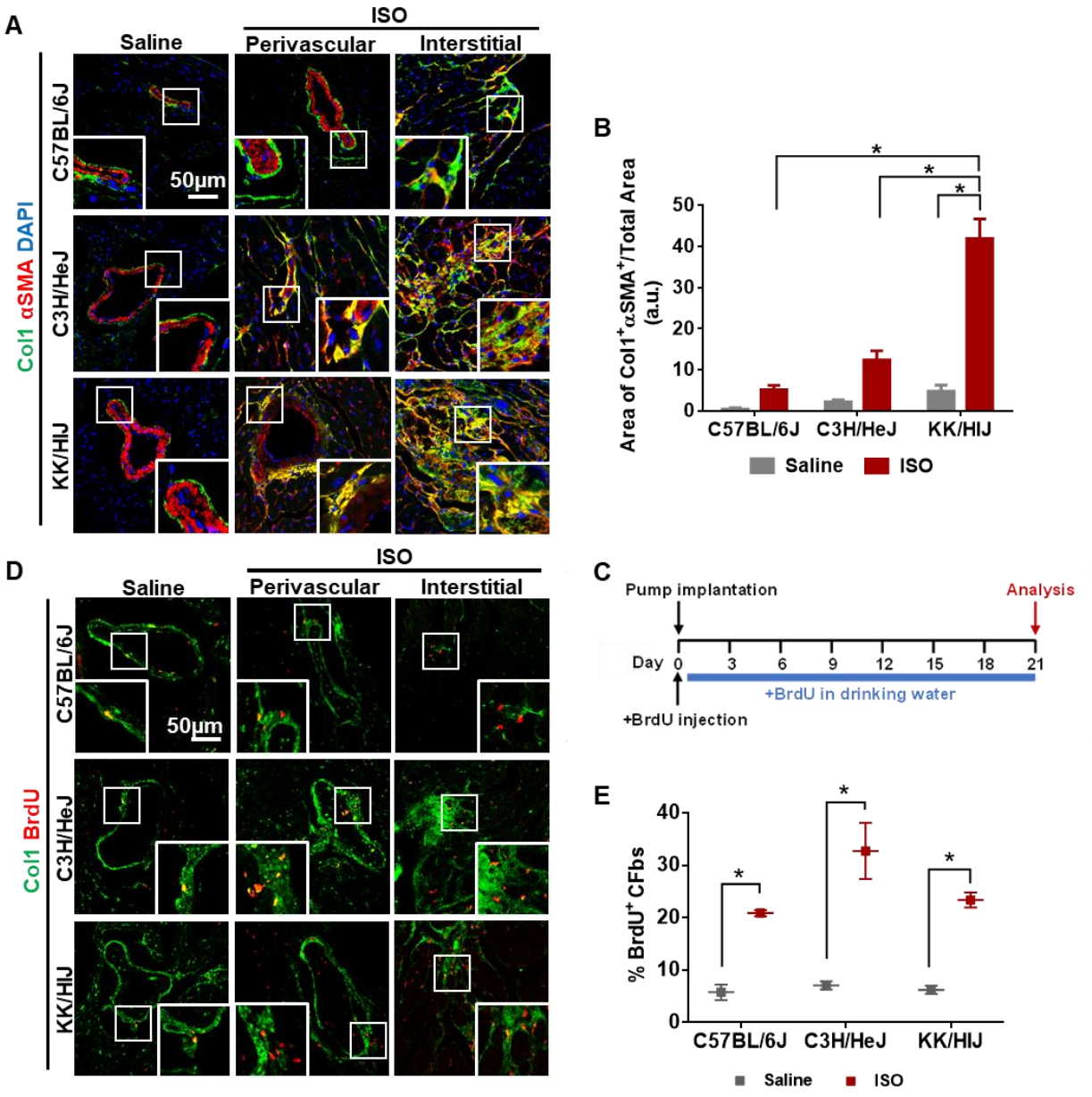
A
Saline
ISO
Perivascular
Interstitial
C57BL/6J
C3H/HeJ
KK/HlJ
Col1 αSMA DAPI
50μm
B
Area of Col1+αSMA+/Total Area (a.u.)
C57BL/6J
C3H/HeJ
KK/HlJ
Saline
ISO
C
Pump implantation
Analysis
Day 0 3 6 9 12 15 18 21
+BrdU in drinking water
+BrdU injection
D
Col1 BrdU
E
% BrdU+ CFbs

Figure 3: CFbs display a distinct pattern of activation and proliferation that is strain-specific after *in vivo* ISO treatment

(A) Heart sections from different strains after treatment with saline or ISO stained for αSMA (red) and Col1 (green) show presence of activated fibroblasts in perivascular and interstitial fibrotic areas. **(B)** Quantification of $Col1^{+}\alpha SMA^{+}$ co-localized areas as a percentage of total heart section area (n=3-4 hearts per strain/condition). **(C)** Schematic of *in vivo* bromodeoxyuridine (BrdU) administration. **(D)** IHC of heart sections from different strains after treatment with saline or ISO shows $BrdU^{+}$ cells within $Col1^{+}$ perivascular and interstitial fibrotic regions. **(E)** The extent of CFb proliferation is depicted as the percentage of $BrdU^{+}$ CFbs within the entire $Thy^{+}HE^{-}$ population in each strain after saline or ISO treatment (n=12/strain/condition). DAPI was used to stain nuclei. Data presented as mean ± SEM. Two-way ANOVA, *P< 0.05. Scale bar: 50μm

Figure 4

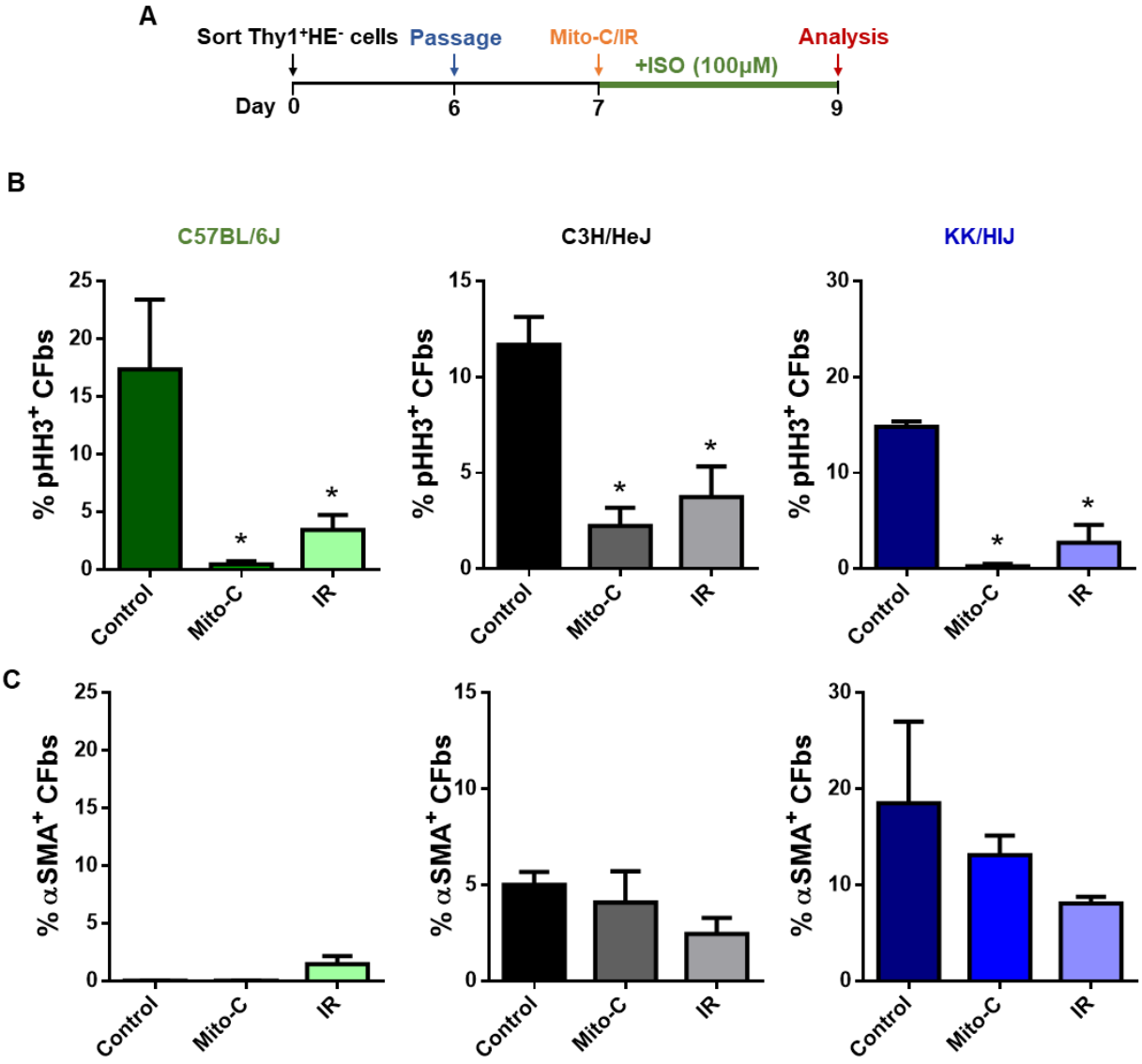
A
Sort Thy1+HE- cells
Passage
Mito-C/IR
Analysis
+ISO (100μM)
Day 0
6
7
9
B
C57BL/6J
C3H/HeJ
KK/HIJ
% pHH3+ CFbs
Control
Mito-C
IR
C
% αSMA+ CFbs
Control
Mito-C
IR

Figure 4: Inhibiting CFb proliferation does not affect CFb activation levels *in vitro*

(A) Schematic diagram outlining the experimental design. Cells were cultured in control media, media with mitomycin-C (mito-C), or irradiated (IR) prior to ISO treatment. **(B)** Proliferation of CFbs after ISO treatment was measured by comparing the number of $pHH3^{+}$ nuclei relative to total nuclei (n=4 wells/strain/condition). **(C)** Activated $Col1^{+}\alpha SMA^{+}$ cells are shown as a percentage of double-positive cells relative to all $Col1^{+}$ cells (n=4 wells/strain/condition). Data presented as mean ± SEM. One-way ANOVA, *P < 0.05.

Figure 5

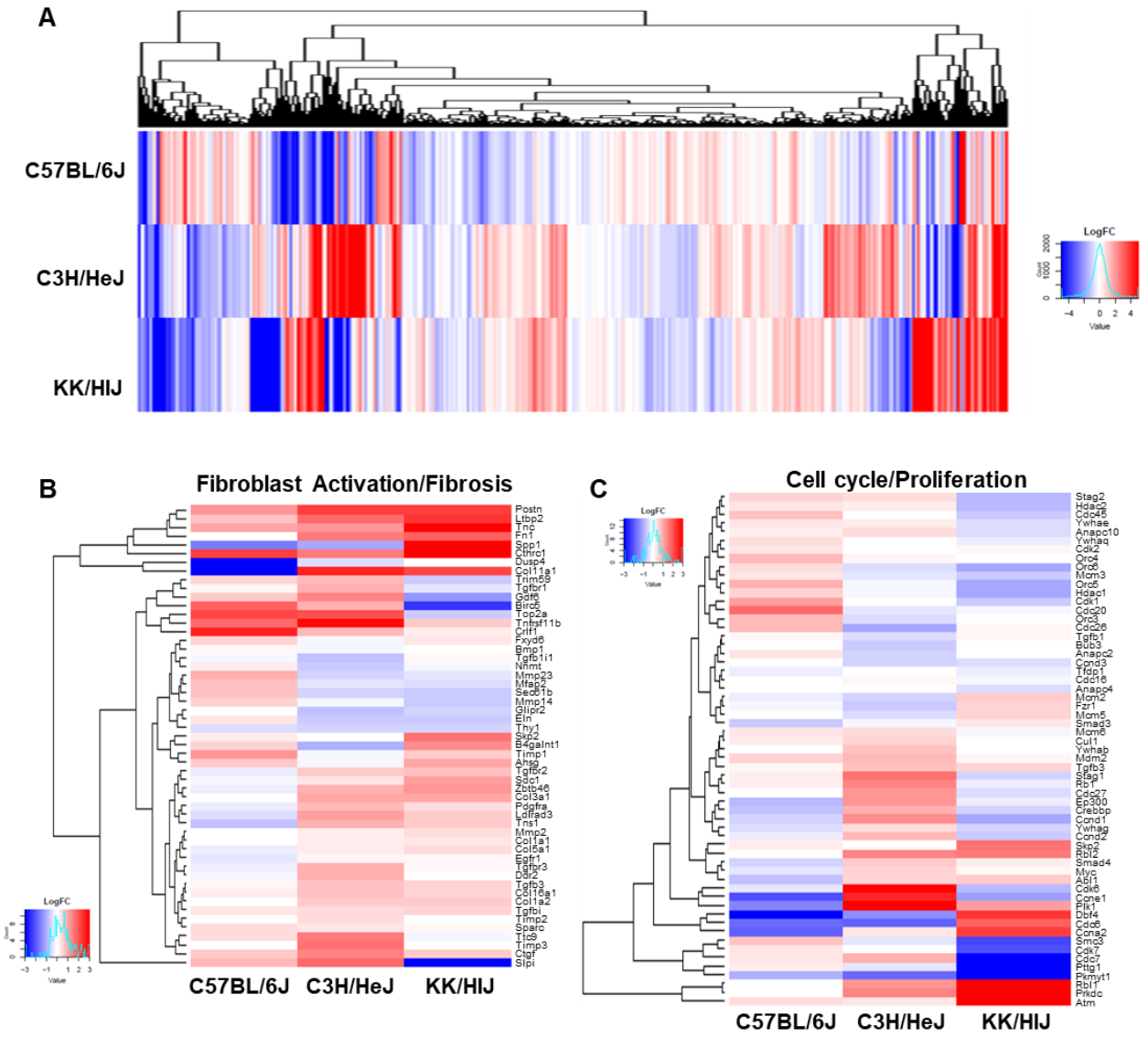
A
C57BL/6J
C3H/HeJ
KK/HlJ
LogFC
B
Fibroblast Activation/Fibrosis
Postn
Ltbp2
Tnc
Fn1
Spp1
Cthrc1
Dusp4
Col11a1
Trim59
Tgfbr1
Gdf6
Birc5
Top2a
Tnfsf11b
Crlf1
Fxyd6
Bmp1
Tgfb1i1
Nnmt
Mmp23
Mfap2
Sec61b
Mmp14
Glipr2
Eln
Thy1
Skp2
B4galnt1
Timp1
Ahsg
Tgfbr2
Sdc1
Zbtb46
Col3a1
Pdgfra
Ldlrad3
Tns1
Mmp2
Col1a1
Col5a1
Egfr1
Tgfbr3
Dkk2
Tgfb3
Col16a1
Col1a2
Tgfbi
Timp2
Sparc
Ttc9
Timp3
Ctgf
Slpi
C57BL/6J
C3H/HeJ
KK/HlJ
C
Cell cycle/Proliferation
Stag2
Hdac2
Cdc45
Ywhae
Anapc10
Ywhaq
Cdk2
Orc4
Orc6
Mcm3
Orc5
Hdac1
Cdk1
Cdc20
Orc3
Cdc26
Tgfb1
Bub3
Anapc2
Ccnd3
Tfdp1
Cdc16
Anapc4
Mcm2
Fzr1
Mcm5
Smad3
Mcm6
Cul1
Ywhab
Mdm2
Tgfb3
Stag1
Rbl1
Cdc27
Ep300
Crebbp
Ccnd1
Ywhag
Ccnd2
Skp2
Rbl2
Smad4
Myc
Abl1
Cdk6
Ccne1
Plk1
Dbf4
Cdc6
Ccna2
Smc3
Cdk7
Cdc7
Ptg1
Pkmyt1
Rbl1
Prkdc
Atm
C57BL/6J
C3H/HeJ
KK/HlJ

Figure 5: ISO treatment induces unique gene expression patterns in CFbs of different strains after 21 days

(A) Heat map showing log2 fold change of differentially expressed genes in CFbs of all strains after 21 days of ISO treatment. **(B)** Heat map representing the log2 fold change value of select differentially expressed genes involved in fibroblast activation and fibrosis. **(C)** Heat map comparing expression changes of select genes involved in cell cycle and proliferation across the three strains.

Figure 6

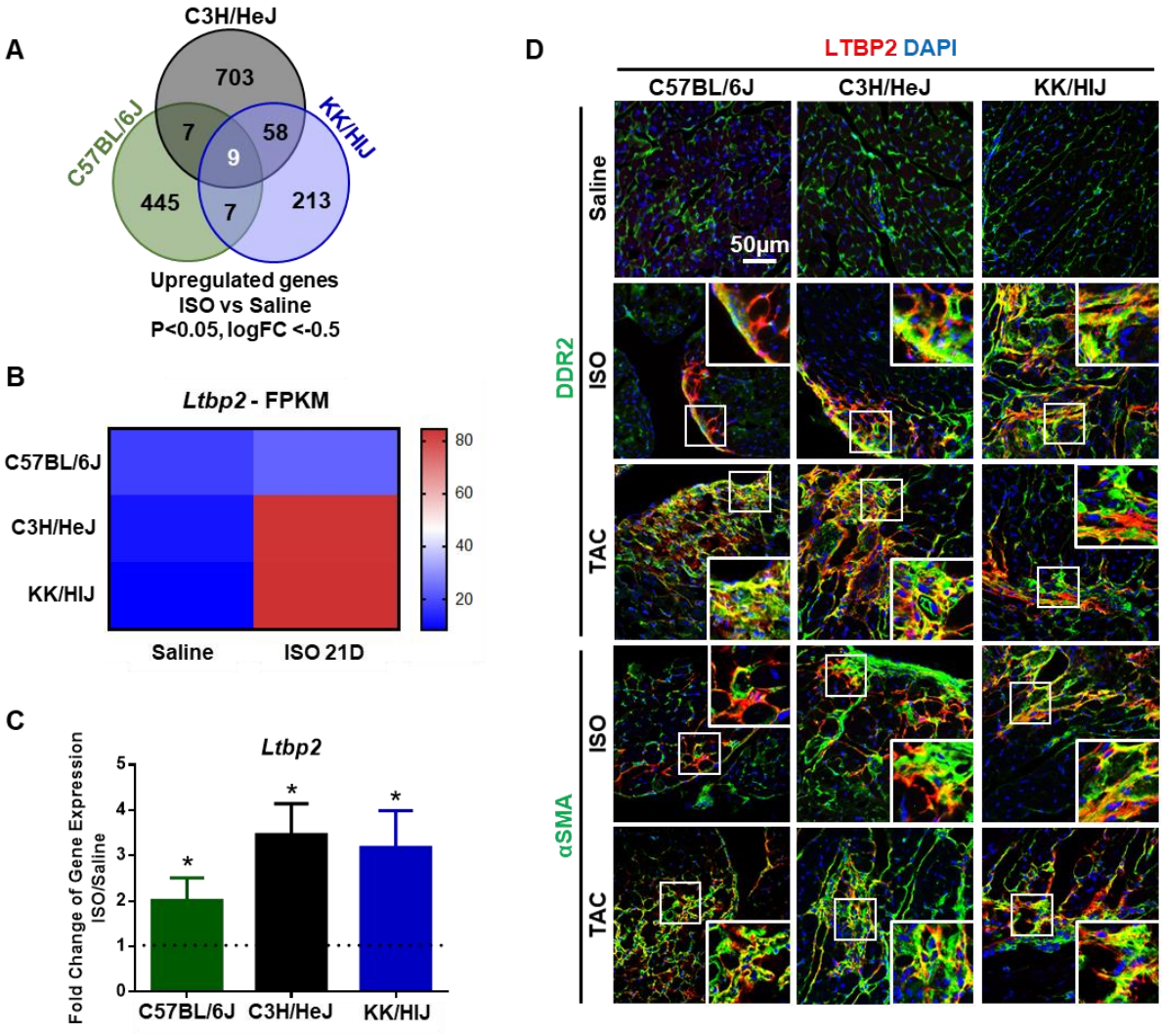
A
C3H/HeJ
703
C57BL/6J
KK/HIJ
7
58
9
445
7
213
Upregulated genes
ISO vs Saline
P<0.05, logFC <-0.5
B
Ltbp2 - FPKM
C57BL/6J
C3H/HeJ
KK/HIJ
80
60
40
20
Saline
ISO 21D
C
Ltbp2
Fold Change of Gene Expression
ISO/Saline
5
4
3
2
1
0
*
*
*
C57BL/6J
C3H/HeJ
KK/HIJ
D
LTBP2 DAPI
C57BL/6J
C3H/HeJ
KK/HIJ
Saline
50μm
DDR2
ISO
TAC
αSMA
ISO
TAC

Figure 6: *Ltbp2* is upregulated in CFbs of all strains after injury.

(A) Venn diagram depicting the number of overlapping upregulated genes across all three strains after ISO treatment. **(B)** Average FPKM values for *Ltbp2* in all three strains after 21 days of ISO treatment. **(C)** RT-qPCR analysis of *Ltbp2* after ISO treatment (n=7-9/strain/condition). **(D)** IHC of heart sections stained for LTBP2 (red) and DDR2 (green) or αSMA (green) after ISO treatment and TAC injury. DAPI was used to stain nuclei. FPKM: fragments per kilobase of transcript per million mapped reads. TAC: transverse aortic constriction. Data presented as mean ± SEM. Student t-test, *P < 0.05. Scale bar: 50μm

Supplementary Figure I

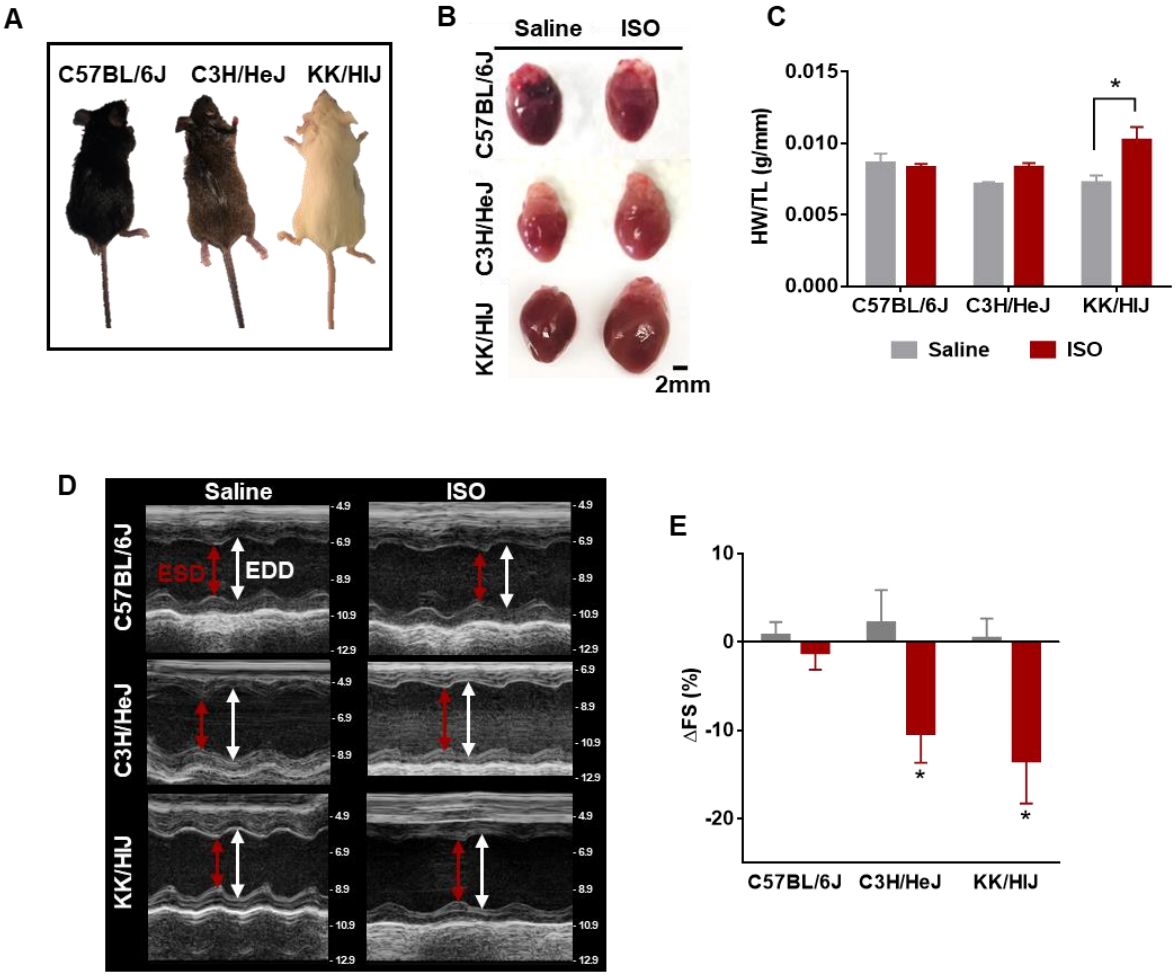

Supplementary Figure I: **Severity of cardiac hypertrophy and cardiac dysfunction varies among select strains in response to ISO treatment**

(A) Representative images of adult, female mice (8-12 weeks) from all three strains: C57BL/6J, C3H/HeJ, and KK/HIJ. **(B)** Whole heart images of the different strains after 21 days of saline or ISO treatment (n=6 mice/condition). **(C)** Heart weight/tibia length (HW/TL) ratios after saline or ISO treatment (n=20 hearts/strain). **(D)** Representative M-mode echocardiographic images of hearts from animals following 21 days of saline or ISO treatment (n=20 mice/strain). **(E)** Fractional shortening (FS) was measured by echocardiography in both saline and ISO groups across the different strains (n=20 mice/strain). ESD: end-systolic dimension. EDD: end-diastolic dimension. Data presented as mean ± SEM. Two-way ANOVA, *P < 0.05. Scale bar: 2mm.

Supplementary Figure II

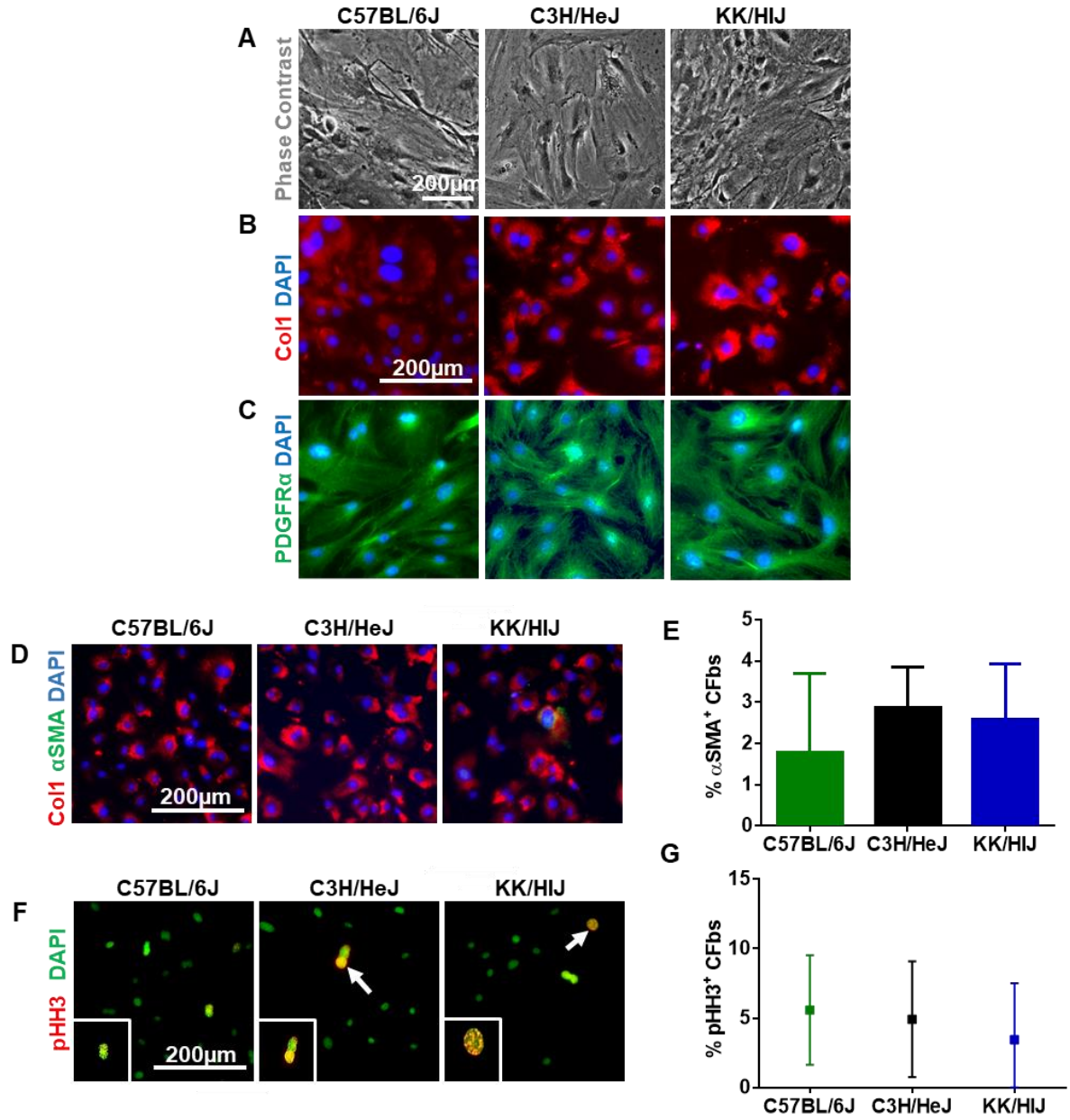

Supplementary Figure II: Strain-specific CFbs exhibit similar characteristics in culture

(A) Phase contrast images of $Thy1^{+}HE^{-}$ cells from the hearts of the three strains that were isolated by FACS and expanded in culture. Cultured $Thy1^{+}HE^{-}$ cells expressed fibroblast associated markers Collagen1 (Col1) (red) **(B)** and PDGFRα (green) **(C)**. Activated CFbs were marked by co-expression of αSMA (green) and Col1 (red) **(D)**. Rare, activated CFbs were observed in the absence of any stimuli. The bar graph demonstrates the percentage of $Col1^{+}αSMA^{+}$ cells relative to all $Col1^{+}$ cells (n=5 wells/strain/condition) **(E)**. Proliferating CFbs were identified by nuclear staining for phospho-Histone H3 (pHH3) (red) **(F)**. The percentage of $pHH3^{+}$ nuclei was measured relative to total nuclei (green) (n=5 wells/strain/condition) **(G)**. DAPI was used to stain nuclei. Data presented as mean ± SEM. Student t-test. Scale bar: 200μm.

Supplementary Figure III

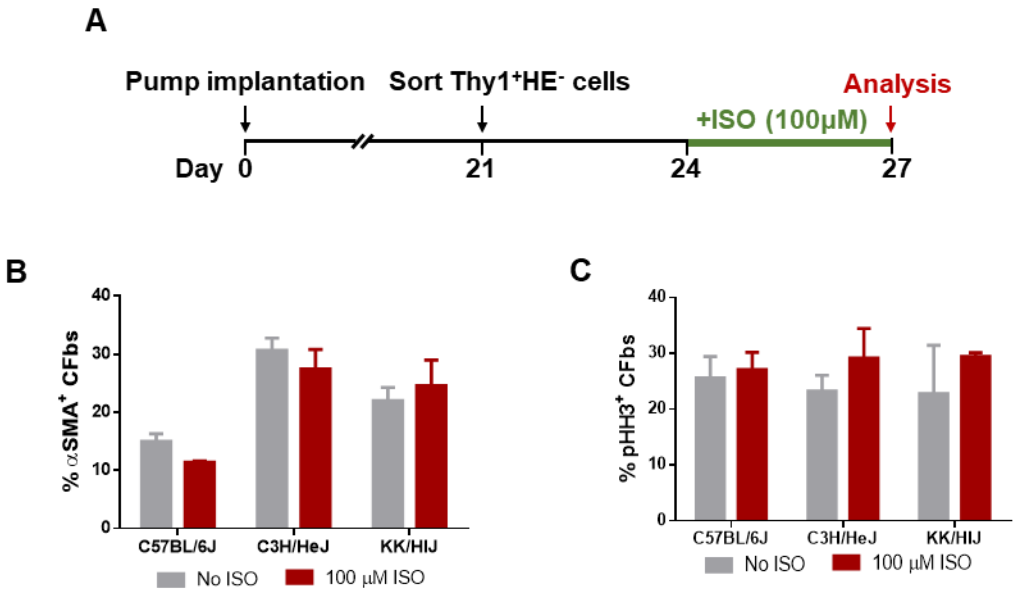

Supplementary Figure III: *In vitro* culture of CFbs isolated from ISO-treated mice exhibit minimal responses

(A) Schematic outlining culture of CFbs from mice that have been treated with ISO prior to CFb isolation. *In vitro* ISO treatment had no significant effect on the percentage of αSMA^+ **(B)** and $pHH3^+$ **(C)** cardiac fibroblasts isolated from ISO-treated mice. Data presented as mean ± SEM. Two-way ANOVA.

Supplementary Figure IV

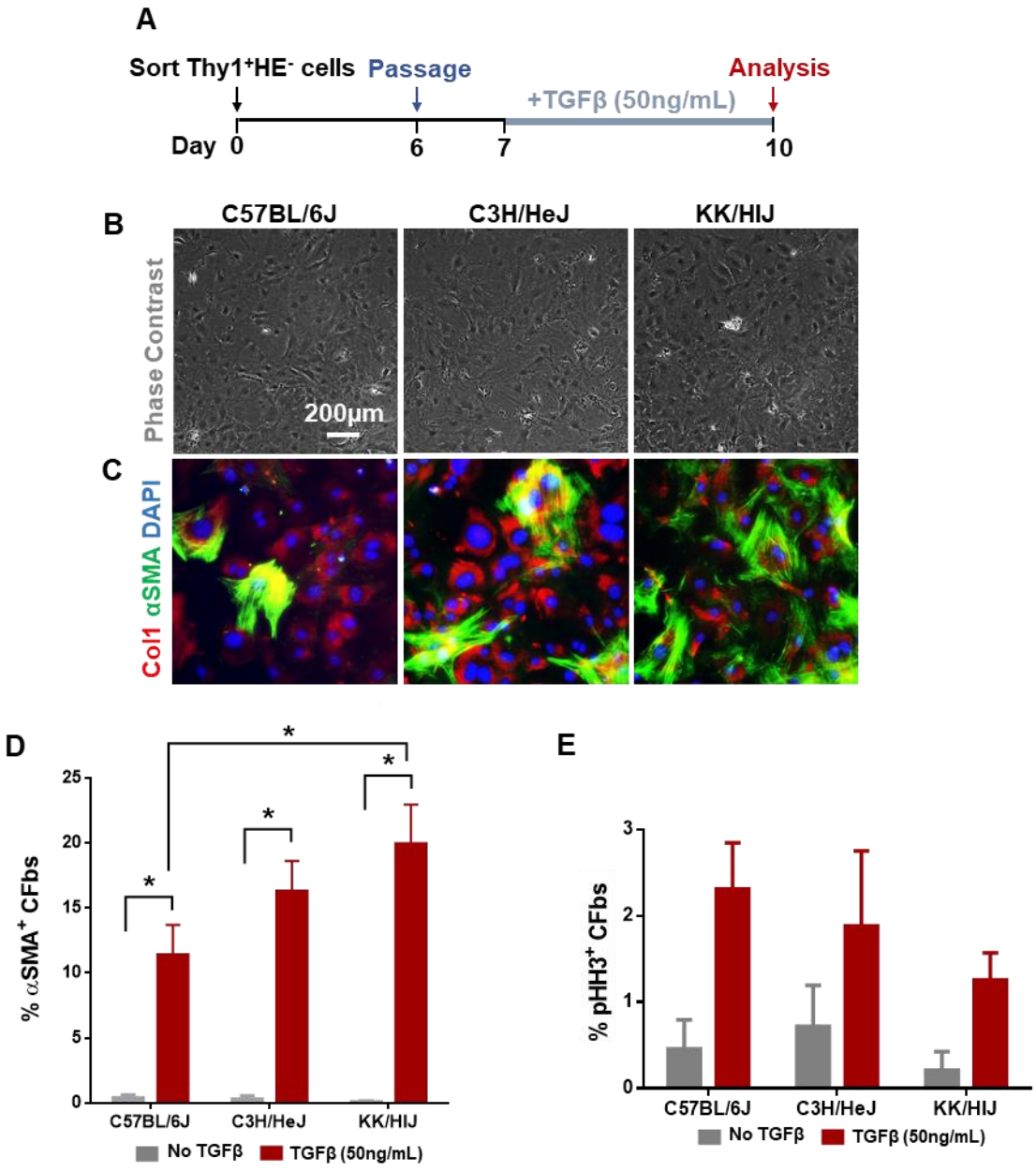

Supplementary Figure IV: Treatment of CFbs from different strains with TGFβ induces differential responses

(A) Schematic of *in vitro* TGFβ treatment. **(B)** Phase contrast images of CFbs from different strains after TGFβ treatment. **(C)** Immunocytochemistry for Col1 (red) and αSMA (green) was used to identify activated fibroblasts. **(D)** CFb activation was quantified as a percentage of $Col1^{+}\alpha SMA^{+}$ cells relative to all $Col1^{+}$ cells. **(E)** Quantification of CFb proliferation is presented as a percentage of $pHH3^{+}$ nuclei of total nuclei. DAPI was used to stain nuclei. Scale bar: 200μm. Data presented as mean ± SEM. Two-way ANOVA, *P<0.05

Supplementary Figure V

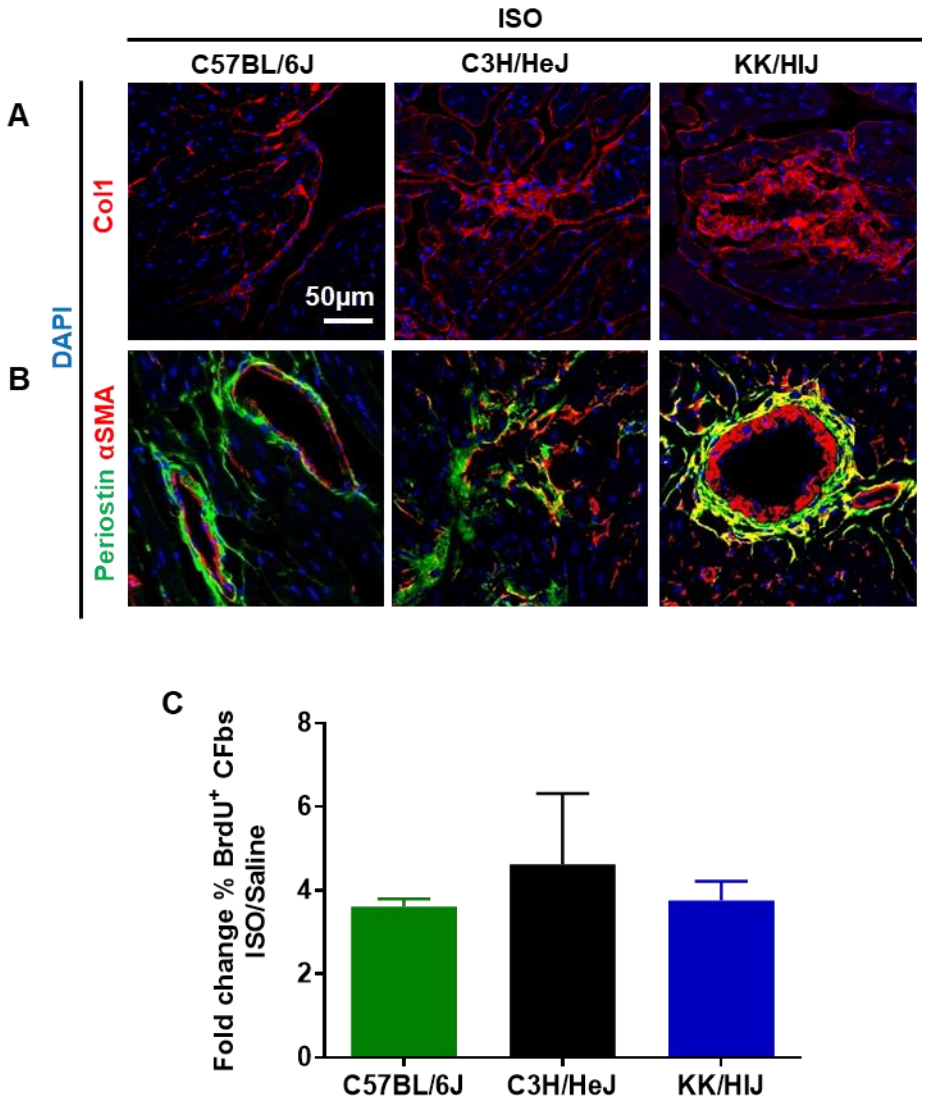

Supplementary Figure V: Levels of CFb activation after ISO treatment correlate with extent of collagen deposition, while CFb proliferation does not

(A) Heart sections after ISO treatment were stained for Col1 (red) to visualize extracellular matrix deposition. **(B)** Immunohistochemistry of ISO-treated heart sections stained for periostin (green) and αSMA (red), which both mark activated fibroblasts. **(C)** Fold change of proliferation rates in response to ISO were compared across the different strains. Each ISO-treated group was normalized to their respective control groups within each strain (n=12/strain/condition). DAPI was used to stain nuclei. Data presented as mean ± SEM. One-way ANOVA. Scale bar: 50μm.

Supplementary Figure VI

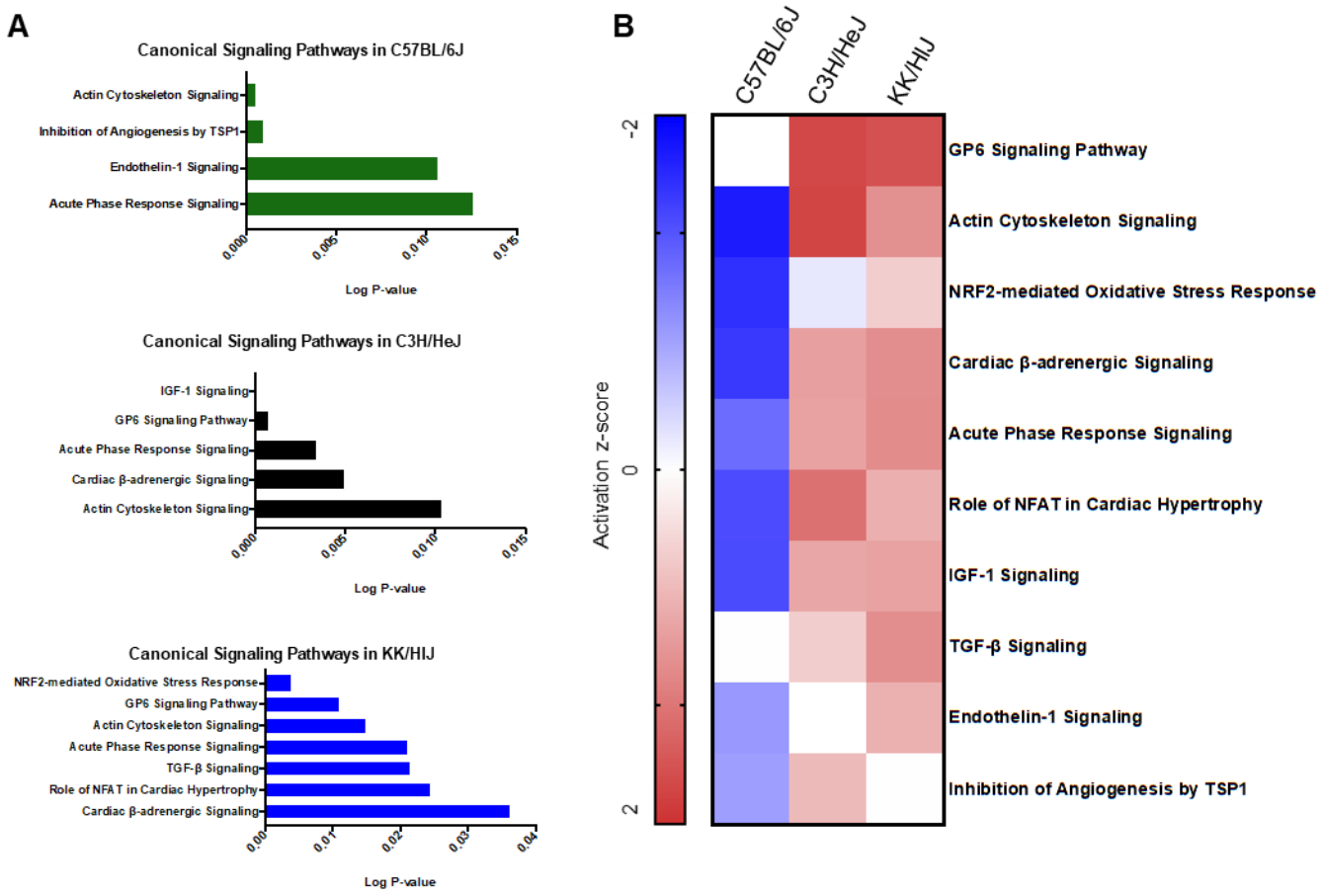

Supplementary Figure VI: CFbs from select strains are enriched for various canonical pathways after 21 days of ISO treatment

(A) Significantly enriched pathways from Ingenuity Pathway Analysis (IPA) in each strain after 21 days of ISO treatment. **(B)** IPA was used to generate a list of activated canonical pathways in CFbs treated with ISO compared to saline. Pathways were selected based on the trends that correlated with the extent of fibrosis seen *in vivo*.

Supplementary Figure VII

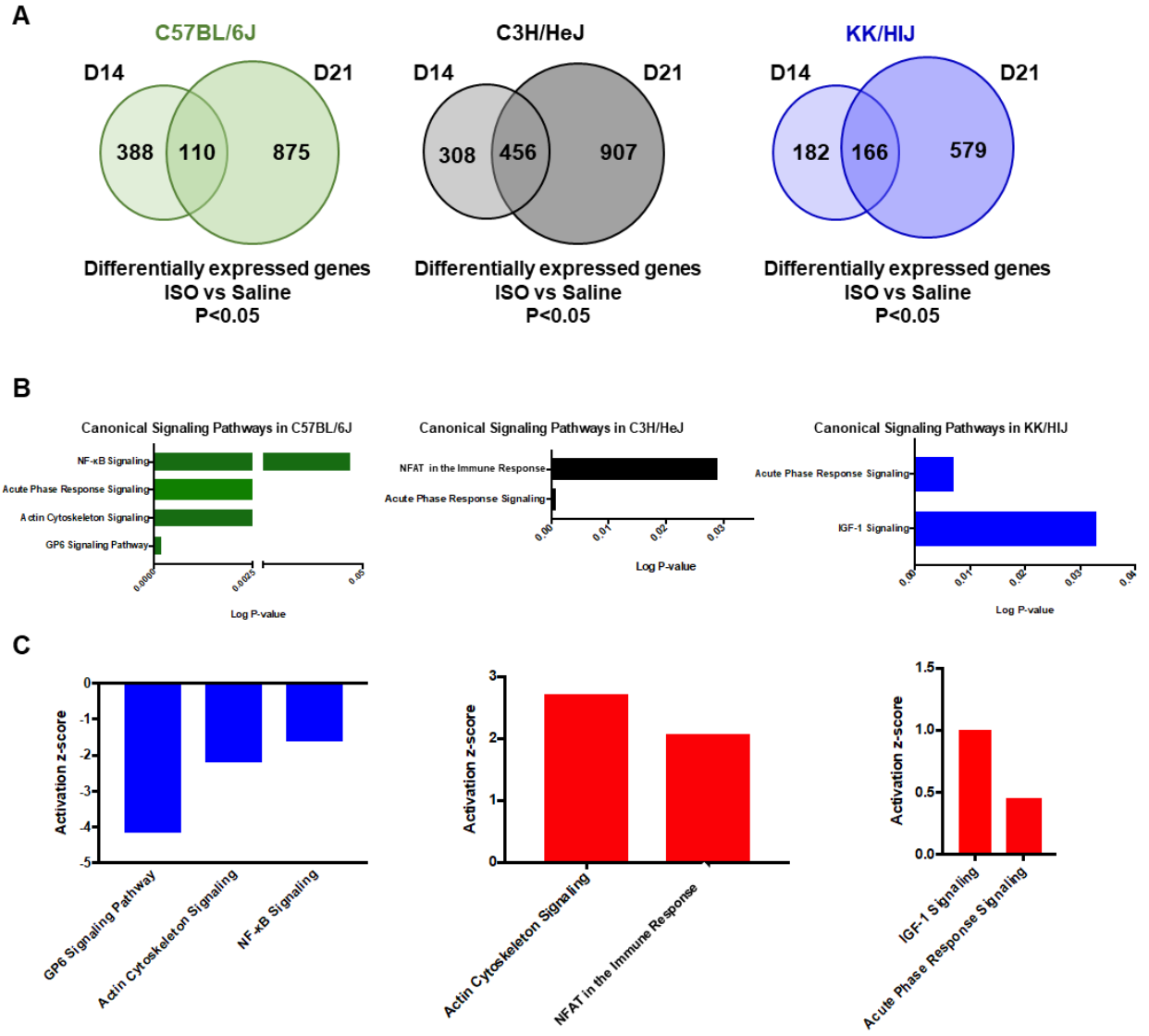

Supplementary Figure VII: CFbs from all strains display unique gene expression changes between 14 and 21 days of ISO treatment

(A) Venn diagrams showing number of differentially expressed genes in CFbs from mice that had been treated with ISO for 14 or 21 days compared to CFbs from saline-treated mice. IPA was also used to determine activation scores **(B)** and canonical pathways that were significantly enriched for **(C)** within each strain between 14 and 21 days of ISO treatment.

Supplementary Figure VIII

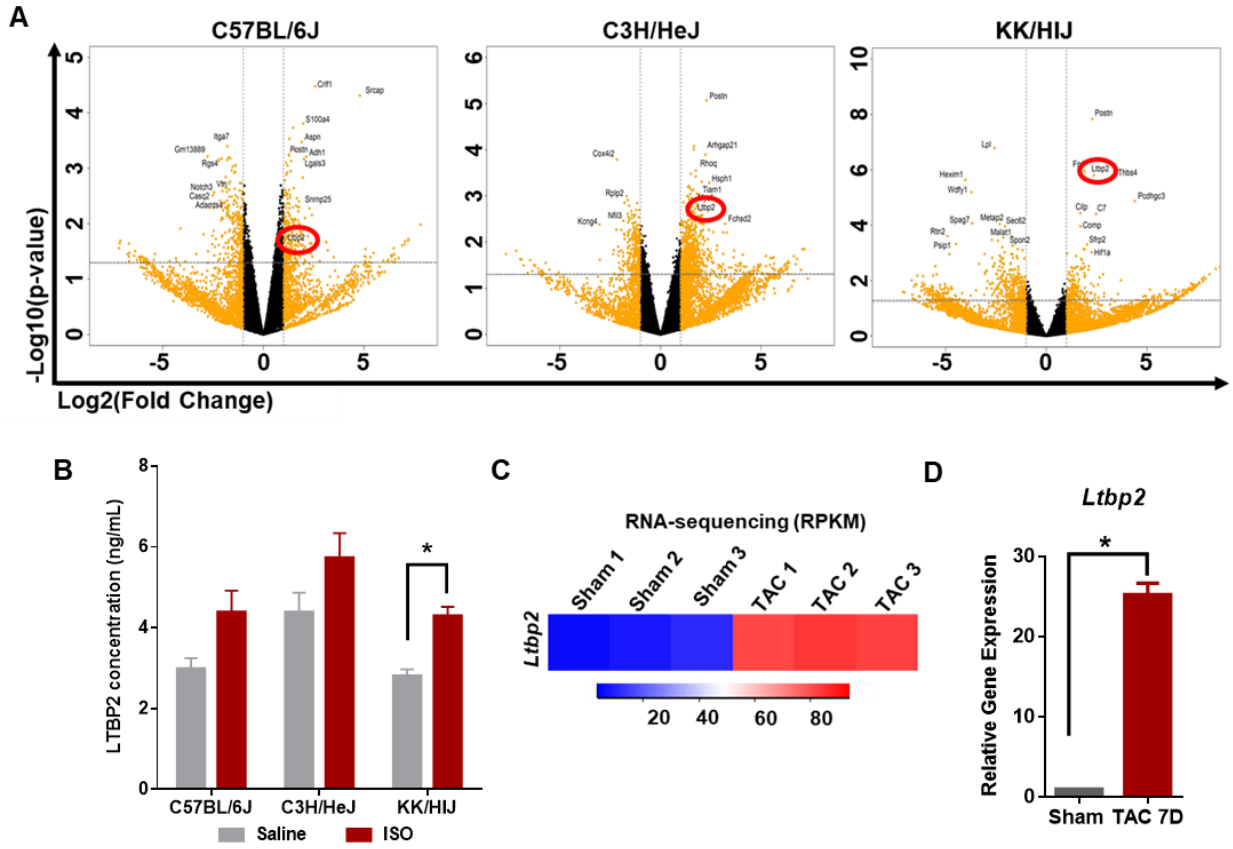

Supplementary Figure VIII: LTBP2 is upregulated in multiple injury models in mice

(A) Volcano plots derived from RNA-sequencing data from all three strains depicting differentially expressed genes 21 days after ISO treatment compared to saline-treated. *Ltbp2* is indicated by the red circles. **(B)** LTBP2 protein levels in mouse plasma samples after ISO treatment, measured by ELISA (n=3/strain/condition). RNA-sequencing **(C)** and RT-qPCR analysis **(D)** of *Ltbp2* gene expression in CFbs isolated from C57BL/6J, 7 days post-sham or TAC operation. (n=3/mice/condition). RPKM: Reads Per Kilobase of transcript, per Million mapped reads. TAC: transverse aortic constriction. Data presented as mean ± SEM. Student t-test, *P < 0.05.

Supplementary Figure IX

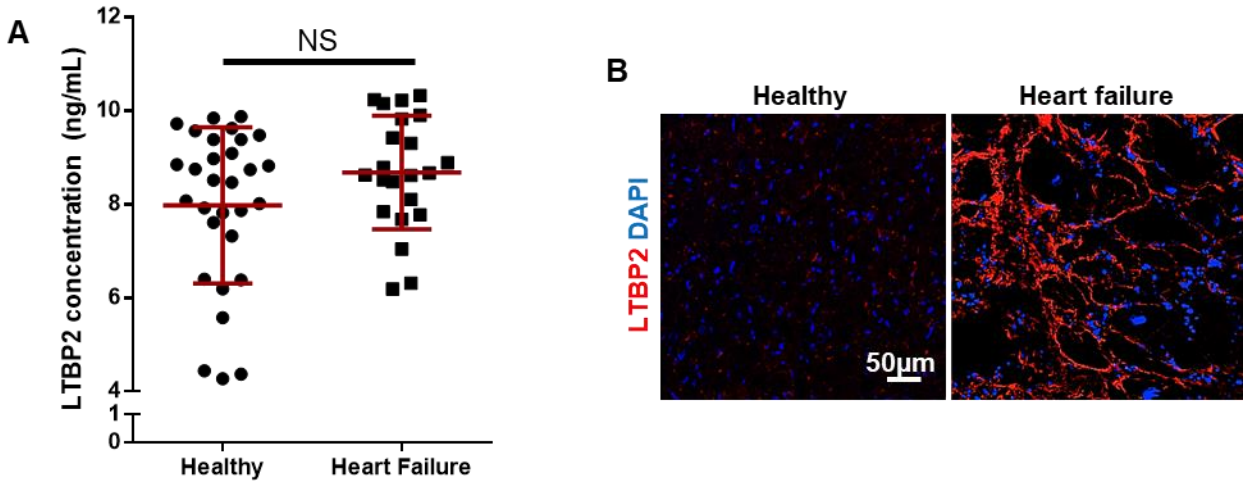

Supplementary Figure IX: LTBP2 expression is upregulated in human heart failure patients

(A) Quantification of LTBP2 levels in plasma samples from healthy individuals and heart failure patients by ELISA. **(B)** Heart sections from healthy and failing human hearts stained for LTBP2 (red). DAPI was used to stain nuclei. Data presented as mean ± SD. Student t-test, NS: non-significant. Scale bar: 50µm.

Supplementary Table I

Antibody	Catalog number	Vendor
Collagen 1 (1:100)	ab34710	Abcam
αSMA (1:100)	A2547	Sigma-Aldrich
PDGFRα (1:100)	Sc-338	Santa Cruz Biotechnology
Periostin (1:100)	AF2955	R&D Systems
LTBP2 (1:200)	Gift from Dr. Marko Hyytiäinen from the University of Helsinki, Finland	
DDR2 (1:100)	MAB25381	R&D Systems
pHH3 (1:50)	ab47297	Abcam
BrdU (1:50)	ab6326	Abcam
Anti-Mouse CD 90.1 APC-eFluor 780	47-0900-82	eBioscience
Anti-Mouse CD 90.2 APC-eFluor 780	47-0900-82	eBioscience
Anti-Mouse CD31 PE-Cyanine7	25-0311-81	eBioscience
Anti-Mouse CD11b PE-Cyanine7	25-0112-81	eBioscience
Anti-Mouse CD45 PE-Cyanine5	48-0451-82	eBioscience
TER-119 PE-Cyanine7	25-5921-81	eBioscience
Donkey Anti-Rabbit Alexa Fluor 647	A-31573	Invitrogen
Rabbit Anti-Mouse Alexa Fluor 647	A-21239	Invitrogen
Goat Anti-Rabbit Alexa Fluor 594	A-11037	Invitrogen
Goat Anti-Rabbit Alexa Fluor 488	A-21206	Invitrogen
Goat Anti-Mouse Alexa Fluor 488	A-11001	Invitrogen

Supplementary Table II

Gene	Forward Primer	Reverse Primer
Gapdh	TTGTCTCCTGCGACTTCAAC	GTCATACCAGGAAATGAGCTTG
Ltbp2	AACAGCACCAACCACTGTATC	CCTGGCATTCTGAGGGTCAAA

Supplementary Table III

Marker	Species	Catalog number	vendor
LTBP2	Mouse	MBS2885029	MyBioSource
LTBP2	Human	MBS2882493	MyBioSource

Supplementary Table IV

	Age (year)	Gender	Etiology	EF (%)	Median BNP (pg/ml)	DM	h/o HTN	Afib
Healthy individuals	50±10	50% Male 50% Female	N/A	≥55	NA	0%	0%	0%
HF-1	56	Male	Non-ischemic	15%	1719	N	h/O	N
HF-2	48	Male	Non-ischemic	20%	1244	Y	Y	Y
HF-3	59	Female	Ischemic	25%	716	N	N	N
HF-4	70	Male	Ischemic	25%	737	Y	N	N
HF-5	60	Female	Non-ischemic	25%	696	N	N	N
HF-6	64	Male	Ischemic	30%	567	Y	Y	Y
HF-7	53	Male	Ischemic	20%	541	Y	Y	N
HF-8	67	Male	Ischemic	25%	710	Y	Y	N
HF-9	57	Male	Ischemic	20%	707	N	N	N
HF-10	69	Male	Ischemic	25%	1107	Y	Y	N
HF-11	50	Male	Non-ischemic	25%	1671	N	Y	N
HF-12	52	Female	Non-ischemic	35%	554	N	N	N
HF-13	49	Male	Non-ischemic	30%	498	N	N	N
HF-14	59	Male	Ischemic	20%	870	Y	N	N
HF-15	62	Female	Ischemic	25%	1104	Y	Y	N
HF-16	49	Male	Non-ischemic	25%	1009	N	N	N
HF-17	53	Male	Non-ischemic	20%	947	N	N	N
HF-18	57	Female	Ischemic	25%	894	Y	Y	N

REFERENCES

1. Fan D, Takawale A, Lee J and Kassiri Z. Cardiac fibroblasts, fibrosis and extracellular matrix remodeling in heart disease. *Fibrogenesis Tissue Repair*. 2012;5:15 doi: 10.1186/1755-1536-5-15.
2. Ali SR, Ranjbarvaziri S, Talkhabi M, Zhao P, Subat A, Hojjat A, Kamran P, Muller AM, Volz KS, Tang Z, Red-Horse K and Ardehali R. Developmental heterogeneity of cardiac fibroblasts does not predict pathological proliferation and activation. *Circ Res*. 2014;115:625-635. doi: 10.1161/CIRCRESAHA.115.303794.
3. Travers JG, Kamal FA, Robbins J, Yutzey KE and Blaxall BC. Cardiac Fibrosis: The Fibroblast Awakens. *Circ Res*. 2016;118:1021-1040. doi: 10.1161/CIRCRESAHA.115.306565.
4. Lusis AJ, Seldin MM, Allayee H, Bennett BJ, Civelek M, Davis RC, Eskin E, Farber CR, Hui S, Mehrabian M, Norheim F, Pan C, Parks B, Rau CD, Smith DJ, Vallim T, Wang Y and Wang J. The Hybrid Mouse Diversity Panel: a resource for systems genetics analyses of metabolic and cardiovascular traits. *J Lipid Res*. 2016;57:925-942. doi: 10.1194/jlr.R066944.
5. Rau CD, Wang J, Avetisyan R, Romay MC, Martin L, Ren S, Wang Y and Lusis AJ. Mapping genetic contributions to cardiac pathology induced by Beta-adrenergic stimulation in mice. *Circ Cardiovasc Genet*. 2015;8:40-49. doi: 10.1161/CIRCGENETICS.113.000732.
6. Wang JJ, Rau C, Avetisyan R, Ren S, Romay MC, Stolin G, Gong KW, Wang Y and Lusis AJ. Genetic Dissection of Cardiac Remodeling in an Isoproterenol-Induced Heart Failure Mouse Model. *PLoS Genet*. 2016;12:e1006038. doi: 10.1371/journal.pgen.1006038.
7. Baum J and Duffy HS. Fibroblasts and myofibroblasts: what are we talking about? *J Cardiovasc Pharmacol*. 2011;57:376-379. doi: 10.1097/FJC.0b013e3182116e39.
8. Crosio C, Fimia GM, Loury R, Kimura M, Okano Y, Zhou H, Sen S, Allis CD and Sassone-Corsi P. Mitotic phosphorylation of histone H3: spatio-temporal regulation by mammalian Aurora kinases. *Mol Cell Biol*. 2002;22:874-885.

9. Squires CE, Escobar GP, Payne JF, Leonardi RA, Goshorn DK, Sheats NJ, Mains IM, Mingoia JT, Flack EC and Lindsey ML. Altered fibroblast function following myocardial infarction. *J Mol Cell Cardiol*. 2005;39:699-707.
10. Leask A. TGFbeta, cardiac fibroblasts, and the fibrotic response. *Cardiovasc Res*. 2007;74:207-212.
11. Kanisicak O, Khalil H, Ivey MJ, Karch J, Maliken BD, Correll RN, Brody MJ, SC JL, Aronow BJ, Tallquist MD and Molkentin JD. Genetic lineage tracing defines myofibroblast origin and function in the injured heart. *Nat Commun*. 2016;7:12260. doi: 10.1038/ncomms12260.
12. Snider P, Standley KN, Wang J, Azhar M, Doetschman T and Conway SJ. Origin of cardiac fibroblasts and the role of periostin. *Circ Res*. 2009;105:934-947. doi: 10.1161/CIRCRESAHA.109.201400.
13. Ponchio L, Duma L, Oliviero B, Gibelli N, Pedrazzoli P and Robustelli della Cuna G. Mitomycin C as an alternative to irradiation to inhibit the feeder layer growth in long-term culture assays. *Cytotherapy*. 2000;2:281-286.
14. Biernacka A, Dobaczewski M and Frangogiannis NG. TGF-beta signaling in fibrosis. *Growth Factors*. 2011;29:196-202. doi: 10.3109/08977194.2011.595714.
15. Ross B, D'Orleans-Juste P and Giaid A. Potential role of endothelin-1 in pulmonary fibrosis: from the bench to the clinic. *Am J Respir Cell Mol Biol*. 2010;42:16-20. doi: 10.1165/rcmb.2009-0175TR.
16. deAlmeida AC, van Oort RJ and Wehrens XH. Transverse aortic constriction in mice. *J Vis Exp*. 2010;38:1729. doi: 10.3791/1729.
17. Chen W and Frangogiannis NG. Fibroblasts in post-infarction inflammation and cardiac repair. *Biochim Biophys Acta*. 2013;1833:945-953. doi: 10.1016/j.bbamcr.2012.08.023.
18. Midgley AC, Rogers M, Hallett MB, Clayton A, Bowen T, Phillips AO and Steadman R. Transforming growth factor-beta1 (TGF-beta1)-stimulated fibroblast to myofibroblast differentiation is mediated by hyaluronan (HA)-facilitated epidermal growth factor receptor

(EGFR) and CD44 co-localization in lipid rafts. *J Biol Chem*. 2013;288:14824-14838. doi: 10.1074/jbc.M113.451336.

19. Manabe I, Shindo T and Nagai R. Gene expression in fibroblasts and fibrosis: involvement in cardiac hypertrophy. *Circ Res*. 2002;91:1103-1113.
20. Watson SP, Auger JM, McCarty OJ and Pearce AC. GPVI and integrin alphaIIb beta3 signaling in platelets. *J Thromb Haemost*. 2005;3:1752-1762.
21. Stranger BE, Stahl EA and Raj T. Progress and promise of genome-wide association studies for human complex trait genetics. *Genetics*. 2011;187:367-383. doi: 10.1534/genetics.110.120907.
22. Rau CD, Lusis AJ and Wang Y. Genetics of common forms of heart failure: challenges and potential solutions. *Curr Opin Cardiol*. 2015;30:222-227. doi: 10.1097/HCO.0000000000000160.
23. Dallas SL, Keene DR, Bruder SP, Saharinen J, Sakai LY, Mundy GR and Bonewald LF. Role of the latent transforming growth factor beta binding protein 1 in fibrillin-containing microfibrils in bone cells in vitro and in vivo. *J Bone Miner Res*. 2000;15:68-81.
24. Penttinen C, Saharinen J, Weikkolainen K, Hyytiainen M and Keski-Oja J. Secretion of human latent TGF-beta-binding protein-3 (LTBP-3) is dependent on co-expression of TGF-beta. *J Cell Sci*. 2002;115:3457-3468.
25. Bultmann-Mellin I, Dinger K, Debuschewitz C, Loewe KMA, Melcher Y, Plum MTW, Appel S, Rappl G, Willenborg S, Schauss AC, Jungst C, Kruger M, Dressler S, Nakamura T, Wempe F, Alejandre Alcazar MA and Sterner-Kock A. Role of LTBP-4 in alveolarization, angiogenesis and fibrosis in lungs. *Am J Physiol Lung Cell Mol Physiol*. 2017;313:L687-L698. doi: 10.1152/ajplung.00031.2017.

CHAPTER 5

Cardiac Fibrosis is Associated with Decreased Circulating Levels of Full-Length CILP in Heart Failure

Cardiac Fibrosis is Associated with Decreased Circulating Levels of Full-Length CILP in Heart Failure

Shuin Park, BS*†‡, Sara Ranjbarvaziri, PhD*†‡§, Peng Zhao, MD, PhD*, and Reza Ardehali, MD, PhD*†‡‖

*Division of Cardiology, Department of Medicine, David Geffen School of Medicine, University of California, Los Angeles, CA

†Eli and Edythe Broad Center of Regenerative Medicine and Stem Cell Research, University of California, Los Angeles, CA

‡Molecular, Cellular, and Integrative Physiology Graduate Program, University of California, Los Angeles, CA

§Current address: Department of Pediatrics and Cardiovascular Institute, Stanford University, CA

‖Molecular Biology Institute, University of California, Los Angeles, CA

DISCLOSURES

This work was completed with no relationships with industry.

ABSTRACT

Objectives

The objective of this study was to identify potential circulating biomarkers for cardiac fibrosis.

Background

Cardiac fibrosis leads to pathological remodeling that can deteriorate cardiac function. Heart failure arising from cardiac fibrosis is a debilitating syndrome, and there is a need to identify circulating biomarkers that can help diagnose the extent of fibrosis.

Methods

We performed experimental pressure overload injury in C57BL/6J mice by transverse aortic constriction (TAC) and isolated cardiac fibroblasts 7 days post injury or sham operation for RNA-sequencing. Potential biomarkers for cardiac fibrosis were identified and results confirmed by reverse transcription-qPCR. Expression of the biomarkers were measured in fibroblasts treated *in vitro* with TGFβ by immunocytochemistry. Immunofluorescence staining confirmed expression in hearts from TAC murine hearts and human heart failure biopsies. Circulating protein levels were measured by ELISA and Western blotting of serum from human subjects.

Results

LTBP2, COMP, and CILP were upregulated in murine and human cardiac fibroblasts after *in vitro* TGFβ treatment. All three proteins were found to be expressed specifically in the fibrotic regions of injured murine and human hearts. Additionally, the full-length CILP protein showed a significant decrease in circulating levels in heart failure patients compared to healthy volunteers.

Conclusions

The full-length CILP protein may be a potential circulating biomarker for cardiac fibrosis. LTBP2 and COMP are additional markers that specifically localized to the fibrotic regions of the injured myocardium. Further studies are warranted to determine the functional contributions of these proteins to the development of cardiac fibrosis.

INTRODUCTION

Myocardial fibrosis is a pathological process associated with various forms of cardiac disease that contributes to impaired cardiac function, development of arrhythmias, and ultimately heart failure[1,2]. The formation of fibrosis can be initiated by either an acute ischemic event to the heart, such as myocardial infarction, or through a chronic progression driven by increased cardiac load. Cardiac fibroblasts (CFbs) are the main participating cells in the development of myocardial fibrosis[3]. Under homeostatic conditions, resident CFbs are responsible for maintaining the structural integrity of the heart by regulating extracellular matrix (ECM) production[4]. However, under pathological conditions, CFbs become activated, proliferate, and secrete an excess amount of ECM proteins, contributing to scar tissue[3,4]. This scar replaces healthy myocardium, renders the substrate arrhythmogenic, induces stiffening of the heart and leads to adverse remodeling. Collectively, the sequela of fibrosis can have deleterious effects on the ability of the heart to pump blood effectively and hinders the recovery of cardiac function. There are currently limited treatment options for the reversal of cardiac fibrosis, and available therapies for heart failure are ineffective at preventing the formation of scar tissue[5]. It has been suggested that identifying diagnostic markers for fibrosis may provide prognostic value for clinicians[6]. Considering the critical role of CFbs in myocardial fibrosis, we hypothesized that CFbs may release factors that could serve as promising biomarkers for cardiac fibrosis[7]. Identification of circulating biomarkers would serve as a non-invasive clinical tool of determining the presence, extent, and progression of fibrosis in cardiac disease patients.

In the present study, we isolated CFbs from C57BL/6J mice that underwent transverse aortic constriction (TAC, a pressure overload injury model) or sham operation and performed RNA-sequencing to identify key upregulated genes in response to injury[8]. From this data, we identified three genes encoding secreted proteins that could be potential biomarkers for myocardial fibrosis: latent TGFβ-binding protein 2 (*Ltbp2*), cartilage oligomeric matrix protein (*Comp*), and cartilage

intermediate layer protein 1 (*Cilp*). *Ltbp2* is part of the latent TGFβ-binding protein family, which consists of key regulators of TGFβ signaling[9]. *Comp* and *Cilp* are mainly known for their roles in the binding of specific ECM proteins, such as collagens, in cartilage[10,11]. LTBP2, COMP, and CILP were upregulated in cultured murine CFbs and in the fibrotic regions of TAC hearts, suggesting that their expression is specific to the formation of scar. Furthermore, there was an increase in expression of these proteins in stimulated human CFbs and within the fibrotic regions of heart sections from heart failure patients, demonstrating their potential as clinical biomarkers for fibrosis. Finally, we show that CILP, specifically the full length CILP protein, demonstrated a significant difference in circulating levels in the serum of mice after TAC and heart failure patients. The findings in this study introduce potential markers for myocardial fibrosis and support the need to pursue studies on CILP as a possible circulating biomarker for the development of cardiac fibrosis.

RESULTS

Murine cardiac fibroblasts express *Ltbp2*, *Comp*, and *Cilp* after injury

To identify secreted proteins expressed by CFbs in fibrotic hearts, we conducted RNA-sequencing on isolated CFbs from female C57BL/6J adult mice (8-12 weeks) that had undergone either sham or TAC surgery (n=3). CFbs were isolated seven days after surgery to observe gene expression changes in the early stages of fibrosis[8]. After TAC, many genes were differentially expressed in CFbs **(Figure 1A, Supplementary Table 3)**. Specifically, CFbs from mice that had undergone TAC showed higher expression of various genes associated with fibrosis **(Figure 1B)**. From these, we selected genes that encoded for secreted proteins and then further filtered the list to those that were novel in the context of heart failure and had previously reported roles in extracellular matrix formation/remodeling. We identified *Ltbp2*, *Comp*, and *Cilp* as potential candidate biomarkers. These results were further validated by RT-qPCR **(Figure 1C)**.

The TGFβ signaling pathway is a major component of injury response in cardiac fibroblasts[12]. Treatment of fibroblasts *in vitro* with TGFβ activates and induces proliferation of cultured cells, imitating *in vivo* responses [13]. To confirm that the TGFβ signaling pathway stimulates a robust increase in the expression of the identified genes, CFbs from uninjured C57BL/6J mice were cultured in media with or without TGFβ for 72 hours **(Figure 2A)**. CFbs were isolated by whole explant culture to encompass the entire CFb population in the heart, rather than a subpopulation[14]. TGFβ treatment induced expression of fibroblast activation genes, such as Periostin (*Postn*) and α-smooth muscle actin (*Acta2*)[15], as well as *Ltbp2*, *Comp*, and *Cilp* **(Figure 2B)**. Furthermore, immunocytochemistry (ICC) confirmed that expression of LTBP2, COMP, and CILP were increased at the protein level in cultured CFbs after exposure to TGFβ **(Figure 2C)**. We observed similar patterns of staining for these proteins when CFbs were isolated by fluorescence-activated cell sorting **(Supplementary Figure I)**[8]. These data confirm that CFbs are a cellular source of LTBP2, COMP, and CILP under stimulatory conditions.

LTBP2, COMP, and CILP are localized to fibrotic regions

Although TAC surgery induces fibrosis, it also causes other cardiac pathologies, such as hypertrophy[16]. In order to confirm that the increase in LTBP2, COMP, and CILP expression after injury was specific to scar formation, we analyzed the anatomic location of LTBP2, COMP, and CILP in the hearts of mice that had undergone TAC surgery. After seven days, there was visible perivascular and interstitial fibrosis in TAC hearts, compared to sham which exhibited no fibrosis **(Figure 3A)**. Immunofluorescence (IF) staining showed minimal expression of the three proteins in sham hearts. In TAC hearts, LTBP2, COMP, and CILP expression appeared to colocalize with Discoidin domain-containing receptor 2 (DDR2), a marker for fibroblasts[17], and α-smooth muscle actin (αSMA)[18] within the fibrotic regions of the myocardium in TAC hearts **(Figure 3B)**. Areas of nonfibrotic myocardium in TAC hearts did not stain for any of the target proteins (data not shown),

indicating that expression of LTBP2, COMP, and CILP are expressed by activated cardiac fibroblasts and localized to regions of fibrosis.

We next sought to determine whether the expression of these biomarkers is also observed in other types of cardiac fibrosis, such as replacement fibrosis after myocardial infarction. Our findings were further confirmed in an ischemic reperfusion (IR) injury model in which the hearts exhibited discrete areas of fibrosis, although not to the severity of TAC injury. LTBP2, COMP, and CILP were found to be specifically co-localized with DDR2 and αSMA in hearts that had undergone IR **(Supplementary Figure II)**. Together, these data suggest that LTBP2, COMP and CILP are expressed by activated cardiac fibroblasts and are localized to regions of fibrosis.

Human cardiac fibroblasts have increased LTBP2, COMP, and CILP levels in response to TGFβ1 treatment

To confirm the clinical utility of our identified proteins as biomarkers for cardiac fibrosis, we sought to assess their expression levels in human ischemic myocardial tissue. RNA-sequencing data of human cardiac tissue from ischemic heart failure patients in a publicly available database (GSE46224) demonstrated that *LTBP2*, *COMP*, and *CILP* are upregulated in ischemic hearts **(Figure 4A)**[19]. We next cultured human CFbs and treated them with TGFβ1 to stimulate their *in vitro* activation **(Figure 4B)**. TGFβ1 treatment led to morphological changes in human CFbs and induced expression of *LTBP2*, *COMP*, and *CILP*, along with fibroblast activation genes **(Figure 4C)**. ICC staining confirmed the upregulation of LTBP2, COMP, and CILP in response to TGFβ1 treatment, as seen in mouse CFbs **(Figure 4D)**. Conditioned media from cells that had undergone TGFβ1 treatment did not show significant differences in the levels of LTBP2, an increasing trend of COMP levels, and decreased levels of CILP **(Supplementary Figure III)**. These results may be due to unknown mechanisms of protein secretion that affect the presence of these proteins in the context of our culture protocol. The results from the *in vitro* culture of human CFbs mirrored

our data from mice, further supporting the potential of these proteins to be biomarkers for cardiac fibrosis.

LTBP2, COMP, and CILP are potential biomarkers for cardiac fibrosis

We used IF staining to observe the expression of LTBP2, COMP, and CILP within the myocardium of heart failure patients compared to healthy hearts. Myocardial tissue from heart failure patients (with a documented diagnosis of ischemic cardiomyopathy) exhibited significant amounts of fibrosis compared to healthy hearts **(Figure 5A)**. In healthy hearts, we observed no or minimal positive staining for the candidate markers throughout the myocardium **(Figure 5B)**. However, sections from diseased hearts demonstrated a significant increase in expression of all three proteins **(Figure 5B)**. Staining for these three proteins were localized to disarrayed regions of the myocardium, indicative of the specificity of these proteins for fibrotic areas.

Full length CILP is significantly decreased in serum from heart failure patients

In addition to increased expression within the fibrotic myocardium, we sought to determine the utility of LTBP2, COMP, and CILP as novel circulating biomarkers for cardiac fibrosis. We measured the protein levels in serum from healthy volunteers and heart failure patients by ELISA **(Supplementary Table 4)**. We observed no significant differences in the circulating levels of LTBP2[20] or COMP **(Figure 6A)**. However, serum from heart failure patients exhibited significantly decreased levels of CILP **(Figure 6B)**. Mice that had undergone TAC injury exhibited a similar trend in decreased levels of circulating CILP compared to sham mice **(Supplementary Figure IV)**. The *CILP* gene encodes a precursor protein that undergoes cleavage into an N-terminal fragment of roughly 75kDa and a C-terminal fragment of about 55kDa[21]. Both of these fragments were shown to inhibit Smad3 phosphorylation, which is normally promoted by active TGFβ signaling. While commercially available ELISA kits target the C-terminal region of CILP (hence detecting both the C-terminal and the full-length fragment), previous work discovered that CFbs

secrete the N-terminal fragment as well as the full-length CILP protein [22]. We specifically used an antibody that spans the cleavage site of the CILP precursor and performed western blotting to confirm levels of circulating full-length CILP. Our results showed that serum from heart failure patients had significantly decreased levels of full-length CILP in circulation **(Figure 6C-D)**. Together, these data suggest while activated fibroblasts in the fibrotic regions of human myocardium express high levels of CILP, the circulating level of CILP is significantly reduced when compared to healthy individuals with no evidence of cardiac fibrosis.

DISCUSSION

With the increasing prevalence of cardiac disease worldwide, there is significant value in identifying a robust biomarker panel to non-invasively measure the presence and progression of cardiac fibrosis. We hypothesized that, as key participants of the fibrotic response, cardiac fibroblasts may be a source of novel biomarkers for myocardial fibrosis. We performed RNA-sequencing of CFbs from TAC and sham murine hearts and identified *Ltbp2*, *Comp*, and *Cilp* to be upregulated in hearts after pressure overload injury. The expression of these proteins by CFbs in response to injury were validated by *in vitro* studies in both murine and human CFbs. Additionally, we demonstrated that these proteins localize in fibrotic regions in murine hearts after pressure overload and ischemic reperfusion injury. These findings were further confirmed by high levels of these three biomarkers in the fibrotic areas of human ischemic myocardial tissue. Notably, the circulating levels of full-length CILP protein were significantly reduced in the serum of ischemic heart failure patients compared to healthy individuals, indicating its potential to be a circulating biomarker.

LTBP2 and COMP expression is specific to fibrotic regions

LTBP2 is a member of the latent TGFβ-binding protein family, which consists of key regulators of TGFβ signaling. TGFβ has diverse and pleiotropic effects on various cell types through its binding

and activation of TGFβ receptors[12,23]. TGFβ is secreted from cells as a multiplex form that is covalently bound to latent TGFβ binding proteins LTBP1, LTBP3, and LTBP4. These proteins target the latent complex to specific sites for storage within the ECM where it awaits activation. Matrix sequestration of latent TGFβ may serve to regulate its immediate bioavailability while achieving critical threshold concentration at sites of intended function[9,23]. However, the functional role of LTBP2 is not well understood. Recent studies suggest that LTBP2 does not bind to latent TGFβ but may interact with other ECM proteins[9]. Other studies have additionally reported on the competitive role of LTBP2 with LTBP1 for binding sites on fibrillin-1 within the ECM[24]. Our data show strong support for increased expression of LTBP2 in response to injury and a strong localization of LTBP2 in activated fibroblasts within the fibrotic regions of the myocardium. Whether LTBP2 is merely a surrogate for cardiac fibrosis or is involved in its pathogenesis is not entirely known.

COMP is another ECM protein that is mainly studied in the context of tendons and cartilage[25]. The main function of COMP is to directly bind with other ECM components, including collagens and TGFβ1, and to facilitate the stability of the ECM network by the formation of collagen fibrils[26]. This role is crucial to maintaining homeostasis of the heart as COMP-knockout mice have been shown to develop dilated cardiomyopathy[27]. However, the role of COMP in pathological remodeling is less understood. Studies have shown that COMP is upregulated in the context of idiopathic pulmonary fibrosis[28] and liver fibrosis[29], although there have been conflicting reports as to whether it can serve as an accurate circulating marker for fibrosis in patients[28,30].

Our results suggest that LTBP2 and COMP both have a strong potential for being markers for cardiac fibrosis as the expression of these proteins are specific to scar formation. However, our data does not support their use as circulating biomarkers after cardiac injury. Although these proteins are known to be secreted, it is possible that they remain within the ECM and participate

in the process of fibrosis and scar formation. Further research is warranted to investigate the specific functional contributions of LTBP2 and COMP to the development of cardiac fibrosis. Due to their known roles in other organ systems, it is possible that these proteins may be markers for general fibrosis and not specific to cardiac fibrosis[31].

Decreased levels of CILP may be indicative of heart failure

The exact function of CILP within cartilage is still unknown, but it has been implicated in cartilage remodeling and maintenance of the ECM[11,32]. The upregulation of CILP has been found in various disease models including osteoarthritis, idiopathic pulmonary fibrosis, and ischemic heart disease[32–35]. However, the contribution of CILP to the development of cardiac fibrosis remains unknown. While most studies suggest that CFbs are the major source of CILP expression in the heart, a recent study has shown evidence of cardiomyocytes being another a major contributor[36,37]. Although we did not explore the expression of CILP in cardiomyocytes, our data supports the claim that CFbs are a major cellular source of CILP. Several studies have reported that cardiac injury causes an upregulation of CILP in CFbs but the potential for CILP to be a potential biomarker for fibrosis had not been previously explored[22,37].

The *CILP* gene encodes for a precursor protein containing a furin cleavage site. The precursor is first synthesized and processed by furin proteases intracellularly prior to being secreted [21]. The N-terminal fragment has been shown to directly interact with TGFβ, suppressing TGFβ signaling in CFbs, while the C-terminal fragment is homologous to a porcine nucleotide pyrophosphohydrolase (NTPPHase) which has been reported to have limited enzymatic activity[21,38]. In contrast to the two fragments, the functional role of full-length CILP protein has not been well-studied. The full-length CILP has been shown to inhibit TGFβ signaling, similarly to the N-terminal fragment, most likely due to the common thrombospondin-1 domain which has been shown to bind to TGFβ[22]. However, further studies to determine any functional differences

between the N-terminal fragment and the full-length CILP are required. Our data specifically demonstrates that circulating levels of the full-length CILP are attenuated in heart failure patients but show an abundance of expression in the fibrotic myocardium. A possible mechanism for this paradox is that full-length CILP is sequestered to the ECM by its binding to TGFβ, therefore reducing circulating levels. Studies have reported that while injury induces increased expression of TGFβ in the myocardium of heart failure patients[39], circulating TGFβ is reduced[40,41]. Due to the inhibitory role of full-length CILP in TGFβ signaling, it is possible that increased levels of CILP may reside in the ECM and promote a negative feedback mechanism to suppress CFb activation[22,42]. Further studies on the dynamics of CILP turnover in the ECM are required to elucidate the significance of both circulating and interstitial CILP.

In conclusion, the present study confirms the potential for LTBP2, COMP, and CILP as novel markers of cardiac fibrosis in both mouse and human heart failure models. Most notably, we discovered a significant reduction in serum levels of full-length CILP in patients with heart failure. Though our data is indicative of this relationship, the small sample size limits the statistical power of our analysis. There is a need to conduct additional validation studies on a larger cohort of patients with varying etiologies of cardiomyopathy to better determine the clinical implications of CILP as a biomarker for the presence of cardiac fibrosis. Nevertheless, our results suggest that LTBP2, COMP, and CILP are worthy of future investigation as participants in cardiac fibrosis and as biomarkers for the development of ischemic heart failure.

METHODS

Study Approvals

All mouse surgery procedures were carried out with the approval of the University of California, Los Angeles (UCLA) Animal Research Committee or the Institutional Animal Care. The study was approved by an IRB (12-001164) and human participants gave written informed consent.

RNA-Sequencing and Analysis

Cardiac fibroblasts were isolated from murine hearts, as previously described, for RNA-sequencing [8]. This data is publicly available on GEO (GSE51620). Downstream analysis was conducted using the DESeq2, Enhanced Volcanoplot and gplots R packages[43,44]. To identify potential candidates for secreted biomarkers of cardiac fibrosis, we first identified genes that were differentially expressed in cardiac fibroblasts after transverse aortic constriction compared to sham operation (GSE51620) ($p<0.05$). We selected for genes that exhibited a minimum fold-change increase of 4 to select for significantly upregulated genes in TAC. We then identified genes that were associated with fibrosis through the literature and screening for genes associated with the following Gene Ontology classes: GO:0062023 (collagen-containing extracellular matrix), GO:0001666 (response to hypoxia), GO:0001968 (fibronectin binding), GO:0030199 (collagen fibril organization), GO:0005201 (extracellular matrix structural constituent) and/or GO:0005615 (extracellular space). From this list, we further selected for genes that encoded for at least one protein product that was reportedly secreted. This was identified using online resources such as Uniprot, the Human Protein Atlas, and previously published literature. This process allowed for the selection of only secreted proteins that may mark the presence of cardiac fibrosis.

Validation of secreted proteins that were identified by our RNA sequencing was conducted using a different cardiac injury, treatment with isoproterenol (ISO). C57BL/6J mice were implanted with ALZET osmotic pumps in the abdominal cavity while under anesthesia with isoflurane. The pumps were filled with saline or ISO (Sigma) at a concentration to treat the mice at a rate of 30mg/kg body weight/day for a treatment period of 21 days. Mouse serum was collected at the end of the treatment period and prepared for analysis as described in the section titled “Serum Preparation”. Western blot and ELISA were used to screen through potential secreted proteins. Proteins that

demonstrated a notable difference between saline- and ISO-treated samples were further selected for experiments.

Mice

Adult C57BL/6J mice (age 8-12 weeks) were used for all experiments. For the *in vivo* experiments, mice were randomly assigned into sham, TAC, and ischemic reperfusion (IR) treatment groups. No phenotypic differences were observed between male and female mice. All procedures were carried out with the approval of the University of California, Los Angeles (UCLA) Animal Research Committee or the Institutional Animal Care.

Transverse Aortic Constriction Surgery, Ischemic-Reperfusion Surgery, and Aftercare

Adult C57BL/6J mice were anesthetized by intraperitoneal injection of ketamine/xylazine (100mg/10mg/kg). Endotracheal intubation was performed using a blunt 20-gauge needle connected to a volume-cycled rodent ventilator (SAR-830/P; CWE, Inc.) with a tidal volume of 0.2 ml and a respiratory rate of 120/min. For transverse aortic constriction surgery, the chest was opened to expose the transverse aorta, located through the second intercostal space. Aortic constriction was performed by tying a 7-0 nylon suture ligature against a 27-gauge blunt needle and then removing the needle to yield a constriction of roughly 0.4mm in diameter. For ischemic-reperfusion surgery, left thoracotomy between ribs four and five was performed. The pericardium was opened, and a suture was placed around the left anterior descending coronary artery 1-2mm from the tip of the left atrium. The suture was tightened to occlude blood flow for 45 minutes and subsequently removed. Mice that underwent sham operations underwent the same procedure, excluding the constriction/occlusion. After the operation, the chest was closed in layers using 5-0 Vicryl sutures and the mice remained on the ventilators until sufficient spontaneous breathing was resumed, at which point the endotracheal tube was removed. The entire surgical procedure was performed under aseptic conditions. Buprenorphine (0.1 mg/kg) was administrated by

subcutaneous injection immediately prior to surgery, followed by every 12 hours for 48 hours, and carprofen (5mg/Kg) was administrated post operation every 24 hours for 48 hours. Mice were additionally treated post-operatively with Sulfamethoxazole and Trimethoprim oral suspension (Aurbindo). Operators blinded to the experimental designs performed all animal surgeries and *in vivo* analyses.

Cardiac fibroblast culture and TGFβ treatment (murine and human)

Adult C57BL/6J mice were sacrificed by isoflurane followed by cervical dislocation. Hearts were dissected from the mice and cannulated with a blunt syringe. The hearts were perfused with 20-30ml PBS, subsequently chopped into small pieces and incubated in 7-10ml enzyme at 37°C on a rotator for an hour with periodic pipetting to digest larger pieces. The enzyme mix consisted of TH and TM liberases (Roche), Dnase (Invitrogen), and Poloxamer. The cells were then passed through a 70μm filter, centrifuged, and the pellet was resuspended in DMEM containing 20% FBS, 1% Penicillin Streptomycin, and 0.1% Ciprofloxacin. The cells from one heart were plated in a single well of a 6-well plate that had been coated with 0.1% gelatin. Twelve hours after plating, the floating cells were removed, and the media was replaced. Media changes were done every other day until cells reached 80% confluency, at which point they were passaged and cultured in serum-free media for 24 hours prior to TGFβ treatment (Cell Signaling, 50ng/mL). Throughout the TGFβ treatment, the media was changed daily. Human fibroblasts were cultured according to the company's instructions (Cell Applications) and similarly passaged for TGFβ treatment (R&D Systems, 10ng/mL).

RNA Extraction and RT-qPCR

RNA was extracted from cells using TRIzol™ LS Reagent (ThermoFisher) and following the manufacturer's instructions. RNA was quantified by NanoDrop, and cDNA was prepared using the iScript™ Reverse Transcription Supermix kit (Bio-Rad). Reverse transcription quantitative-

PCR (RT-qPCR) reactions were prepared using SYBR Green (Bio-Rad) and primers (IDT) unique for each gene of interest **(Supplementary Table 1)**. The reactions were run on a CFX96™ Real-Time PCR Detection System.

The PCR conditions for RT-qPCR had the following steps:

1. Initial denaturation – 95°C – 2 minutes and 10 seconds
2. Denaturation – 95°C – 15 seconds
3. Annealing – 60°C – 30 seconds
4. Extension – 72°C – 30 seconds
5. Repeat steps 2-4 for a total of 39 cycles
6. Final extension – 72°C – 10 minutes

The mean cycle threshold (Ct) values were taken from triplicate measurements to determine relative gene expression, as normalized to *Gapdh/GAPDH* expression.

Immunocytochemical/Immunofluorescence Staining

Cells were cultured on 8-well chamber slides (Falcon) and washed with PBS prior to fixation with 4% paraformaldehyde (PFA). For *in vivo* staining, murine hearts were isolated and fixed with 4% PFA overnight prior to being incubated in 30% sucrose and embedded in Optimal Cutting Temperature (OCT) compound (Fisher). Hearts were sectioned at a thickness of 8µm in a cryostat, mounted on Colorfrost Plus microscope slides (Fisher), and stored at -20°C until ready to stain. For immunocytochemical staining, the fixed cells were blocked with blocking buffer (10% NGS, PBS-0.1%Tween 20) for 1 hour at room temperature and then incubated in diluted primary antibodies **(Supplementary Table 2)** overnight at 4°C. The slides were then washed 3 times with PBS-0.1%Tween and then incubated in diluted secondary antibodies **(Supplementary Table 2)** for an hour at room temperature. After another round of washing with PBS-0.1%Tween 20, the coverslips were mounted using mounting medium containing DAPI (Vector Laboratories). For immunofluorescence staining, slides were incubated at room temperature for 10 minutes prior to

3 washes with PBS. The sections were treated with 0.25% Triton X-100 in PBS to permeabilize for 10 minutes. The subsequent blocking and staining protocol mirrored immunocytochemical staining as described. Slides were incubated with antibodies outlined in **Supplementary Table 2**. Imaging was done on either a Zeiss confocal microscope (LSM880) or a Leica fluorescent microscope (LEICACTR6500). Image processing and analysis was done through either ZEN 2 (blue edition) or LAS AF Lite.

Conditioned Media Preparation

Cells were cultured in 6-well plates and culture media was collected every day during the treatment period for a total of three times. The collected media was centrifuged for 10,000rpm for 10 minutes at 4°C and the supernatant was transferred to a separate tube to remove any cellular contamination. The media was stored at -80°C until ready for analysis. For ELISA, the media from each day was pooled into a single sample per well. The media was concentrated by Amicon® Ultra Centrifugal Filters and the final concentrated volume was noted for total concentration calculations after ELISA.

Serum Preparation

Healthy human samples were purchased from Equitech Enterprises. Blood samples from heart failure patients were collected with informed consent **(Supplementary Table 4)**. Serum was isolated using Ficoll and stored at -80°C until enough samples were collected for experiments. For western blots, albumin was removed from the samples with the AlbuSorb™ Albumin Depletion Kit (Biotech Support Group).

ELISA and Western Blot

ELISA kits were purchased from MyBiosource and the manufacturer's protocol was followed. For western blot, protein concentration was measured by a Pierce™ BCA Protein assay kit

(ThermoScientific) and 20µg was loaded into each well of 4-20% Mini-PROTEAN TGX Precast Protein gels (Bio-Rad). After transferring the gel onto a PVDF membrane, detection of CILP was conducted by incubating the membrane with primary antibody followed by secondary antibody conjugated with HRP **(Supplementary Table 2)**. The signal was developed using the Pierce® ECL Western Blotting Substrate (ThermoScientific).

Statistical Analysis

Continuous data are presented using the mean ± standard error of the mean (SEM) and comparisons between groups were performed using Student's t-test. A p-value < 0.05 was considered statistically significant and data were analyzed using GraphPad Prism 6.

ACKNOWLEDGEMENTS

S.P., S.R., and R.A. conceived the project and designed the experiments. S.P. performed all experiments, analyzed data and prepared the figures. S.P. and R.A. wrote the manuscript. P.Z. performed all surgeries. All authors reviewed the manuscript. We would like to acknowledge Fides Lay for assisting in the RNA-sequencing analysis and Jasmeet S. Dhaliwal for helping with the trichrome staining. The LTBP2 antibody was a gift from Dr. Marko Hyytiäinen from the University of Helsinki, Finland. We also acknowledge the UCLA Technology Center for Genomics & Bioinformatics, Broad Stem Cell Research Center Flow Cytometry Core, and Confocal Microscopy Core for their expert technical assistance. We acknowledge James L. Engel, Arash Pezhouman, and Ngoc B. Nguyen for their critical reading of this article.

FUNDING SUPPORT

This work was supported in part by the National Institute of Health DP2 (HL127728) and AHA Innovative Award (18IPA34170309). S.P. was supported by the Ruth L. Kirschstein National Research Service Award (T32HL69766).

Figure 1

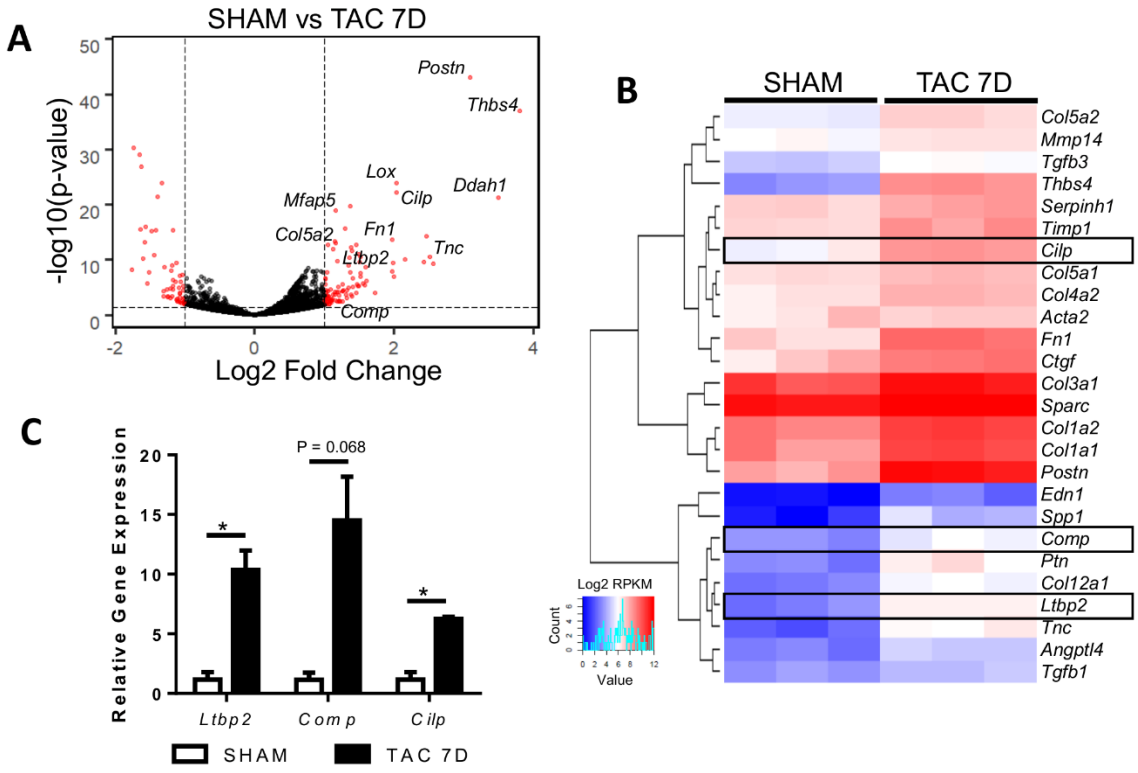

Figure 1: Identification of potential biomarkers for cardiac fibrosis

(A) Volcano plot depicting highly differentially expressed genes in cardiac fibroblasts after TAC. **(B)** Heatmap of pro-fibrotic genes that are upregulated in cardiac fibroblasts isolated from sham and TAC mouse hearts. Select genes (*Ltbp2*, *Comp*, and *Cilp*) are boxed. **(C)** RT-qPCR confirmation of upregulation of *Ltbp2*, *Comp*, and *Cilp* in cardiac fibroblasts after 7D TAC (n=3). TAC: Transverse Aortic Constriction. P*<0.050 (t-test).

Figure 2

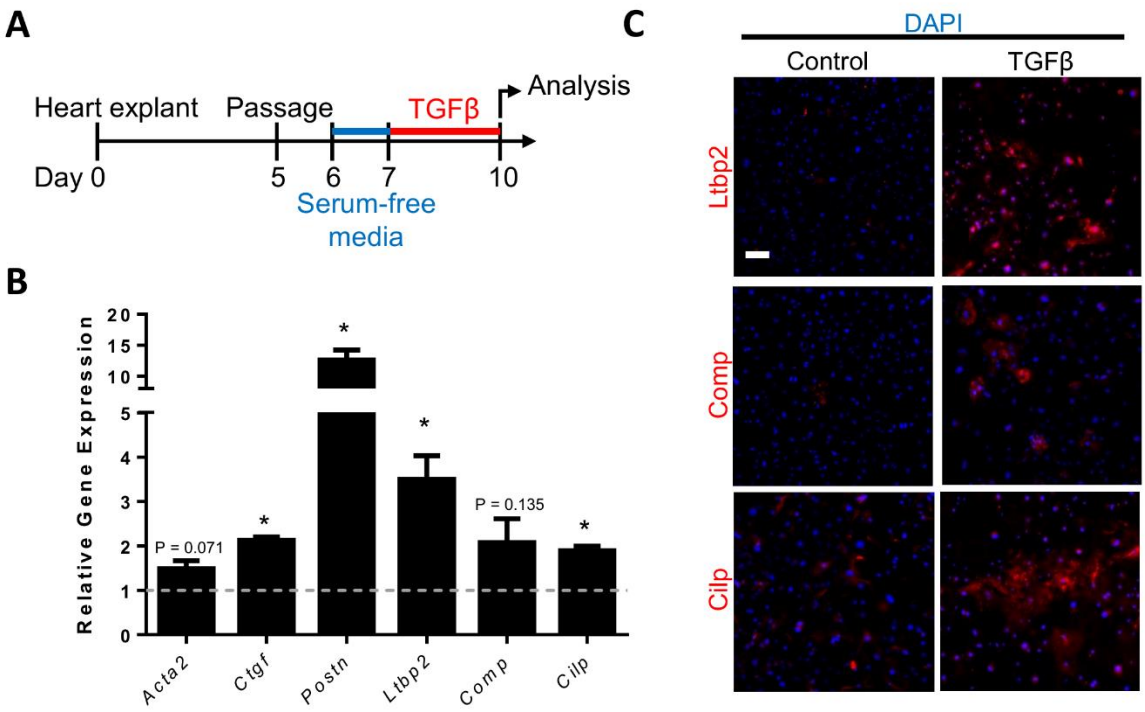

Figure 2: LTBP2, COMP, and CILP are upregulated in cultured cardiac fibroblasts after TGFβ treatment

(A) Schematic of cardiac fibroblast culture and TGFβ treatment. **(B)** RT-qPCR of cardiac fibroblasts treated with TGFβ normalized to untreated controls (indicated by dotted line at y=1) (n=4). **(C)** Immunocytochemistry for LTBP2, COMP, and CILP show significant increase in expression after TGFβ treatment (n=4). DAPI (blue) stained for nuclei. Scale bar: 100μm. TGFβ: Transforming Growth Factor-β. P*<0.050 (t-test).

Figure 3

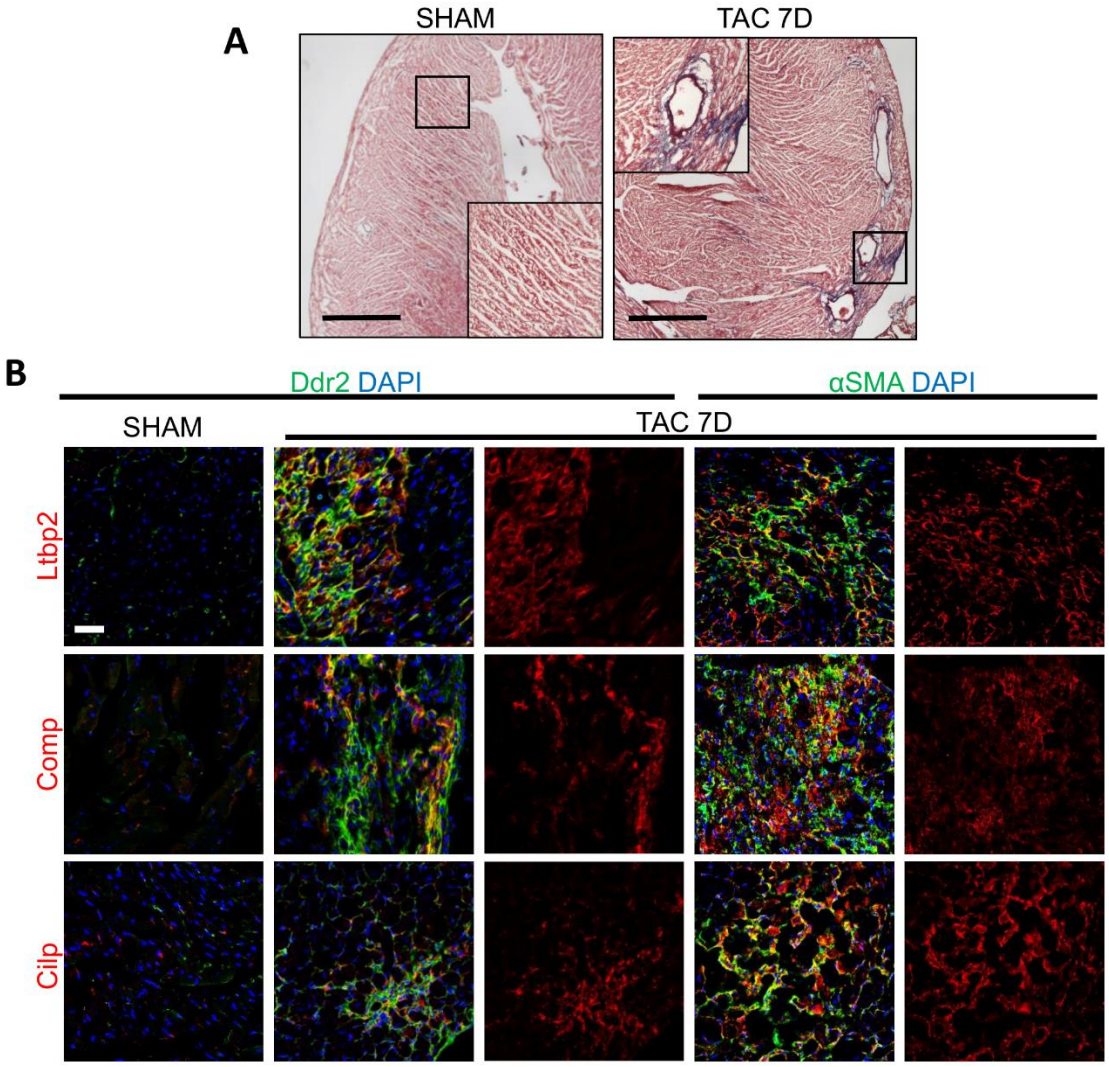

Figure 3: LTBP2, COMP, and CILP localize to the fibrotic myocardium

(A) Mice that had undergone TAC surgery exhibited myocardial fibrosis as shown by Masson's trichrome staining. **(B)** Immunofluorescence staining shows colocalization of LTBP2, COMP, and CILP (red) with fibroblast marker DDR2 (green, left) and activated fibroblast marker αSMA (green, right). Red channel images are shown separately for clarity. DAPI (blue) stained for nuclei. Scale bar: 50μm. DDR2: Discoidin Domain Receptor Tyrosine Kinase 2. αSMA: α-Smooth Muscle Actin.

Figure 4

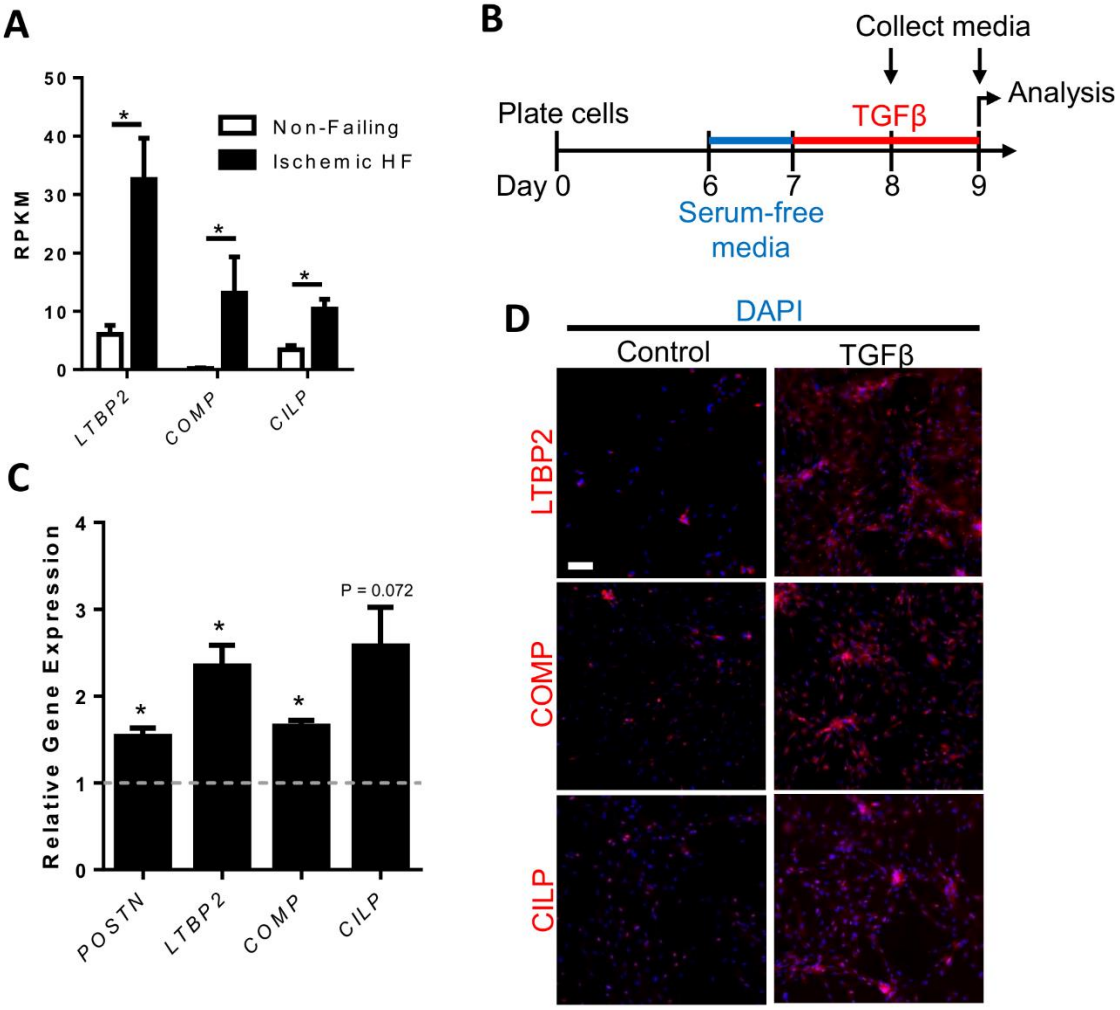
A
RPKM
Non-Failing
Ischemic HF
LTBP2
COMP
CILP
B
Collect media
Analysis
Plate cells
TGFβ
Day 0
6
7
8
9
Serum-free media
C
Relative Gene Expression
P = 0.072
POSTN
LTBP2
COMP
CILP
D
DAPI
Control
TGFβ
LTBP2
COMP
CILP

Figure 4: LTBP2, COMP, and CILP are upregulated in human cardiac fibroblasts in response to TGFβ

(A) RNA-sequencing data from a public database (GSE46224) show that expression of *LTBP2*, *COMP*, and *CILP* are upregulated in heart biopsies from ischemic heart failure (HF) patients compared to healthy patients. **(B)** Schematic of culture and TGFβ treatment of human cardiac fibroblasts. **(C**) RT-qPCR of human cardiac fibroblasts treated with TGFβ normalized to untreated controls (indicated by dotted line at y=1) (n=3). **(D)** Immunocytochemistry shows increased expression of LTBP2, COMP, and CILP in cultured human cardiac fibroblasts after TGFβ treatment. DAPI (blue) stained for nuclei (n=4). RPKM: Reads Per Kilobases Mapped. Scale bar: 100μm. *P<0.050 (t-test).

Figure 5

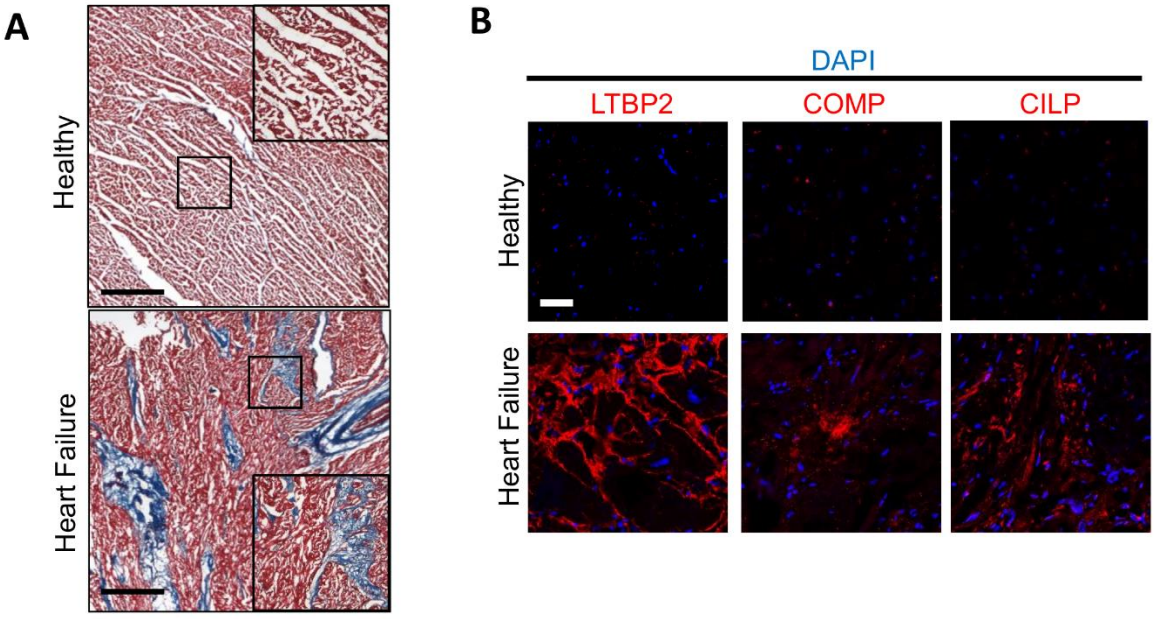

Figure 5: LTBP2, COMP, and CILP are upregulated in the myocardium of human heart failure patients

(A) Masson's trichrome staining show extensive fibrosis in heart sections of heart failure patients. Insets are higher magnification images of boxed area. **(B)** LTBP2, COMP, and CILP (red) expression is significantly increased in hearts undergoing heart failure. DAPI (blue) stained for nuclei. Scale bar: 50μm.

Figure 6

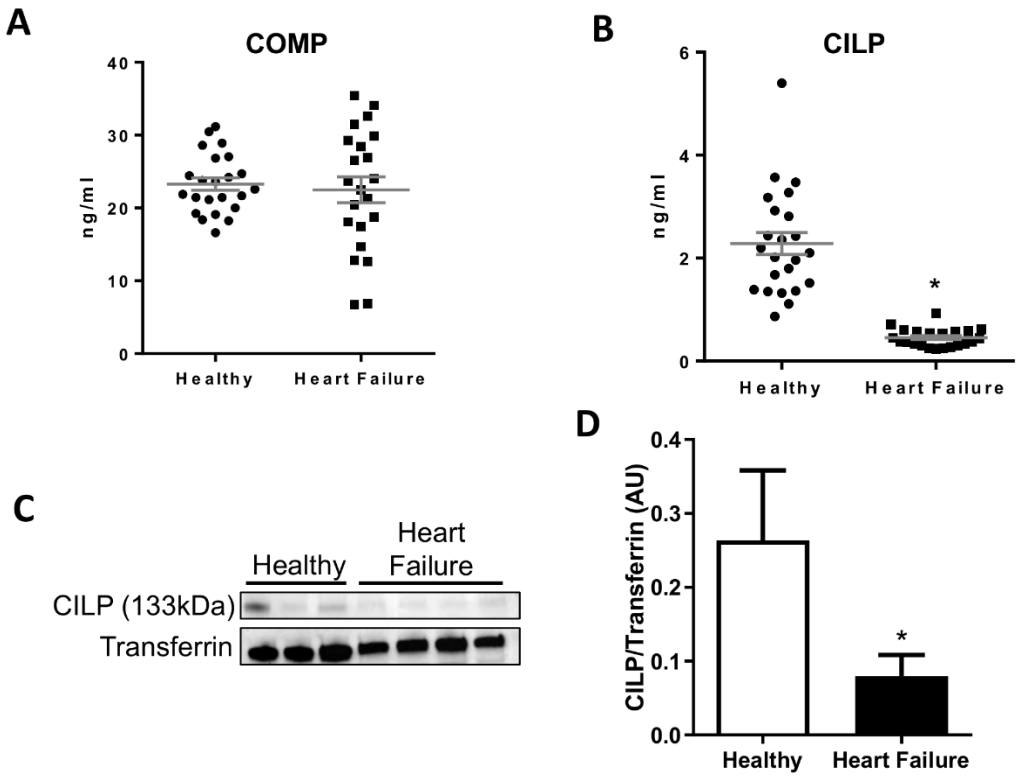

Figure 6: Full length CILP is downregulated in the serum of heart failure patients

(A) ELISA demonstrates non-significant changes in levels of COMP in the serum of heart failure patients compared to healthy individuals (Healthy n=23, Heart Failure n=22). **(B)** Heart failure patients had a significant decrease in circulating CILP levels (Healthy n=23, Heart Failure n=22). **(C)** Representative western blotting shows decreased levels of full length CILP (~133kDa) in heart failure patient serum. Quantified data is shown in **(D)** (Healthy n= 5, Heart Failure n=5). a.u.: arbitrary units. *P<0.050 (t-test).

Supplementary Figure I

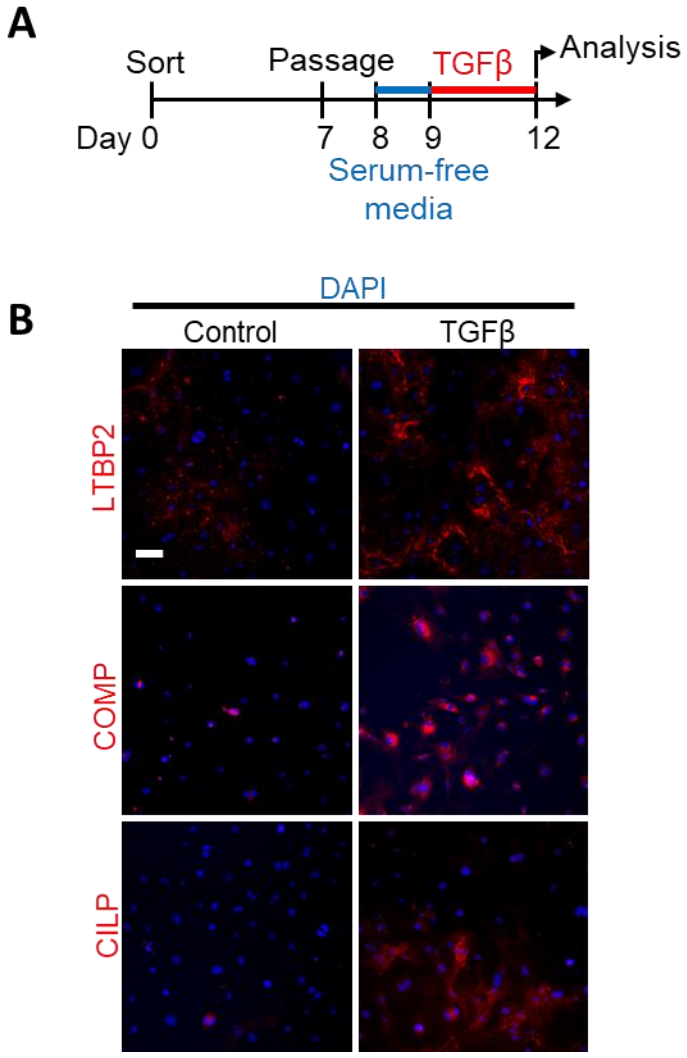

Supplementary Figure I: LTBP2, COMP, and CILP are upregulated in Thy1+ sorted cardiac fibroblasts after TGFβ treatment

(A) Schematic of cardiac fibroblast sort, culture and TGFβ treatment. **(B)** Immunocytochemistry show that TGFβ treatment induces increased expression of LTBP2, COMP, and CILP. DAPI (blue) stained for nuclei. Scale bar: 100μm. TGFβ: Transforming Growth Factor-β

Supplementary Figure II

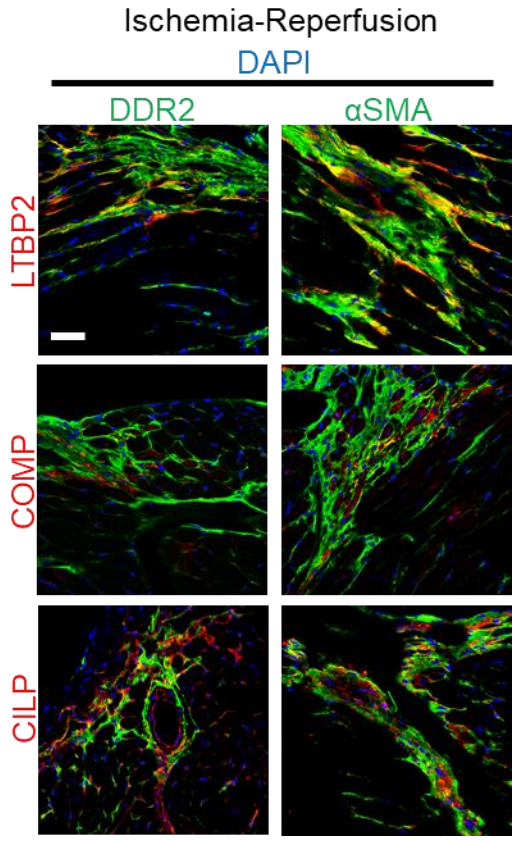

Supplementary Figure II: Expression of LTBP2, COMP, and CILP are elevated in ischemia-reperfusion injury

Immunofluorescence staining of heart sections from mice that had undergone ischemia-reperfusion injury shows colocalization of LTBP2, COMP, and CILP (red) with fibroblast marker DDR2 (green) and activated fibroblast marker αSMA (green). DAPI (blue) stained for nuclei. Scale bar: 50μm. DDR2: Discoidin Domain Receptor Tyrosine Kinase 2. αSMA: α-Smooth Muscle Actin.

Supplementary Figure III

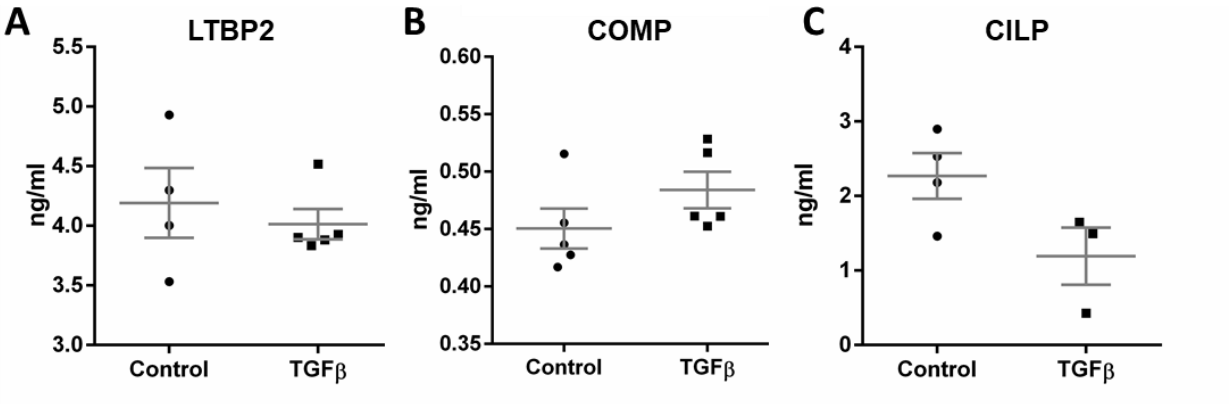

Supplementary Figure III: Levels of LTBP2, COMP, and CILP in conditioned media from cultured human CFbs

There were no statistically significant differences in levels of LTBP2 **(A)**, COMP **(B)**, and CILP **(C)** in collected media from human CFbs treated with TGFβ (n=3-5).

Supplementary Figure IV

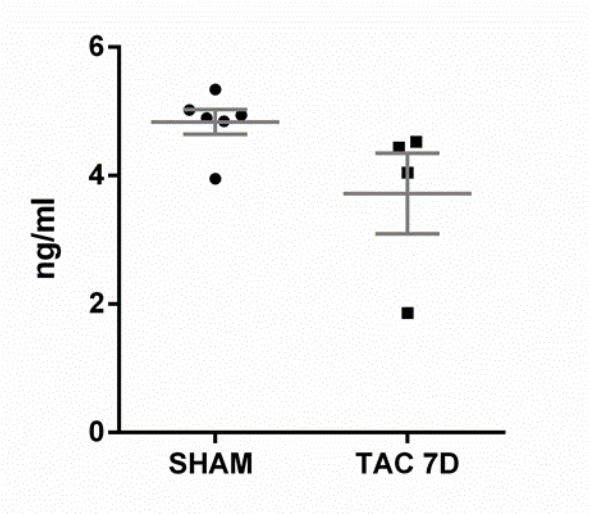

Supplementary Figure IV: CILP levels are decreased in the serum of mice that have undergone TAC

ELISA demonstrate a decrease in levels of CILP in the serum of mice 7 days after TAC surgery (n=4-6).

Supplementary Table 1

RT-qPCR Primers

Target Gene	Forward Primer (5'-3')	Reverse Primer (5'-3')
Gapdh (Mouse and *Human)*	TTGTCTCCTGCGACTTCAAC	GTCATACCAGGAAATGAGCTTG
Ltbp2 (Mouse)	AACAGCACCAACCACTGTATC	CCTGGCATTCTGAGGGTCAAA
Comp (Mouse)	ACTGCCTGCGTTCTAGTGC	CGCCGCATTAGTCTCCTGAA
Cilp (Mouse)	ATGGCAGCAATCAAGACTTGG	AGGCTGGACTCTTCTCACTGA
Acta2 (Mouse)	TGACGCTGAAGTATCCGATAGA	CGAAGCTCGTTATAGAAAGAGTGG
Ctgf (Mouse)	GACCCAACTATGATGCGAGCC	CCCATCCCACAGGTCTTAGAA
Postn (Mouse)	GACTGCTTCAGGGAGACACA	TGATCGTCTTCTAGGCCCTT
POSTN (Human)	TAGCCCAATTAGGCTTGGCATCC	TAAGAAGGCGTTGGTCCATGCT
LTBP2 (Human)	AGCACCAACCACTGTATCAAAC	CTCATCGGGAATGACCTCCTC
COMP (Human)	CAGGGAGATCACGTTCCTGA	GGCCGGTGCGTACTGAC
CILP (Human)	GCAAAAGCATCCTGAAGATCAC	GGAGTCTCTGCCCTCACAAAC

Supplementary Table 2

Primary and secondary antibodies

Target Protein	Technique	Catalog no.	Dilution
LTBP2 (Mouse/Human)	ICC	From Dr. Marko Hyytiäinen (University of Helsinki, Finland)	1:200
COMP (Mouse)	ICC	Santa Cruz sc-25163	1:50
CILP (Mouse)	ICC	Biomatik CAU24345	1:50
DDR2 (Mouse)	IF	R&D Systems MAB25381	1:100
αSMA (Mouse)	IF	Sigma-Aldrich A2547	1:100
COMP (Human)	ICC	Abcam ab74524	1:100
CILP (Human)	ICC/Western	Biomatik CAU24346	1:50/1:1000
Secondary Target	**Fluorophore**	**Catalog no.**	**Dilution**
Anti-Rabbit IgG	Alexa Fluor™ 488	Invitrogen A11034	1:200
Anti-Rabbit IgG	Alexa Fluor™ 594	Invitrogen A11037	1:200
Anti-Mouse IgG	Alexa Fluor™ 488	Invitrogen A11029	1:200
Anti-Rabbit IgG	HRP	Invitrogen 31460	1:5000

Supplementary Table 3

Significantly up-regulated genes in mouse CFbs in TAC (Fold change > 4, p-value < 0.05)

Gene	FC	p-value		Gene	FC	p-value
Ltbp2	9.866	2.432E-05		*Cthrc1*	28.773	5.914E-03
Runx1	4.990	1.298E-04		*Synpo*	5.143	5.944E-03
Cilp	5.149	1.891E-04		*Npl*	8.374	6.748E-03
1110006O17Rik	5.530	2.261E-04		*Col12a1*	7.391	6.839E-03
Cx3cl1	6.097	3.026E-04		*Col8a2*	11.705	6.854E-03
Kif26b	14.386	3.688E-04		*Dnajc15*	5.776	6.930E-03
Casc5	10.002	4.061E-04		*Col11a1*	45.058	6.980E-03
Ass1	4.474	4.249E-04		*Dclk3*	5.165	7.230E-03
Frem1	21.151	4.304E-04		*Clca1*	4.590	7.804E-03
Palld	5.074	4.792E-04		*Adam12*	4.649	7.959E-03
Pole	5.574	5.022E-04		*Top2a*	6.817	8.380E-03
Ncaph	4.194	5.375E-04		*Bub1*	9.958	8.398E-03
Gtse1	9.913	5.594E-04		*Cst6*	4.562	8.483E-03
Clec11a	4.100	5.617E-04		*1500015O10Rik*	7.017	8.553E-03
EG432466	5.367	5.760E-04		*Siglec1*	8.049	9.065E-03
A930038C07Rik	4.840	5.876E-04		*Fhl2*	4.151	9.132E-03
Mki67	8.226	5.932E-04		*2310033K02Rik*	4.108	9.422E-03
Ccdc99	8.726	5.999E-04		*Pik3ap1*	7.383	9.442E-03
Erg	8.030	6.239E-04		*Pik3r5*	4.736	9.548E-03
Meox1	4.588	1.200E-03		*Spink2*	7.795	9.730E-03
Fn1	5.676	1.343E-03		*LOC100043741*	4.470	1.010E-02
Mdk	4.842	1.379E-03		*Stoml1*	4.101	1.051E-02
Cenpe	10.971	1.447E-03		*2810433D01Rik*	5.737	1.150E-02
Lox	5.109	1.576E-03		*D0H4S114*	4.442	1.186E-02
9930013L23Rik	26.326	1.626E-03		*Cenpa*	4.174	1.210E-02
Nek2	6.204	1.878E-03		*Postn*	9.933	1.303E-02
Aspm	5.494	1.910E-03		*EG620473*	4.520	1.309E-02
C1qtnf6	4.071	1.914E-03		*Ckap2*	5.395	1.313E-02
LOC668063	13.173	1.944E-03		*Tnc*	15.646	1.334E-02
Fut4	8.096	2.028E-03		*Hcls1*	6.586	1.379E-02
Cenpf	5.151	2.148E-03		*Pbk*	5.895	1.396E-02
4930547N16Rik	9.489	2.180E-03		*Ccl6*	9.021	1.416E-02
Mybl2	5.978	2.213E-03		*Hmmr*	9.735	1.420E-02
Wisp2	4.899	2.692E-03		*Cmya3*	5.253	1.474E-02
Wisp1	11.264	2.699E-03		*Ttk*	16.145	1.506E-02
Accn2	5.408	2.815E-03		*3830403N18Rik*	6.792	1.517E-02
Tnfrsf10b	4.671	2.839E-03		*Lhfpl1*	10.304	1.538E-02
5830483C08Rik	4.309	3.180E-03		*Matn3*	14.104	1.557E-02
Gpr176	9.108	3.314E-03		*Gdf6*	4.978	1.576E-02
Tlr13	8.906	4.260E-03		*1600015H20Rik*	4.691	1.581E-02
Gmpr	10.113	4.342E-03		*Tlr5*	6.436	1.594E-02
Sgol2	4.654	4.357E-03		*Fmod*	4.628	1.613E-02
Neil3	9.379	4.391E-03		*Crlf1*	12.408	1.623E-02
LOC100043901	4.927	4.405E-03		*Psrc1*	6.821	1.624E-02
Kif15	14.284	4.641E-03		*Comp*	4.697	1.680E-02
EG622657	5.319	4.725E-03		*Soat2*	8.366	1.695E-02
D530008I22	4.767	4.883E-03		*6330512M04Rik*	10.837	1.699E-02
Thbs4	35.578	5.158E-03		*1500005K14Rik*	6.481	1.714E-02
Fbn2	4.778	5.238E-03		*Camk2n2*	4.614	1.743E-02
Arhgap11a	6.946	5.350E-03		*Zdhhc12*	4.614	1.743E-02

Gene	FC	p-value		Gene	FC	p-value
Gm22	4.101	1.794E-02		*Cx3cr1*	4.900	3.846E-02
Ckap2l	22.239	1.796E-02		*Nxt1*	5.255	3.904E-02
4921517D22Rik	6.339	1.864E-02		*Ptn*	10.726	3.909E-02
Ddah1	33.473	1.917E-02		*Zfp185*	6.172	4.021E-02
LOC100043526	8.292	1.934E-02		*Cit*	6.924	4.073E-02
Nanp	6.634	1.942E-02		*LOC100038957*	5.608	4.199E-02
Ccdc122	7.697	1.946E-02		*EG432951*	6.210	4.254E-02
Pmch	5.984	1.960E-02		*Pdgfc*	5.766	4.327E-02
5730590G19Rik	17.335	2.084E-02		*EG218444*	4.344	4.335E-02
Gm444	4.428	2.102E-02		*Sfrp2*	4.335	4.455E-02
Iqgap3	4.773	2.144E-02		*Ccnb2*	5.077	4.539E-02
LOC667005	6.256	2.193E-02		*Kif4*	13.148	4.542E-02
Scube2	26.108	2.221E-02		*5033413D22Rik*	5.739	4.612E-02
Racgap1	4.186	2.236E-02		*Lilrb4*	4.658	4.663E-02
Bub1b	8.066	2.268E-02		*Gpr65*	6.596	4.675E-02
Depdc1a	6.871	2.289E-02		*Tmem132e*	6.594	4.675E-02
Ccl5	5.734	2.411E-02		*Padi4*	4.066	4.686E-02
LOC665939	5.978	2.435E-02		*Bcas1*	6.097	4.725E-02
Ngef	4.325	2.445E-02		*Cdca7*	4.606	4.758E-02
Anln	7.915	2.471E-02		*Espl1*	4.174	4.914E-02
Prc1	5.860	2.482E-02		*Ect2*	20.594	4.918E-02
Ccdc40	5.628	2.545E-02				
LOC621880	4.778	2.584E-02				
Gp49a	4.767	2.597E-02				
5330437I02Rik	4.756	2.618E-02				
Kif23	6.567	2.632E-02				
H19	17.780	2.634E-02				
Nrg1	12.142	2.658E-02				
Tmeff1	6.108	2.783E-02				
LOC619973	4.331	2.801E-02				
3000004C01Rik	11.536	2.809E-02				
Cdt1	4.570	2.922E-02				
BC038925	5.308	2.973E-02				
Kif2c	23.975	3.006E-02				
LOC100040305	6.952	3.012E-02				
Comtd1	6.332	3.016E-02				
Acan	7.390	3.068E-02				
LOC100043431	13.185	3.081E-02				
Fgfrl1	5.192	3.090E-02				
Kcnj15	4.101	3.231E-02				
Ankrd41	5.459	3.309E-02				
Fbxo40	5.599	3.323E-02				
Tpx2	5.887	3.340E-02				
Tm7sf2	4.041	3.436E-02				
Il3ra	5.406	3.461E-02				
Pbp2	10.606	3.519E-02				
EG624855	5.004	3.586E-02				
Cep55	5.174	3.597E-02				
Edn1	6.339	3.602E-02				
D230039L06Rik	12.520	3.613E-02				
Diap3	4.384	3.695E-02				
Ccna2	4.552	3.780E-02				
Trim29	4.913	3.819E-02				

Supplementary Table 4

Characteristics of human samples

	Healthy Individuals (n=23)	HF Patients (n=22)
Age (years)	50±10	59±10
Gender	50% M 50% F	64% M 36% F
Etiology	N/A	59% Ischemic 41% Non-iCMY
EF (%)	≥55	26±6
Median BNP (pg/ml)	N/A	696±369
DM	0%	Y: 37% N: 63%
h/o HTN	0%	Y: 45% N: 50%
Medications	N/A	D: 73% BB: 100% Ent: 41% ACE-I: 32% ARB: 18% AA: 36%

Non-iCMY: Non-ischemic cardiomyopathy

D: Diuretics

BB: Beta blockers

Ent: Entresto

ACE-I: Ace-inhibitors

ARB: Angiotensin receptor blockers

AA: Aldosterone antagonists

REFERENCES

1. Kong, P., Christia, P. & Frangogiannis, N. G. The Pathogenesis of Cardiac Fibrosis. *Cell Mol Life Sci* **71**, 549–574 (2014).
2. Khan, R. & Sheppard, R. Fibrosis in heart disease: understanding the role of transforming growth factor-beta in cardiomyopathy, valvular disease and arrhythmia. *Immunology* **118**, 10–24 (2006).
3. Travers, J. G., Kamal, F. A., Robbins, J., Yutzey, K. E. & Blaxall, B. C. Cardiac Fibrosis: The Fibroblast Awakens. *Circ. Res.* **118**, 1021–1040 (2016).
4. Fan, D., Takawale, A., Lee, J. & Kassiri, Z. Cardiac fibroblasts, fibrosis and extracellular matrix remodeling in heart disease. *Fibrogenesis & Tissue Repair* **5**, 15 (2012).
5. Park, S., Nguyen, N. B., Pezhouman, A. & Ardehali, R. Cardiac Fibrosis: Potential Therapeutic Targets. *Translational Research* (2019) doi:10.1016/j.trsl.2019.03.001.
6. Pitt Bertram & Zannad Faiez. The Detection of Myocardial Fibrosis. *Circulation: Cardiovascular Imaging* **5**, 9–11 (2012).
7. Lajiness, J. D. & Conway, S. J. The Dynamic Role of Cardiac Fibroblasts in Development and Disease. *J Cardiovasc Transl Res* **5**, 739–748 (2012).
8. Ali, S. R. *et al.* Developmental heterogeneity of cardiac fibroblasts does not predict pathological proliferation and activation. *Circ. Res.* **115**, 625–635 (2014).
9. Robertson, I. B. *et al.* Latent TGF-β-binding proteins. *Matrix Biology* **47**, 44–53 (2015).
10. Acharya, C. *et al.* Cartilage oligomeric matrix protein and its binding partners in the cartilage extracellular matrix: Interaction, regulation and role in chondrogenesis. *Matrix Biology* **37**, 102–111 (2014).
11. Lorenzo, P., Bayliss, M. T. & Heinegård, D. A Novel Cartilage Protein (CILP) Present in the Mid-zone of Human Articular Cartilage Increases with Age. *J. Biol. Chem.* **273**, 23463–23468 (1998).

12. Meng, X.-M., Nikolic-Paterson, D. J. & Lan, H. Y. TGF-β: the master regulator of fibrosis. *Nat Rev Nephrol* **12**, 325–338 (2016).
13. Clark, R. A., McCoy, G. A., Folkvord, J. M. & McPherson, J. M. TGF-beta 1 stimulates cultured human fibroblasts to proliferate and produce tissue-like fibroplasia: a fibronectin matrix-dependent event. *J. Cell. Physiol.* **170**, 69–80 (1997).
14. Lynch, M. D. & Watt, F. M. Fibroblast heterogeneity: implications for human disease. *J Clin Invest* **128**, 26–35 (2018).
15. Snider Paige *et al.* Origin of Cardiac Fibroblasts and the Role of Periostin. *Circulation Research* **105**, 934–947 (2009).
16. Patten Richard D. & Hall-Porter Monica R. Small Animal Models of Heart Failure. *Circulation: Heart Failure* **2**, 138–144 (2009).
17. Goldsmith, E. C. *et al.* Organization of fibroblasts in the heart. *Dev. Dyn.* **230**, 787–794 (2004).
18. Leslie, K. O., Taatjes, D. J., Schwarz, J., vonTurkovich, M. & Low, R. B. Cardiac myofibroblasts express alpha smooth muscle actin during right ventricular pressure overload in the rabbit. *Am. J. Pathol.* **139**, 207–216 (1991).
19. Yang, K.-C. *et al.* Deep RNA sequencing reveals dynamic regulation of myocardial noncoding RNAs in failing human heart and remodeling with mechanical circulatory support. *Circulation* **129**, 1009–1021 (2014).
20. Park, S. *et al.* Genetic Regulation of Fibroblast Activation and Proliferation in Cardiac Fibrosis. *Circulation* (2018).
21. Lorenzo, P., Neame, P., Sommarin, Y. & Heinegård, D. Cloning and Deduced Amino Acid Sequence of a Novel Cartilage Protein (CILP) Identifies a Proform Including a Nucleotide Pyrophosphohydrolase. *J. Biol. Chem.* **273**, 23469–23475 (1998).
22. Shindo, K. *et al.* Cartilage Intermediate Layer Protein 1 Suppresses TGF-β Signaling in Cardiac Fibroblasts. *International Journal of Gerontology* **11**, 67–74 (2017).

23. Dobaczewski, M., Chen, W. & Frangogiannis, N. G. Transforming growth factor (TGF)-β signaling in cardiac remodeling. *J. Mol. Cell. Cardiol.* **51**, 600–606 (2011).
24. Hirani, R., Hanssen, E. & Gibson, M. A. LTBP-2 specifically interacts with the amino-terminal region of fibrillin-1 and competes with LTBP-1 for binding to this microfibrillar protein. *Matrix Biol.* **26**, 213–223 (2007).
25. Hedbom, E. *et al.* Cartilage matrix proteins. An acidic oligomeric protein (COMP) detected only in cartilage. *J. Biol. Chem.* **267**, 6132–6136 (1992).
26. Rosenberg, K., Olsson, H., Mörgelin, M. & Heinegård, D. Cartilage Oligomeric Matrix Protein Shows High Affinity Zinc-dependent Interaction with Triple Helical Collagen. *J. Biol. Chem.* **273**, 20397–20403 (1998).
27. Huang, Y. *et al.* Deficiency of cartilage oligomeric matrix protein causes dilated cardiomyopathy. *Basic Res. Cardiol.* **108**, 374 (2013).
28. Vuga, L. J. *et al.* Cartilage oligomeric matrix protein in idiopathic pulmonary fibrosis. *PLoS ONE* **8**, e83120 (2013).
29. Magdaleno, F. *et al.* Cartilage oligomeric matrix protein participates in the pathogenesis of liver fibrosis. *J. Hepatol.* **65**, 963–971 (2016).
30. Hesselstrand, R. *et al.* Increased serum COMP predicts mortality in SSc: results from a longitudinal study of interstitial lung disease. *Rheumatology (Oxford)* **51**, 915–920 (2012).
31. Zachou, K. *et al.* COMP serum levels: A new non-invasive biomarker of liver fibrosis in patients with chronic viral hepatitis. *Eur. J. Intern. Med.* **38**, 83–88 (2017).
32. Bernardo, B. C. *et al.* Cartilage Intermediate Layer Protein 2 (CILP-2) Is Expressed in Articular and Meniscal Cartilage and Down-regulated in Experimental Osteoarthritis. *J. Biol. Chem.* **286**, 37758–37767 (2011).
33. Luzina, I. G. *et al.* Transcriptomic evidence of immune activation in macroscopically normal-appearing and scarred lung tissues in idiopathic pulmonary fibrosis. *Cell. Immunol.* **325**, 1–13 (2018).

34. Sanders, Y. Y. *et al.* Altered DNA methylation profile in idiopathic pulmonary fibrosis. *Am. J. Respir. Crit. Care Med.* **186**, 525–535 (2012).

35. Barallobre-Barreiro Javier *et al.* Proteomics Analysis of Cardiac Extracellular Matrix Remodeling in a Porcine Model of Ischemia/Reperfusion Injury. *Circulation* **125**, 789–802 (2012).

36. Zhang, C.-L. *et al.* Cartilage intermediate layer protein-1 alleviates pressure overload-induced cardiac fibrosis via interfering TGF-β1 signaling. *Journal of Molecular and Cellular Cardiology* **116**, 135–144 (2018).

37. Nieuwenhoven, F. A. van *et al.* Cartilage intermediate layer protein 1 (CILP1): A novel mediator of cardiac extracellular matrix remodelling. *Scientific Reports* **7**, 16042 (2017).

38. Seki, S. *et al.* A functional SNP in *CILP*, encoding cartilage intermediate layer protein, is associated with susceptibility to lumbar disc disease. *Nature Genetics* **37**, 607–612 (2005).

39. Edgley, A. J., Krum, H. & Kelly, D. J. Targeting Fibrosis for the Treatment of Heart Failure: A Role for Transforming Growth Factor-β. *Cardiovascular Therapeutics* **30**, e30–e40 (2012).

40. Aukrust, P. *et al.* Cytokine network in congestive heart failure secondary to ischemic or idiopathic dilated cardiomyopathy. *The American Journal of Cardiology* **83**, 376–382 (1999).

41. Kapur Navin K. Transforming Growth Factor-β. *Circulation: Heart Failure* **4**, 5–7 (2011).

42. Lehr, S. *et al.* Identification and validation of novel adipokines released from primary human adipocytes. *Mol. Cell Proteomics* **11**, M111.010504 (2012).

43. Love, M. I., Huber, W. & Anders, S. Moderated estimation of fold change and dispersion for RNA-seq data with DESeq2. *Genome Biology* **15**, 550 (2014).

44. Blighe, K. EnhancedVolcano: Publication-ready volcano plots with enhanced colouring and labeling. *R package version 1.2.0* https://github.com/kevinblighe/EnhancedVolcano (2019).

APPENDIX I:

Cardiac Fibrosis: Potential Therapeutic Targets

Cardiac fibrosis: potential therapeutic targets

SHUIN PARK, NGOC B. NGUYEN, ARASH PEZHOUMAN, and REZA ARDEHALI

LOS ANGELES, CALIFORNIA

Cardiovascular disease is a leading cause of mortality in the world and is exacerbated by the presence of cardiac fibrosis, defined by the accumulation of noncontractile extracellular matrix proteins. Cardiac fibrosis is directly linked to cardiac dysfunction and increased risk of arrhythmia. Despite its prevalence, there is a lack of efficacious therapies for inhibiting or reversing cardiac fibrosis, largely due to the complexity of the cell types and signaling pathways involved. Ongoing research has aimed to understand the mechanisms of cardiac fibrosis and develop new therapies for treating scar formation. Major approaches include preventing the formation of scar tissue and replacing fibrous tissue with functional cardiomyocytes. While targeting the renin-angiotensin-aldosterone system is currently used as the standard line of therapy for heart failure, there has been increased interest in inhibiting the transforming growth factor-β signaling pathway due its established role in cardiac fibrosis. Significant advances in cell transplantation therapy and biomaterials engineering have also demonstrated potential in regenerating the myocardium. Novel techniques, such as cellular direct reprogramming, and molecular targets, such as noncoding RNAs and epigenetic modifiers, are uncovering novel therapeutic options targeting fibrosis. This review provides an overview of current approaches and discuss future directions for treating cardiac fibrosis. (Translational Research 2019; 209:121–137)

Abbreviations: AAV = adeno-associated viruses; AdV = adenovirus; Ang = angiotensin; CM = cardiomyocyte; CPC = cardiac progenitor cell; cTnT = cardiac troponin T; CVD = cardiovascular diseases; ECM = extracellular matrix; HF = heart failure; HFpEF = heart failure with preserved ejection fraction; HFrEF = heart failure with reduced ejection fraction; HGF = hepatocyte growth factor; hPSC = human pluripotent stem cell; LAD = left anterior descending artery; LVEDP = left ventricular end diastolic pressure; MI = myocardial infarction; MMP1 = matrix metalloproteinase-1; MSC = mesenchymal stem cell; PRR = (pro)renin receptor; RAAS = renin-angiotensin-aldosterone system; SeV = sendai virus; TGFβ = transforming growth factor β; TNFα = tumor necrosis factor α; αMHC = α-myosin heavy chain

INTRODUCTION

Cardiac fibrosis is a major pathologic disorder associated with a multitude of cardiovascular diseases (CVD) and is characterized by excessive extracellular matrix (ECM) protein deposition in the heart.[1,2] Upon ischemic injury or pressure overload, the heart undergoes a dynamic remodeling process that is driven by a multitude of cells including cardiomyocytes (CMs),

From the Division of Cardiology, Department of Internal Medicine, David Geffen School of Medicine, University of California, Los Angeles, Los Angeles, California; Eli and Edythe Broad Center for Regenerative Medicine and Stem Cell Research, University of California, Los Angeles, Los Angeles, California; Molecular, Cellular and Integrative Physiology Graduate Program, University of California, Los Angeles, Los Angeles, California; Molecular Biology Institute, University of California, Los Angeles, Los Angeles, California.

Submitted for Publication January 4, 2019; received submitted March 1, 2019; accepted for publication March 5, 2019.

Authorship: All authors have read the journal's authorship agreement and have reviewed and approved this manuscript.

Reprint requests: Reza Ardehali, MacDonald Medical Research Laboratory, Room 3760, 675 Charles E Young Dr S, Los Angeles, CA 90095. E-mail: rardehali@mednet.ucla.edu.

1931-5244/$ - see front matter

https://doi.org/10.1016/j.trsl.2019.03.001

endothelial cells, immune cells, and cardiac fibroblasts.[2-4] At the onset of acute injury, CMs rapidly become apoptotic and endothelial cells play a critical role in modulating the inflammatory response.[5,6] In the initial phases of remodeling, immune cells proliferate, infiltrate damaged myocardium to clear dead tissue, and release profibrotic cytokines.[3,7] In response to these cytokines, cardiac fibroblasts become activated and increase production of ECM proteins such as collagens and fibronectin to form scar tissue.[1,4,8] At first, these responses are critical in removing apoptotic CMs and for stabilizing the chamber walls to prevent rupture. The scar that is formed at this stage is deemed as reparative fibrosis. However, the persistent presence of noncontractile ECM leads to the maturation of scar tissue and adverse remodeling, the effects of which include an increased risk of arrhythmias and reduced contractility.[9,10] These effects can have a devastating impact on the clinical outcomes of CVD patients, creating a need to develop strategies to prevent or reverse cardiac fibrosis.

Several obstacles that have limited the development of antifibrotic therapies available for CVD patients. First, the regenerative potential of the adult human heart is limited and CMs are unable to proliferate at a level that can replace damaged myocardium.[11] This restricts therapies that aim to inhibit fibrosis entirely as the endogenous CMs are unable to replace lost muscle tissue, thus increasing risk of cardiac rupture. Second, the molecular mechanisms driving cardiac fibrosis are complex and not fully understood. Although cardiac fibroblasts are the major contributory cells of cardiac fibrosis, further studies are needed to unravel the mechanistic regulation of these cells. There is a need to understand their mechanisms of activation, the temporal nature of their molecular changes, and whether these cells can be "deactivated" or eliminated.[12] Finally, the injured heart, particularly after myocardial infarction (MI), is a volatile microenvironment with dramatic levels of CM apoptosis, immune cell infiltration, and fibroblast proliferation.[4,7,13] This hostile environment may hinder the efficacy of delivering antifibrosis therapies. In this review, we aim to describe prominent research areas that are being explored for the treatment of cardiac fibrosis with potential clinical promise.

RENIN-ANGIOTENSIN-ALDOSTERONE SYSTEM

Overview of the RAAS system. The renin-angiotensin-aldosterone system (RAAS) plays an integral role in the homeostatic control of arterial pressure, tissue perfusion, and extracellular volume.[14] This pathway is initiated by the secretion of renin from the juxtaglomerular cells of the kidney in response to various stimuli such as decreased renal perfusion, decreased sodium chloride concentration, or increased sympathetic activity.[15,16] Renin goes on to cleave angiotensinogen, to form a biologically inert peptide, Angiotensin (Ang) I. AngI is then hydrolyzed by angiotensin-converting enzyme (ACE) to form an active AngII, which is a potent vasoconstrictor. AngII is the primary effector of a variety of RAAS-induced physiological and pathophysiological actions. Within the cardiovascular system, these effects include vasoconstriction, increased blood pressure, increased cardiac contractility, and vascular and cardiac hypertrophy.[17] Another important action of AngII includes stimulating the production and release of aldosterone from the adrenal cortex. Aldosterone is a major regulator of sodium and potassium balance and thus plays a role in regulating extracellular volume.[18] Together, the resulting effects of AngII and aldosterone on their target organs serve to maintain blood pressure and restore renal perfusion. Although the RAAS plays an important role in normal circulatory homeostasis, continued or inappropriate activation of this system is thought to contribute to the pathophysiology of diseases such as hypertension and heart failure (HF).

Role of RAAS in cardiac fibrosis. *In vitro* experiments using adult rat cardiac fibroblasts have shown that AngII[19-21] and aldosterone[19] stimulate collagen synthesis in a dose-dependent manner. AngII additionally suppresses the activity of matrix metalloproteinase-1, a key enzyme of interstitial collagen degradation[19], that synergistically leads to progressive collagen accumulation within the myocardial interstitium. AngII induces expression of TGFβ1 within cardiac fibroblasts through the Ang type-I receptor (AT_1).[22] After MI, increased wall stress resulting from elevated left ventricular end diastolic pressure (LVEDP) stimulates mechanoreceptors that lead to activation of RAAS. Upregulated AngII increases tissue inflammation, and TGFβ, IL-1β, and TNFα secretion,[23-26] leading to enhanced generation of myofibroblasts. Within experimental models of hypertensive heart disease and chronic HF, circulating and local levels of renin-angiotensin-aldosterone promote the development of myocardial fibrosis and diastolic dysfunction.[27,28] Given the significant role of RAAS in the pathogenesis of cardiac fibrosis, therapies have been developed to antagonize or modulate the activity of various components of this system.

Direct renin inhibitors and renin receptor blockers. Direct renin inhibition may be a promising antifibrotic therapy as it attenuates the profibrotic effects of renin in addition to that of other effectors of the renin-angiotensin pathway.[29] Renin inhibitors interfere with the

initial rate limiting step in the synthesis of AngII by binding directly to renin.[30] Aliskiren is the first orally active renin inhibitor approved by the FDA for the treatment of hypertension in adults.[31] Zhi et al showed that aliskiren has direct effects on collagen metabolism in cardiac fibroblasts and prevented myocardial collagen deposition in a nonhypertrophic mouse model of myocardial fibrosis.[29] Other groups have shown that aliskiren functions through inhibition of AngII-dependent as well as AngII-independent effects mediated via the (pro)renin receptor (PRR).[32,33] Cardiac expression of PRR is upregulated in hypertension and HF and has been shown to be associated with the development of cardiac fibrosis and hypertrophy as well as cardiac dysfunction.[34-39] Ellmers et al reported that PRR blockade in a mouse model of MI significantly reduced infarct size and attenuated cardiac fibrosis and adverse remodeling.[38]

ACE inhibitors and angiotensin receptor blockers. ACE inhibitors such as enalapril, lisinopril, and trandolapril, prevent the conversion of inactive AngI into active AngII and are considered first-line therapy for many cardiovascular and renal diseases. There is a large body of evidence that ACE inhibitors regress myocardial fibrosis and are associated with reduction of ventricular arrhythmias and improvement of myocardial function.[40-45] Angiotensin receptor blockers (ARBs) are also commonly prescribed clinically and work by preventing the binding of AngII to its receptor (with greater affinity for AT_1 than AT_2). Wu et al showed that valsartan, an ARB, improved coronary arterial thickening and perivascular fibrosis in a pressure overload mouse model.[46] Similarly, Frimm et al found that rats treated with losartan had a reduction in cardiac infarct size and collagen content 1 month after experimental MI.[47] However, despite the efficacy of ACEs and ARBs in a variety of cardiac diseases including HF with reduced ejection fraction (HFrEF), recent clinical trials have not shown their benefit in HF patients with preserved ejection fraction (HFpEF).[48-50]

Aldosterone antagonists. Aldosterone is a steroid hormone produced by the zona glomerulosa of the adrenal cortex. It plays a key role in regulating blood pressure and plasma sodium levels through its actions on renal tubules to promote sodium retention and extracellular volume expansion. It has also been reported that aldosterone can be produced within the heart.[51] This local aldosterone system responds to short- and long-term physiological stimuli, suggesting that the cardiac-generated aldosterone has possible autocrine or paracrine actions.[52] Billa et al demonstrated that chronic administration of aldosterone in the setting of high salt intake causes both interstitial and perivascular fibrosis in the heart[53] and that treatment with an aldosterone antagonist, spironolactone, prevents the increase in total and interstitial collagen in rats.[54,55] Several clinical studies have confirmed survival benefit when aldosterone antagonists are used in HFrEF patients.[56-59] However, the risk of hyperkalemia requires frequent monitoring.[60]

Therapies targeting the RAAS have been extensively studied and shown to be effective in preventing collagen deposition and reducing cardiac fibrosis. While RAAS inhibition is the mainstay of clinical care, especially for HFrEF patients, further studies are needed to examine the efficacy and safety of these therapies for patients with HFpEF and other forms of cardiac fibrosis.

TGF-β SIGNALING PATHWAY

Overview of TGF-β signaling. The Transforming Growth Factor-β (TGFβ) family of peptides is one of the most well-studied regulators of the fibrotic response that plays a central role in the maladaptive remodeling of the heart after injury.[61-63] The expression of TGFβ in myocardial tissue is markedly increased in both animal experimental models of MI and in HF patients.[62,64] The targeting of the TGFβ signaling pathway has long been explored as a potential therapy to curtail fibrosis.[65,66] One of the challenges of studying the TGFβ family includes the complexity of effects that TGFβ peptides can stimulate across multiple cell types and conditions. TGFβ is known to play key roles in regulating inflammation and ECM deposition, 2 processes that constitute major phases of the fibrotic response. In inflammation, TGFβ signaling inhibits the synthesis of proinflammatory cytokines, such as TNFα.[67,68] TGFβ1-null mice demonstrate high levels of autoimmunity, supporting the importance of TGFβ in mediating the inflammatory response.[69] On the other hand, TGFβ signaling has been shown to induce fibroblast transition into activated myofibroblasts, the major cellular source for ECM protein deposition that makes up the fibrotic area.[4] Due to the multifunctional roles of TGFβ signaling, several studies have revealed that the specificity and timing of targeting this pathway are crucial for effective outcomes.[70]

Inhibitors of TGFβ receptors I and II. TGFβ signaling is activated by the binding of TGFβ to a tetrameric receptor complex made up of 2 type I (TGFβR1 or ALK5) and 2 type II (TGFβR2) receptors.[71] Studies inhibiting either ALK5 or TGFβR2 have shown reduced cardiac fibrosis in mouse models, although adverse effects such as increased mortality and inflammation were

observed.[72,73] Furthermore, long-term inhibition has serious side effect such as cardiac toxicities, which limits its clinical application.[74] Despite these limitations, there have been promising reports of novel TGFβ receptor inhibitors on treating cardiac fibrosis. GW788388 was recently identified as a more potent inhibitor of both ALK5 and TGFβR2 with an improved pharmacokinetic profile[75] and minimal toxic effects.[76] Multiple studies have demonstrated that GW788388 reduces myocardial fibrosis in murine heart disease models.[77-79] These studies reveal that GW788388 may be a promising antifibrotic agent that requires further exploration.

Clinical inhibitors of TGFβ—pirfenidone and tranilast. Pirfenidone and tranilast are 2 clinically-approved drugs that have a broad range of effects on inflammation and other fibrotic pathways. However, it has additionally been established that these drugs are inhibitory of TGFβ signaling. Both have recently been garnering interest in potentially treating cardiac fibrosis.[80] Pirfenidone is an oral antifibrotic drug that was approved by the FDA in 2014 for the treatment of idiopathic pulmonary fibrosis.[81] Pirfenidone has been shown to inhibit the transcription of TGFβ and suppress downstream effects of TGFβ signaling, such as ECM protein upregulation.[82] Several recent studies have additionally demonstrated the antifibrotic effects of pirfenidone in cardiac disease. Mirkovic et al and Nguyen et al independently showed reduced cardiac scarring after treatment of pirfenidone in hypertensive rats and rats with MI, respectively.[83,84] Similar effects were seen in murine pressure-overload injury; pirfenidone increased survival and attenuated collagen deposition.[85,86] Clinical trials are ongoing to explore the antifibrotic effects of pirfenidone in patients with HF and preserved ejection fraction (PIROUETTE).

Tranilast was originally used as an antihistamine to treat bronchial asthma, however, since its conception in the 1980s,[87] investigators have found efficacy of tranilast in other medical conditions. One of the main modes of action of tranilast is the suppression of TGFβ expression and activity.[87] Several studies have reported that tranilast induces downregulation of collagen production in fibroblasts.[88-90] Subsequently, the PRESTO (Prevention of REStenosis with Tranilast and its Outcomes) clinical trial, despite finding little effects of tranilast on restenosis, noted a reduction in the development of MI in patients treated with tranilast.[91] The effects of tranilast on attenuating myocardial fibrosis have been additionally supported by multiple animal models of cardiomyopathy, including experimental diabetes in rats[92] and viral myocarditis in mice.[93] While the antifibrotic effects of tranilast have been attributed to its regulation of TGFβ signaling, Kagitani et al reported that tranilast treatment is associated with decreased monocyte infiltration, which may also contribute to the reduced fibrosis.[94] Others have reported the anti-inflammatory effect of tranilast to be related to its ability to inhibit prostaglandin E2, thromboxane B2, or interleukin-8. Additionally, the timing of tranilast administration in relation to time of injury is a significant factor to consider. See et al showed that early tranilast treatment of rats with left anterior descending artery (LAD) ligation (day 0-7 after injury) exacerbated infarct size, implying a potential hazard when used early after injury.[95]

Despite the evidences supporting the antifibrotic effects of both pirfenidone and tranilast, studies have shown that prolonged dosages of either of these drugs can have hepatic toxicity and may lead to liver failure.[66] Therefore, more research is warranted to explore alternative methods that can safely, but efficaciously, target TGFβ signaling for reduction of cardiac fibrosis.

BIOMATERIAL APPLICATIONS

Overview of biomaterials. Biomaterials are natural or engineered substances that interact with biological systems and are used to replace or repair tissues of the body. There has been a vast array of applications of biomaterials for controlling cardiac fibrosis. In addition to providing a platform for controlled release of antifibrotic compounds, biomaterials may also provide mechanical support to the infarcted tissue and decrease elevated wall stress, resulting in improved cardiac function.[96] Both naturally-derived biomaterials such as collagen,[97-99] fibrin,[100-102] and alginate,[103-105] in addition to synthetic materials including metals and polymers,[106] have been used in cardiac applications. While natural biomaterials tend to offer better compatibility and low immunogenicity, the main benefits of synthetic materials are their strength and durability.[107] When combined with cells or cytokines/growth factors, biomaterials may offer enhanced retention of their payload leading to improved engraftment or biological function.[108] This review will focus on 2 main classes of biomaterials with cardiovascular applications.

Injectable biomaterials. In recent years, injectable biomaterials have seen a significant increase in application toward treating MI.[108-110] Hydrogels based on alginate and chitosan have been shown to decrease cardiac fibrosis, reduce tissue inflammation, and improve vascularization.[103,104] Combined with antifibrotic/anti-inflammatory compounds or stem cells, the therapeutic potential of injectable biomaterials can be further expanded. In a rat chronic myocarditis model, gelatin hydrogel sheets containing hepatocyte growth factor were found to improve cardiac function and fibrosis.[111]

Hepatocyte growth factor (HGF) serves as a favorable candidate as it suppresses fibrosis by inhibiting TGFβ (suppressing collagen synthesis) and activating metalloproteinase-1 to increase collagen degradation.[112,113] In addition to its antifibrotic effects, reports have also indicated their role in angiogenesis[114-116] and tissue regeneration.[117] Other growth factors incorporated with injectable biomaterials include basic fibroblast growth factor,[118,119] vascular endothelial growth factor,[120-122] and platelet-derived growth factor.[123,124] Collectively, there is significant amount of research on the development of injectable biomaterials with antifibrotic compounds or biologics to reduce fibrosis and promote healing.

Cardiac patches. Cardiac patches generally contain cells combined with a natural or synthetic biomaterial, although acellular patch therapies and cell sheets have also been investigated. While many *in vivo* studies in small animals have shown an improvement in cardiac function, one limitation with this application is the thickness of the material due to diffusion limitations.[125,126] The use of a collagen scaffold for cardiac patch has been well studied in combination with a variety of cell types.[98,127-129] Fibrin cardiac patches have also contributed to improved cell delivery and cardiac function in large animal models.[100,130,131] Processed decellularized cardiac ECM has also shown promise as an injectable hydrogel[132-134] and patch.[135,136] This is a naturally-derived matrix that provides cells with tissue-specific biochemical cues important for cell migration and differentiation, and tissue regeneration. Pieces of the myocardium (or the entire heart) may be chemically or enzymatically digested to obtain cardiac ECM.[132] The major compositions of decellularized cardiac ECM include collagen, elastin, and fibronectin. It should be noted that although fibronectin has been shown to activate cardiac fibroblasts into myofibroblasts,[137] it is thought that other factors or cytokines within the cardiac ECM matrix may offset this activation and lead to overall benefit.[112] Other clinical studies on the use of ECM are underway.[138-140]

Injectable biomaterials and cardiac patches for the treatment of MI have recently been launched in clinical trials. While many promising studies have been completed in rodent and large animal models, further studies are needed to better understand the mechanisms behind their observed effects as well as utility for clinical applications.

CELL TRANSPLANTATION THERAPY

Overview of cardiac cell therapy. Reduction of blood flow and oxygen to the heart resulting from ischemia can lead to irreversible loss of CMs and replacement with fibrotic scar tissue. Although traditional medical therapies are beneficial, many patients eventually progress to end-stage HF, with cardiac transplantation as the only definitive option. Due to the limited supply of donor hearts and potential complications from chronic immunosuppressive therapy, investigators have turned to therapeutic approaches aimed at improving myocardial function by cell transplantation.[141-143] The inception of the use of stem cells as a form of cardiac therapy initially emerged in animal studies over 20 years ago[144] and reached clinical trials 10 years thereafter.[145] Despite early promises, there is no evidence to suggest that current approaches for cardiac cell therapy offer any clinical benefit. Although there are many strategies of cell therapy, this review will focus on 2 main avenues: (1) direct remuscularization of injured heart and (2) targeting endogenous mechanisms of repair.

Direct remuscularization of fibrotic tissue in injured heart. The concept behind this approach is that transplantation of cells into the injured area may lead to integration with viable cells in the host myocardium, thereby improving cardiac contraction and reducing the risk of ventricular rupture or aneurysms. For this reason, many different cell types have been explored as a source for cell transplantation, including autologous skeletal myoblasts,[146] bone marrow-derived CD34+ cells (endothelial progenitor cells),[147] C-kit surface antigen-selected cells,[148] ESC/iPSC-derived CM precursors,[149-153] and ESC/iPSC-derived CM.[154-156]

Clinical application of skeletal myoblasts failed due to concerns over arrhythmias generated by the transplanted cells.[157] C-kit surface antigen-selected cardiac progenitor cells initially showed some promise owing to their potential to proliferate and differentiate into the new myocardium, although later studies have challenged the existence of such cells that could generate new CMs.[158,159] Human pluripotent stem cells (hPSC) were first characterized in 1998 and[160] have been used to generate CMs in vitro and in vivo. Nevertheless, injection of hPSC-derived CMs or progenitors in large animal models after an acute MI have raised safety concerns such as ventricular fibrillation/tachycardia.[154,161,162] One possibility is the potential contamination of noncardiac or pacemaker cells in the hPSC-derived population capable of inducing arrhythmias. Another possibility is failure of transplanted hPSC-derived cardiac cells to physiologically couple with endogenous CMs, leading to disruption of cardiac action potential propagation. Alternative to direct injection of cells into the injured myocardium, others have used bioengineering approaches such as scaffolds or patches for cell therapy (discussed in detail above).

Menasché and others developed a sheet of PSC-derived CMs and applied it onto the surface of the scar and border zone in MI hearts.[149] This single case report study was the first clinical application of hPSC-derived cardiac cell therapy and no safety issues were reported. However, epicardially-administered cells are unlikely to engraft, migrate, and integrate into the host myocardial tissue. Despite the promising advancement in developing contractile cardiac cell products and successfully applying them in animal models,[153] further studies are still needed to optimize this strategy to enhance the safety and long-term engraftment of transplanted cells.[163]

Stimulation of endogenous cardiovascular progenitors and/or CMs for regenerative therapy. This approach aims to use cells or their by-products to induce endogenous progenitors or CMs to proliferate and replace fibrotic tissue in the injured myocardium via paracrine-mediated effects. However, no study has yet provided unequivocal evidence for the existence of cardiac progenitors in adult human hearts. Studies have shown that certain cells have myogenic differentiation capacity[164] or release by-products, such as exosomes,[165] that may stimulate cardiac regeneration. Other studies have used adult undifferentiated progenitor cells such as bone marrow aspirated mononuclear cells,[166] marrow-derived mesenchymal stem cells (MSCs),[167,168] and resident adult cardiac progenitors (CPCs)[169] to stimulate endogenous pathway for regenerative therapy. A clinical trial involving the use of MSCs is ongoing, despite its uncertain efficacy.[170] Some studies have revealed an improvement in scar size,[171] while others have shown no benefit.[172] Preclinical studies of CPCs suggested that these cells possess myogenic differentiation capacity, however, further mechanistic studies revealed their anti-inflammatory and antifibrotic properties, as well as ability to stimulate endogenous cardiac progenitor and CMs.[173-176] Other genetic fate-mapping studies have shown that endogenous CPCs[158,177] and MSCs[173,178,179] produce new CMs, although the percentage of CMs emerging from the CPCs and MSCs was extremely low. Altogether, engraftment of MSCs and CPCs is lower compared to ESC/iPSC-based strategies but leads to significant improvement in left ventricular function and reduction of scar size.[153,169,180] These findings promised a paradigm shift in cardiac biology and new opportunities for future regenerative therapy. However, several years after these findings, a consensus on the biological role of these populations remains obscure.

In summary, although significant advancements have been made in cell therapy, several critical issues remain. In order to expedite clinical application of cell therapy, a better understanding of the mechanism of action, improvement in cellular delivery and retention, purification of the desired cell types, and functional integration of transplanted cells need to be addressed.

DIRECT REPROGRAMMING OF FIBROBLASTS

Overview of cardiac direct reprogramming. The development of cardiac fibrosis is driven by the proliferation and activation of cardiac fibroblasts, which become the main cellular components of scar tissue.[1,4,8] Considering the abundance of this cell type within the fibrotic region, they may be an ideal target for direct reprogramming to generate CMs to replace the scar and restore cardiac function.[181] In 2010, Ieda et al demonstrated the ability to reprogram postnatal murine dermal and cardiac fibroblasts into induced CM-like cells by transducing the cells with 3 factors (Gata4, Mef2c, and Tbx5, hereafter collectively referred to as GMT).[182] The resulting cells expressed CM-specific markers such as cardiac troponin T and α-myosin heavy chain.[182] Wada et al further demonstrated that transduction with GMT plus additional factors Mesp1 and Myocardin could produce induced CM-like cells from human fibroblasts.[183] This has generated enthusiasm for improving and utilizing direct reprogramming for potential therapeutic purposes.

In vivo direct reprogramming by retroviral delivery of transcription factors. The potential of direct reprogramming to be used for treating ischemic heart disease was first explored in 2012 by several groups that attempted to apply successful in vitro results to an in vivo setting. Qian et al and Song et al independently reported successful reprogramming of resident fibroblasts to induced CMs in murine hearts after LAD ligation by retroviral transduction of GMT and GMT plus Hand2, respectively.[184,185] Both groups observed increased reprogramming efficiency in vivo compared to in vitro, suggesting that the cardiac environment may influence the reprogramming process. However, the percentage of cells that were successfully reprogrammed remained low. Inagawa et al reported an improvement in the reprogramming efficiency with GMT by using a retroviral polycistronic vector.[186] All 3 studies demonstrated that retroviral delivery of GMT or GMHT into the murine heart after an experimental MI could reduce the extent of cardiac fibrosis, solidifying the therapeutic potential for direct reprogramming.

While numerous groups have reported successful direct reprogramming of cardiac fibroblasts in murine ischemic heart disease models, the clinical translation of this approach has not been fully addressed. Retroviral delivery involves random insertion of DNA into the

host cell's genome which makes this mechanism of reprogramming potentially pathogenic.[187] Therefore, nonintegrative methods of reprogramming that can be safely applied to human patients are warranted. There is an additional need to verify the safety and efficacy of direct reprogramming of cardiac fibroblasts to induced CMs-like cells in large animal models as a preclinical prelude to future human studies.

Potential clinical applications of direct reprogramming. Nonintegrative viral vectors such as Adenovirus (AdV), Adeno-associated viruses (AAV), and Sendai virus (SeV) have recently garnered interest in the reprogramming field. AdVs are a widely used research tool that can transduce a variety of cells with high efficiency. A recent report demonstrated that AdVs encoding GMT were able to induce cardiac reprogramming in a rat infarct model to a similar degree as an integrative viral vector (lentivirus).[188] However, clinical applications of AdVs have been dampened by their high immunogenicity.[189] AAVs, on the other hand, are a more viable option as they are able to target various cell types similar to AdVs but exhibit significantly reduced immunogenicity.[190] Clinical trials investigating the use of AAVs for gene therapy in various conditions are currently underway.[191] Yoo et al demonstrated that chimeric-AAVs encoding GMT are able to induce direct cardiac reprogramming and reduce infarct size after LAD ligation in mice.[192] Finally, SeVs are a relatively new tool for gene therapy that is gaining attention due to their lack of integration and high expression of viral genes.[193] Indeed, SeV vectors expressing GMT have been shown to significantly increase the efficiency of cardiac reprogramming in mouse infarct hearts, compared to retroviral vectors, and resulted in lower levels of fibrosis.[194,195]

Several studies have also explored the potential to directly reprogram fibroblasts into CMs by nonviral methods. Recent reports have shown the ability to reprogram mouse fibroblasts into CMs by addition of small molecules in vitro.[196,197] Additionally, another group has demonstrated the capabilities of miRNA transfection in cardiac reprogramming in vivo.[198] These advancements have laid a framework for a future in vivo reprogramming without the need for viral transduction.

EMERGING NOVEL ANTIFIBROTIC THERAPEUTIC STRATEGIES

Noncoding RNAs in cardiac fibrosis. There have been several exciting findings for other novel antifibrotic therapeutic strategies. Several studies have identified a variety of noncoding RNAs (miRNAs and lncRNA) which may modulate fibrosis.[199,200] miRNA-21,[201] miRNA-29,[202] and miRNA-34[203] are a few of the identified miRNAs that are being extensively characterized for their role in regulating cardiac fibrosis. Silencing of miRNA-21 and miRNA-34 reduced fibrosis while downregulation of miRNA-29 exacerbated collagen production. These data suggest that a variety of

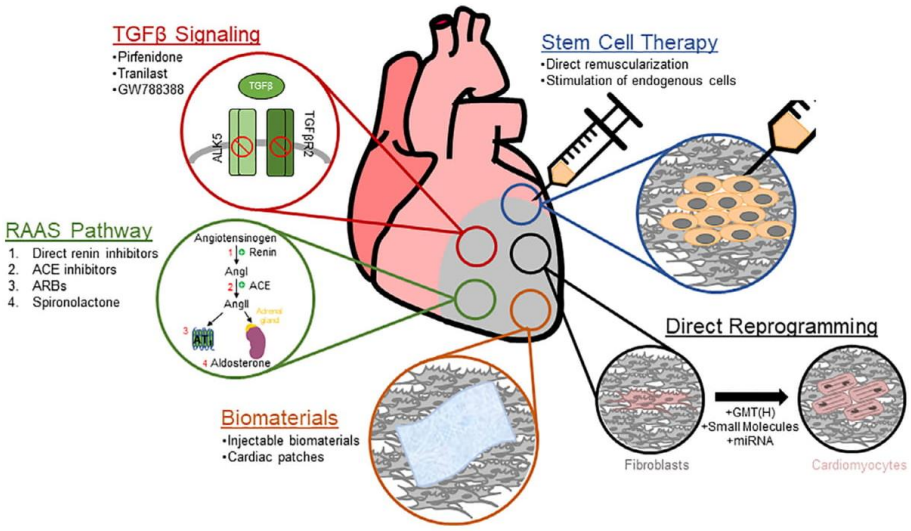

Fig 1. Schematic diagram depicting potential therapeutic strategies for targeting cardiac fibrosis.

Table 1. Animal and clinical studies assessing cardiac fibrosis therapies.

Therapeutic Target	Strategy	Dosage	Year	Model of Fibrosis	Species	Ref
RAAS	Renin inhibition (aliskiren)*	0.5-50mg/kg#/day	2013	Hyperhomocysteinemia-induced myocardial fibrosis	Mice	29
	Pro-renin receptor blockade (mouse HRP)	0.1mg/kg#/day	2016	Myocardial infarction	Mice	38
	ACE inhibition (lisinopril)*	2.5-20mg/kg#/day	1991	Spontaneous hypertension	Rat	40
	ACE inhibition (trandolapril)*	0.3mg/kg#/day	1995	Spontaneous hypertension	Rat	43
	ACE inhibition (captopril)*	2g/L water	1997	Spontaneous hypertension	Rat	44
	ACE inhibition (lisinopril)*	20mg/day	2000	Patients with primary HTN, LV hypertrophy, and LV diastolic dysfunction	Human	42
	ACE inhibition (perindopril)*	4mg/day	2006	HFpEF	Human	48
	ACE inhibition (captopril)*	10-100mg/kg#	2017	LPS-induced inflammation	Rat	45
	ARB (losartan)*	10mg/kg#/day	1997	Myocardial infarction	Rat	47
	ARB (valsartan)*	1mg/kg#/day	2002	Transaortic constriction	Mice	46
	ARB (candesartan)*	32mg/day	2003	HFpEF	Human	49
	ARB (irbesartan)*	300mg/day	2008	HFpEF	Human	50
	Aldosterone antagonist (spironolactone)*	20-200mg/kg#/day	1992	Renovascular hypertension	Rat	54
	Aldosterone antagonist (spironolactone)*	12-75mg/day	1996	Chronic HF patients	Human	58
	Aldosterone antagonist (spironolactone)*	25mg/day	1999	HFrEF	Human	59
	Aldosterone antagonist (spironolactone)*	15-45mg/day	2014	HFpEF	Human	57
	Aldosterone antagonist (spironolactone)*	15mg/day	2018	HFpEF	Human	60
TGFβ Signaling	TGFβRII plasmid transfection	N/A	2004	Myocardial infarction	Mice	73
	SM16 (inhibitor of ALK5)	0.45g/kg chow	2014	Pressure overload	Mice	72
	GW788388 (inhibitor of ALK5 and TGFβRII)	50mg/kg#/day	2010	Myocardial infarction	Rats	79
	GW788388 (inhibitor of ALK5 and TGFβRII)	3mg/kg#	2012	Chagas	Mice	77
	GW788388 (inhibitor of ALK5 and TGFβRII)	5mg/kg#/day	2017	Scn5a+/-	Mice	78
	Pirfenidone	250-300mg/kg#/day	2002	DOCA-salt hypertension	Rats	83
	Pirfenidone	1.2% in chow	2010	Myocardial infarction	Rats	84
	Pirfenidone	200mg/kg#	2013	Pressure overload	Mice	85
	Pirfenidone	400mg/kg#	2015	Pressure overload	Mice	86
	Tranilast	100mg/kg#/day	2004	DOCA-salt hypertension	Rats	94
	Tranilast	300mg/kg#	2013	Myocardial infarction	Rats	95
	Tranilast	200mg/kg#/day	2016	Viral myocarditis	Mice	93
Biomaterials	Hydrogel (alginate)	N/A	2009	Myocardial infarction	Porcine	104
	Hydrogel (polyester-VEGF)	N/A	2011	Myocardial infarction	Rats	121
	Hydrogel (decellularized ECM)	N/A	2012	Myocardial infarction	Rats	133
	Hydrogel (alginate-chitosan)	N/A	2014	Myocardial infarction	Rats	103
	Hydrogel (gelatin-HGF)	N/A	2014	Chronic myocarditis	Rats	111
	Hydrogel (CorMatrix®-ECM)	N/A	ongoing	CABG after myocardial infarction	Human	138
	Hydrogel (VentriGel)	N/A	ongoing	STEMI undergoing PCI	Human	140

(*continued*)

Table 1. (*Continued*)

Therapeutic Target	Strategy	Dosage	Year	Model of Fibrosis	Species	Ref
	Patch (alginate-neonatal rat CMs)	N/A	2009	Myocardial infarction	Rats	120
	Patch (hiPS-CMs)	N/A	2012	Myocardial infarction	Porcine	130
	Patch (decellularized ECM)	N/A	2016	Ischemia-reperfusion	Porcine	136
	Glue (fibrin-FGF)	N/A	2010	Myocardial infarction	Canine	118
	Microspheres	N/A	2006	Myocardial infarction	Canine	119
	Self-assembling peptides (skeletal myoblasts-PDGF)	N/A	2008	Myocardial infarction	Rats	123
	Self-assembling peptides (PDGF-FGF)	N/A	2011	Myocardial infarction	Rats	124
	Scaffold (fibrin-ECs-SMCs)	N/A	2011	Myocardial infarction	Porcine	100
Cell Transplantation	Direct Remuscularization skeletal (myoblasts)	N/A	1993		Mice	146
	Direct Remuscularization (BM-MSCs)	N/A	2004	Myocardial infarction	Human	145
	Direct Remuscularization	N/A	2005	Myocardial infarction	Human	141
	Direct Remuscularization (hematopoietic BM stem cell)	N/A	2006	Myocardial infarction	Human	142
	Direct Remuscularization (BM-derived progenitor cells)	N/A	2006	Myocardial infarction	Human	143
	Direct Remuscularization (myoblast)	N/A	2008	Ischemic Cardiomyopathy	Human	157
	Direct Remuscularization (cardiac stem cell)	N/A	2012	Ischemic Cardiomyopathy	Human	210
	Direct Remuscularization (hESC-CMs)	N/A	2014	Myocardial infarction	Monkey	154
	Direct Remuscularization (hESC-CMs)	N/A	2014	Myocardial infarction	Pig	156
	Direct Remuscularization (hESC-CMs and hESC-CVPs)	N/A	2015	Myocardial infarction	Rat	153
	Direct Remuscularization (hESC-CVPs)	N/A	2015	Severe heart failure	Human	149
	Direct Remuscularization (hESC-CMs)	N/A	2015	Myocardial infarction	Rat	155
	Direct Remuscularization (CD34+ Cell)	N/A	2016	Refractory Angina	Human	147
	Direct Remuscularization (myoblast)	N/A	2016	Myocardial infarction	Monkey	161
	Stimulation of Endogenous CVPs	N/A	2001	Myocardial infarction	Mice	166
	Stimulation of Endogenous CVPs (BM-MSCs)	N/A	2008	Ischemic heart disease	Human	168
	Stimulation of Endogenous CVPs (BM-MSCs)	N/A	2009	Myocardial infarction	Pig	178
	Stimulation of Endogenous CVPs (BM-MSCs)	N/A	2010	Myocardial infarction	Pig	173
	Stimulation of Endogenous	N/A	2011	Myocardial infarction	Mice	174

(*continued*)

Table 1. (*Continued*)

Therapeutic Target	Strategy	Dosage	Year	Model of Fibrosis	Species	Ref
	CVPs (cardiac stem cell c-kit$^+$)					
	Stimulation of Endogenous CVPs (cardiac stem cell c-kit$^+$)	N/A	2012	Heart failure due to Ischemia	Human	169
	Stimulation of Endogenous CVPs (BM-MSCs)	N/A	2013	Myocardial infarction & Ischemic heart disease	Human	171
	Stimulation of Endogenous CVPs (cardiosphere-derived cells)	N/A	2013	Myocardial infarction	Mice	175
	Stimulation of Endogenous CVPs (MSCs and cardiac progenitor cells)	N/A	2015	Myocardial infarction	Pig	176
	Stimulation of Endogenous CVPs	N/A	2017	Myocardial infarction	Pig	165
Direct Reprogramming	GMT (retrovirus/lentivirus)	N/A	2010	N/A	*In vitro -> in vivo* (Mice)	182
	GMT/GMTMM (retrovirus/lentivirus)	N/A	2013	N/A	*in vitro* (Human)	183
	Small molecule cocktail + Oct4	N/A	2014	N/A	*In vitro* (Mouse)	196
	Chemical cocktail	N/A	2015	N/A	*In vitro* (Mouse)	197
	GMT (retrovirus)	N/A	2012	Myocardial infarction	Mice	184
	GMHT (retrovirus)	N/A	2012	Myocardial infarction	Mice	185
	GMHT (retrovirus, polycistronic)	N/A	2012	Myocardial infarction	Mice	186
	miRNAs (1, 133, 208, and 499)	N/A	2015	Myocardial infarction	Mice	198
	GMT (adenovirus)	N/A	2017	Myocardial infarction	Rats	188
	GMT (chimeric AAV)	N/A	2018	Myocardial infarction	Mice	192
	GMT (sendai virus)	N/A	2018	Myocardial infarction	Mice	194

*Currently used clinical therapy
#Body weight

miRNAs possess both antifibrotic and profibrotic roles. Additionally, lncRNAs have gained interest as another family of regulatory noncoding RNAs in cardiac fibrosis. Wisper and MIAT are 2 recently identified lncRNAs that function to regulate fibrosis-related genes.[204,205] There remain challenges in targeting miRNAs and lncRNAs for therapy due to their broad and nonspecific effects. Ongoing efforts to identify the molecular targets of these noncoding RNAs will undoubtedly shed light on this novel therapeutic approach.

Epigenetic modifiers in cardiac fibrosis. The contribution of epigenetics to the development of cardiac fibrosis is an additional growing field. Evidences have shown that modifications to the epigenetic landscape of various cell types can arise from different stimuli and stresses. These changes can regulate the expression of proinflammatory and profibrotic genes in immune cells and cardiac fibroblasts.[206] Therefore, therapies targeting epigenetic modifiers may be promising in reversing pathologic symptoms in cardiac fibrosis. Preliminary studies have shown that histone deacetylase inhibitors, such as Mocetinostat, can reverse cardiac fibrosis by targeting cardiac fibroblast activation.[207,208] Additionally, inhibition of the epigenetic reader BRD4 was shown to reduce fibrosis in mice undergoing MI.[209] These findings have been mainly from preclinical studies and require further exploration as a promising tool for treating cardiac fibrosis in the future.

CONCLUSIONS

In this review, we discussed several potential therapeutic options for preventing or reducing cardiac fibrosis (Fig 1). While the research conducted in these fields has exhibited great promise, there remain challenges for translating these data into clinical practice. Both the RAAS and TGFβ pathway are major signaling cascades that significantly regulate the development of cardiac fibrosis. Targeting the RAAS has shown notable promise in the clinic, but it is unknown whether their effects can be seen in patients with different types of CVD. Inhibitors of components from the TGFβ pathway have shown strong evidences of reducing fibrosis in animal models, although their applications in the clinic require further investigation. The goal of cell transplantation has been to replenish cardiac muscle and replace fibrotic tissue. Questions remain regarding the most suitable cell type for transplantation and how to promote functional integration of transplanted cells into the recipient hearts. The development of engineered biomaterials in the form of hydrogels or cardiac patches has begun to address some of these limiting factors. It is likely that the future success of cell therapy will ultimately involve a combinatorial approach where the ideal cell types are embedded within a scaffold for optimal cell survival, differentiation, and functional integration into the host myocardium while replacing the scar tissue. Direct reprogramming provides a novel method of replacing pathologic fibroblasts with induced CMs. However, the safety of in vivo reprogramming still requires validation in large animal models. It is likely that a combination of various therapies will be necessary to address the complex pathology of cardiac fibrosis.

An obstacle not discussed in detail in this review is the significant difficulty in translating results from animal studies to human subjects. The majority of translational research is conducted in rodents (mice or rats), which exhibit significantly different characteristics in cardiac physiology compared with humans (Table I). These differences have been reflected by poor clinical trial outcomes despite promising preclinical data. There has been a movement in recent preclinical work to be conducted in larger animal models (pigs and nonhuman primates), which more closely resemble human physiology. However, there are still species-specific differences that can hinder the development of efficacious therapies. Continued research, considering these factors, on potential antifibrosis therapeutic strategies will help to progress these therapies to the clinic.

ACKNOWLEDGEMENTS

Conflicts of Interest: All authors have read the journal's policy on disclosure of potential conflicts of interest. The authors have no conflicts of interest to declare.

Funding: Park, S is supported by the Ruth L. Kirschstein National Research Service Award (NRSA) T32HL69766. Nguyen, NB is supported by the Ruth L. Kirschstein NRSA Predoctoral Fellowship F31HL144057. Pezhouman, A is supported by the Eli & Edythe Broad Center of Regenerative Medicine and Stem Cell Research at UCLA Training Program. Ardehali, R is supported in part by the National Institute of Health DP2 (HL127728), California Institute for Regenerative Medicine (RN3-06378) and the American Heart Association Innovative Research Grant (18IPA34170309).

REFERENCES

1. Fan D, Takawale A, Lee J, Kassiri Z. Cardiac fibroblasts, fibrosis and extracellular matrix remodeling in heart disease. Fibrogenesis Tissue Repair 2012;5:15.
2. Kong P, Christia P, Frangogiannis NG. The pathogenesis of cardiac fibrosis. Cell Mol Life Sci 2014;71:549–74.
3. Nicoletti A, Michel J-B. Cardiac fibrosis and inflammationinteraction with hemodynamic and hormonal factors. Cardiovasc Res 1999;41:532–43.
4. Travers JG, Kamal FA, Robbins J, Yutzey KE, Blaxall BC. Cardiac fibrosis: the fibroblast awakens. Circ Res 2016;118:1021–40.
5. Dumont Ewald AWJ, Hofstra L, van Heerde Waander L, et al. Cardiomyocyte death induced by myocardial ischemia and reperfusion. Circulation 2000;102:1564–8.
6. Singhal AK, Symons JD, Boudina S, Jaishy B, Shiu YT. Role of endothelial cells in myocardial ischemia-reperfusion injury. Vasc Dis Prev 2010;7:1–14.
7. Frangogiannis NG. The inflammatory response in myocardial injury, repair and remodeling. Nat Rev Cardiol 2014;11:255–65.
8. Krenning G, Zeisberg EM, Kalluri R. The origin of fibroblasts and mechanism of cardiac fibrosis. J Cell Physiol 2010;225:631–7.
9. Khan R, Sheppard R. Fibrosis in heart disease: understanding the role of transforming growth factor-beta in cardiomyopathy, valvular disease and arrhythmia. Immunology 2006;118:10–24.
10. Baicu CF, Stroud JD, Livesay VA, et al. Changes in extracellular collagen matrix alter myocardial systolic performance. Am J Physiol Heart Circulatory Physiol 2003;284:H122–32.
11. Steinhauser ML, Lee RT. Regeneration of the heart. EMBO Mol Med 2011;3:701–12.
12. Ma Y, Iyer RP, Jung M, Czubryt MP, Lindsey ML. Cardiac fibroblast activation post-myocardial infarction: current knowledge gaps. Trends Pharmacol Sci 2017;38:448–58.
13. Akasaka Y, Morimoto N, Ishikawa Y, et al. Myocardial apoptosis associated with the expression of proinflammatory cytokines during the course of myocardial infarction. Mod Pathol 2006;19:588.
14. Atlas SA. The renin-angiotensin aldosterone system: pathophysiological role and pharmacologic inhibition. J Manag Care Pharm 2007;13(8 Supp B):9–20.

15. J Brown M. Direct renin inhibition − a new way of targeting the renin system. J Renin-Angiotensin-Aldosterone Syst Vol 72006, S7-S11.
16. Laragh JH, Sealey JE. Renin-angiotensin-aldosterone system and the renal regulation of sodium, potassium, and blood pressure homeostasis. Compr Physiol 2011:1409–541.
17. Carey RM, Siragy HM. Newly recognized components of the renin-angiotensin system: potential roles in cardiovascular and renal regulation. Endocr Rev 2003;24:261–71.
18. Funder JW. New biology of aldosterone, and experimental studies on the selective aldosterone blocker eplerenone. Am Heart J 2002;144(5, Supplement):S8–S11.
19. Brilla CG, Zhou G, Matsubara L, Weber KT. Collagen metabolism in cultured adult rat cardiac fibroblasts: response to angiotensin II and aldosterone. J Mol Cell Cardiol 1994; 26:809–20.
20. Villarreal FJ, Kim NN, Ungab GD, Printz MP, Dillmann WH. Identification of functional angiotensin II receptors on rat cardiac fibroblasts. Circulation 1993;88:2849–61.
21. Sadoshima J, Izumo S. Molecular characterization of angiotensin II−induced hypertrophy of cardiac myocytes and hyperplasia of cardiac fibroblasts. Critical role of the AT1 receptor subtype. Circ Res 1993;73:413–23.
22. Campbell SE, Katwa LC. Angiotensin II stimulated expression of transforming growth factor-β1 in cardiac fibroblasts and myofibroblasts. J Mol Cell Cardiol 1997;29:1947–58.
23. Sutton Martin GSJ, Sharpe N. Left ventricular remodeling after myocardial infarction. Circulation 2000;101:2981–8.
24. Lahera V, Cachofeiro V, de las Heras N. Interplay of hypertension, inflammation, and angiotensin II. Am J Hypertens 2011; 24:1059.
25. Haudek SB, Cheng J, Du J, et al. Monocytic fibroblast precursors mediate fibrosis in angiotensin-II-induced cardiac hypertrophy. J Mol Cell Cardiol 2010;49:499–507.
26. Bodiga S, Zhong JC, Wang W, et al. Enhanced susceptibility to biomechanical stress in ACE2 null mice is prevented by loss of the p47 phox NADPH oxidase subunit. Cardiovasc Res 2011;91:151–61.
27. Brilla CG, Pick R, Tan LB, Janicki JS, Weber KT. Remodeling of the rat right and left ventricles in experimental hypertension. Circ Res 1990;67:1355–64.
28. Weber KT, Brilla CG. Pathological hypertrophy and cardiac interstitium. Fibrosis and renin-angiotensin-aldosterone system. Circulation 1991;83:1849–65.
29. Zhi H, Luptak I, Alreja G, et al. Effects of direct renin inhibition on myocardial fibrosis and cardiac fibroblast function. PLoS One 2013;8:e81612.
30. Kleinert HD. Hemodynamic effects of renin inhibitors. Am J Nephrol 1996;16:252–60.
31. Staessen JA, Li Y, Richart T. Oral renin inhibitors. Lancet 2006;368:1449–56.
32. Gross O, Girgert R, Rubel D, Temme J, Theissen S, Müller G-A. Renal protective effects of aliskiren beyond its antihypertensive property in a mouse model of progressive fibrosis. Am J Hypertens 2011;24:355–61.
33. Montes E, Ruiz V, Checa M, et al. Renin is an angiotensin-independent profibrotic mediator: role in pulmonary fibrosis. Eur Respir J 2012;39:141.
34. Danser AHJ, van Kesteren Catharina AM, Bax Willem A, et al. Prorenin, renin, angiotensinogen, and angiotensin-converting enzyme in normal and failing human hearts. Circulation 1997;96:220–6.
35. Ichihara A, Kaneshiro Y, Takemitsu T, et al. Nonproteolytic activation of prorenin contributes to development of cardiac fibrosis in genetic hypertension. Hypertension 2006;47:894–900.
36. Hirose T, Mori N, Totsune K, et al. Gene expression of (pro) renin receptor is upregulated in hearts and kidneys of rats with congestive heart failure. Peptides 2009;30:2316–22.
37. Moilanen A-M, Rysä J, Serpi R, et al. (Pro)renin receptor triggers distinct angiotensin II-independent extracellular matrix remodeling and deterioration of cardiac function. PLoS One 2012;7:e41404.
38. Ellmers LJ, Rademaker MT, Charles CJ, Yandle TG, Richards AM. (Pro)renin receptor blockade ameliorates cardiac injury and remodeling and improves function after myocardial infarction. J Card Fail 2016;22:64–72.
39. Nguyen G. The (pro)renin receptor: pathophysiological roles in cardiovascular and renal pathology. Curr Opin Nephrol Hypertens 2007;16:129–33.
40. Brilla CG, Janicki JS, Weber KT. Impaired diastolic function and coronary reserve in genetic hypertension. Role of interstitial fibrosis and medial thickening of intramyocardial coronary arteries. Circ Res 1991;69:107–15.
41. Brilla CG, Janicki JS, Weber KT. Cardioreparative effects of lisinopril in rats with genetic hypertension and left ventricular hypertrophy. Circulation 1991;83:1771–9.
42. Brilla Christian G, Funck Reinhard C, Rupp H. Lisinopril-mediated regression of myocardial fibrosis in patients with hypertensive heart disease. Circulation 2000;102:1388–93.
43. Chevalier B, Heudes D, Heymes C, et al. Trandolapril Decreases prevalence of ventricular ectopic activity in middle-aged SHR. Circulation 1995;92:1947–53.
44. Brooks Wesley W, Bing Oscar HL, Robinson Kathleen G, Slawsky Mara T, Chaletsky David M, Conrad Chester H. Effect of angiotensin-converting enzyme inhibition on myocardial fibrosis and function in hypertrophied and failing myocardium from the spontaneously hypertensive rat. Circulation 1997;96: 4002–10.
45. Abareshi A, Norouzi F, Asgharzadeh F, et al. Effect of angiotensin-converting enzyme inhibitor on cardiac fibrosis and oxidative stress status in lipopolysaccharide-induced inflammation model in rats. Int J Preventive Med 2017;8:69-69.
46. Wu L, Iwai M, Nakagami H, et al. Effect of angiotensin II type 1 receptor blockade on cardiac remodeling in angiotensin II Type 2 receptor null mice. Arterioscler Thromb Vasc Biol 2002; 22:49–54.
47. De Carvalho Frimm C, Sun Y, Weber KT. Angiotensin II receptor blockade and myocardial fibrosis of the infarcted rat heart. J Lab Clin Med 1997;129:439–46.
48. Cleland JGF, Tendera M, Adamus J, et al. The perindopril in elderly people with chronic heart failure (PEP-CHF) study. Eur Heart J 2006;27:2338–45.
49. Yusuf S, Pfeffer MA, Swedberg K, et al. Effects of candesartan in patients with chronic heart failure and preserved left-ventricular ejection fraction: the CHARM-Preserved Trial. Lancet 2003;362:777–81.
50. Massie BM, Carson PE, McMurray JJ, et al. Irbesartan in patients with heart failure and preserved ejection fraction. N Engl J Med 2008;359:2456–67.
51. Silvestre JS, Robert V, Heymes C, et al. Myocardial production of aldosterone and corticosterone in the rat. Physiological regulation. J Biol Chem 1998;273:4883–91.
52. Lijnen P, Petrov V. Induction of cardiac fibrosis by aldosterone. J Mol Cell Cardiol 2000;32:865–79.
53. Brilla CG, Weber KT. Mineralocorticoid excess, dietary sodium, and myocardial fibrosis. J Lab Clin Med 1992;120:893–901.
54. Brilla CG, Weber KT. Reactive and reparative myocardial fibrosis in arterial hypertension in the rat. Cardiovasc Res 1992;26:671–7.

55. Brilla CG, Matsubara LS, Weber KT. Antifibrotic effects of spironolactone in preventing myocardial fibrosis in systemic arterial hypertension. Am J Cardiol 1993;71:A12–6.
56. Brewster UC, Perazella MA, Setaro JF. The renin-angiotensin-aldosterone system: cardiorenal effects and implications for renal and cardiovascular disease states. Am J Med Sci 2003;326:15–24.
57. Pitt B, Pfeffer MA, Assmann SF, et al. Spironolactone for heart failure with preserved ejection fraction. N Engl J Med 2014; 370:1383–92.
58. Effectiveness of spironolactone added to an angiotensin-converting enzyme inhibitor and a loop diuretic for severe chronic congestive heart failure (The Randomized Aldactone Evaluation Study [RALES]). Am J Cardiol 1996;78:902–7.
59. Pitt B, Zannad F, Remme WJ, et al. The effect of spironolactone on morbidity and mortality in patients with severe heart failure. N Engl J Med 1999;341:709–17.
60. Desai AS, Liu J, Pfeffer MA, et al. Incident hyperkalemia, hypokalemia, and clinical outcomes during spironolactone treatment of heart failure with preserved ejection fraction: analysis of the TOPCAT trial. J Card Fail 2018;24:313–20.
61. Meng X-M, Nikolic-Paterson DJ, Lan HY. TGF-β: the master regulator of fibrosis. Nat Rev Nephrol 2016;12:325–38.
62. Yue Y, Meng K, Pu Y, Zhang X. Transforming growth factor beta (TGF-β) mediates cardiac fibrosis and induces diabetic cardiomyopathy. Diabetes Res Clin Pract 2017;133: 124–30.
63. Bujak M, Frangogiannis NG. The role of TGF-beta signaling in myocardial infarction and cardiac remodeling. Cardiovasc Res 2007;74:184–95.
64. Khan S, Joyce J, Margulies KB, Tsuda T. Enhanced bioactive myocardial transforming growth factor-β in advanced human heart failure. Circ J 2014;78:2711–8.
65. Walton KL, Johnson KE, Harrison CA. Targeting TGF-β mediated SMAD signaling for the prevention of fibrosis. Front Pharmacol 2017;8:1–11.
66. Fang L, Murphy AJ, Dart AM. A clinical perspective of anti-fibrotic therapies for cardiovascular disease. Front Pharmacol 2017;8:186.
67. Letterio JJ, Roberts AB. Regulation of immune responses by TGF-beta. Annu Rev Immunol 1998;16:137–61.
68. Wahl SM, Hunt DA, Wakefield LM, et al. Transforming growth factor type beta induces monocyte chemotaxis and growth factor production. Proc Natl Academy Sci USA 1987;84:5788–92.
69. Yaswen L, Kulkarni AB, Fredrickson T, et al. Autoimmune manifestations in the transforming growth factor-beta 1 knockout mouse. Blood 1996;87:1439–45.
70. Liao R. Yin and Yang of myocardial transforming growth factor-beta1: timing is everything. Circulation 2005;111:2416–7.
71. Massagué J. TGFβ signalling in context. Nat Rev Mol Cell Biol 2012;13:616–30.
72. Engebretsen KVT, Skårdal K, Bjørnstad S, et al. Attenuated development of cardiac fibrosis in left ventricular pressure overload by SM16, an orally active inhibitor of ALK5. J Mol Cell Cardiol 2014;76:148–57.
73. Ikeuchi M, Tsutsui H, Shiomi T, et al. Inhibition of TGF-beta signaling exacerbates early cardiac dysfunction but prevents late remodeling after infarction. Cardiovasc Res 2004;64:526–35.
74. Herbertz S, Sawyer JS, Stauber AJ, et al. Clinical development of galunisertib (LY2157299 monohydrate), a small molecule inhibitor of transforming growth factor-beta signaling pathway. Drug Des Dev Ther 2015;9:4479–99.
75. Gellibert F, de Gouville AC, Woolven J, et al. Discovery of 4-{4-[3-(pyridin-2-yl)-1H-pyrazol-4-yl]pyridin-2-yl}-N-(tetrahydro-2H- pyran-4-yl)benzamide (GW788388): a potent, selective, and orally active transforming growth factor-beta type I receptor inhibitor. J Med Chem 2006;49: 2210–21.
76. Petersen M, Thorikay M, Deckers M, et al. Oral administration of GW788388, an inhibitor of TGF-beta type I and II receptor kinases, decreases renal fibrosis. Kidney Int 2008;73:705–15.
77. Oliveira FLD, Araújo-Jorge TC, Souza EMD, et al. Oral Administration of GW788388, an inhibitor of transforming growth factor beta signaling, prevents heart fibrosis in chagas disease. PLoS Negl Trop Dis 2012;6:e1696.
78. Derangeon M, Montnach J, Cerpa CO, et al. Transforming growth factor β receptor inhibition prevents ventricular fibrosis in a mouse model of progressive cardiac conduction disease. Cardiovasc Res 2017;113:464–74.
79. Tan SM, Zhang Y, Connelly KA, Gilbert RE, Kelly DJ. Targeted inhibition of activin receptor-like kinase 5 signaling attenuates cardiac dysfunction following myocardial infarction. Am J Physiol Heart Circ Physiol 2010;298:H1415–25.
80. Edgley AJ, Krum H, Kelly DJ. Targeting fibrosis for the treatment of heart failure: a role for transforming growth factor-β. Cardiovasc Ther 2012;30:e30–40.
81. King TE, Bradford WZ, Castro-Bernardini S, et al. A phase 3 trial of pirfenidone in patients with idiopathic pulmonary fibrosis. N Engl J Med 2014;370:2083–92.
82. Iyer SN, Gurujeyalakshmi G, Giri SN. Effects of pirfenidone on transforming growth factor-beta gene expression at the transcriptional level in bleomycin hamster model of lung fibrosis. J Pharmacol Exp Ther 1999;291:367–73.
83. Mirkovic S, Seymour A-ML, Fenning A, et al. Attenuation of cardiac fibrosis by pirfenidone and amiloride in DOCA-salt hypertensive rats. Br J Pharmacol 2002;135:961–8.
84. Nguyen DT, Ding C, Wilson E, Marcus GM, Olgin JE. Pirfenidone mitigates left ventricular fibrosis and dysfunction after myocardial infarction and reduces arrhythmias. Heart Rhythm 2010;7:1438–45.
85. Wang Y, Wu Y, Chen J, Zhao S, Li H. Pirfenidone attenuates cardiac fibrosis in a mouse model of TAC-induced left ventricular remodeling by suppressing NLRP3 inflammasome formation. Cardiology 2013;126:1–11.
86. Yamagami K, Oka T, Wang Q, et al. Pirfenidone exhibits cardioprotective effects by regulating myocardial fibrosis and vascular permeability in pressure-overloaded hearts. Am J Physiol Heart Circ Physiol 2015;309:H512–22.
87. Darakhshan S, Pour AB. Tranilast: a review of its therapeutic applications. Pharmacol Res 2015;91:15–28.
88. Isaji M, Aruga N, Naito J, Miyata H. Inhibition by tranilast of collagen accumulation in hypersensitive granulomatous inflammation in vivo and of morphological changes and functions of fibroblasts in vitro. Life Sci 1994;55:PL287–92.
89. Suzawa H, Kikuchi S, Arai N, Koda A. The mechanism involved in the inhibitory action of tranilast on collagen biosynthesis of keloid fibroblasts. Jpn J Pharmacol 1992;60:91–6.
90. Ikeda H, Inao M, Fujiwara K. Inhibitory effect of tranilast on activation and transforming growth factor beta 1 expression in cultured rat stellate cells. Biochem Biophys Res Commun 1996;227:322–7.
91. Holmes DR, Savage M, LaBlanche JM, et al. Results of prevention of restenosis with tranilast and its outcomes (PRESTO) trial. Circulation 2002;106:1243–50.

92. Martin J, Kelly DJ, Mifsud SA, et al. Tranilast attenuates cardiac matrix deposition in experimental diabetes: role of transforming growth factor-beta. Cardiovasc Res 2005;65:694–701.
93. Wen C, Xie G, Zeng P, Huang L-F, Chen C-Y. Tranilast inhibits myocardial fibrosis in mice with viral myocarditis. Zhongguo Dang Dai Er Ke Za Zhi = Chin J Contemporary Pediatr 2016;18:446–54.
94. Kagitani S, Ueno H, Hirade S, Takahashi T, Takata M, Inoue H. Tranilast attenuates myocardial fibrosis in association with suppression of monocyte/macrophage infiltration in DOCA/salt hypertensive rats. J Hypertens 2004;22:1007–15.
95. See F, Watanabe M, Kompa AR, et al. Early and delayed tranilast treatment reduces pathological fibrosis following myocardial infarction. Heart, Lung Circ 2013;22:122–32.
96. Wang F, Guan J. Cellular cardiomyoplasty and cardiac tissue engineering for myocardial therapy. Adv Drug Deliv Rev 2010;62:784–97.
97. Blackburn NJR, Sofrenovic T, Kuraitis D, et al. Timing underpins the benefits associated with injectable collagen biomaterial therapy for the treatment of myocardial infarction. Biomaterials 2015;39:182–92.
98. Pozzobon M, Bollini S, Iop L, et al. Human bone marrow-derived CD133+ cells delivered to a collagen patch on cryoinjured rat heart promote angiogenesis and arteriogenesis. Cell Transplant 2010;19:1247–60.
99. Dai W, Hale SL, Kay GL, Jyrala AJ, Kloner RA. Delivering stem cells to the heart in a collagen matrix reduces relocation of cells to other organs as assessed by nanoparticle technology. Regenerative Med 2009;4:387–95.
100. Xiong Q, Hill KL, Li Q, et al. A fibrin patch-based enhanced delivery of human embryonic stem cell-derived vascular cell transplantation in a porcine model of postinfarction left ventricular remodeling. Stem Cells 2011;29:367–75.
101. Nakamuta JS, Danoviz ME, Marques FLN, et al. Cell therapy attenuates cardiac dysfunction post myocardial infarction: effect of timing, routes of injection and a fibrin scaffold. PLoS One 2009;4:e6005.
102. Zhang X, Wang H, Ma X, et al. Preservation of the cardiac function in infarcted rat hearts by the transplantation of adipose-derived stem cells with injectable fibrin scaffolds. Exp Biol Med 2010;235:1505–15.
103. Deng B, Shen L, Wu Y, et al. Delivery of alginate-chitosan hydrogel promotes endogenous repair and preserves cardiac function in rats with myocardial infarction. J Biomed Mat Res Part A 2014;103:907–18.
104. Leor J, Tuvia S, Guetta V, et al. Intracoronary injection of in situ forming alginate hydrogel reverses left ventricular remodeling after myocardial infarction in swine. J Am Coll Cardiol 2009;54:1014–23.
105. Landa N, Miller L, Feinberg Micha S, et al. Effect of injectable alginate implant on cardiac remodeling and function after recent and old infarcts in rat. Circulation 2008;117:1388–96.
106. Bridges AW, García AJ. Anti-inflammatory polymeric coatings for implantable biomaterials and devices. J Diabetes Sci Technol 2008;2:984–94.
107. Lam MT, Wu JC. Biomaterial applications in cardiovascular tissue repair and regeneration. Expert Rev Cardiovasc Ther 2012;10:1039–49.
108. Segers Vincent FM, Lee Richard T, Dimmeler S, Losordo D. Biomaterials to enhance stem cell function in the heart. Circ Res 2011;109:910–22.
109. Rane AA, Christman KL. Biomaterials for the treatment of myocardial infarction: a 5-year update. J Am Coll Cardiol 2011;58:2615–29.
110. Venugopal JR, Prabhakaran MP, Mukherjee S, Ravichandran R, Dan K, Ramakrishna S. Biomaterial strategies for alleviation of myocardial infarction. J R Soc Interface 2012;9:1–19.
111. Nakano J, Marui A, Muranaka H, et al. Effects of hepatocyte growth factor in myocarditis rats induced by immunization with porcine cardiac myosin. Interact Cardiovasc Thoracic Surg 2014;18:300–7.
112. Nakamura T, Matsumoto K, Mizuno S, Sawa Y, Matsuda H, Nakamura T. Hepatocyte growth factor prevents tissue fibrosis, remodeling, and dysfunction in cardiomyopathic hamster hearts. Am J Physiol Heart Circ Physiol 2005;288:H2131–9.
113. Taniyama Y, Morishita R, Aoki M, et al. Angiogenesis and antifibrotic action by hepatocyte growth factor in cardiomyopathy. Hypertension 2002;40:47–53.
114. Aoki M, Morishita R, Taniyama Y, et al. Angiogenesis induced by hepatocyte growth factor in non-infarcted myocardium and infarcted myocardium: up-regulation of essential transcription factor for angiogenesis, ets. Gene Ther 2000;7:417.
115. Bussolino F, Di Renzo MF, Ziche M, et al. Hepatocyte growth factor is a potent angiogenic factor which stimulates endothelial cell motility and growth. J Cell Biol 1992;119:629–41.
116. Van Belle E, Witzenbichler B, Chen D, et al. Potentiated angiogenic effect of scatter factor/hepatocyte growth factor via induction of vascular endothelial growth factor. Circulation 1998;97:381–90.
117. Balkovetz DF, Lipschutz JH. Hepatocyte growth factor and the kidney: it is not just for the liver. In: Jeon KW, ed. International review of cytology, 186, Academic Press, 1998:225–60.
118. Nie S-P, Wang X, Qiao S-B, et al. Improved myocardial perfusion and cardiac function by controlled-release basic fibroblast growth factor using fibrin glue in a canine infarct model. J Zhejiang Univ Sci B 2010;11:895–904.
119. Liu Y, Sun L, Huan Y, Zhao H, Deng J. Effects of basic fibroblast growth factor microspheres on angiogenesis in ischemic myocardium and cardiac function: analysis with dobutamine cardiovascular magnetic resonance tagging. Eur J Cardiothorac Surg 2006;30:103–7.
120. Dvir T, Kedem A, Ruvinov E, et al. Prevascularization of cardiac patch on the omentum improves its therapeutic outcome. Proc Natl Academy Sci USA 2009;106:14990–5.
121. Wu J, Zeng F, Huang X-P, et al. Infarct stabilization and cardiac repair with a VEGF-conjugated, injectable hydrogel. Biomaterials 2011;32:579–86.
122. Simón-Yarza T, Formiga FR, Tamayo E, Pelacho B, Prosper F, Blanco-Prieto MJ. Vascular endothelial growth factor-delivery systems for cardiac repair: an overview. Theranostics 2012;2:541–52.
123. Dubois G, Segers VFM, Bellamy V, et al. Self-assembling peptide nanofibers and skeletal myoblast transplantation in infarcted myocardium. J Biomed Mat Res Part B 2008;87B:222–8.
124. Kim JH, Jung Y, Kim S-H, et al. The enhancement of mature vessel formation and cardiac function in infarcted hearts using dual growth factor delivery with self-assembling peptides. Biomaterials 2011;32:6080–8.
125. Christman KL, Lee RJ. Biomaterials for the treatment of myocardial infarction. J Am Coll Cardiol 2006;48:907–13.
126. Sarig U, Machluf M. Engineering cell platforms for myocardial regeneration. Expert Opin Biol Ther 2011;11:1055–77.

127. Callegari A, Bollini S, Iop L, et al. Neovascularization induced by porous collagen scaffold implanted on intact and cryoinjured rat hearts. Biomaterials 2007;28:5449–61.
128. Simpson D, Liu H, Fan T-HM, Nerem R, Dudley Jr SC. A tissue engineering approach to progenitor cell delivery results in significant cell engraftment and improved myocardial remodeling. Stem Cells 2007;25:2350–7.
129. Chachques JC, Trainini JC, Lago N, Cortes-Morichetti M, Schussler O, Carpentier A. Myocardial assistance by grafting a new bioartificial upgraded myocardium (MAGNUM trial): clinical feasibility study. Ann Thorac Surg 2008;85:901–8.
130. Kawamura M, Miyagawa S, Miki K, et al. Feasibility, safety, and therapeutic efficacy of human induced pluripotent stem cell-derived cardiomyocyte sheets in a Porcine Ischemic Cardiomyopathy Model. Circulation 2012;126(11_suppl_1):S29–37.
131. Xiong Q, Ye L, Zhang P, et al. Functional consequences of human induced pluripotent stem cell therapy: myocardial ATP turnover rate in the in vivo swine heart with postinfarction remodeling. Circulation 2013;127:997–1008.
132. Wang RM, Christman KL. Decellularized myocardial matrix hydrogels: In basic research and preclinical studies. Adv Drug Deliv Rev 2016;96:77–82.
133. Singelyn JM, Sundaramurthy P, Johnson TD, et al. Catheter-deliverable hydrogel derived from decellularized ventricular extracellular matrix increases endogenous cardiomyocytes and preserves cardiac function post-myocardial infarction. J Am Coll Cardiol 2012;59:751–63.
134. Singelyn JM, DeQuach JA, Seif-Naraghi SB, Littlefield RB, Schup-Magoffin PJ, Christman KL. Naturally derived myocardial matrix as an injectable scaffold for cardiac tissue engineering. Biomaterials 2009;30:5409–16.
135. Ott HC, Matthiesen TS, Goh S-K, et al. Perfusion-decellularized matrix: using nature's platform to engineer a bioartificial heart. Nat Med 2008;14:213.
136. Mewhort HEM, Turnbull JD, Satriano A, et al. Epicardial infarct repair with bioinductive extracellular matrix promotes vasculogenesis and myocardial recovery. J Heart Lung Transplant 2016;35:661–70.
137. Turner NA. Inflammatory and fibrotic responses of cardiac fibroblasts to myocardial damage associated molecular patterns (DAMPs). J Mol Cell Cardiol 2016;94:189–200.
138. Fedak P. Epicardial infarct repair using CorMatrix®-ECM: clinical feasibility study (EIR) https://clinicaltrials.gov/ct2/show/NCT02887768; Published 2017. Accessed December 16, 2018.
139. Aziyo Biologics I. Obtain additional information on use of CorMatrix ECM (Extracellular Matrix) (RECON) https://clinicaltrials.gov/ct2/show/study/NCT02073331; Published 2018. Accessed December 16, 2018.
140. Ventrix I. A study of ventrigel in post-MI patients https://clinicaltrials.gov/ct2/show/NCT02305602?term=NCT02305602&rank=1; Published 2018. Accessed December 16, 2018.
141. Cleland JGF, Freemantle N, Coletta AP, Clark AL. Clinical trials update from the American Heart Association: REPAIR-AMI, ASTAMI, JELIS, MEGA, REVIVE-II, SURVIVE, and PROACTIVE. Eur J Heart Fail 2005;8:105–10.
142. Mansour S, Vanderheyden M, De Bruyne B, et al. Intracoronary delivery of hematopoietic bone marrow stem cells and luminal loss of the infarct-related artery in patients with recent myocardial infarction. J Am Coll Cardiol 2006;47:1727–30.
143. Schächinger V, Erbs S, Elsässer A, et al. Improved clinical outcome after intracoronary administration of bone-marrow-derived progenitor cells in acute myocardial infarction: final 1-year results of the REPAIR-AMI trial. Eur Heart J 2006;27:2775–83.
144. Marelli D, Desrosiers C, el-Alfy M, Kao RL, Chiu RC. Cell transplantation for myocardial repair: an experimental approach. Cell Transplant 1992;1:383–90.
145. Chen S-L, Fang W-w, Qian J, et al. Improvement of cardiac function after transplantation of autologous bone marrow mesenchymal stem cells in patients with acute myocardial infarction. Chin Med J 2004;117:1443–8.
146. Koh GY, Klug MG, Soonpaa MH, Field LJ. Differentiation and long-term survival of C2C12 myoblast grafts in heart. J Clin Invest 1993;92:1548–54.
147. Povsic TJ, Henry TD, Traverse JH, et al. The RENEW trial: efficacy and safety of intramyocardial autologous CD34+ cell administration in patients with refractory angina. JACC 2016;9:1576–85.
148. Beltrami AP, Barlucchi L, Torella D, et al. Adult cardiac stem cells are multipotent and support myocardial regeneration. Cell 2003;114:763–76.
149. Menasché P, Vanneaux V, Hagège A, et al. Human embryonic stem cell-derived cardiac progenitors for severe heart failure treatment: first clinical case report. Eur Heart J 2015;36:2011–7.
150. Skelton RJP, Brady B, Khoja S, et al. CD13 and ROR2 permit isolation of highly enriched cardiac mesoderm from differentiating human embryonic stem cells. Stem Cell Rep 2016;6:95–108.
151. Skelton RJP, Kamp TJ, Elliott DA, Ardehali R. Biomarkers of human pluripotent stem cell-derived cardiac lineages. Trends Mol Med 2017;23:651–68.
152. Skelton RJ, Costa M, Anderson DJ, et al. SIRPA, VCAM1 and CD34 identify discrete lineages during early human cardiovascular development. Stem Cell Res 2014;13:172–9.
153. Fernandes S, Chong JJH, Paige SL, et al. Comparison of human embryonic stem cell-derived cardiomyocytes, cardiovascular progenitors, and bone marrow mononuclear cells for cardiac repair. Stem Cell Rep 2015;5:753–62.
154. Chong JJ, Yang X, Don CW, et al. Human embryonic-stem-cell-derived cardiomyocytes regenerate non-human primate hearts. Nature 2014;510:273–7.
155. Riegler J, Tiburcy M, Ebert A, et al. Human engineered heart muscles engraft and survive long term in a Rodent Myocardial Infarction Model. Circ Res 2015;117:720–30.
156. Ye L, Chang Y-H, Xiong Q, et al. Cardiac repair in a porcine model of acute myocardial infarction with human induced pluripotent stem cell-derived cardiovascular cells. Cell Stem Cell 2014;15:750–61.
157. Menasché P, Alfieri O, Janssens S, et al. The Myoblast Autologous Grafting in Ischemic Cardiomyopathy (MAGIC) trial: first randomized placebo-controlled study of myoblast transplantation. Circulation 2008;117:1189–200.
158. van Berlo JH, Kanisicak O, Maillet M, et al. C-kit+ cells minimally contribute cardiomyocytes to the heart. Nature 2014;509:337–41.
159. The Lancet Editors. Expression of concern: the SCIPIO trial. Lancet 2014;383:1279.
160. Thomson JA, Itskovitz-Eldor J, Shapiro SS, et al. Embryonic stem cell lines derived from human blastocysts. Science 1998;282:1145.
161. Shiba Y, Gomibuchi T, Seto T, et al. Allogeneic transplantation of iPS cell-derived cardiomyocytes regenerates primate hearts. Nature 2016;538:388–91.
162. Almeida SO, Skelton RJ, Adigopula S, Ardehali R. Arrhythmia in stem cell transplantation. Card Electrophysiol Clin 2015;7:357–70.

163. Fox IJ, Daley GQ, Goldman SA, Huard J, Kamp TJ, Trucco M. Stem cell therapy. Use of differentiated pluripotent stem cells as replacement therapy for treating disease. Science 2014;345:1247391.
164. Laflamme MA, Murry CE. Heart regeneration. Nature 2011; 473:326–35.
165. Gallet R, Dawkins J, Valle J, et al. Exosomes secreted by cardiosphere-derived cells reduce scarring, attenuate adverse remodelling, and improve function in acute and chronic porcine myocardial infarction. Eur Heart J 2017;38:201–11.
166. Orlic D, Kajstura J, Chimenti S, et al. Bone marrow cells regenerate infarcted myocardium. Nature 2001;410:701–5.
167. Wang LT, Ting CH, Yen ML, et al. Human mesenchymal stem cells (MSCs) for treatment towards immune- and inflammation-mediated diseases: review of current clinical trials. J Biomed Sci 2016;23:76.
168. Behfar A, Faustino RS, Arrell DK, Dzeja PP, Perez-Terzic C, Terzic A. Guided stem cell cardiopoiesis: discovery and translation. J Mol Cell Cardiol 2008;45:523–9.
169. Chugh AR, Beache GM, Loughran JH, et al. Administration of cardiac stem cells in patients with ischemic cardiomyopathy: the SCIPIO trial: surgical aspects and interim analysis of myocardial function and viability by magnetic resonance. Circulation 2012;126(11 Suppl 1):S54–64.
170. Mathur A, Fernández-Avilés F, Dimmeler S, et al. The consensus of the Task Force of the European Society of Cardiology concerning the clinical investigation of the use of autologous adult stem cells for the treatment of acute myocardial infarction and heart failure: update 2016. Eur Heart J 2017;38:2930–5.
171. Jeevanantham V, Afzal MR, Zuba-Surma EK, Dawn B. Clinical trials of cardiac repair with adult bone marrow- derived cells. Methods Mol Biol 2013;1036:179–205.
172. Nowbar AN, Mielewczik M, Karavassilis M, et al. Discrepancies in autologous bone marrow stem cell trials and enhancement of ejection fraction (DAMASCENE): weighted regression and meta-analysis. BMJ 2014;348:g2688.
173. Hatzistergos KE, Quevedo H, Oskouei BN, et al. Bone marrow mesenchymal stem cells stimulate cardiac stem cell proliferation and differentiation. Circ Res 2010;107:913–22.
174. Loffredo FS, Steinhauser ML, Gannon J, Lee RT. Bone marrow-derived cell therapy stimulates endogenous cardiomyocyte progenitors and promotes cardiac repair. Cell Stem Cell 2011;8:389–98.
175. Malliaras K, Zhang Y, Seinfeld J, et al. Cardiomyocyte proliferation and progenitor cell recruitment underlie therapeutic regeneration after myocardial infarction in the adult mouse heart. EMBO Mol Med 2013;5:191–209.
176. Quijada P, Salunga HT, Hariharan N, et al. Cardiac stem cell hybrids enhance myocardial repair. Circ Res 2015;117:695–706.
177. Hatzistergos KE, Takeuchi LM, Saur D, et al. C-kit+ cardiac progenitors of neural crest origin. Proc Natl Academy Sci USA 2015;112:13051–6.
178. Quevedo HC, Hatzistergos KE, Oskouei BN, et al. Allogeneic mesenchymal stem cells restore cardiac function in chronic ischemic cardiomyopathy via trilineage differentiating capacity. Proc Natl Acad Sci USA 2009;106:14022–7.
179. Chong JJ, Chandrakanthan V, Xaymardan M, et al. Adult cardiac-resident MSC-like stem cells with a proepicardial origin. Cell Stem Cell 2011;9:527–40.
180. Gomes SA, Rangel EB, Premer C, et al. S-nitrosoglutathione reductase (GSNOR) enhances vasculogenesis by mesenchymal stem cells. Proc Natl Acad Sci USA 2013;110:2834–9.
181. Engel JL, Ardehali R. Direct cardiac reprogramming: progress and promise. Stem Cells Int 2018;2018:1–10.
182. Ieda M, Fu J-D, Delgado-Olguin P, et al. Direct reprogramming of fibroblasts into functional cardiomyocytes by defined factors. Cell 2010;142:375–86.
183. Wada R, Muraoka N, Inagawa K, et al. Induction of human cardiomyocyte-like cells from fibroblasts by defined factors. Proc Natl Academy Sci USA 2013;110:12667–72.
184. Qian L, Huang Y, Spencer CI, et al. In vivo reprogramming of murine cardiac fibroblasts into induced cardiomyocytes. Nature 2012;485:593–8.
185. Song K, Nam Y-J, Luo X, et al. Heart repair by reprogramming non-myocytes with cardiac transcription factors. Nature 2012;485:599–604.
186. Inagawa K, Miyamoto K, Yamakawa H, et al. Induction of cardiomyocyte-like cells in infarct hearts by gene transfer of Gata4, Mef2c, and Tbx5. Circ Res 2012;111:1147–56.
187. Edelstein ML, Abedi MR, Wixon J, Edelstein RM. Gene therapy clinical trials worldwide 1989−2004—an overview. J Gene Med 2004;6:597–602.
188. Mathison M, Singh VP, Chiuchiolo MJ, et al. In situ reprogramming to transdifferentiate fibroblasts into cardiomyocytes using adenoviral vectors: implications for clinical myocardial regeneration. J Thorac Cardiovasc Surg 2017;153: 329–39, e323.
189. Wold WSM, Toth K. Adenovirus vectors for gene therapy, vaccination and cancer gene therapy. Curr Gene Ther 2013; 13:421–33.
190. Anne KZaDAM. Immune Responses to Adeno-Associated Virus Vectors. Curr Gene Ther 2005;5:323–31.
191. Colella P, Ronzitti G, Mingozzi F. Emerging Issues in AAV-Mediated In Vivo Gene Therapy. Mol Ther Methods Clin Dev 2017;8:87–104.
192. Yoo SY, Jeong S-N, Kang J-I, Lee S-W. Chimeric adeno-associated virus-mediated cardiovascular reprogramming for ischemic heart disease. ACS Omega 2018;3:5918–25.
193. Nakanishi M, Otsu M. Development of sendai virus vectors and their potential applications in gene therapy and regenerative medicine. Curr Gene Ther 2012;12:410–6.
194. Miyamoto K, Akiyama M, Tamura F, et al. Direct In vivo reprogramming with sendai virus vectors improves cardiac function after myocardial infarction. Cell Stem Cell 2018;22: 91–103, e105.
195. Engel JL, Ardehali R. Sendai virus based direct cardiac reprogramming: what lies ahead. Stem Cell Investig 2018; 5:37.
196. Wang H, Cao N, Spencer CI, et al. Small molecules enable cardiac reprogramming of mouse fibroblasts with a single factor. Cell Rep 2014;6:951–60.
197. Fu Y, Huang C, Xu X, et al. Direct reprogramming of mouse fibroblasts into cardiomyocytes with chemical cocktails. Cell Res 2015;25:1013–24.
198. Jayawardena TM, Finch EA, Zhang L, et al. MicroRNA induced cardiac reprogramming in vivo: evidence for mature cardiac myocytes and improved cardiac function. Circ Res 2015;116:418–24.
199. Dong D-L, Yang B-F. Role of microRNAs in cardiac hypertrophy, myocardial fibrosis and heart failure. Acta Pharmaceutica Sinica B 2011;1:1–7.
200. Qu X, Song X, Yuan W, et al. Expression signature of lncRNAs and their potential roles in cardiac fibrosis of post-infarct mice. Biosci Rep 2016;36:e00337.

201. Thum T, Gross C, Fiedler J, et al. MicroRNA-21 contributes to myocardial disease by stimulating MAP kinase signalling in fibroblasts. Nature 2008;456:980–4.
202. van Rooij E, Sutherland LB, Thatcher JE, et al. Dysregulation of microRNAs after myocardial infarction reveals a role of miR-29 in cardiac fibrosis. Proc Natl Acad Sci USA 2008;105: 13027–32.
203. Huang Y, Qi Y, Du JQ, Zhang DF. MicroRNA-34a regulates cardiac fibrosis after myocardial infarction by targeting Smad4. Expert Opin Ther Targets 2014;18:1355–65.
204. Micheletti R, Plaisance I, Abraham BJ, et al. The long noncoding RNA Wisper controls cardiac fibrosis and remodeling. Sci Transl Med 2017;9:eaai9118.
205. Qu X, Du Y, Shu Y, et al. MIAT is a pro-fibrotic long non-coding rna governing cardiac fibrosis in post-infarct myocardium. Sci Rep 2017;7:42657.
206. Felisbino MB, McKinsey TA. Epigenetics in cardiac fibrosis: emphasis on inflammation and fibroblast activation. JACC Basic translation Sci 2018;3:704–15.
207. Nural-Guvener HF, Zakharova L, Nimlos J, Popovic S, Mastroeni D, Gaballa MA. HDAC class I inhibitor, mocetinostat, reverses cardiac fibrosis in heart failure and diminishes CD90+ cardiac myofibroblast activation. Fibrogenesis Tissue Repair 2014;7:10.
208. Yoon S, Eom GH. HDAC and HDAC inhibitor: from cancer to cardiovascular diseases. Chonnam Med J 2016;52:1–11.
209. Duan Q, McMahon S, Anand P, et al. BET bromodomain inhibition suppresses innate inflammatory and profibrotic transcriptional networks in heart failure. Sci Transl Med 2017;9:1–15.
210. Bolli R, Chugh A, Loughran J, Kajstura J, Anversa P. Cardiac stem cells in patients with ischaemic cardiomyopathy−authors' reply. Lancet 2012;379:891–2.